ALMA MATER STUDIORUM
UNIVERSITÀ DI BOLOGNA

DOTTORATO DI RICERCA IN

NANOSCIENZE PER LA MEDICINA E PER L'AMBIENTE

Ciclo 37

Settore Concorsuale: 03/C1 - CHIMICA ORGANICA

Settore Scientifico Disciplinare: CHIM/06 - CHIMICA ORGANICA

CHEMICAL TAILORING OF GRAPHENE OXIDE AND RELATED COMPOSITES FOR ENHANCED ADSORPTION OF WATER EMERGING CONTAMINANTS

Presentata da: Francesca Tunioli

Coordinatore Dottorato

Matteo Calvaresi

Supervisore

Manuela Melucci

Co-supervisore

Matteo Calvaresi

Esame finale anno 2025

Index

Abstract

Water purification is a critical global issue and the pollution by emerging contaminants (ECs), such as per- and polyfluoroalkyl substances (PFAS), pharmaceuticals, and personal care products, poses significant risks to human health and the environment. Traditional water treatment methods are often insufficient for removing these persistent contaminants, calling for the urgent development of new technologies and materials. In this context, graphene related materials (GRM) have gained increasing attention due to their exceptional properties, allowing innovative and efficient solutions. This thesis explores the potential of GRM as sorbents for the removal of ECs from drinking water, with a focus on the development of advanced composites that exploit both biopolymers and synthetic polymers as support matrices for GRM.

This work examines the adsorption behaviour of water-dispersed GRM, in particular graphene oxide (GO), which forms stable water dispersion due to its surface oxygen groups (i.e. carboxyl, epoxy and hydroxyl groups). Moreover, GO adsorption properties, i.e. selectivity and capacity, can be tailored by modifying its surface through covalent functionalization. Epoxide ring-opening reactions were used to graft various functional groups, including amino acids and β-cyclodextrin (βCD), onto the GO surface. In particular, functionalization with βCD was proven to be effective in the removal of perfluorobutanoic acid (PFBA), a persistent PFAS. By controlling the length of the alkyl chain used to bind the βCD to the GO, the adsorption efficiency in tap water was significantly improved from no removal with pristine GO to 65% removal with the best performing GO-βCD, and confirmed also by molecular dynamic simulations.

Although GRM have excellent adsorption properties, their need for dispersion and subsequent removal from water presents challenges, often requiring complex techniques or additional steps. To overcome these limitations, the study focused on incorporating GRM into a polymer matrix, creating a macroscopic structure that allows for easy removal and recovery after treatment, while retaining partial access to the GRM surface area for effective adsorption. With this aim, alginate was used as a biopolymer to produce hydrogels, incorporating GRM to form a stable composite material. These sorbents were tested for the removal of a selection of ECs, including bisphenol A, ofloxacin, and diclofenac, from tap water. The results demonstrated excellent adsorption

capacity and selectivity, as well as promising reusability after multiple adsorption-desorption cycles, highlighting the potential for sustainable applications.

In addition to biopolymer-based composites, synthetic polymer systems were investigated, particularly polysulfone (PSU) hollow fiber membranes coextruded with GO. These membranes were developed for point-of-use water treatment technologies and tested for their efficiency in removing pharmaceuticals, heavy metals, and PFAS. A novel approach was also introduced to recycle PSU-GO industrial scraps into granular sorbents, which were tested in pilot plants under real tap water conditions. Safety assessments, including surface-enhanced Raman spectroscopy, confirmed that GO release was negligible, ensuring the suitability of PSU-GO for practical water treatment applications.

List of acronyms and abbreviations

AC	*Activated carbon*
AOPs	*Advances oxidation processes*
ATR-FTIR	*Attenuated total reflection - Fourier transform infrared spectroscopy*
βCD	*β-cyclodextrin*
BET	*Brunauer–Emmett–Teller*
BP3	*Bisphenone-3*
BP4	*Bisphenone-4*
BPA	*Bisphenol A*
CAF	*Caffeine*
CBZ	*Carbamazepine*
CIPRO	*Ciprofloxacin*
DCF	*Diclofenac*
DWD	*Drinking water directive*
DWTPs	*Drinking water treatment plants*
EA	*Elemental analysis*
EBCT	*Empty bed contact time*
ECs	*Emerging contaminants*
EDCs	*Endocrine-disrupting chemicals*
EPA	*Environmental protection agency*
GAC	*Granular activated carbon*
GNP	*Graphene nanoplatelets*
GO	*Graphene oxide*
GRM	*Graphene related materials*
HF	*Hollow fibers*
HPLC	*High performance liquid chromatography*
ICP-MS	*Inductively coupled plasma mass spectrometry*
Lys	*Lysine*
LOQ	*Limit of quantification*
MB	*Methylene blue*
MD	*Molecular dynamic*
MF	*Microfiltration*

NF	*Nanofiltration*
NMR	*Nuclear magnetic resonance spectroscopy*
NOM	*Natural organic matter*
OFLOX	*Ofloxacin*
PAC	*Powder activated carbon*
PCL	*Poly(ε-caprolactone)*
PES	*Polyethersulfone*
PET	*Polyethylene terephthalate*
PFAS	*Per- and polyfluorinated substances*
PFBA	*Perfluorobutanoic acid*
PFCA	*Perfluoroalkyl carboxylic acids*
PFOA	*Perfluorooctanoic acid*
PFSA	*Perfluoroalkyl sulfonic acids*
PLA	*Polylactice acid*
POE	*Point-of-entry*
POU	*Point-of-use*
PP	*Polypropylene*
PPCPs	*Pharmaceutical and personal care products*
PS	*Polystyrene*
PSU	*Polysulfone*
PVC	*Polyvinylchloride*
PVDF	*Polyvinylidene fluoride*
Qm	*Maximum monolayer adsorption capacity*
rGO	*Reduced graphene oxide*
RhB	*Rhodamine B*
RO	*Reverse osmosis*
SD	*Standard deviation*
SDGs	*Sustainable development goals*
SEM	*Scanning electron spectroscopy*
SERS	*Surface enhanced Raman spectroscopy*
TFA	*Trifluoroacetic acid*
TGA	*Thermogravimetric analysis*

UF	*Ultrafiltration*
UPLC-MS/MS	*Ultrahigh performance liquid chromatography - mass spectroscopy*
XPS	*X-ray photoelectron spectroscopy*

1 Introduction

1.1 Water issues: scarcity and pollution

Water is an essential natural resource that is required for the existence of all living organisms. It is known that the world is facing a water crisis characterized by two main issues: scarcity and pollution. Over the past decades, water pollution has significantly increased, evolving into a severe global issue, posing significant risks to human health and ecological systems.[1-3] Various pollution sources, including urban development, industrial effluents and improper waste disposal, contribute to the contamination of water bodies.[4] Population growth and urban expansion have intensified the demand for water, putting a strain on existing resources , also due to sub-optimal water use practices and inadequate infrastructure.[5] Additionally, climate change has exacerbated water scarcity through altered precipitation patterns, leading to droughts and reduced water availability in many regions worldwide.[6]

To address this global issue a coordinated effort and shared actions are needed. On this line, United Nations established the Sustainable Development Goals (SDGs), 17 global targets set in 2015 as part of the 2030 Agenda for Sustainable Development.[7] These goals aim to address social, economic and environmental challenges to achieve a more sustainable and equitable world by the year 2030. Among them, SDG 6 is focused on water-related issues, specifically on “ensuring the availability and sustainable management of water and sanitation for all”. Emphasis is placed on improving water quality, its use efficiency and reducing pollution. Integrated water resources management is required, with a focus on the preservation of related ecosystems to preserve its quality and availability. The goal also promotes international collaboration in water and sanitation programmes. SDG 6 is crucial for the achievement of sustainable development, as water and sanitation are essential for public health, economic development, environmental sustainability and, ultimately, human well-being.

European Union policies about water are consistent with the ones promoted by the United Nations. At the end of 2020, the European Commission promulgated the new Drinking Water Directive (DWD) 2020/2184,[8] which represents an important step in the history of water management in this continent. This directive emphasises the need to improve water quality standards and treatment techniques by setting quality parameters

for drinking water throughout the European Union. The directive, revised in 2022,[9] introduces defined parameters and maximum allowable concentrations for a range of substances and microorganisms in drinking water, including chemicals, bacteria and parasites. It also introduces a risk-based approach to the monitoring of water bodies and distribution lines, to identify and address potential risks to drinking water quality, and to elaborate the most efficient and cost-effective solution to the problem. Furthermore, the DWD facilitates the access to the information and data about monitoring and evaluation for the public and the scientific community.

The new DWD imposes the limit values to a great variety of substances, elements and microorganisms of concern for human health that should be carefully monitored by the Europe Union member states. Several of these limits have been updated since the previous directive (98/83/EC)[10], but many others have been introduced for the first time in this occasion. This list includes some metals (lead and chromium), industrial chemicals (i.e. pharmaceuticals, pesticides, UV filters) and per- and polyfluoroalkyl substances (PFAS).

The above examples are commonly known as “emerging contaminants” (ECs), a term that refers primarily to pollutants that are not currently regulated or monitored in water supplies or wastewater. This category comprises a vast and articulated family of substances and microorganisms (more than 1˙000), including pharmaceuticals (such as antibiotics and painkillers), diagnostic products, steroids and hormones, antiseptics, personal care products (such as sunscreens and perfumes), pesticide and herbicides, fuel additives, surfactants, endocrine disruptors and more.[11-13]

ECs originate from a variety of anthropogenic sources and activities.[13] Pharmaceuticals and personal care products are major contributors, entering the aquatic environment through domestic wastewater discharges, improper disposal of pharmaceuticals and agricultural runoff. Industrial processes also play a major role, with chemicals from manufacturing, textile and electronics industries often entering water bodies. Agricultural activities contribute through the use of pesticides, herbicides and veterinary medicines, which can leach into groundwater or run off into surface waters. Although waste water treatment plants are designed to remove conventional pollutants, they often fail to remove ECs completely, leading to their persistence in the treated waste water and sludge.[14, 15] As a result, ECs have been detected in various environmental

compartments, including rivers, surface and groundwater, municipal wastewater, and, in the worst cases, even drinking water and food sources.[16, 17]

Interest in ECs has increased significantly over the years, as reflected in the growing number of publications on the subject.[12, 15-18] However, their effects on the environment and human health remain largely unknown and are still being assessed. The development of environmentally friendly and economically viable water purification technologies that meet the needs of society without compromising the natural environment requires urgent cooperation between academia, scientists and industry. These actions are crucial to ensure sustainable water quality and protect public health.

1.2 Emerging contaminants

The US Environmental Protection Agency (EPA) defines ECs as chemicals or materials that pose a perceived, potential or actual threat to human health or the environment or by a lack of published health standards. A contaminant can be considered ECs because a new source or a new pathway to human has been discovered or a new detection method or treatment technology has been developed.[19] Emerging contaminants enter aquatic environments through various pathways, such as the release of untreated or treated wastewater from municipal and industrial facilities. In addition, they may originate from sewage overflows, leaks from waste disposal sites and runoff from urban and agricultural land where sewage sludge or manure are used for irrigation. Over the last decade, several ECs have been detected in both raw influent and treated effluents of municipal wastewater treatment plants at concentrations ranging from ng/L to µg/L.[20] Global production of ECs is estimated to have increased from 1 million to 500 million tons per year.[21]

The list of emerging contaminants is extensive and many class of molecules and products are considered ECs,[20-23] including:

- *Pharmaceutical and personal care products* (PPCPs): antibiotics, anti-inflammatory, hormones, drugs, cormetics, UV-filters, fragrances and cleaning products.

- *Per- and polyfluoroalkyl substances* (PFAS): synthetic organofluorine chemical compounds used in a variety of products including waterproof clothing, furniture, adhesives, food packaging, heat-resistant non-stick cooking surfaces.

- *Endocrine-disrupting chemicals* (EDCs): substances that can interfere with the hormonal system of humans and wildlife. They include chemicals used in plastics, pesticides, and certain industrial processes.[24]

These contaminants are increasingly found in surface, ground and even drinking water due to their persistence and resistance to conventional wastewater treatment processes, becoming ubiquitous in the environment (Figure 1.1). For example, more than 80 ECs have been found in the drinking water of Milan, the most populous and industrialized city in Italy.[25] These ECs include pharmaceuticals, illicit drugs, PFAS, anthropogenic markers, and plasticizers, and they have been detected in trace amounts (ng/L) in each water source tested, indicating a negligible risk to human health. Furthermore, a significant PFAS contamination was discovered in May 2013 in some areas of the Veneto Region (northern Italy), mainly associated with an industrial plant activity located in the area.[26]

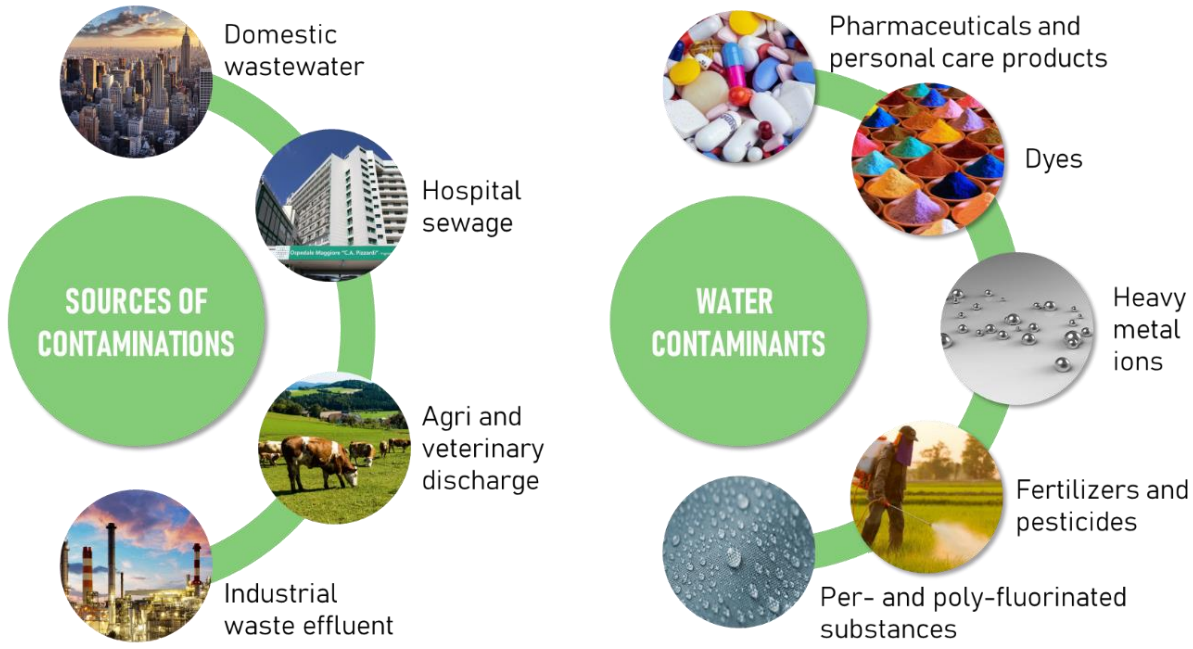

Figure 1.1 *Sources and classification of hazardous emerging contaminants.*

The widespread presence of ECs in drinking water underlines the urgent need for extensive research into their presence, behaviour, fate and potential risks. This research is crucial for the development of regulatory guidelines and the inclusion of the most hazardous contaminants in future legislation. While the toxicity of some ECs has already been confirmed, most of these substances are still under evaluation.[21] Consequently, many of them have been included in the European watch list, along with heavy metals,

which have been extensively studied.[27] Contrarily to ECs, heavy metals have well-documented toxicity and carcinogenic properties at specific exposure levels. However, they are released into water daily from various natural and anthropogenic sources, raising serious health concerns.[28-30]

The following sections provide an overview of the contaminants of environmental concern that I focused on during my PhD research, including organic contaminants, PFAS and heavy metals.

1.2.1 Pharmaceutical and personal care products

Pharmaceuticals and personal care products (PPCPs) have emerged as significant environmental contaminants in aquatic systems. These substances, which include a wide range of products such as prescription drugs, over-the-counter medicines, cosmetics, sunscreens and fragrances, are continuously introduced into water bodies through various pathways.[31, 32] PPCPs have revolutionised modern human life, becoming essential commodities. The increasing population and evolving lifestyles have resulted in their growing utilization and demand, with global consumption levels equal to those of agrochemicals. Consequently, they now constitute one of the largest sources of persistent ECs in surface and groundwater systems globally.

These consumer products are regularly disposed of or discharged into aquatic systems through domestic and industrial sewage systems. As a result, over the past decade, PPCPs have frequently been detected in wastewater treatment plants. The persistence and bioactivity of many PPCPs pose potential risks to aquatic ecosystems and human health, as they can alter endocrine functions and induce antibiotic resistance.[33] Despite their widespread presence, PPCPs are still not fully regulated, necessitating comprehensive research into their presence, behaviour, fate and impacts.[21]

Figure 1.2 shows the chemical structure of a selection of eight PPCPs. Among the pharmaceuticals frequently reported in both drinking and wastewater, there are diclofenac (anti-inflammatory),[34] carbamazepine (anti-epileptic drug),[35] ofloxacin and ciprofloxacin (antibiotics).[36] Also caffeine, bisphenol A and benzophenones can be frequently monitored in PPCPs, as stimulant, additives or UV filters, respectively. Rhodamine B, used as a textile dye, is also frequently detected in PPCP products.

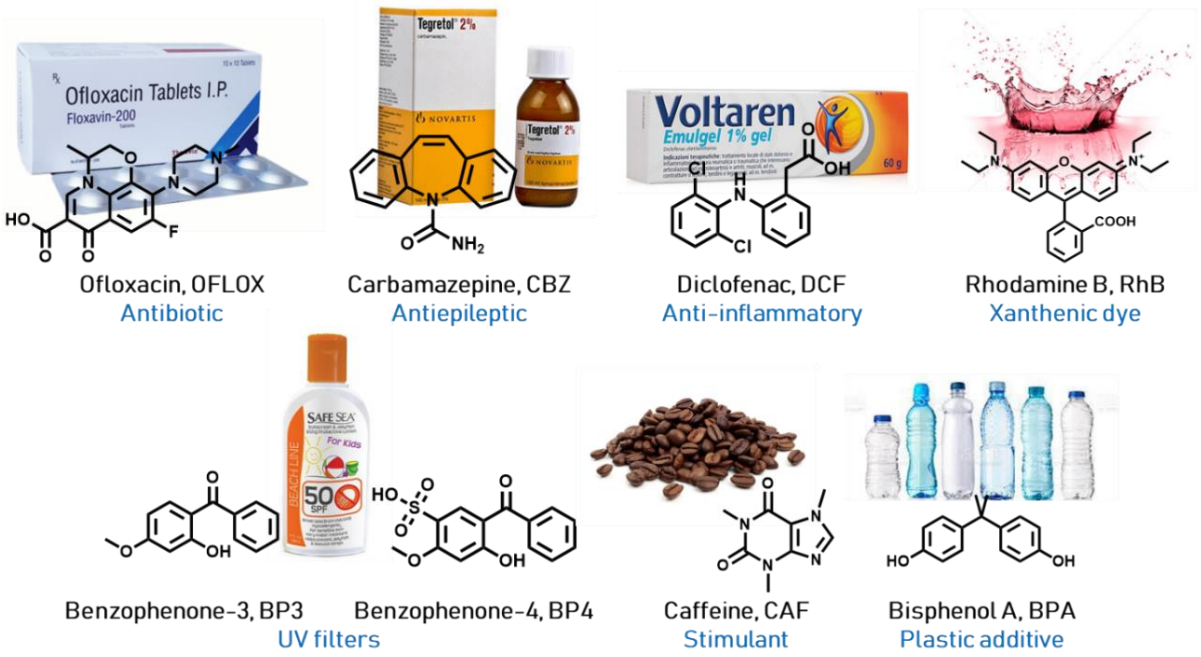

Figure 1.2 *Chemical structure of a selection of PPCPs.*

Ciprofloxacin (CIPRO) and Ofloxacin (OFLOX) are quinolone antibiotics used for the treatment of various types of bacterial infections.[36, 37] They have gained increased concern due to their widespread use, and their presence in aquatic environments is associated with the potential to induce antibiotic resistance.[38] Over the past decade, CIPRO has been widely detected in the environment, with the highest concentrations recorded in India, where a maximum concentration of 2500-6500 mg/L was detected. [39, 40] These concentrations are significantly higher than those observed in the United States and Europe, where CIPRO is typically found at much lower ng/L levels in surface and groundwater.[38, 41] OFLOX, on the other hand, is usually found in lower concentrations and less frequently, but it is one of the most important antibiotic compounds present in effluents from treatment plants and surface waters.[38]

Carbamazepine (CBZ) is an anti-epileptic drug used in the treatment of neuropathic pain and certain psychiatric disorders with a global usage amount of 1˙014 tons per year.[42-44] In the human body, CBZ is extensively metabolised, with only a small fraction (< 2%) being excreted in an unchanged form.[42] However, due to low removal rates in wastewater treatment processes (<45%), CBZ is continuously released into the environment.[45] It exhibits resistance to degradation in the environment and can persist in both freshwater and marine systems, with concentrations ranging from ng/L to a few µg/L. Notably, it has been widely detected in Milan's drinking water, with levels reaching

up to 0.18 ng/L.[42, 46-48] Exposure to CBZ can cause adverse effects in aquatic and terrestrial organisms, including reproduction toxicity, developmental delay and carcinogenicity.[49-52] Consequently, CBZ is considered a contaminant of environmental and human health concern[52] and has even been proposed as a potential marker of human activity in water bodies.[50]

Diclofenac (DCF), a common non-steroidal anti-inflammatory drug, has emerged as a growing environmental concern in aquatic systems. Widely used for the treatment of pain and inflammation, DCF is extensively consumed and consequently released into the environment through domestic and industrial wastewater.[53] Moreover, this compound exhibits a remarkable resistance to degradation in conventional wastewater treatment, resulting in its persistence in both freshwater and marine environments. Environmental concentrations of Diclofenac generally range from ng/L to a few µg/L, with traces also detected in drinking water at concentrations up to 10 ng/L.[54] Long-term exposure has been shown to have adverse effects on ecosystem health and has been the cause of severe visceral gout or kidney failure in humans, even at low concentrations.[55-57]

Another class of contaminants closely linked to the growing use of PPCPs are synthetic organic dyes, which are widely used in various sectors, such as textiles, leather, cosmetics, food and pharmaceuticals, for both human and animal use.[58] Due to rapid industrialisation and population growth, the textile sector produces about 7 x 10^5 tons/year of synthetic dyes. Almost 10% of these toxic dyes are released into the environment, as there are no regulations to prevent their discharge into watercourses.[59-61] In the textile industry, Rhodamine B (RhB) is a common water-soluble organic dye, used as fabric colouring. Even at very low concentrations (1.0 mg/L), it imparts vivid colour to water, but 140 µg/L is the limit for protection against harmful effects.[62, 63] RhB presence in aquatic ecosystems has been associated with environmental problems and potential health hazards for both humans and animals.[62] In fact, RhB is harmful if ingested and may cause soreness of the skin, eyes and respiratory tract, and may also affect photosynthesis and respiration rates.[61, 64]

Benzophenones, particularly Benzophenone-3 (BP3) and Benzophenone-4 (BP4), are widely used in personal care products like sunscreens, lotions, and cosmetics to minimize sun exposure and protect from UV rays.[36, 65] Although UV filters can protect

the skin, benzophenones show potential endocrine disrupting activity and genotoxicity, and are therefore classified as Group 2B of the AIRC Classification (possibly carcinogenic to humans).[66] BP3 and BP4 are commonly detected in various aquatic environments, including wastewater, swimming pools, rivers, lakes, with concentrations reaching up to 700 ng/L for BP3 and up to 13.3 µg/L for BP4 in specific cases.[66] Although these substances are widespread and can reach high concentrations in specific environments, there is a lack of research on their ecological impact, and they are not currently included in any environmental regulations or discharge standards.[66]

In addition to the pharmaceutical compounds mentioned above, central nervous system stimulants are also frequently detected in environmental compartments at relevant concentrations.[67] One notable example is caffeine (CAF), which is contained in many medications, drugs, cosmetics and beverages. In small doses, CAF stimulates the nervous system, while larger doses can lead to nerve cell depletion, and extremely high doses may even be fatal.[68] Moreover, even at low concentrations, CAF can negatively affect the metabolism of fish, amphibians, and reptiles.[69] Approximately 5% of CAF is not metabolized and enters the aquatic environment via wastewater, in addition to the disposal of food, beverages and medications containing caffeine. As a result, caffeine is frequently detected in drinking surface waters with concentrations ranging from 1 ng/L to 750 µg/L.[70]

Bisphenol A (BPA) is a plastic additive used primarily in the production of polycarbonate plastics and epoxy resins. Its widespread application includes products like water bottles, food containers, and thermal paper. Despite not being intentionally added as ingredient, BPA might be contained in certain PPCPs (i.e. toothpaste, soaps, cosmetics, and medical products) due to migration from plastic containers or component degradation.[71-74] BPA is classified as EDC and has the potential to affect human health, from prenatal development through adulthood, can exhibiting genotoxic, neurotoxic, cytotoxic, reproductive, and endocrine-disrupting effects.[73] Recent research has revealed the widespread presence of BPA in groundwater, categorizing it as a ubiquitous pollutant, frequently found in various water sources.[75, 76] Since groundwater is a vital source of fresh water for about one third of the world's population, this issue is of crucial relevance.[73, 77]

1.2.2 Per- and polyfluoroalkyl substances

Per- and polyfluoroalkyl substances (PFAS) are a wide class of synthetic chemicals characterised by carbon-fluorine bonds, which confer exceptional stability and resistance to degradation, making them highly persistent in the environment.[78] PFAS consist of an aliphatic carbon backbone of different length in which hydrogen atoms have been completely or partially replaced by fluorine atoms, and including a charged functional groups, commonly sulfonic (PFSA) or carboxylic (PFCA) acids (Figure 1.3).[79] These substances display outstanding chemical and thermal stability: they withstand acids, bases, heat, reducing and oxidizing degradation processes. Moreover, the hydrophobic chain and the hydrophilic functional group, attached at one end of the molecules, make PFAS amphiphilic compounds and excellent surfactants. Therefore in recent years they have been used in several applications, such as food packaging, non-stick cookware, paints, waterproof clothing, stain repellent, cosmetics and firefighting foams.[80-82]

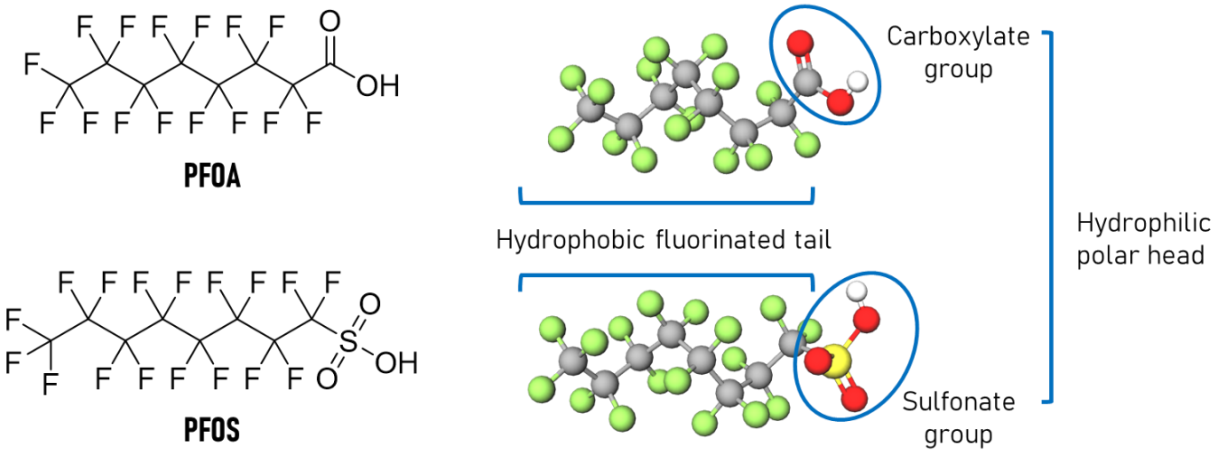

Figure 1.3 *Chemical structure and 3D molecules of two representative PFAS: perfluorooctanoic acid (PFOA) and perfluorooctane sulfonic acid (PFOS).*

The wide use of PFAS in industrial processes and consumer products has led to their release into the environment and their accumulation in water, including surface water, rainwater, drinking water, and groundwater.[83-89] Since water solubility increase with the decreasing carbon-chain length, “short-chain” PFAS (i.e. PFCA with eight or fewer carbons and PFSA with six or fewer carbons) are the most soluble and persistent in water and are therefore resistant to conventional water treatment methods.[90, 91] These chemicals are also commonly found in various consumer products, such as cosmetics,[92] food packaging,[93] agricultural food items[94] as well as toilet paper.[17]

The toxicity of PFAS is continually being evaluated, and they are categorized under Group 2B in the AIRC classification, indicating potential carcinogenicity in humans.[95] Studies have linked PFAS exposure to various acute and chronic human diseases, including thyroid disorders, immune toxicity, cardiovascular disease, activation of nuclear receptors, tissue-level changes, and potential impacts on embryonic development and motor functions. [96-98] The risk depends on factors like exposure source, concentration and frequency of exposure. There are many aspects to consider and it is not easy to give clear guidance due to the lack of reliable and reproducible data.

The ubiquity of these contaminants is of particular concern in the Veneto region of Italy, where groundwater has been found to be contaminated with PFAS from the activities of manufacturing plants that have been operating since 1960. Residents have been exposed to elevated levels of PFAS in their drinking water for over 60 years (up to 1.4 µg/L of PFOA, 0.6 µg/L of PFBA), resulting in an average tested concentration of 44.4 µg/L of PFOA in the blood of citizens.[99] More recently, PFAS have been ubiquitously found in drinking water of Milan, even though at non-risky concentrations (i.e. 0.07 ng/L). Higher concentrations have been found worldwide,[100] with groundwater concentrations up to 3.7 µg/L for PFCA and 25 µg/L PFSA.[100]

In recent years, significant measures have been taken globally to limit PFAS contamination and several countries have published administrative guidelines for level of PFAS in water.[82] The European Commission has declared PFAS emerging contaminants and PFOS priority hazardous substances. The revised European Drinking Water Directive2020/2184 sets the combined maximum concentration of all PFAS compounds at 0.5 µg/L in water. Alternatively, Member States have to monitor the total of 20 PFAS compounds, with a maximum limit of 0.1 µg/L. The EPA has also developed a policy to regulate PFAS in drinking water, which is regularly updated to reflect the latest science and health warnings. In fact, an update was published in 2024 that sets a zero maximum contaminant level target, a non-enforceable health-based target, for PFOA and PFOS. This reflects the latest scientific evidence showing that there is no level of exposure to these contaminants without risk of health effects, including some cancers.[101] Additionally, many countries have banned or phased out the use of certain PFAS in consumer products and industrial processes, promoting the development and use of safer alternatives. These actions aim to reduce PFAS release into the environment and mitigate their impact on human health and ecosystems.

1.2.3 Heavy metals

Although heavy metals are not classified as ECs, they are listed as potential environmental hazards due to their well-documented adverse effects on both human health and the ecosystem.[102] Heavy metals and metalloids are a group of elements characterized by their high density (> 4 g/cm^3) and atomic weight. Heavy metals commonly occurring as contaminants within domestic water supplies include copper (Cu), cadmium (Cd), zinc (Zn), lead (Pb), mercury (Hg), arsenic (As), chromium (Cr), iron (Fe), nickel (Ni) and manganese (Mn). Although heavy metals are naturally occurring elements found on Earth, most environmental contamination arises from anthropogenic activities such as mining and smelting operations, industrial production, as well as domestic and agricultural applications of metal-containing compounds.[103] These toxic elements persist in the environment as highly stable and non-degradable contaminants, leading to their bioaccumulation.[104, 105] It has been reported that approximately 40% of the lakes and rivers of the planet are polluted by heavy metals and several regions worldwide exhibit alarmingly high concentrations of metals in their drinking water.[105-108]

Acute heavy metal intoxication can damage central nervous function, the cardiovascular and gastrointestinal systems, lungs, kidneys, liver, endocrine glands and bones. The toxicity has been discussed since 1980, when the first attempt to limit their harmful effects was done (Table 1.1).[109] Their toxicity arises from the ability to bind protein site in blood, displacing the original essential metals and bioaccumulation on bodies, leading to harmful effect.[109] Moreover, heavy metals can lead to the occurrence of genetic abnormalities, physiological and morphological issues, hindered developmental progress, carcinogenic effects, and increased mortality rates.[110]

Table 1.1 *Comparison of EPA and UE drinking water guidelines for heavy metals.*

	Maximum concentration limit (µg/L)		
Heavy metals	EPA	UE DW directive	Effect
Cu	1300	2000	Liver damage, Wilson disease, insomnia
Cd	5	5	Kidney damage, renal disorder, human carcinogen
Zn	5000	3000	Gastrointestinal distress, depression, lethargy, neurological signs and increased thirst
Pb	15	10	Demage to fetal brain, disease of kidneys, nervous system
Hg	2	1	Rheumatoid arthritis, disease of kidneys, nervous system
As	10	10	Skin damage, vascular disease, visceral cancers
Cr	100	25	Lung and stomach cancer, increased risk lymphomas
Fe	300	200	Haemochromatosis
Ni	100	20	Dermatitis, nausea, chronic asthma, human carcinogen
Mn	50	50	Staining and discoloration

1.3 Conventional technologies for water treatments

Traditional drinking water treatment plants (DWTPs) play a crucial role in ensuring the safety and quality of drinking water. These plants often source water from rivers, lakes and other natural bodies, which are often contaminated due to inadequate wastewater management by industries, agricultural runoff and urbanisation.[111] As a result, these water sources can contain a variety of pollutants, including suspended solids, organic matter, bacteria and ECs. DWTPs utilize a multi-stage process divided into primary, secondary, and tertiary treatment steps, combining physical, chemical and biological processes, to ensure the safety and quality of potable water.[20, 112] The specific treatment steps employed may vary depending on the type and quality of the source water.

Primary treatment focuses on the removal of large particles and suspended solids and includes coagulation and flocculation.[113] Secondary treatment aims to remove dissolved and fine particulate matter that remains after primary treatment using chemical and biological processes. Tertiary treatment is the final purification stage, focusing on the

removal of residual contaminants and disinfection of the water. It includes several technologies such as filtration, oxidation processes (e.g. ozonation, UV treatment, chlorination, photocatalysis) and adsorption.

Although these traditional methods are generally effective in producing safe drinking water, they are not primarily designed to remove ECs.[114] The removal efficiencies of all treatment technologies significantly depend on the physicochemical properties (e.g., hydrophobicity, functionalities, charge, size, dissociation constant, and morphology) and nature of targeted ECs, but also on the employed treatment technologies, and operating/environmental conditions.[115] Tertiary treatment steps are generally the most effective at removing ECs from water (removal >90%), compared to primary (removal 20-50%) and secondary (removal 30-70%) treatments.[116, 117] Tertiary treatment includes advanced processes such as membrane filtration, advance adsorption techniques, biological treatments and advances oxidation processes (AOPs), which are the most appropriate and promising techniques to remove ECs.

Despite the advanced processes employed in tertiary treatment, several factors contribute to its occasional inability to completely remove ECs.[118] The diverse and complex chemical structures of ECs make it challenging for a single treatment method to be universally effective. Some advanced oxidation processes may not fully mineralize ECs, leading to the formation of by-products that can still be harmful.[115] Adsorption techniques, like activated carbon, can reach saturation, reducing their efficacy, and membrane filtration can suffer from fouling and selectivity issues.[112, 119] Consequently, DWTPs often fail to achieve satisfactory removal efficiency, allowing a portion of these contaminants to enter the environment, which raises concerns about human health.[120]

To further reduce the release of ECs and address these drawbacks, it is essential to enhance and upgrade water treatment technologies.[116, 121] Membrane filtration and adsorption are among the most promising methods for the removal of ECs.[112, 122] These technologies will be discussed individually in the following sections to explore their effectiveness and potential for widespread application.

1.3.1 Membrane filtration

Among physical treatment systems, membrane filtration has proven to be highly effective in the removal of many persistent ECs.[123] This method exploits filtration of water stream to isolate the contaminants, allowing water to flow through the membrane

while molecules are retained and concentrated at the membrane surface. Membrane filtration separates contaminants based on the membrane pore size, solution concentration, applied pressure, size and physio-chemical properties of contaminants.[124] Selectivity and efficiency of the membranes depend on the material they are composed of, which defined pore size, hydrophilicity and surface charge. Metal, ceramics, glasses, and most of all, polymers may be used to produce membrane for water treatment.[125]

Based on the pore size of the membrane, filtration can be classified as microfiltration (MF, pore size = 0.1–1 μm), ultrafiltration (UF, pore size = 0.01–0.1 μm), nanofiltration (NF, pore size = 0.001–0.01 μm), and reverse osmosis (RO, pore size = 0.1-1 nm) (Figure 1.4).[126] MF is primarily used to remove suspended solids, bacteria, and large pathogens. Although MF is effective for particulate removal, it is less capable of removing ECs.[127] UF can filter viruses, colloids, and larger organic molecules, making it more effective than MF for certain ECs. However, UF still struggles with removing smaller molecular contaminants and highly polar substances.[128] NF is effective in the removal of small organic molecules, bivalent ions, and certain pharmaceuticals, making it a promising technology for removing ECs. It can retain molecules in the size range of 200-1000 Daltons.[129] RO features the smallest pore sizes, making it the most advanced filtration method. RO operates by applying external pressure that is higher than the natural osmotic pressure to water (between 30 and 50 atm), forcing it through a semipermeable membrane that allows water molecules to pass while blocking most dissolved salts, organic molecules, and ECs.[116]

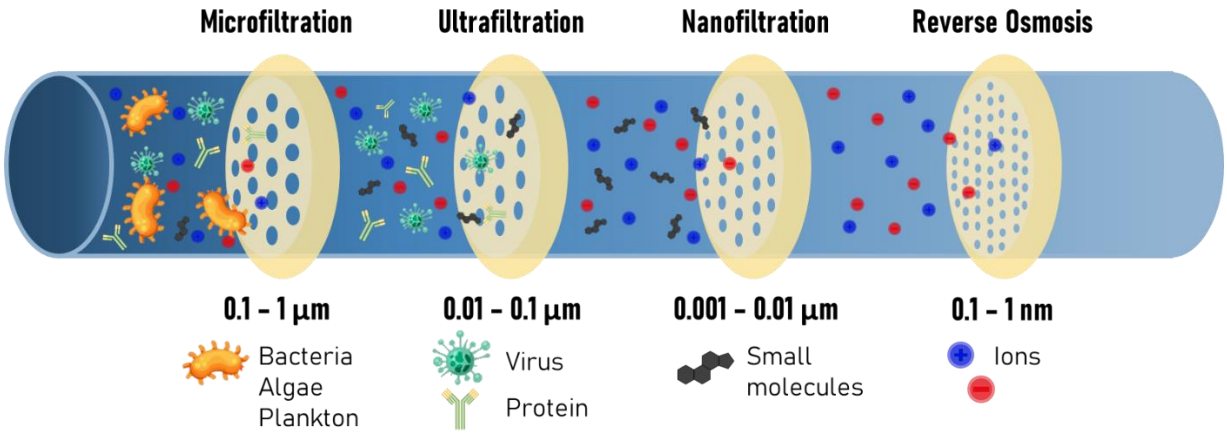

Figure 1.4 *Classification of filtration membranes based on pore size.*

In addition to the membrane's characteristics, also physio-chemical properties of ECs (size, concentration, functional group, charge, polarity) and operating conditions (pH, temperature and redox condition) influence the efficiency of treatment. Non-polar ECs are mainly removed due to their hydrophobic interactions with the membrane material or the biofilm layer, which can lead to adsorption and retention. On the other hand, polar ECs pass more easily through membranes, especially those with higher hydrophilicity, unless they are large enough to be retained by size exclusion, which can only be significantly achieved with NF and RO membranes. Charged polar ECs can interact electrostatically with the membrane surface and the removal efficiency depend on the charge characteristics of the contaminants and the membrane (Figure 1.5).[130]

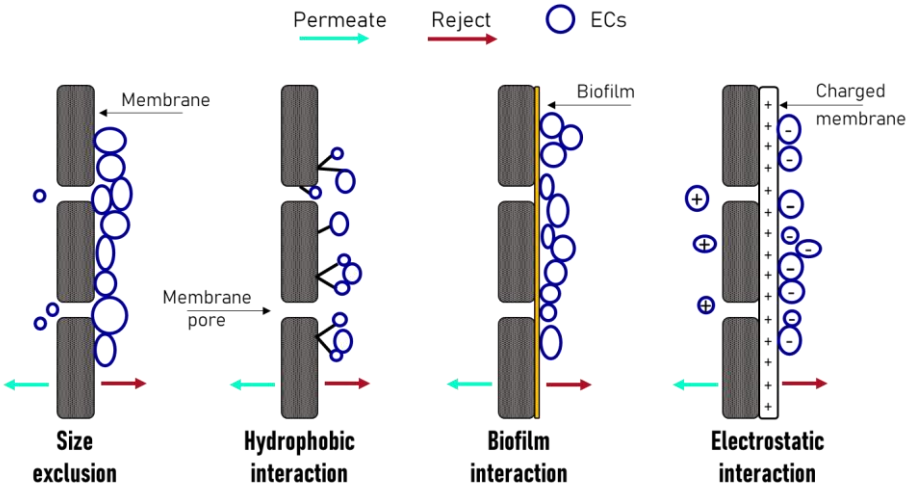

Figure 1.5 *Possible mechanism of ECs removal in membrane filtration.*

Membrane filtration has proven to be sustainable and highly effective strategies for removing ECs. In addition, the possibility of incorporating nanocomposites into the polymer matrix of membranes to enhance their selectivity towards ECs represent a promising frontier in materials innovation to further enhance water treatments.[115]

However, membrane filtration has some drawbacks that must be taken into account. Firstly, maintenance costs are generally higher than with conventional systems, partly due to the high energy consumption required, particularly for NF and OR.[131, 132] In addition, membrane fouling can significantly reduce filtration efficiency and increase operating costs by requiring frequent cleaning and replacement due to the accumulation of material (organic, inorganic, particulate, microbiological organisms) on the surface or within the pores of the membrane.[133] Finally, ECs removed from water are concentrated on the surface of the membrane and still require further treatment for disposal.

1.3.2 Adsorption

Adsorption is a surface phenomenon based on a phase change mechanism in which the contaminant (*adsorbate*) is removed from water through an adsorption on a solid phase (*sorbent*). This technique has been extensively explored for the removal of ECs [134] and it is one of the most efficient and reliable, due to its simplicity of use, flexibility and low operation cost. Additionally, it offers the possibility to recover and reuse the sorbent.[112]

The adsorption efficiency depends on several factors, including the properties of ECs (molecular size, polarity, functional group, K_{OW}, Kd, pKa), environmental conditions (pH, temperature, water matrix) and on the properties of the sorbent (particle size, surface area, pore diameter, mineral content).

A wide variety of sorbents are currently used to remove ECs from water sources, including activated carbons, zeolites, metal organic frameworks (MOFs), bio chars, carbon nanotubes and graphene.[126, 135] Among them all, activated carbon (AC) is the most extensively sorbent used, and it is considered as the benchmark, mainly due to his high porosity, large specific surface area and the high degree of surface interactions.[136] The adsorption efficiency is directly related to the characteristics of the sorbent, such as particle size, which distinguishes powdered activated carbon (PAC, ~44 μm) and granular activated carbon (GAC, 0.6-4 mm). On the other hand, AC can be classified by the pore size, as macroporous (≥ 50 nm), mesoporous (2–50 nm), and microporous (2−0.8 nm). Moreover, the source of the raw material for AC may led to different carbon structure of the final sorbent, determining a different adsorption capacity.[134]

AC treatments appear to be an attractive method for upgrading DWTPs, also due to the easy integration methods. PAC can be added directly in the activated sludge tank or as a post-treatment system, like a tertiary filter, but it is difficult to pack in fixed bed and has higher costs than GAC. On the other hand, GAC, which is hard and abrasion-resistant, can be incorporated into existing sand filters or as a replacement for the top layer of a tertiary filter. [137]

AC is a promising sorbent material but has some drawbacks to be addressed. The production of AC requires a high primary energy demand and is therefore not sustainable. GAC has a smaller CO_2 footprint if compared to PAC due to the possibility to be reactivated and reused again. However, the regeneration and reuse require high

energy to desorb the adsorbed compounds of higher molecular weight. Adsorption processes can be affected by the presence of natural organic matter (NOM) in water, which can compete with ECs for adsorption active sites. Furthermore, the saturated sorbent must be properly disposed and treated, for example, using a hot stream that becomes a hazardous waste itself. [138]

The cost of high quality sorbents, especially advanced materials such as MOFs and graphene, is still prohibitive for large-scale applications, but it is extensively studied at laboratory and pilot plant scale.[139-141] Those limitations requires ongoing research to develop cost-effective, high-capacity sorbents that can be efficiently regenerated and have minimal environmental impact at disposal.

Table 1.2 summarises the advantages and disadvantages of membrane filtration and adsorption reported in the previous sections.

Table 1.2 *Advantages and disadvantages of membrane filtration and adsorption.*

Technique	Advantages	Limitations
Membrane filtration	• Small space required • Commercial membrane • Fast and efficient process with high quality effluent	• High investment, maintenance and operating cost • High energy required • Membrane fouling
Adsorption	• Simple technique • Wide variety of sorbents to treat various contaminants • Numerous commercial sorbent	• High cost for sorbent regeneration • Regeneration not always effective • pH-dependant • Pre-post-treatment required

1.3.3 Point-of-use systems

As reported in the previous sections, current drinking water treatment plants are occasionally inefficient in the removal of ECs from water. This is not due to an intrinsic limit of this type of facility, but to the rapidity and complexity that characterized the insurgence of the ECs issue. DWTPs are huge and expansive structures and usually work non-stop to supply water to tens or hundreds thousands of people. Technological progress in DWTPs is extremely slow, mainly because the integration of research results requires time and money. This slow progress is insufficient to address the emergence of new ECs that have the potential to enter water bodies.

An effective way to address this issue are point-of-use (POU) systems, which have emerged as a solution to allow people to improve the quality of drinking water at home through simple, safe and low-cost treatment methods.[142] POU systems are small and relatively cheap device which can be installed on the water supply lines directly on the tap or dispenser, performing purification *in situ* where water is ultimately consumed. They are installed to adjust water taste, hardness and also to remove some traces of persistent contaminants to conventional drinking water treatment technologies.[143] Their market is significantly increased in the recent years (>$20 billion per year), due to their simplicity and customization capacities.[142, 144] Similar to DWTPs, POU systems employ a series of treatments, including activated carbon, membrane filtration units, UV purifiers and ceramic filters. [145-147]

The high spare parts turnover, high sales volumes, small size and low costs greatly facilitate the implementation of new technologies in POU systems. This market is therefore an optimal environment for research on water purification and for the transfer of new technologies from small scales.

1.4 Nanomaterials in water remediation

In the past decades, nanomaterials have gained considerable attention due to their unique physical and chemical properties, which are suitable for their potential applications in water treatment.[148 149] These materials, characterised by at least one dimension in the range 1-100 nm, offer a high surface area-to-volume ratio, enhanced reactivity, and the ability to tailor surface properties for specific interactions with contaminants. Nanomaterials offer versatile solutions for a wide range of environmental applications and can be synthesized through top-down or bottom-up approaches using a variety of methods, including chemical, physical and mechanical processes.[149 150]

Nanotechnology has made significant progress, finding many applications in various fields of science and technology, including catalysis, functional coatings, nanoelectronics, sensors [151] and mainly in adsorption.[138, 152] Several types of nanomaterials, including metal oxides nanoparticles (TiO_2, ZnO, CdS), carbon-based nanomaterials, metal-organic frameworks and polymer-based nanocomposites, have been studied to remove contaminants from water. Ceramic nanomaterials and 2D crystalline materials, like borophene, germanene, and 2D silica, are also making significant contributions in various applications.[150]

Nanomaterials have proven effective in the purification of air and water, enhancing processes like filtration, adsorption, and oxidation.[153] Their high surface area, together with their porosity, provides numerous active sites to interact with different chemical species, making them excellent sorbents. Among all nanomaterials, carbon-based sorbents (i.e. activated carbon, carbon nanotubes, fullerenes and graphene), stand out for their high adsorption capacity and remarkable thermal stability. [153]

1.4.1 Graphene related materials

Graphene related materials (GRM) have received great attention in past years due to their exceptional electronic, optical, thermal, morphological and mechanical properties. As a result, GRM have been applied in a wide range of scientific and technological fields, including energy storage, catalysis, sensing, drug delivery, optoelectronics and environmental remediation.[154]

Graphene is an allotrope of carbon consisting of a single layer of sp^2 hybridized atom arranged in a honeycomb lattice. The honeycomb structure is the building block for other allotropes classified as GRM (Figure 1.6), including 0D materials (such as graphene quantum dots and fullerenes), 1D materials (carbon nanotubes) and 3D materials (graphite). Even more interesting are graphene 2D derivatives, in which the nanosheets structure is retained. For example, graphene nanoplatelets (GNP) are nanoparticles made of stacks of graphene nanosheets with thickness in the range 1-15 nm and radius up to hundreds of microns, they may be treated as nanoparticles in several application.[155] Another example of 2D derivative is defective graphene, which maintained the same structure of graphene, but its surface is scattered with holes and defects, that modify its conductivity and its adsorption properties.[156]

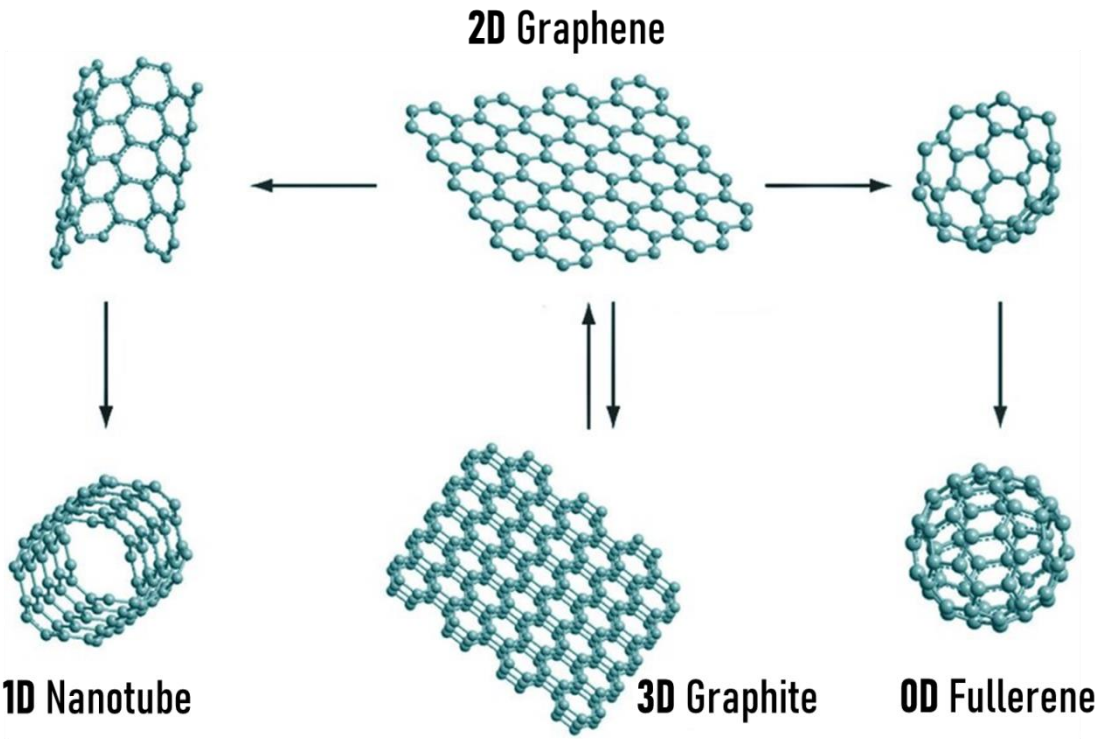

Figure 1.6 *Structure of 2D graphene and other carbon allotrope: 0D fullerene, 1D nanotube and 3D graphite.*

In the field of water treatment, the above-mentioned GRM have shown attractive properties. However, most of them are highly hydrophobic and therefore tend to aggregate when dispersed in water, decreasing the active surface area exploitable for the adsorption of contaminants. This leads to the most important GRM for the present work, which is graphene oxide.

Graphene oxide (GO) presents the same 2D nanosheets structure of graphene, but several oxygenated groups, such as epoxy, hydroxyl, carbonyl and carboxyl groups, are present on the surface (Figure 1.7).[157] The oxidation degree of the material is expressed by the O/C ratio and varies according to the synthesis method, usually ranging between 0.2 and 0.45.[158] Epoxides and hydroxides are the most abundant oxygen groups and are found on the surface, while carbonyl and carboxyl groups are located on the edges.[159]

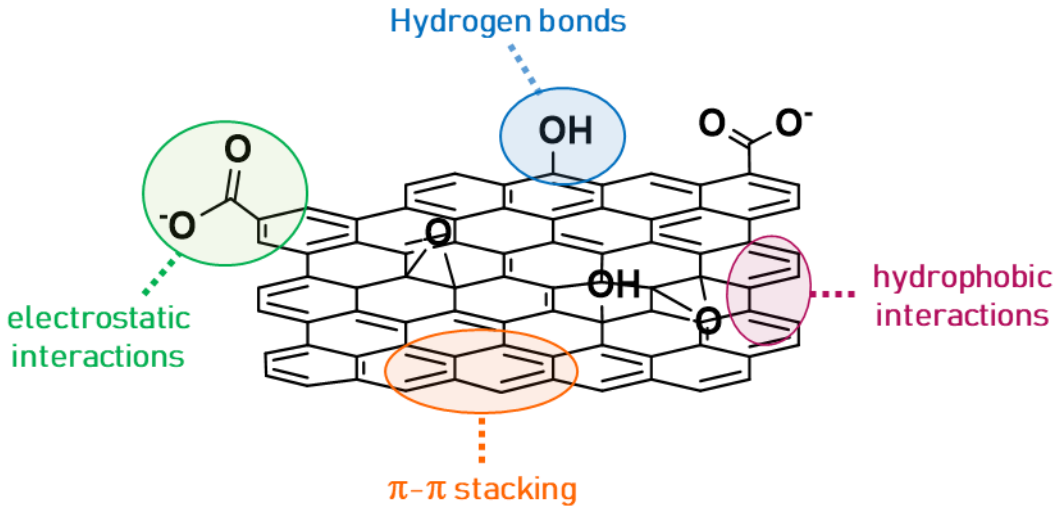

Figure 1.7 *Representative chemical structure of graphene oxide and possible interactions between GO and contaminants.*

The presence of oxygenated groups makes GO dispersible in various polar solvents, including water, making it very attractive as a sorbent for water treatment. In addition, oxygen groups are crucial because they broaden the possible interaction between GO and contaminants (Figure 1.7). Indeed, these oxygen functionalities introduce a negative charge to the GO surface, enabling electrostatic interactions with cationic organic contaminants. GO also act as a potential sorbent for metal ion complexation through both electrostatic and coordinate bonding approaches. [160] Hydrogen bonding can occur through the oxygen groups, covalently bonded to GO, and hydrogen atoms of contaminant, bonded to a highly electro-negative atom. In aqueous media, hydrophobic molecules can interact with non-polar regions of GO. Finally, GO sp^2 regions enable π-π interactions with aromatic organic pollutants, resulting in noncovalent bonds with contaminants possessing an extended π core and a compatible geometry.[161]

Moreover, the functional groups present on GO provide reactive sites for further functionalization, allowing a broad range of modifications and enhancing its selectivity toward contaminants (Figure 1.8).[162] The chemistry of GO is mainly inspired by the classical organic reactions of epoxy, hydroxyl and carboxyl groups, as well as C=C bonds. Carboxyl groups on the edges of GO can react with amines via amide bond formation or with alcohols through esterification. However, given the low presence of carboxyl groups, these derivatization strategies lead to low levels of functionalisation. Due to the abundance of epoxide and hydroxyl moieties on the surface of GO, most of the functionalization strategies are aimed at these functional groups. Although hydroxyl

groups are not particularly reactive nucleophiles or electrophiles, they can still participate in many chemical reactions. The most common method to modify GO through the hydroxyl functions is silanization, which involves the reaction with organosilanes to form covalent Si–O bonds.[163] The epoxy can be functionalized through a ring opening reaction by a nucleophile such as amines, thiols and the azide anion (N_3^-).[164, 165] Nucleophilic epoxide ring-opening is one of the most widely used methods for GO functionalisation because it is simple to perform and occurs under mild and environmentally friendly conditions (in water and without catalysts).[159]

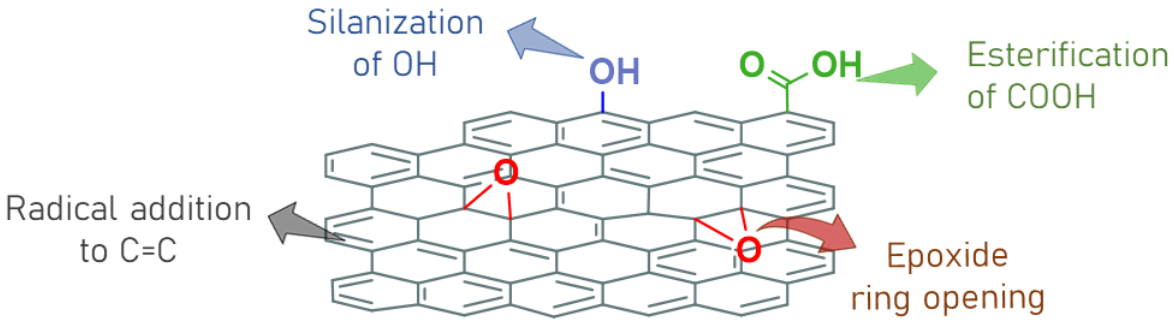

Figure 1.8 *Overview of possible chemical reaction that can occur through the oxygen groups.*

Despite all the above-mentioned advantages, the oxygenated groups on GO can also lead to disadvantages such as electrical insulation. Nevertheless, the conductivity of GO can be partially restored by chemically reducing it with agents like hydrazine or ascorbic acid. The obtained material, reduced graphene oxide (rGO), recovers a conjugated structure and shares properties with pristine graphene, differing for the presence of some residual functional oxygenated groups on the surface. By regulating the quantity of retained functional groups, the electrical performance and solubility of rGO can be easily controlled.[166]

1.4.2 Graphene-polymer composites for water treatment

As seen in the previous section, GRM, particularly GO, are excellent candidates as sorbents for water treatment. In recent years, numerous publications have demonstrated the high capacity and selectivity of GRM toward different classes of contaminants, including ECs.[167, 168] For further insight, Table 1.3 shows the adsorption properties of GO towards some ECs of concern compared to those of GAC, the industry benchmark for adsorption. In this table, absorption values are expressed in terms of maximum

absorption capacity (Qm), a quantity obtained from absorption isotherm studies that expresses the amount of contaminant adsorbed per weight of sorbent.

Table 1.3 *Maximum adsorption capacity (Qm) expressed in mg/g of GO and GAC toward RhB,[169] MB,[170] OFLOX[170] and Pb.[171, 172]*

Sorbent	RhB	MB	OFLOX	Pb
GO	439	428	204	555
GAC	191	187	95	30

Predictably, GRM perform most effectively when dispersed in water as nanosheets, maximizing their surface area and enhancing their adsorption efficiency. However, when used in dispersion, these promising nanomaterials have one significant disadvantage: the challenge of separation once the water has been treated. On a laboratory scale, GRM are typically recovered by centrifugation, a method that is impractical on an industrial scale, or by filtration, which requires an additional step and can lead to clogging of the filtration modules.[173] The difficulty in efficiently separating GRM from treated water not only complicates the treatment process, but also poses potential environmental and operational challenges due to the risk of secondary contamination.[174]

To overcome this issue, GO nanosheets can be processed into 3D macrostructures, with different geometries such as sponges, membranes and fibers. These highly porous structures are being developed for applications where specific surface area is a critical parameter, such as water and air treatment, supercapacitors, batteries and sensors.[175]

Another viable and widely studied approach is the embedding of GO within polymer matrix to obtain graphene-polymer composites.[176] They combined the advantages of polymers and graphene, providing a promising adsorbent that can improve the fouling resistance, the selectivity/permeability, the chlorine resistance, and the mechanical stress.[177] The polymers used in these composites were mainly classified according to their source. They were divided into biopolymers and synthetic polymers.

1.4.2.1 Graphene-biopolymer composites

Biopolymers can be classified into polymers derived from natural sources, such as sodium alginate[178] (obtained from brown seaweed) and chitosan[179] (obtained from insects, algae, fungi, molluscs and crustaceans), or biodegradable polymers, such as

poly(ε-caprolactone)[180] (PCL) and polylactic acid[181] (PLA). GRM and biopolymers can be combined to create different composite structures, including hydrogel and aerogel beads, sponges and membranes. The effectiveness of these composites in treating water from various contaminants has been demonstrated in several publications. For example, Zhang et al. have reported the preparation of free-standing, low-density chitosan-GO sponges that are able to effectively remove Co^{2+} (224.8 mg/g) and Ni^{2+} (423.7 mg/g), and in addition they have also demonstrated the possibility of regenerating and reusing the composites.[182] De Luna et al. investigated the effect of gluteraldehyde as a cross-linker for the formation of chitosan-GO composites, and then studied their adsorption properties towards dyes. The addition of GO enabled the composites to adsorb not only anionic but also cationic dyes, increasing the adsorption capacity of methylene blue from 4 to 169 mg/g.[183] Chitosan was also used by Kovtun et al. to form two types of GO-doped 3D chitosan-gelatin aerogels with GO nanosheets embedded in the bulk or deposited on the surface of the sponge. The adsorption capacity of both systems was tested on two pharmaceuticals (ofloxacin and ciprofloxacin) and a heavy metal (Pb^{2+}). For Pb^{2+}, embedded GO aerogels showed higher adsorption capacities than GO-coated ones (11.1 *vs.* 1.5 mg/g), while for organic contaminants, only minor differences were found between the two approaches, with an adsorption capacity between 5 and 8 mg/g. However, no adsorption was found for chitosan-gelatin without GO neither towards pharmaceuticals nor heavy metals, showing that even small amounts of GO (2% w/w) can significantly change the adsorption properties of materials.[184]

GRM and sodium alginate, a low-cost biopolymer with high processability, have also been investigated for the realisation of porous aerogels and hydrogels for adsorption of contaminants.[185-188] It has already been reported that encapsulating GO in an alginate matrix makes the resulting composite material more porous and introduces stabilising C-O bonds between GO and alginate.[189] The adsorption of such composites toward heavy metals, such as Cd^{2+}, Cu^{2+} and Pb^{2+}, and ciprofloxacin from aqueous solutions by alginate-graphene beads has been demonstrated.[190-192] Tuning the amount of GO as well as GO pre-functionalization was tested to increase the adsorption capacity. In this context, M. Majdoub et al. showed that hexamethylenediamine (HMDA) covalent binding on GO led to remarkably high adsorption rates for Pb^{2+}, Cu^{2+} and Cd^{2+}, with only 15 wt% of GO-HMDA incorporated into the alginate beads, in both single contaminant or mixed

solutions in tap water.[191] Similarly, amino post-functionalization of the alginate shell increased its maximum adsorption capacity (expressed in mg/g) by 130% and 182% towards Cu^{2+} and ciprofloxacin, respectively.[193]

1.4.2.2 Graphene-synthetic polymer composites

Composite materials of GRM with synthetic polymers have been widely studied.[194-196] Their wide range of applications relies on the structure versatility of such membranes, with morphology and porosity that can be tuned by the choice of several parameters including processing solvent/non solvent, coagulation temperature, casting solution composition and humidity.[197, 198] With the rapid development of membrane technology for various applications, including POU systems for water purification,[199] a wide range of polymers, such as polyvinylidene fluoride (PVDF),[200] polypropylene (PP),[201] polystyrene (PS),[202] polysulfone (PSU),[203] polyethersulfone (PES)[204] have been used as matrices and GRM as dopant nanomaterials.[195] These membranes, in both flat and hollow fibre structures, enhance the capabilities of GRM in desalination and ECs adsorption combining the microfiltration (MF) or ultrafiltration (UF) properties of polymer membranes.[205] For example, Kafiah et al. proposed planar microfiltration membranes made of PP and PVDF with a monolayer of graphene, transferred by chemical vapour deposition followed by interfacial polymerization to seal surface defects. The composite membranes were tested in water desalination and the PVDF-graphene membrane blocked 67% of KCl, while PP-graphene membrane reached 84% of ion blockage.[201] Badrinezhad et al. demonstrated methylene blue adsorption from water with removal efficiency of about 80% for PSU planar membranes doped with 0.75% w/w of GO and desorption of about 40% which was lower that than observed in graphene free membranes.[206] Khaliha et al. proposed PSU-GO hollow fibers membranes with simultaneous adsorption and ultrafiltration capabilities and the composites were prepared by phase inversion extrusion in a customized semi-industrial plant. The PSU hollow fibers membranes doped with 3.5% w/w of GO showed same ultrafiltration capability of PSU standard filters and they also showed high removal capabilities towards heavy metals (Pb^{2+}, Cu^{2+} and Cr^{3+}) and PFAS from tap water.[207]

1.5 References

1. Shah, A.; Arjunan, A.; Baroutaji, A.; Zakharova, J., A review of physicochemical and biological contaminants in drinking water and their impacts on human health. *Water Science and Engineering* **2023,** *16* (4), 333-344.
2. Rathi, B.; Kumar, P.; Vo, D.-V., Critical review on hazardous pollutants in water environment: Occurrence, monitoring, fate, removal technologies and risk assessment. *Sci. Total Environ.* **2021,** *797*, 149134.
3. Sharma, S.; Bhattacharya, A., Drinking water contamination and treatment techniques. *Appl. Water Sci.* **2017,** *7* (3), 1043-1067.
4. Altalhi, T.; Alrooqi, A., *Handbook of Water Pollution*. John Wiley & Sons: 2024.
5. Akhtar, N.; Syakir Ishak, M. I.; Bhawani, S. A.; Umar, K., Various Natural and Anthropogenic Factors Responsible for Water Quality Degradation: A Review. **2021,** *13* (19), 2660.
6. Konapala, G.; Mishra, A. K.; Wada, Y.; Mann, M. E., Climate change will affect global water availability through compounding changes in seasonal precipitation and evaporation. *Nature Communications* **2020,** *11* (1), 3044.
7. https://sdgs.un.org/goals.
8. https://eur-lex.europa.eu/legal-content/EN/TXT/?uri=CELEX%3A32020L2184.
9. https://environment.ec.europa.eu/publications/implementing-decision-drinking-water-directive-watch-list_en.
10. https://eur-lex.europa.eu/legal-content/EN/ALL/?uri=CELEX%3A31998L0083.
11. Togola, A.; Lopez, B.; Ollivier, P.; Baran, N.; Ghestem, J. P., *Pharmaceuticals and PCPs in groundwater: Results from French National screening*. 2014.
12. Petrie, B.; Barden, R.; Kasprzyk-Hordern, B., A review on emerging contaminants in wastewaters and the environment: Current knowledge, understudied areas and recommendations for future monitoring. *Water Res.* **2015,** *72*, 3-27.
13. Tröger, R.; Ren, H.; Yin, D.; Postigo, C.; Nguyen, P. D.; Baduel, C.; Golovko, O.; Been, F.; Joerss, H.; Boleda, M. R.; Polesello, S.; Roncoroni, M.; Taniyasu, S.; Menger, F.; Ahrens, L.; Yin Lai, F.; Wiberg, K., What's in the water? – Target and suspect screening of contaminants of emerging concern in raw water and drinking water from Europe and Asia. *Water Res.* **2021,** *198*, 117099.
14. Rizzo, L.; Malato, S.; Antakyali, D.; Beretsou, V. G.; Đolić, M. B.; Gernjak, W.; Heath, E.; Ivancev-Tumbas, I.; Karaolia, P.; Lado Ribeiro, A. R.; Mascolo, G.; McArdell, C. S.; Schaar, H.; Silva, A. M. T.; Fatta-Kassinos, D., Consolidated vs new advanced treatment methods for the removal of contaminants of emerging concern from urban wastewater. *Sci. Total Environ.* **2019,** *655*, 986-1008.
15. Kumar, L.; Deitch, M. J.; Tunio, I. A.; Kumar, A.; Memon, S. A.; Williams, L.; Tagar, U.; Kumari, R.; Basheer, S., Case Studies in Chemical and Environmental Engineering.
16. Puri, M.; Gandhi, K.; Kumar, M. S., Emerging environmental contaminants: A global perspective on policies and regulations. *J. Environ. Manage.* **2023,** *332*, 117344.
17. Thompson, J. T.; Chen, B.; Bowden, J. A.; Townsend, T. G., Per- and Polyfluoroalkyl Substances in Toilet Paper and the Impact on Wastewater Systems. *Env. Sci. Technol. Lett.* **2023,** *10* (3), 234-239.
18. Riva, F.; Castiglioni, S.; Fattore, E.; Manenti, A.; Davoli, E.; Zuccato, E. J. I. j. o. h.; health, e., Monitoring emerging contaminants in the drinking water of Milan and assessment of the human risk. **2018,** *221* (3), 451-457.
19. https://nepis.epa.gov/Exe/ZyPURL.cgi?Dockey=P100LTG6.txt.

20. Tran, N. H.; Reinhard, M.; Gin, K. Y.-H., Occurrence and fate of emerging contaminants in municipal wastewater treatment plants from different geographical regions-a review. *Water Res.* **2018,** *133*, 182-207.
21. Khan, S.; Naushad, M.; Govarthanan, M.; Iqbal, J.; Alfadul, S. M., Emerging contaminants of high concern for the environment: Current trends and future research. *Environ. Res.* **2022,** *207*, 112609.
22. Luo, Y.; Guo, W.; Ngo, H. H.; Nghiem, L. D.; Hai, F. I.; Zhang, J.; Liang, S.; Wang, X. C., A review on the occurrence of micropollutants in the aquatic environment and their fate and removal during wastewater treatment. *Sci. Total Environ.* **2014,** *473-474*, 619-641.
23. Morin-Crini, N.; Lichtfouse, E.; Liu, G.; Balaram, V.; Ribeiro, A. R. L.; Lu, Z.; Stock, F.; Carmona, E.; Teixeira, M. R.; Picos-Corrales, L. A.; Moreno-Piraján, J. C.; Giraldo, L.; Li, C.; Pandey, A.; Hocquet, D.; Torri, G.; Crini, G., Worldwide cases of water pollution by emerging contaminants: a review. *Environ. Chem. Lett.* **2022,** *20* (4), 2311-2338.
24. Caporale, N.; Leemans, M.; Birgersson, L.; Germain, P.-L.; Cheroni, C.; Borbély, G.; Engdahl, E.; Lindh, C.; Bressan, R. B.; Cavallo, F. J. S., From cohorts to molecules: Adverse impacts of endocrine disrupting mixtures. *Science (New York, N.Y.)* **2022,** *375* (6582), eabe8244.
25. Riva, F.; Zuccato, E.; Davoli, E.; Fattore, E.; Castiglioni, S., Risk assessment of a mixture of emerging contaminants in surface water in a highly urbanized area in Italy. *J. Hazard. Mater.* **2019,** *361*, 103-110.
26. Giglioli, S.; Colombo, L.; Azzellino, A., Cluster and multivariate analysis to study the diffuse contamination of emerging per- and polyfluoroalkyl substances (PFAS) in the Veneto Region plain (North-eastern Italy). *Chemosphere* **2023,** *319*, 137916.
27. Du, M.; Zheng, M.; Liu, A.; Wang, L.; Pan, X.; Liu, J.; Ran, X. J. S. o. t. T. E., Effects of emerging contaminants and heavy metals on variation in bacterial communities in estuarine sediments. **2022,** *832*, 155118.
28. Zamora-Ledezma, C.; Negrete-Bolagay, D.; Figueroa, F.; Zamora-Ledezma, E.; Ni, M.; Alexis, F.; Guerrero, V. H. J. E. T.; Innovation, Heavy metal water pollution: A fresh look about hazards, novel and conventional remediation methods. **2021,** *22*, 101504.
29. Gupta, G.; Khan, J.; Singh, N. J. M. T. P., Application and efficacy of low-cost adsorbents for metal removal from contaminated water: A review. **2021,** *43*, 2958-2964.
30. Triassi, M.; Cerino, P.; Montuori, P.; Pizzolante, A.; Trama, U.; Nicodemo, F.; D'Auria, J. L.; De Vita, S.; De Rosa, E.; Limone, A., Heavy Metals in Groundwater of Southern Italy: Occurrence and Potential Adverse Effects on the Environment and Human Health. **2023,** *20* (3), 1693.
31. Dey, S.; Bano, F.; Malik, A., 1 - Pharmaceuticals and personal care product (PPCP) contamination—a global discharge inventory. In *Pharmaceuticals and Personal Care Products: Waste Management and Treatment Technology*, Prasad, M. N. V.; Vithanage, M.; Kapley, A., Eds. Butterworth-Heinemann: 2019; pp 1-26.
32. Nikolaou, A.; Meric, S.; Fatta, D., Occurrence patterns of pharmaceuticals in water and wastewater environments. *Anal. Bioanal. Chem.* **2007,** *387* (4), 1225-1234.
33. Samal, K.; Mahapatra, S.; Hibzur Ali, M., Pharmaceutical wastewater as Emerging Contaminants (EC): Treatment technologies, impact on environment and human health. *Energy Nexus* **2022,** *6*, 100076.
34. Lonappan, L.; Brar, S. K.; Das, R. K.; Verma, M.; Surampalli, R. Y., Diclofenac and its transformation products: Environmental occurrence and toxicity - A review. *Environ. Int.* **2016,** *96*, 127-138.

35. Clara, M.; Strenn, B.; Kreuzinger, N., Carbamazepine as a possible anthropogenic marker in the aquatic environment: investigations on the behaviour of Carbamazepine in wastewater treatment and during groundwater infiltration. *Water Res.* **2004,** *38* (4), 947-954.
36. Chaturvedi, P.; Shukla, P.; Giri, B. S.; Chowdhary, P.; Chandra, R.; Gupta, P.; Pandey, A., Prevalence and hazardous impact of pharmaceutical and personal care products and antibiotics in environment: A review on emerging contaminants. *Environ. Res.* **2021,** *194*, 110664.
37. de Ilurdoz, M. S.; Sadhwani, J. J.; Reboso, J. V., Antibiotic removal processes from water & wastewater for the protection of the aquatic environment - a review. *J. Water Process Eng.* **2022,** *45*, 102474.
38. Kovalakova, P.; Cizmas, L.; McDonald, T. J.; Marsalek, B.; Feng, M.; Sharma, V. K., Occurrence and toxicity of antibiotics in the aquatic environment: A review. *Chemosphere* **2020,** *251*, 126351.
39. Hernández-Tenorio, R.; González-Juárez, E.; Guzmán-Mar, J. L.; Hinojosa-Reyes, L.; Hernández-Ramírez, A., Review of occurrence of pharmaceuticals worldwide for estimating concentration ranges in aquatic environments at the end of the last decade. *Journal of Hazardous Materials Advances* **2022,** *8*, 100172.
40. Oliveira, M. G.; Spaolonzi, M. P.; Duarte, E. D. V.; Costa, H. P. S.; da Silva, M. G. C.; Vieira, M. G. A., Adsorption kinetics of ciprofloxacin and ofloxacin by green-modified carbon nanotubes. *Environ. Res.* **2023,** *233*, 116503.
41. Kumar, M.; Ram, B.; Honda, R.; Poopipattana, C.; Canh, V. D.; Chaminda, T.; Furumai, H., Concurrence of antibiotic resistant bacteria (ARB), viruses, pharmaceuticals and personal care products (PPCPs) in ambient waters of Guwahati, India: Urban vulnerability and resilience perspective. *Sci. Total Environ.* **2019,** *693*, 133640.
42. Almeida, Â.; Soares, A. M. V. M.; Esteves, V. I.; Freitas, R., Occurrence of the antiepileptic carbamazepine in water and bivalves from marine environments: A review. *Environ. Toxicol. Pharmacol.* **2021,** *86*, 103661.
43. Zhang, Y.; Geißen, S.-U.; Gal, C., Carbamazepine and diclofenac: Removal in wastewater treatment plants and occurrence in water bodies. *Chemosphere* **2008,** *73* (8), 1151-1161.
44. Ambrósio, A. F.; Soares-da-Silva, P.; Carvalho, C. M.; Carvalho, A. P., Mechanisms of Action of Carbamazepine and Its Derivatives, Oxcarbazepine, BIA 2-093, and BIA 2-024. *Neurochem. Res.* **2002,** *27* (1), 121-130.
45. Verlicchi, P.; Al Aukidy, M.; Zambello, E., Occurrence of pharmaceutical compounds in urban wastewater: Removal, mass load and environmental risk after a secondary treatment—A review. *Sci. Total Environ.* **2012,** *429*, 123-155.
46. Ebrahimzadeh, S.; Castiglioni, S.; Riva, F.; Zuccato, E.; Azzellino, A., Carbamazepine Levels Related to the Demographic Indicators in Groundwater of Densely Populated Area. **2021,** *13* (18), 2539.
47. Riva, F.; Castiglioni, S.; Fattore, E.; Manenti, A.; Davoli, E.; Zuccato, E., Monitoring emerging contaminants in the drinking water of Milan and assessment of the human risk. *Int. J. Hyg. Environ. Health* **2018,** *221* (3), 451-457.
48. Biel-Maeso, M.; Baena-Nogueras, R. M.; Corada-Fernández, C.; Lara-Martín, P. A., Occurrence, distribution and environmental risk of pharmaceutically active compounds (PhACs) in coastal and ocean waters from the Gulf of Cadiz (SW Spain). *Sci. Total Environ.* **2018,** *612*, 649-659.

49. Décima, M. A.; Marzeddu, S.; Barchiesi, M.; Di Marcantonio, C.; Chiavola, A.; Boni, M. R., A Review on the Removal of Carbamazepine from Aqueous Solution by Using Activated Carbon and Biochar. **2021,** *13* (21), 11760.
50. Hai, F. I.; Yang, S.; Asif, M. B.; Sencadas, V.; Shawkat, S.; Sanderson-Smith, M.; Gorman, J.; Xu, Z.-Q.; Yamamoto, K., Carbamazepine as a Possible Anthropogenic Marker in Water: Occurrences, Toxicological Effects, Regulations and Removal by Wastewater Treatment Technologies. **2018,** *10* (2), 107.
51. Santos, L. H. M. L. M.; Araújo, A. N.; Fachini, A.; Pena, A.; Delerue-Matos, C.; Montenegro, M. C. B. S. M., Ecotoxicological aspects related to the presence of pharmaceuticals in the aquatic environment. *J. Hazard. Mater.* **2010,** *175* (1), 45-95.
52. Webb, S.; Ternes, T.; Gibert, M.; Olejniczak, K., Indirect human exposure to pharmaceuticals via drinking water. *Toxicol. Lett.* **2003,** *142* (3), 157-167.
53. Shamsudin, M. S.; Azha, S. F.; Ismail, S., A review of diclofenac occurrences, toxicology, and potential adsorption of clay-based materials with surfactant modifier. *J. Environ. Chem. Eng.* **2022,** *10* (3), 107541.
54. Rigobello, E. S.; Dantas, A. D. B.; Di Bernardo, L.; Vieira, E. M., Removal of diclofenac by conventional drinking water treatment processes and granular activated carbon filtration. *Chemosphere* **2013,** *92* (2), 184-191.
55. Parida, V. K.; Saidulu, D.; Majumder, A.; Srivastava, A.; Gupta, B.; Gupta, A. K., Emerging contaminants in wastewater: A critical review on occurrence, existing legislations, risk assessment, and sustainable treatment alternatives. *J. Environ. Chem. Eng.* **2021,** *9* (5), 105966.
56. Patel, M.; Kumar, R.; Kishor, K.; Mlsna, T.; Pittman, C. U., Jr.; Mohan, D., Pharmaceuticals of Emerging Concern in Aquatic Systems: Chemistry, Occurrence, Effects, and Removal Methods. *Chem. Rev.* **2019,** *119* (6), 3510-3673.
57. Xiong, T.; Yuan, X.; Wang, H.; Wu, Z.; Jiang, L.; Leng, L.; Xi, K.; Cao, X.; Zeng, G., Highly efficient removal of diclofenac sodium from medical wastewater by Mg/Al layered double hydroxide-poly(m-phenylenediamine) composite. *Chem. Eng. J.* **2019,** *366*, 83-91.
58. Sharma, P.; Kaur, H.; Sharma, M.; Sahore, V., A review on applicability of naturally available adsorbents for the removal of hazardous dyes from aqueous waste. *Environ. Monit. Assess.* **2011,** *183* (1), 151-195.
59. Singh, S.; Parveen, N.; Gupta, H., Adsorptive decontamination of rhodamine-B from water using banana peel powder: A biosorbent. *Environmental Technology & Innovation* **2018,** *12*, 189-195.
60. Rathi, B. S.; Kumar, P. S.; Vo, D.-V. N., Critical review on hazardous pollutants in water environment: Occurrence, monitoring, fate, removal technologies and risk assessment. *Sci. Total Environ.* **2021,** *797*, 149134.
61. Al-Buriahi, A. K.; Al-Gheethi, A. A.; Senthil Kumar, P.; Radin Mohamed, R. M. S.; Yusof, H.; Alshalif, A. F.; Khalifa, N. A., Elimination of rhodamine B from textile wastewater using nanoparticle photocatalysts: A review for sustainable approaches. *Chemosphere* **2022,** *287*, 132162.
62. Yusuf, T. L.; Orimolade, B. O.; Masekela, D.; Mamba, B.; Mabuba, N., The application of photoelectrocatalysis in the degradation of rhodamine B in aqueous solutions: a review. *RSC Advances* **2022,** *12* (40), 26176-26191.
63. Sharma, J.; Sharma, S.; Bhatt, U.; Soni, V., Toxic effects of Rhodamine B on antioxidant system and photosynthesis of Hydrilla verticillata. *Journal of Hazardous Materials Letters* **2022,** *3*, 100069.

64. Imran, M.; Crowley, D. E.; Khalid, A.; Hussain, S.; Mumtaz, M. W.; Arshad, M., Microbial biotechnology for decolorization of textile wastewaters. *Reviews in Environmental Science and Bio/Technology* **2015,** *14* (1), 73-92.
65. Kim, S.; Choi, K., Occurrences, toxicities, and ecological risks of benzophenone-3, a common component of organic sunscreen products: A mini-review. *Environ. Int.* **2014,** *70*, 143-157.
66. Esperanza, M.; Seoane, M.; Rioboo, C.; Herrero, C.; Cid, Á., Differential toxicity of the UV-filters BP-3 and BP-4 in Chlamydomonas reinhardtii: A flow cytometric approach. *Sci. Total Environ.* **2019,** *669*, 412-420.
67. Vieira, L. R.; Soares, A. M. V. M.; Freitas, R., Caffeine as a contaminant of concern: A review on concentrations and impacts in marine coastal systems. *Chemosphere* **2022,** *286*, 131675.
68. Anastopoulos, I.; Pashalidis, I.; Orfanos, A. G.; Manariotis, I. D.; Tatarchuk, T.; Sellaoui, L.; Bonilla-Petriciolet, A.; Mittal, A.; Núñez-Delgado, A., Removal of caffeine, nicotine and amoxicillin from (waste)waters by various adsorbents. A review. *J. Environ. Manage.* **2020,** *261*, 110236.
69. Bouhcain, B.; Carrillo-Peña, D.; El Mansouri, F.; Ez Zoubi, Y.; Mateos, R.; Morán, A.; Quiroga, J. M.; Zerrouk, M. H., Removal of Emerging Contaminants as Diclofenac and Caffeine Using Activated Carbon Obtained from Argan Fruit Shells. **2022,** *12* (6), 2922.
70. Santos-Silva, T. G.; Montagner, C. C.; Martinez, C. B. R., Evaluation of caffeine effects on biochemical and genotoxic biomarkers in the neotropical freshwater teleost Prochilodus lineatus. *Environ. Toxicol. Pharmacol.* **2018,** *58*, 237-242.
71. Vandenberg, L. N.; Hauser, R.; Marcus, M.; Olea, N.; Welshons, W. V., Human exposure to bisphenol A (BPA). *Reprod. Toxicol.* **2007,** *24* (2), 139-177.
72. Lu, S.; Yu, Y.; Ren, L.; Zhang, X.; Liu, G.; Yu, Y., Estimation of intake and uptake of bisphenols and triclosan from personal care products by dermal contact. *Sci. Total Environ.* **2018,** *621*, 1389-1396.
73. Dueñas-Moreno, J.; Mora, A.; Cervantes-Avilés, P.; Mahlknecht, J., Groundwater contamination pathways of phthalates and bisphenol A: origin, characteristics, transport, and fate – A review. *Environ. Int.* **2022,** *170*, 107550.
74. Deng, M.; Han, X.; Ge, J.; Liang, X.; Du, B.; Li, J.; Zeng, L., Prevalence of phthalate alternatives and monoesters alongside traditional phthalates in indoor dust from a typical e-waste recycling area: Source elucidation and co-exposure risk. *J. Hazard. Mater.* **2021,** *413*, 125322.
75. Qian, Y.; Jia, X.; Ding, T.; Yang, M.; Yang, B.; Li, J., Occurrence and removal of bisphenol analogues in wastewater treatment plants and activated sludge bioreactor. *Sci. Total Environ.* **2021,** *758*, 143606.
76. Lesser, L. E.; Mora, A.; Moreau, C.; Mahlknecht, J.; Hernández-Antonio, A.; Ramírez, A. I.; Barrios-Piña, H., Survey of 218 organic contaminants in groundwater derived from the world's largest untreated wastewater irrigation system: Mezquital Valley, Mexico. *Chemosphere* **2018,** *198*, 510-521.
77. Li, P.; Karunanidhi, D.; Subramani, T.; Srinivasamoorthy, K., Sources and Consequences of Groundwater Contamination. *Arch. Environ. Contam. Toxicol.* **2021,** *80* (1), 1-10.
78. Lenka, S. P.; Kah, M.; Padhye, L. P., A review of the occurrence, transformation, and removal of poly- and perfluoroalkyl substances (PFAS) in wastewater treatment plants. *Water Res.* **2021,** *199*, 117187.

79. Kancharla, S.; Alexandridis, P.; Tsianou, M., Sequestration of per- and polyfluoroalkyl substances (PFAS) by adsorption: Surfactant and surface aspects. *Curr. Opin. Colloid Interface Sci.* **2022,** *58*, 101571.
80. Gaines, L. G. T., Historical and current usage of per- and polyfluoroalkyl substances (PFAS): A literature review. **2023,** *66* (5), 353-378.
81. Longendyke, G. K.; Katel, S.; Wang, Y., PFAS fate and destruction mechanisms during thermal treatment: a comprehensive review. *Environmental Science: Processes & Impacts* **2022,** *24* (2), 196-208.
82. Kurwadkar, S.; Dane, J.; Kanel, S. R.; Nadagouda, M. N.; Cawdrey, R. W.; Ambade, B.; Struckhoff, G. C.; Wilkin, R., Per- and polyfluoroalkyl substances in water and wastewater: A critical review of their global occurrence and distribution. *Sci. Total Environ.* **2022,** *809*, 151003.
83. Dickman, R. A.; Aga, D. S., A review of recent studies on toxicity, sequestration, and degradation of per- and polyfluoroalkyl substances (PFAS). *J. Hazard. Mater.* **2022,** *436*, 129120.
84. Gobelius, L.; Persson, C.; Wiberg, K.; Ahrens, L., Calibration and application of passive sampling for per- and polyfluoroalkyl substances in a drinking water treatment plant. *J. Hazard. Mater.* **2019,** *362*, 230-237.
85. Guardian, M. G. E.; Boongaling, E. G.; Bernardo-Boongaling, V. R. R.; Gamonchuang, J.; Boontongto, T.; Burakham, R.; Arnnok, P.; Aga, D. S., Prevalence of per- and polyfluoroalkyl substances (PFASs) in drinking and source water from two Asian countries. *Chemosphere* **2020,** *256*, 127115.
86. Sun, M.; Arevalo, E.; Strynar, M.; Lindstrom, A.; Richardson, M.; Kearns, B.; Pickett, A.; Smith, C.; Knappe, D. R. U., Legacy and Emerging Perfluoroalkyl Substances Are Important Drinking Water Contaminants in the Cape Fear River Watershed of North Carolina. *Environmental Science & Technology Letters* **2016,** *3* (12), 415-419.
87. Houtz, E. F.; Higgins, C. P.; Field, J. A.; Sedlak, D. L., Persistence of Perfluoroalkyl Acid Precursors in AFFF-Impacted Groundwater and Soil. *Environ. Sci. Technol.* **2013,** *47* (15), 8187-8195.
88. Barzen-Hanson, K. A.; Roberts, S. C.; Choyke, S.; Oetjen, K.; McAlees, A.; Riddell, N.; McCrindle, R.; Ferguson, P. L.; Higgins, C. P.; Field, J. A., Discovery of 40 Classes of Per- and Polyfluoroalkyl Substances in Historical Aqueous Film-Forming Foams (AFFFs) and AFFF-Impacted Groundwater. *Environ. Sci. Technol.* **2017,** *51* (4), 2047-2057.
89. Xu, B.; Liu, S.; Zhou, J. L.; Zheng, C.; Weifeng, J.; Chen, B.; Zhang, T.; Qiu, W., PFAS and their substitutes in groundwater: Occurrence, transformation and remediation. *J. Hazard. Mater.* **2021,** *412*, 125159.
90. Gagliano, E.; Sgroi, M.; Falciglia, P. P.; Vagliasindi, F. G. A.; Roccaro, P., Removal of poly- and perfluoroalkyl substances (PFAS) from water by adsorption: Role of PFAS chain length, effect of organic matter and challenges in adsorbent regeneration. *Water Res.* **2020,** *171*, 115381.
91. Li, F.; Duan, J.; Tian, S.; Ji, H.; Zhu, Y.; Wei, Z.; Zhao, D., Short-chain per- and polyfluoroalkyl substances in aquatic systems: Occurrence, impacts and treatment. *Chem. Eng. J.* **2020,** *380*, 122506.
92. Mousavi, S. E.; Delgado-Saborit, J. M.; Godderis, L., Exposure to per- and polyfluoroalkyl substances and premature skin aging. *J. Hazard. Mater.* **2021,** *405*, 124256.

93. Zabaleta, I.; Bizkarguenaga, E.; Bilbao, D.; Etxebarria, N.; Prieto, A.; Zuloaga, O., Fast and simple determination of perfluorinated compounds and their potential precursors in different packaging materials. *Talanta* **2016,** *152*, 353-363.
94. Genualdi, S.; Jeong, N.; deJager, L.; Begley, T., Investigation into perfluoroalkyl substances (PFASs) in a cranberry bog: method development and sampling results. *Food Additives & Contaminants: Part A* **2017,** *34* (12), 2181-2189.
95. https://monographs.iarc.who.int/list-of-classifications.
96. Brunn, H.; Arnold, G.; Körner, W.; Rippen, G.; Steinhäuser, K. G.; Valentin, I., PFAS: forever chemicals—persistent, bioaccumulative and mobile. Reviewing the status and the need for their phase out and remediation of contaminated sites. *Environmental Sciences Europe* **2023,** *35* (1), 20.
97. Ruan, T.; Jiang, G., Analytical methodology for identification of novel per- and polyfluoroalkyl substances in the environment. *TrAC, Trends Anal. Chem.* **2017,** *95*, 122-131.
98. Caporale, N.; Leemans, M.; Birgersson, L.; Germain, P.-L.; Cheroni, C.; Borbély, G.; Engdahl, E.; Lindh, C.; Bressan, R. B.; Cavallo, F.; Chorev, N. E.; D'Agostino, G. A.; Pollard, S. M.; Rigoli, M. T.; Tenderini, E.; Tobon, A. L.; Trattaro, S.; Troglio, F.; Zanella, M.; Bergman, Å.; Damdimopoulou, P.; Jönsson, M.; Kiess, W.; Kitraki, E.; Kiviranta, H.; Nånberg, E.; Öberg, M.; Rantakokko, P.; Rudén, C.; Söder, O.; Bornehag, C.-G.; Demeneix, B.; Fini, J.-B.; Gennings, C.; Rüegg, J.; Sturve, J.; Testa, G., From cohorts to molecules: Adverse impacts of endocrine disrupting mixtures. **2022,** *375* (6582), eabe8244.
99. Pitter, G.; Re, F. D.; Canova, C.; Barbieri, G.; Jeddi, M. Z.; Daprà, F.; Manea, F.; Zolin, R.; Bettega, A. M.; Stopazzolo, G.; Vittorii, S.; Zambelli, L.; Martuzzi, M.; Mantoan, D.; Russo, F., Serum Levels of Perfluoroalkyl Substances (PFAS) in Adolescents and Young Adults Exposed to Contaminated Drinking Water in the Veneto Region, Italy: A Cross-Sectional Study Based on a Health Surveillance Program. **2020,** *128* (2), 027007.
100. Johnson, G. R.; Brusseau, M. L.; Carroll, K. C.; Tick, G. R.; Duncan, C. M., Global distributions, source-type dependencies, and concentration ranges of per- and polyfluoroalkyl substances in groundwater. *Sci. Total Environ.* **2022,** *841*, 156602.
101. https://www.epa.gov/newsreleases/biden-harris-administration-finalizes-first-ever-national-drinking-water-standard#:~:text=For%20PFOA%20and%20PFOS%2C%20EPA,health%20impacts%2C%20including%20certain%20cancers.
102. Sankhla, M. S.; Kumari, M.; Nandan, M.; Kumar, R.; Agrawal, P. J. I. J. C. M. A. S., Heavy metals contamination in water and their hazardous effect on human health-a review. **2016,** *5* (10), 759-766.
103. Tchounwou, P. B.; Yedjou, C. G.; Patlolla, A. K.; Sutton, D. J., Heavy Metal Toxicity and the Environment. In *Molecular, Clinical and Environmental Toxicology: Volume 3: Environmental Toxicology*, Luch, A., Ed. Springer Basel: Basel, 2012; pp 133-164.
104. Kumar, A.; Cabral-Pinto, M.; Kumar, A.; Kumar, M.; Dinis, P. A., Estimation of Risk to the Eco-Environment and Human Health of Using Heavy Metals in the Uttarakhand Himalaya, India. **2020,** *10* (20), 7078.
105. Zamora-Ledezma, C.; Negrete-Bolagay, D.; Figueroa, F.; Zamora-Ledezma, E.; Ni, M.; Alexis, F.; Guerrero, V. H., Heavy metal water pollution: A fresh look about hazards, novel and conventional remediation methods. *Environmental Technology & Innovation* **2021,** *22*, 101504.
106. Cabral-Pinto, M. M. S.; Inácio, M.; Neves, O.; Almeida, A. A.; Pinto, E.; Oliveiros, B.; Ferreira da Silva, E. A., Human Health Risk Assessment Due to Agricultural Activities

and Crop Consumption in the Surroundings of an Industrial Area. *Exposure and Health* **2020,** *12* (4), 629-640.
107. Cabral Pinto, M. M. S.; Marinho-Reis, P.; Almeida, A.; Pinto, E.; Neves, O.; Inácio, M.; Gerardo, B.; Freitas, S.; Simões, M. R.; Dinis, P. A.; Diniz, L.; Ferreira da Silva, E.; Moreira, P. I., Links between Cognitive Status and Trace Element Levels in Hair for an Environmentally Exposed Population: A Case Study in the Surroundings of the Estarreja Industrial Area. **2019,** *16* (22), 4560.
108. Zhou, Q.; Yang, N.; Li, Y.; Ren, B.; Ding, X.; Bian, H.; Yao, X., Total concentrations and sources of heavy metal pollution in global river and lake water bodies from 1972 to 2017. *Global Ecology and Conservation* **2020,** *22*, e00925.
109. García-Miranda Ferrari, A.; Carrington, P.; Rowley-Neale, S. J.; Banks, C. E., Recent advances in portable heavy metal electrochemical sensing platforms. *Environ. Sci. Water Res. Technol.* **2020,** *6* (10), 2676-2690.
110. Rajendran, S.; Priya, T. A. K.; Khoo, K. S.; Hoang, T. K. A.; Ng, H.-S.; Munawaroh, H. S. H.; Karaman, C.; Orooji, Y.; Show, P. L., A critical review on various remediation approaches for heavy metal contaminants removal from contaminated soils. *Chemosphere* **2022,** *287*, 132369.
111. Crini, G.; Lichtfouse, E., Advantages and disadvantages of techniques used for wastewater treatment. *Environ. Chem. Lett.* **2019,** *17* (1), 145-155.
112. Rathi, B. S.; Kumar, P. S.; Show, P.-L., A review on effective removal of emerging contaminants from aquatic systems: Current trends and scope for further research. *J. Hazard. Mater.* **2021,** *409*, 124413.
113. Pivokonsky, M.; Novotna, K.; Petricek, R.; Cermakova, L.; Prokopova, M.; Naceradska, J., Fundamental chemical aspects of coagulation in drinking water treatment – Back to basics. *J. Water Process Eng.* **2024,** *57*, 104660.
114. Stackelberg, P. E.; Gibs, J.; Furlong, E. T.; Meyer, M. T.; Zaugg, S. D.; Lippincott, R. L., Efficiency of conventional drinking-water-treatment processes in removal of pharmaceuticals and other organic compounds. *Sci. Total Environ.* **2007,** *377* (2), 255-272.
115. Shahid, M. K.; Kashif, A.; Fuwad, A.; Choi, Y., Current advances in treatment technologies for removal of emerging contaminants from water – A critical review. *Coord. Chem. Rev.* **2021,** *442*, 213993.
116. Rout, P. R.; Zhang, T. C.; Bhunia, P.; Surampalli, R. Y., Treatment technologies for emerging contaminants in wastewater treatment plants: A review. *Sci. Total Environ.* **2021,** *753*, 141990.
117. de Oliveira, M.; Frihling, B. E. F.; Velasques, J.; Filho, F. J. C. M.; Cavalheri, P. S.; Migliolo, L., Pharmaceuticals residues and xenobiotics contaminants: Occurrence, analytical techniques and sustainable alternatives for wastewater treatment. *Sci. Total Environ.* **2020,** *705*, 135568.
118. Radwan, E. K.; Abdel Ghafar, H. H.; Ibrahim, M.; Moursy, A. S. J. E. Q. M., Recent trends in treatment technologies of emerging contaminants. **2023,** *32* (3), 7-25.
119. Gao, W.; Liang, H.; Ma, J.; Han, M.; Chen, Z.-l.; Han, Z.-s.; Li, G.-b. J. D., Membrane fouling control in ultrafiltration technology for drinking water production: A review. **2011,** *272* (1-3), 1-8.
120. Mohapatra, D. P.; Kirpalani, D. M., Advancement in treatment of wastewater: Fate of emerging contaminants. **2019,** *97* (10), 2621-2631.
121. Roccaro, P., Treatment processes for municipal wastewater reclamation: The challenges of emerging contaminants and direct potable reuse. *Current Opinion in Environmental Science & Health* **2018,** *2*, 46-54.

122. Pesqueira, J. F. J. R.; Pereira, M. F. R.; Silva, A. M. T., Environmental impact assessment of advanced urban wastewater treatment technologies for the removal of priority substances and contaminants of emerging concern: A review. *Journal of Cleaner Production* **2020,** *261*, 121078.
123. Cevallos-Mendoza, J.; Amorim, C. G.; Rodríguez-Díaz, J. M.; Montenegro, M. d. C. B. J. M., Removal of contaminants from water by membrane filtration: a review. **2022,** *12* (6), 570.
124. Xiang, H.; Min, X.; Tang, C.-J.; Sillanpää, M.; Zhao, F., Recent advances in membrane filtration for heavy metal removal from wastewater: A mini review. *J. Water Process Eng.* **2022,** *49*, 103023.
125. Gupta, V.; Ali, I. J. E. W., Water treatment by membrane filtration techniques. **2013,** *135*.
126. Liang, R.; Hu, A.; Hatat-Fraile, M.; Zhou, N. J. N. f. W. T.; Purification, Fundamentals on adsorption, membrane filtration, and advanced oxidation processes for water treatment. **2014**, 1-45.
127. Anis, S. F.; Hashaikeh, R.; Hilal, N. J. J. o. W. P. E., Microfiltration membrane processes: A review of research trends over the past decade. **2019,** *32*, 100941.
128. Li, X.; Jiang, L.; Li, H. In *Application of ultrafiltration technology in water treatment*, IOP Conference Series: Earth and Environmental Science, IOP Publishing: 2018; p 012009.
129. Guo, H.; Li, X.; Yang, W.; Yao, Z.; Mei, Y.; Peng, L. E.; Yang, Z.; Shao, S.; Tang, C. Y., Nanofiltration for drinking water treatment: a review. *Frontiers of Chemical Science and Engineering* **2022,** *16* (5), 681-698.
130. Schäfer, R. B.; von der Ohe, P. C.; Kühne, R.; Schüürmann, G.; Liess, M., Occurrence and Toxicity of 331 Organic Pollutants in Large Rivers of North Germany over a Decade (1994 to 2004). *Environ. Sci. Technol.* **2011,** *45* (14), 6167-6174.
131. Arkhangelsky, E.; Levitsky, I.; Gitis, V., Considering energy efficiency in filtration of engineering nanoparticles. *Water Supply* **2017,** *17* (5), 1212-1218.
132. Chew, C. M.; Aroua, M. K.; Hussain, M. A.; Ismail, W. M. Z. W., Evaluation of ultrafiltration and conventional water treatment systems for sustainable development: an industrial scale case study. *Journal of Cleaner Production* **2016,** *112*, 3152-3163.
133. Guo, W.; Ngo, H.-H.; Li, J., A mini-review on membrane fouling. *Bioresour. Technol.* **2012,** *122*, 27-34.
134. Rodriguez-Narvaez, O. M.; Peralta-Hernandez, J. M.; Goonetilleke, A.; Bandala, E. R., Treatment technologies for emerging contaminants in water: A review. *Chem. Eng. J.* **2017,** *323*, 361-380.
135. Dotto, G. L.; McKay, G. J. J. o. E. C. E., Current scenario and challenges in adsorption for water treatment. **2020,** *8* (4), 103988.
136. Bhatnagar, A.; Hogland, W.; Marques, M.; Sillanpää, M. J. C. E. J., An overview of the modification methods of activated carbon for its water treatment applications. **2013,** *219*, 499-511.
137. Soni, R.; Bhardwaj, S.; Shukla, D. P., Chapter 14 - Various water-treatment technologies for inorganic contaminants: current status and future aspects. In *Inorganic Pollutants in Water*, Devi, P.; Singh, P.; Kansal, S. K., Eds. Elsevier: 2020; pp 273-295.
138. Shah, A. I.; Din Dar, M. U.; Bhat, R. A.; Singh, J. P.; Singh, K.; Bhat, S. A., Prospectives and challenges of wastewater treatment technologies to combat contaminants of emerging concerns. *Ecol. Eng.* **2020,** *152*, 105882.
139. Yao, Y.; Wang, C.; Na, J.; Hossain, M. S. A.; Yan, X.; Zhang, H.; Amin, M. A.; Qi, J.; Yamauchi, Y.; Li, J. J. S., Macroscopic MOF architectures: Effective strategies for practical application in water treatment. **2022,** *18* (8), 2104387.

140. Ali, I.; Alharbi, O. M.; Tkachev, A.; Galunin, E.; Burakov, A.; Grachev, V. A. J. E. S.; Research, P., Water treatment by new-generation graphene materials: hope for bright future. **2018,** *25*, 7315-7329.
141. Khaliha, S.; Tunioli, F.; Foti, L.; Bianchi, A.; Kovtun, A.; Marforio, T.; Zambianchi, M.; Bettini, C.; Briñas, E.; Vázquez, E.; Bocchi, L.; Palermo, V.; Calvaresi, M.; Navacchia, M. L.; Melucci, M., Upcycling of plastic membrane industrial scraps and reuse as sorbent for emerging contaminants in water. *Environmental Science: Water Research & Technology* **2024,** *10*.
142. Freitas, B. L. S.; Terin, U. C.; Fava, N. M. N.; Maciel, P. M. F.; Garcia, L. A. T.; Medeiros, R. C.; Oliveira, M.; Fernandez-Ibañez, P.; Byrne, J. A.; Sabogal-Paz, L. P., A critical overview of household slow sand filters for water treatment. *Water Res.* **2022,** *208*, 117870.
143. Wu, J.; Cao, M.; Tong, D.; Finkelstein, Z.; Hoek, E. M. V., A critical review of point-of-use drinking water treatment in the United States. *npj Clean Water* **2021,** *4* (1), 40.
144. Westerhoff, P.; Alvarez, P.; Li, Q.; Gardea-Torresdey, J.; Zimmerman, J., Overcoming implementation barriers for nanotechnology in drinking water treatment. *Environ. Sci.: Nano* **2016,** *3* (6), 1241-1253.
145. Fewtrell, L.; Majuru, B.; Hunter, P. R., A re-assessment of the safety of silver in household water treatment: rapid systematic review of mammalian in vivo genotoxicity studies. *Environ. Health* **2017,** *16* (1), 66.
146. Menya, E.; Jjagwe, J.; Kalibbala, H. M.; Storz, H.; Olupot, P. W., Progress in deployment of biomass-based activated carbon in point-of-use filters for removal of emerging contaminants from water: A review. *Chem. Eng. Res. Des.* **2023,** *192*, 412-440.
147. Magdalera, J.; Sanchez, P. A.; Sobremisana, M.; Bautista, R., Drinking Water Treatment using Hybrid Biosand Filter with Locally Produced Coconut Shell Carbon for Brgy. San Juan, Kalayaan, Laguna, Philippines. **2020**, 19-5080.
148. Lu, H.; Wang, J.; Stoller, M.; Wang, T.; Bao, Y.; Hao, H., An Overview of Nanomaterials for Water and Wastewater Treatment. *Advances in Materials Science and Engineering* **2016,** *2016*, 4964828.
149. Singh, K. K.; Singh, A.; Rai, S., A study on nanomaterials for water purification. *Materials Today: Proceedings* **2022,** *51*, 1157-1163.
150. Saleh, T. A., Nanomaterials: Classification, properties, and environmental toxicities. *Environmental Technology & Innovation* **2020,** *20*, 101067.
151. Kolahalam, L. A.; Kasi Viswanath, I. V.; Diwakar, B. S.; Govindh, B.; Reddy, V.; Murthy, Y. L. N., Review on nanomaterials: Synthesis and applications. *Materials Today: Proceedings* **2019,** *18*, 2182-2190.
152. Baig, N.; Ihsanullah; Sajid, M.; Saleh, T. A., Graphene-based adsorbents for the removal of toxic organic pollutants: A review. *J. Environ. Manage.* **2019,** *244*, 370-382.
153. Santhosh, C.; Velmurugan, V.; Jacob, G.; Jeong, S. K.; Grace, A. N.; Bhatnagar, A., Role of nanomaterials in water treatment applications: A review. *Chem. Eng. J.* **2016,** *306*, 1116-1137.
154. Mazari, S. A.; Ali, E.; Abro, R.; Khan, F. S. A.; Ahmed, I.; Ahmed, M.; Nizamuddin, S.; Siddiqui, T. H.; Hossain, N.; Mubarak, N. M.; Shah, A., Nanomaterials: Applications, waste-handling, environmental toxicities, and future challenges – A review. *J. Environ. Chem. Eng* **2021,** *9* (2), 105028.
155. Berktas, I.; Ghafar, A. N.; Fontana, P.; Caputcu, A.; Menceloglu, Y.; Okan, B. S., Facile Synthesis of Graphene from Waste Tire/Silica Hybrid Additives and Optimization

Study for the Fabrication of Thermally Enhanced Cement Grouts. *Molecules* **2020,** *25* (4), 886.
156. Khaliha, S.; Marforio, T. D.; Kovtun, A.; Mantovani, S.; Bianchi, A.; Luisa Navacchia, M.; Zambianchi, M.; Bocchi, L.; Boulanger, N.; Iakunkov, A.; Calvaresi, M.; Talyzin, A. V.; Palermo, V.; Melucci, M., Defective graphene nanosheets for drinking water purification: Adsorption mechanism, performance, and recovery. *FlatChem* **2021,** *29*, 100283.
157. Farjadian, F.; Abbaspour, S.; Sadatlu, M. A. A.; Mirkiani, S.; Ghasemi, A.; Hoseini-Ghahfarokhi, M.; Mozaffari, N.; Karimi, M.; Hamblin, M. R. J. C., Recent developments in graphene and graphene oxide: Properties, synthesis, and modifications: A review. **2020,** *5* (33), 10200-10219.
158. Trikkaliotis, D. G.; Christoforidis, A. K.; Mitropoulos, A. C.; Kyzas, G. Z. J. C., Graphene oxide synthesis, properties and characterization techniques: a comprehensive review. **2021,** *5* (3), 64.
159. Guo, S.; Garaj, S.; Bianco, A.; Ménard-Moyon, C. J. N. R. P., Controlling covalent chemistry on graphene oxide. **2022,** *4* (4), 247-262.
160. Thines, R. K.; Mubarak, N. M.; Nizamuddin, S.; Sahu, J. N.; Abdullah, E. C.; Ganesan, P., Application potential of carbon nanomaterials in water and wastewater treatment: A review. *J. Taiwan Inst. Chem. Eng.* **2017,** *72*, 116-133.
161. Yap, P. L.; Nine, M. J.; Hassan, K.; Tung, T. T.; Tran, D. N.; Losic, D. J. A. F. M., Graphene-based sorbents for multipollutants removal in water: a review of recent progress. **2021,** *31* (9), 2007356.
162. Yap, P. L.; Kabiri, S.; Auyoong, Y. L.; Tran, D. N. H.; Losic, D., Tuning the Multifunctional Surface Chemistry of Reduced Graphene Oxide via Combined Elemental Doping and Chemical Modifications. *ACS Omega* **2019,** *4* (22), 19787-19798.
163. Melucci, M.; Treossi, E.; Ortolani, L.; Giambastiani, G.; Morandi, V.; Klar, P.; Casiraghi, C.; Samorì, P.; Palermo, V. J. J. o. M. C., Facile covalent functionalization of graphene oxide using microwaves: bottom-up development of functional graphitic materials. **2010,** *20* (41), 9052-9060.
164. Mantovani, S.; Khaliha, S.; Favaretto, L.; Bettini, C.; Bianchi, A.; Kovtun, A.; Zambianchi, M.; Gazzano, M.; Casentini, B.; Palermo, V.; Melucci, M., Scalable synthesis and purification of functionalized graphene nanosheets for water remediation. *Chem. Commun.* **2021,** *57* (31), 3765-3768.
165. Mantovani, S.; Khaliha, S.; Marforio, T. D.; Kovtun, A.; Favaretto, L.; Tunioli, F.; Bianchi, A.; Petrone, G.; Liscio, A.; Palermo, V.; Calvaresi, M.; Navacchia, M. L.; Melucci, M., Facile high-yield synthesis and purification of lysine-modified graphene oxide for enhanced drinking water purification. *Chem. Commun.* **2022,** *58* (70), 9766-9769.
166. Zhu, W.-P.; Sun, S.-P.; Gao, J.; Fu, F.-J.; Chung, T.-S., Dual-layer polybenzimidazole/polyethersulfone (PBI/PES) nanofiltration (NF) hollow fiber membranes for heavy metals removal from wastewater. *J. Membr. Sci.* **2014,** *456*, 117-127.
167. Rout, D. R.; Jena, H. M.; Baigenzhenov, O.; Hosseini-Bandegharaei, A. J. S. o. T. T. E., Graphene-based materials for effective adsorption of organic and inorganic pollutants: A critical and comprehensive review. **2023,** *863*, 160871.
168. Perreault, F.; Fonseca de Faria, A.; Elimelech, M., Environmental applications of graphene-based nanomaterials. *Chem. Soc. Rev.* **2015,** *44* (16), 5861-5896.
169. Tunioli, F.; Khaliha, S.; Mantovani, S.; Bianchi, A.; Kovtun, A.; Xia, Z.; Bafqi, M. S. S.; Okan, B. S.; Marforio, T. D.; Calvaresi, M.; Palermo, V.; Navacchia, M. L.; Melucci,

M., Adsorption of emerging contaminants by graphene related materials and their alginate composite hydrogels. *J. Environ. Chem. Eng.* **2023,** *11* (2), 109566.
170. Khaliha, S.; Marforio, T. D.; Kovtun, A.; Mantovani, S.; Bianchi, A.; Navacchia, M. L.; Zambianchi, M.; Bocchi, L.; Boulanger, N.; Iakunkov, A.; Calvaresi, M.; Talyzin, A. V.; Palermo, V.; Melucci, M., Defective graphene nanosheets for drinking water purification: Adsorption mechanism, performance, and recovery. *FlatChem* **2021,** *29*, 100283.
171. Jun, B.-M.; Kim, S.; Kim, Y.; Her, N.; Heo, J.; Han, J.; Jang, M.; Park, C. M.; Yoon, Y., Comprehensive evaluation on removal of lead by graphene oxide and metal organic framework. *Chemosphere* **2019,** *231*, 82-92.
172. Goel, J.; Kadirvelu, K.; Rajagopal, C.; Garg, V. K. J. J. o. h. m., Removal of lead (II) by adsorption using treated granular activated carbon: batch and column studies. **2005,** *125* (1-3), 211-220.
173. Avornyo, A.; Chrysikopoulos, C. V., Applications of graphene oxide (GO) in oily wastewater treatment: Recent developments, challenges, and opportunities. *J. Environ. Manage.* **2024,** *353*, 120178.
174. Anegbe, B.; Ifijen, I. H.; Maliki, M.; Uwidia, I. E.; Aigbodion, A. I., Graphene oxide synthesis and applications in emerging contaminant removal: a comprehensive review. *Environmental Sciences Europe* **2024,** *36* (1), 15.
175. Yousefi, N.; Lu, X.; Elimelech, M.; Tufenkji, N., Environmental performance of graphene-based 3D macrostructures. *Nat Nanotechnol* **2019,** *14* (2), 107-119.
176. Gandhi, M. R.; Vasudevan, S.; Shibayama, A.; Yamada, M., Graphene and Graphene-Based Composites: A Rising Star in Water Purification - A Comprehensive Overview. *ChemistrySelect* **2016,** *1* (15), 4358-4385.
177. Berber, M. R., Current Advances of Polymer Composites for Water Treatment and Desalination. **2020,** *2020* (1), 7608423.
178. Zheng, D.; Wang, K.; Bai, B., A critical review of sodium alginate-based composites in water treatment. *Carbohydr. Polym.* **2024,** *331*, 121850.
179. Bhatt, P.; Joshi, S.; Urper Bayram, G. M.; Khati, P.; Simsek, H., Developments and application of chitosan-based adsorbents for wastewater treatments. *Environ. Res.* **2023,** *226*, 115530.
180. Kayan, G. Ö.; Kayan, A., Polycaprolactone Composites/Blends and Their Applications Especially in Water Treatment. **2023,** *7* (6), 104.
181. Mokoena, L. S.; Mofokeng, J. P. J. M., A review on graphene (GN) and graphene oxide (GO) based biodegradable polymer composites and their usage as selective adsorbents for heavy metals in water. **2023,** *16* (6), 2527.
182. Zhang, D.; Li, N.; Cao, S.; Liu, X.; Qiao, M.; Zhang, P.; Zhao, Q.; Song, L.; Huang, X. J. C. R. i. C. U., A layered chitosan/graphene oxide sponge as reusable adsorbent for removal of heavy metal ions. **2019,** *35* (3), 463-470.
183. De Luna, M. S.; Ascione, C.; Santillo, C.; Verdolotti, L.; Lavorgna, M.; Buonocore, G.; Castaldo, R.; Filippone, G.; Xia, H.; Ambrosio, L. J. C. p., Optimization of dye adsorption capacity and mechanical strength of chitosan aerogels through crosslinking strategy and graphene oxide addition. **2019,** *211*, 195-203.
184. Kovtun, A.; Campodoni, E.; Favaretto, L.; Zambianchi, M.; Salatino, A.; Amalfitano, S.; Navacchia, M. L.; Casentini, B.; Palermo, V.; Sandri, M.; Melucci, M., Multifunctional graphene oxide/biopolymer composite aerogels for microcontaminants removal from drinking water. *Chemosphere* **2020,** *259*, 127501.
185. Zhao, H.; Ouyang, X.-K.; Yang, L.-Y., Adsorption of lead ions from aqueous solutions by porous cellulose nanofiber–sodium alginate hydrogel beads. *J. Mol. Liq.* **2021,** *324*, 115122.

186. Shen, J.; Xu, X.; Ouyang, X.-k.; Jin, M.-c., Adsorption of Pb(II) from Aqueous Solutions Using Nanocrystalline Cellulose/Sodium Alginate/K-Carrageenan Composite Hydrogel Beads. *J Polym Environ* **2022,** *30* (5), 1995-2006.
187. Fan, L.; Lu, Y.; Yang, L.-Y.; Huang, F.; Ouyang, X.-k., Fabrication of polyethylenimine-functionalized sodium alginate/cellulose nanocrystal/polyvinyl alcohol core–shell microspheres ((PVA/SA/CNC)@PEI) for diclofenac sodium adsorption. *J Colloid Interface Sci* **2019,** *554*, 48-58.
188. Li, H.; Zhu, X.; Zhao, J.; Ling, G.; Zhang, P., Emerging adsorbents: Applications of sodium alginate/graphene oxide composite materials in wastewater treatment. *J. Water Process Eng.* **2024,** *59*, 105100.
189. Platero, E.; Fernandez, M. E.; Bonelli, P. R.; Cukierman, A. L., Graphene oxide/alginate beads as adsorbents: Influence of the load and the drying method on their physicochemical-mechanical properties and adsorptive performance. *J Colloid Interface Sci* **2017,** *491*, 1-12.
190. Algothmi, W. M.; Bandaru, N. M.; Yu, Y.; Shapter, J. G.; Ellis, A. V., Alginate-graphene oxide hybrid gel beads: an efficient copper adsorbent material. *J Colloid Interface Sci* **2013,** *397*, 32-8.
191. Majdoub, M.; Amedlous, A.; Anfar, Z.; Jada, A.; El Alem, N., Engineering of amine-based binding chemistry on functionalized graphene oxide/alginate hybrids for simultaneous and efficient removal of trace heavy metals: Towards drinking water. *J Colloid Interface Sci* **2021,** *589*, 511-524.
192. Fei, Y.; Li, Y.; Han, S.; Ma, J., Adsorptive removal of ciprofloxacin by sodium alginate/graphene oxide composite beads from aqueous solution. *J Colloid Interface Sci* **2016,** *484*, 196-204.
193. Sun, Y.; Zhou, T.; Li, W.; Yu, F.; Ma, J., Amino-functionalized alginate/graphene double-network hydrogel beads for emerging contaminant removal from aqueous solution. *Chemosphere* **2020,** *241*, 125110.
194. An, D.; Yang, L.; Wang, T.-J.; Liu, B., Separation Performance of Graphene Oxide Membrane in Aqueous Solution. *Industrial & Engineering Chemistry Research* **2016,** *55* (17), 4803-4810.
195. Joshi, R. K.; Alwarappan, S.; Yoshimura, M.; Sahajwalla, V.; Nishina, Y., Graphene oxide: the new membrane material. *Applied Materials Today* **2015,** *1* (1), 1-12.
196. Nauman Javed, R. M.; Al-Othman, A.; Tawalbeh, M.; Olabi, A. G., Recent developments in graphene and graphene oxide materials for polymer electrolyte membrane fuel cells applications. *Renewable and Sustainable Energy Reviews* **2022,** *168*, 112836.
197. Gao, J.; Wang, K. Y.; Chung, T.-S., Design of nanofiltration (NF) hollow fiber membranes made from functionalized bore fluids containing polyethyleneimine (PEI) for heavy metal removal. *Journal of Membrane Science* **2020,** *603*, 118022.
198. Abdelrasoul, A.; Doan, H.; Lohi, A.; Cheng, C.-H., Morphology Control of Polysulfone Membranes in Filtration Processes: a Critical Review. **2015,** *2* (1), 22-43.
199. An, Y.-C.; Gao, X.-X.; Jiang, W.-L.; Han, J.-L.; Ye, Y.; Chen, T.-M.; Ren, R.-Y.; Zhang, J.-H.; Liang, B.; Li, Z.-L.; Wang, A.-J.; Ren, N.-Q., A critical review on graphene oxide membrane for industrial wastewater treatment. *Environ. Res.* **2023,** *223*, 115409.
200. Fan, Y.; Quan, X.; Zhao, H.; Chen, S.; Yu, H.; Zhang, Y.; Zhang, Q., Poly(vinylidene fluoride) hollow-fiber membranes containing silver/graphene oxide dope with excellent filtration performance. **2017,** *134* (15).

201. Kafiah, F. M.; Khan, Z.; Ibrahim, A.; Karnik, R.; Atieh, M.; Laoui, T., Monolayer graphene transfer onto polypropylene and polyvinylidenedifluoride microfiltration membranes for water desalination. *Desalination* **2016,** *388*, 29-37.
202. Nasseri, S.; Ebrahimi, S.; Abtahi, M.; Saeedi, R., Synthesis and characterization of polysulfone/graphene oxide nano-composite membranes for removal of bisphenol A from water. *J. Environ. Manage.* **2018,** *205*, 174-182.
203. Sewerin, T.; Elshof, M. G.; Matencio, S.; Boerrigter, M.; Yu, J.; de Grooth, J., Advances and Applications of Hollow Fiber Nanofiltration Membranes: A Review. **2021,** *11* (11), 890.
204. Gholami, N.; Mahdavi, H., Nanofiltration composite membranes of polyethersulfone and graphene oxide and sulfonated graphene oxide. **2018,** *37* (8), 3529-3541.
205. Junaidi, N. F. D.; Othman, N. H.; Shahruddin, M. Z.; Alias, N. H.; Marpani, F.; Lau, W. J.; Ismail, A. F., Fabrication and characterization of graphene oxide–polyethersulfone (GO–PES) composite flat sheet and hollow fiber membranes for oil–water separation. **2020,** *95* (5), 1308-1320.
206. Badrinezhad, L.; Ghasemi, S.; Azizian-Kalandaragh, Y.; Nematollahzadeh, A., Preparation and characterization of polysulfone/graphene oxide nanocomposite membranes for the separation of methylene blue from water. *Polym. Bull.* **2018,** *75* (2), 469-484.
207. Zambianchi, M.; Khaliha, S.; Bianchi, A.; Tunioli, F.; Kovtun, A.; Navacchia, M. L.; Salatino, A.; Xia, Z.; Briñas, E.; Vázquez, E.; Paci, D.; Palermo, V.; Bocchi, L.; Casentini, B.; Melucci, M., Graphene oxide-polysulfone hollow fibers membranes with synergic ultrafiltration and adsorption for enhanced drinking water treatment. *J. Membr. Sci.* **2022,** *658*, 120707.

2 Aim of the thesis

The aim of this thesis is the development of chemically modified graphene based nano- and composite materials, their application as sorbents for the removal of emerging contaminants from drinking water, and the understanding of structure-property relationships to enable predictive chemical tailoring. In the following chapters, the adsorption mechanism on water-dispersed graphene nanosheets has been studied to determine the adsorption selectivity and capacity. Then, the impact of chemical modifications on graphene oxide has been evaluated to assess how they can improve the existing selectivity towards particularly persistent contaminants. Finally, composites with GRM and both biopolymers and synthetic polymers have been investigated for the potential implementation of GRM in water treatment technologies.

Chapter 3 describes several covalent modifications on GO obtained by epoxide ring-opening reactions. Among the building blocks chosen for chemical modification there are a set of amino acids (lysine, methionine, glutamate) for adsorption of organic contaminants and β-cyclodextrin for specific application against PFAS. This last modification example is taken as a case study to focus on the synthesis, characterisation and application in water treatment of a graphene-based modified material. β-cyclodextrins with different sized alkyl linkers were grafted on GO surface. The obtained materials were characterised by X-ray photoelectron spectroscopy, elemental analysis and scanning electron microscopy. The modified GO materials were then tested in the adsorption of perfluorobutanoic acid, one of the most persistent PFAS, showing a strong influence of the alkyl chain length on the adsorption efficiency in tap water. In addition, to gain insight into the adsorption mechanism, the experimental results were integrated with molecular dynamic simulations.

In **Chapter 4**, different types of composite materials based on GRM and biopolymers are introduced and described. Among others, alginate-based hydrogel composites are presented as a case study. GRM-alginate composites were prepared by ionic gelation and the resulting gel beads were characterised by a combination of scanning electron microscopy and confocal Raman microscopy mapping. The composite beads were tested in the removal of eight emerging contaminants from tap water, including bisphenol A, ofloxacin and diclofenac. In addition to selectivity studies, the maximum adsorption capacity was investigated through adsorption isotherms. Finally,

regeneration tests were performed to evaluate the possibility of reusing the obtained composites.

Chapter 5 presents composites of GRM and synthetic polymers. In particular, a technology based on hollow fibers membranes of polysulphone (PSU) coextruded with GO is presented for point-of-use applications in water treatment. The preparation, characterization and performance of these filtration systems were briefly described. In addition, a strategy for converting scrap obtained as waste from PSU-GO industrial production into granular sorbent material was presented. The granules were tested for the removal of several emerging contaminants in mixtures, including pharmaceuticals, heavy metals and PFAS. The safety of the materials was assessed by surface enhanced Raman spectroscopy to exclude GO release and combined potability tests. Finally, the granules were tested in a pilot plants that simulate real tap operation conditions.

3 Graphene oxide modification for enhanced selectivity

As mentioned in the introduction, GO exhibits remarkable properties that make it an excellent sorbent for ECs. In addition, the oxygen groups present on its surface enable chemical reactions to covalently bind moieties on the nanosheets. This ability is crucial to extending the selectivity of GO towards more persistent ECs. Indeed, the adsorption is highly dependent on a combination of factors such as surface area, surface chemistry, and morphology of the sorbent, and on the chemical structure of the targeted contaminants.[1] Among the various chemical reactions available, the epoxide ring opening reaction is one of the most widely used for covalent modification of GO.[2] This is due to the abundance of epoxides on the nanosheets and the mild conditions under which the reaction can take place (aqueous environment and room temperature). The reaction occurs via a nucleophilic attack, e.g. by amino-terminated molecules, which leads to the opening of the epoxy ring.

During my PhD, the research group I joined has synthesised and studied a class of modified GO with different amino acids to enhance GO selectivity towards ECs.[3, 4] Briefly, GO modified with L-lysine (Lys), L-methionine (Met) and L-glutamate (Glu) was synthetized by microwave assisted epoxide ring opening reaction (Scheme 3.1). The obtained materials were fully characterised to confirm the presence of the amino acids and a loading of 5-15% was estimated by X-ray photoelectron spectroscopy.

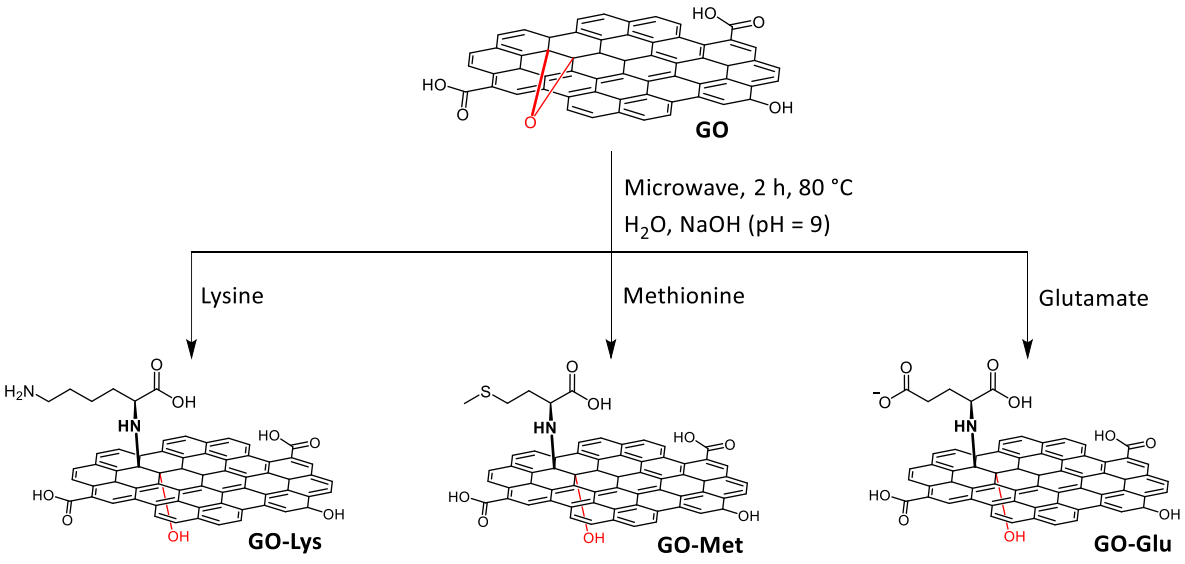

Scheme 3.1 *Synthetic pathway to amino acid-modified GO.*

The three materials were then tested in the removal of eight organic ECs and the results are reported in Figure 3.1. Most of the adsorption occurred during the first hours of treatment, showing fast kinetics for all the sorbent materials tested. Focusing on selectivity, pristine GO showed lower performance for caffeine (CAF), benzophenone-4 (BP4), carbamazepine (CBZ), bisphenol A (BPA) and diclofenac (DCF). Amino acid functionalisation changes the surface chemistry of the nanosheets and increases the adsorption selectivity towards the selected contaminants. GO-Glu, GO-Lys and GO-Met showed better performance than unmodified GO in the removal of the contaminants that were not fully adsorbed (i.e. CAF, BP4, CBZ, BPA and DCF).

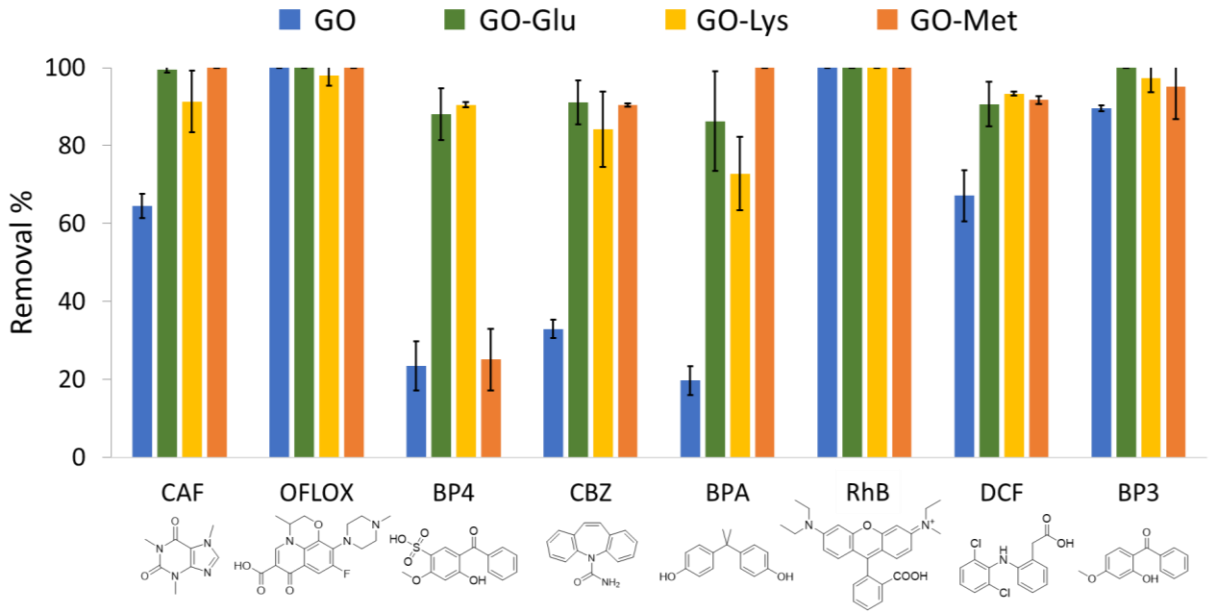

Figure 3.1 *Removal of eight ECs (molecular structure in the bottom) from the mixture in tap water (contact time = 1 h, volume = 10 mL, sorbent amount = 25 mg, c_{IN} = 5 mg/L) by GO (blue), GO-Glu (green), GO-Lys (yellow), and GO-Met (orange).*

Accordingly, molecular dynamics simulations revealed higher interaction energies for amino acid-modified GO than for unmodified GO, which can be attributed to the higher van der Waals and hydrophobic interactions between the amino acid hydrophobic chain and the contaminants. The grafting of amino acids creates 3D recognition sites on the surface of the on the surface of the GO nanosheets, which enhance the removal capacity of the modified materials.

More detailed information can be found in the full article (Mantovani et al).[3] However, the results reported here demonstrate that it is possible to synthesise modified graphene materials with tuneable and predictable adsorption properties on selected contaminants.

With this in mind, during my PhD we focused on the synthesis and characterisation of a graphene material capable of adsorbing PFAS, a family of persistent contaminants described in the introduction. β-cyclodextrin molecules (βCD), having seven glucose units in its structure, has already proved high removal capability toward several emerging contaminants, including PFAS, through the ability to form a stable host-guest complex.[5-13] Indeed, PFAS can enter the cavity of βCD due to the complementary cross-sectional sizes (28 $Å^2$ for PFAS and 30 $Å^2$ for βCD) and create a stable host-guest complex where the dominant force is the hydrophobic interaction between the fluorinated PFAS chain and the βCD cavity.[14] Based on this, we modified the βCD unit with linkers of different lengths to include a terminal amine, which was used to functionalize GO. The synthesized materials were then tested in the removal of PFAS and the results obtained are collected in the following paper.

3.1 Chemical Tailoring of β-Cyclodextrin-Graphene Oxide for Enhanced Per- and Polyfluoroalkyl Substances (PFAS) Adsorption from Drinking Water

Adapted with permission from Chemistry—A European Journal, 29, 2023, e202301854

DOI 10.1002/chem.202301854

Abstract

We report on the synthesis of β-cyclodextrin (βCD) modified graphene oxide (GO) nanosheets, having different sized alkyl linkers (GO-C_n-βCD) and their exploitation as sorbent of per- and polyfluoroalkyl substances (PFAS) from drinking water. βCD were functionalized with a pending amino group, and the resulting precursors grafted to GO nanosheets by epoxide ring opening reaction. Loading of βCD units in the range 12-36% was estimated by combined XPS and elemental analysis. Adsorption tests on perfluorobutanoic acid (PFBA), a particularly persistent PFAS selected as case study, revealed a strong influence of the alkyl linker length on the adsorption efficiency, with the hexyl linker derivative GO-C_6-βCD outperforming both pristine GO and granular activated carbon (GAC), the standard sorbent benchmark. Molecular dynamic simulations ascribed this evidence to the favorable orientation of the βCD unit on the surface of GO which enables a strong contaminant molecules retention.

3.1.1 Introduction

Per- and polyfluoroalkyl substances (PFAS), also known as *forever chemicals*, are currently subject of global concern for their massive use in every-day products, their persistency in the environment and human bodies, and proved eco- and human toxicity.[15, 16] PFAS are nowadays used in hundreds of thousands of industrial products for food packaging, non-stick cookware, paints, waterproof clothing, stain repellent, cosmetics, and firefighting foams. The disposal of such products or their wastes leads to the release of PFAS and their accumulation in different environmental compartments, including water bodies.[17, 18]

Surprisingly, recent studies have shown that toilet paper is one of the major sources of PFAS entering wastewater treatment systems, contributing to the introduction of up to 80 µg/person-year, corresponding to 60 kg/year in Europe region alone, of 6:2 fluorotelomer phosphate diester (6:2 diPAP) in wastewaters.[19] Given the resistance of this class of molecules to current water treatment technologies, PFAS occurrence in drinking water has been reported in several areas, such as the Italian Northern region of Veneto[20-22] or in southern Sweden, where residents showed PFAS blood levels 100 times higher than the reference group.[23, 24]

Adsorption on granular activated carbon (GAC) is one of the most common strategies for PFAS removal.[25-28] However, GAC performances are strongly related to the carbon-chain length of PFAS.[29, 30] Short chain PFAS (i.e. PFAS with eight or fewer carbon atoms),[31] which include perfluorobutanoic acid (PFBA), have higher water solubility,[29] and therefore they are adsorbed to a lesser extent by GAC in the operational conditions used in potabilization plant (i.e. average contact time of 10-20 min).[17, 32] In addition a fast drop of initial adsorption performance of GAC from 100% to 20% has been documented for short change PFAS in real water treatment plants.[33]

Recently, the suitability of graphene oxide (GO) and its derivatives on the removal of emerging contaminants from drinking water has been widely documented.[34, 35] In particular, our group demonstrated GO high adsorption capacity of PFAS (C>5) by using GO nanosheets[3, 4, 36-38] and GO-doped[39, 40] or coated[41] hollow fiber membranes. The adsorption on GO nanosheets was mainly related to the van der Waals interaction, which depends on hydrophobicity and thus on the perfluoroalkyl chain size of these molecules. For short-chain PFAS, such as PFBA, the negative charges of both PFAS

and GO overcome hydrophobic interactions, consequently lowering the adsorption capacity of GO.[37, 39]

Here, aiming at enhancing the interaction capability between short-chain PFAS and GO we report on the covalent modification of GO with β-cyclodextrin units (βCD). βCD, having seven glucose units in its structure, has already proved high removal capability toward several emerging contaminants, including PFAS, through the ability to form a stable host-guest complex.[5-13] Indeed, PFAS can enter the cavity of βCD due to the complementary cross-sectional sizes (28 $Å^2$ for PFAS and 30 $Å^2$ for βCD) and create a stable host-guest complex where the dominant force is the hydrophobic interaction between the fluorinated PFAS chain and the βCD cavity.[14]

Here, we report on the synthesis and full characterization of a class of GO functionalized with βCD bearing differently sized alkyl linkers between GO and the βCD units. We also report on the study of their adsorption of PFBA from tap water, in comparison to pristine GO and GAC (the industrial sorbent benchmark). Adsorption-structure relationships investigation through molecular dynamic simulations were also performed for a deeper understanding of the working mechanism driving the PFBA capture.

3.1.2 Results and Discussion

Synthesis and characterization

The synthesis of GO derivatives was achieved by epoxide ring opening reaction, starting from amino-ending βCD.[42] Amino-ending βCD precursors synthesis involves the preparation of mono tosyl and azide intermediates from commercially available βCD (Scheme 3.2a). Following published procedures,[43, 44] amino alkyl pendants of different length, i.e. (C_0) and three different diamino-alkyl linkers, 1,2-ethylenediamine (C_2), 1,6-hexamethylenediamine (C_6), and 1,12-dodecanediamine (C_{12}) were selected to tailor the distance between the βCD unit and GO nanosheets. NMR characterization of the C_n-βCD derivatives was achieved, and data are reported in the experimental section. The modified amino-ending βCD were then grafted through epoxide ring opening reaction to give GO-C_n-βCD derivatives (Scheme 3.2b). Two control samples were prepared under the same reaction conditions using commercial βCD (without amino-alkyl linker) (GO@βCD) and without the addition of βCD (GO-control). Purification of crude materials was performed by microfiltration on Plasmart modules (Medica Spa), according to previously reported conditions.[4]

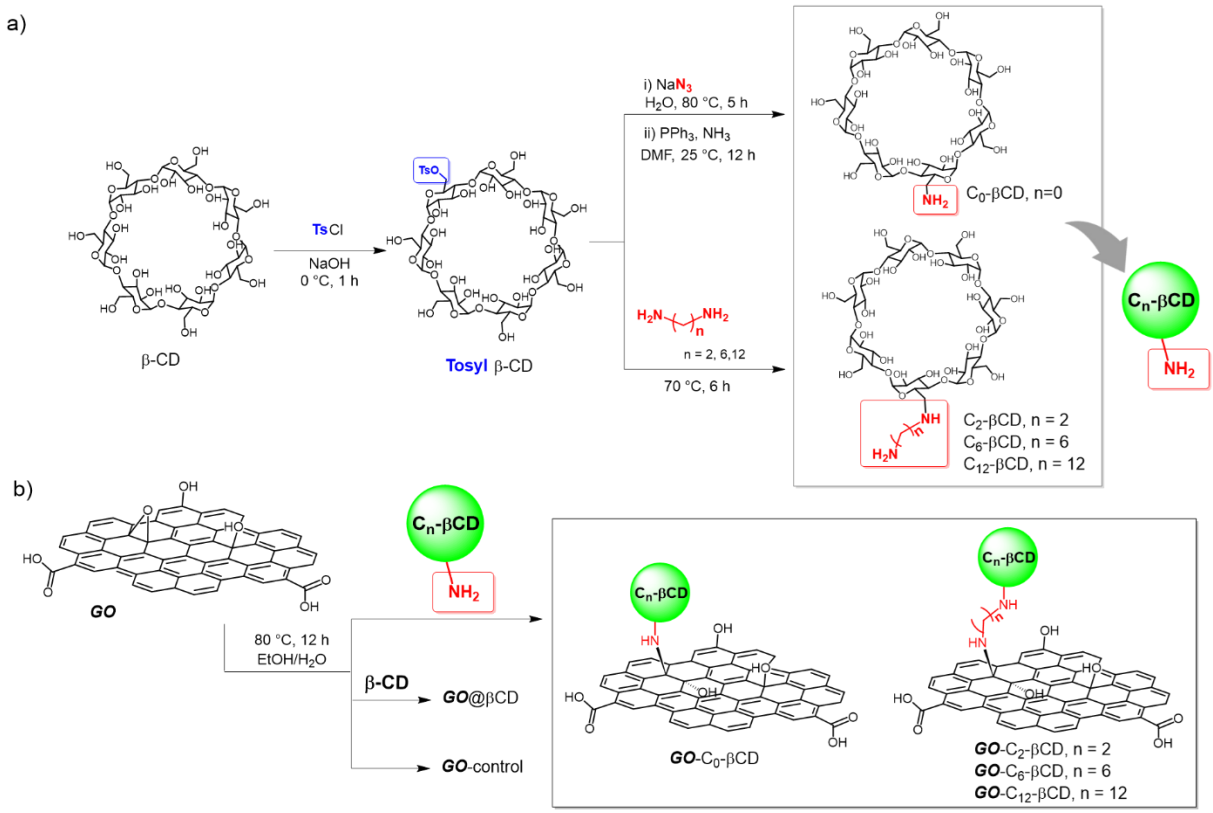

Scheme 3.2 *Synthetic routes to a) amino-ended βCD (NH_2-C_n-βCD), and b) targeted GO-C_n-βCD and control samples: GO@βCD and GO-control.*

Figure 3.2 shows the attenuated total reflection infrared (ATR-FTIR) spectra of GO-C_6-βCD, taken as a case study. Every GO derivatives showed the typical peaks of pristine GO (O-H stretching vibrations) at 3700-3000 cm^{-1} and that typical of βCD at 2920 cm^{-1} (C-H stretching vibrations)[45] (Figure 7.1, Appendix), confirming the presence of βCD in each modified GO. Contrarily, the spectrum of the control material GO@βCD showed only the fingerprint of pristine GO (Figure 3.2), confirming that, in our experimental conditions, βCD without amino pendants did not react with GO.

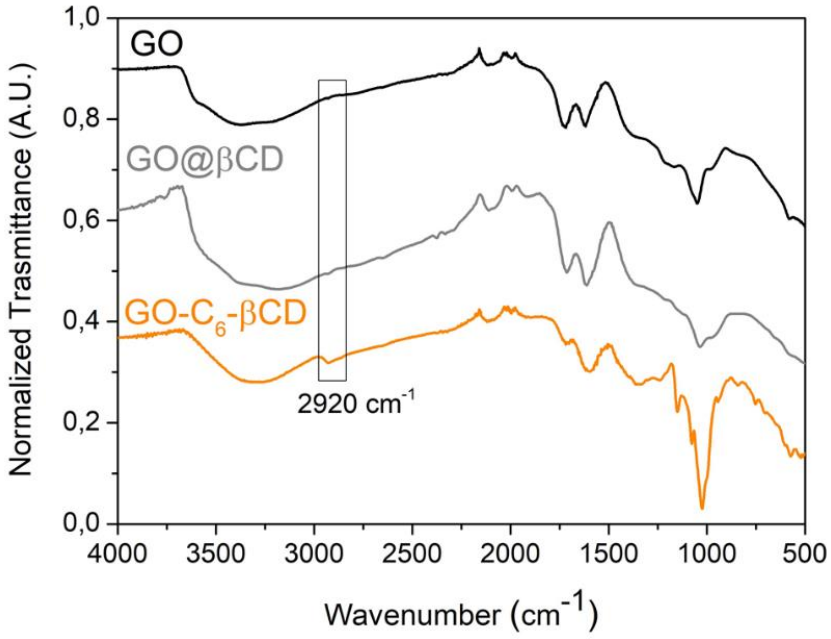

Figure 3.2 *ATR-FTIR spectra of GO (black), GO-C_6-βCD (orange) and GO@βCD (grey).*

Accordingly, thermogravimetric analysis (TGA) of each GO-C_n-βCD revealed the presence of an inflection point at 300 °C (peak in derivative) ascribed to βCD and absent in pristine GO and in the control material GO@βCD (Figure 3.3, and Figure 7.2, Appendix).

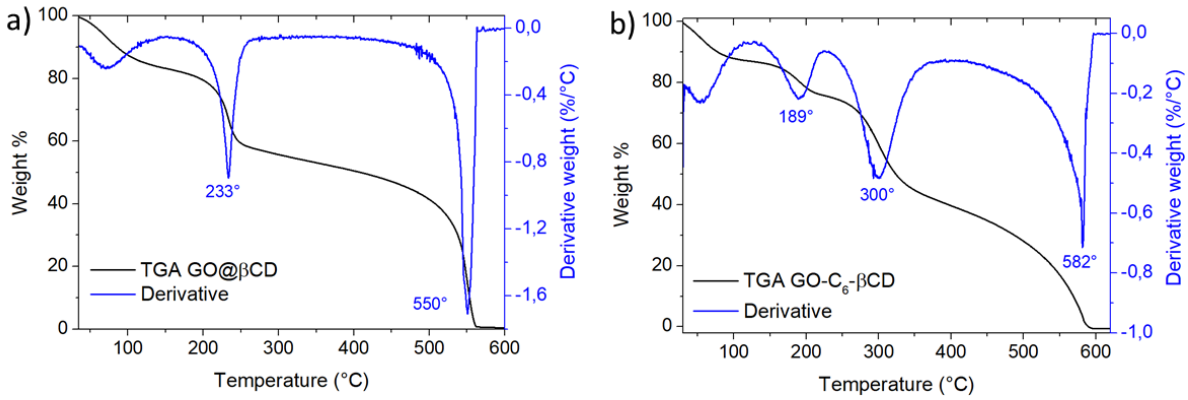

Figure 3.3 *TGA of a) GO@βCD, and b) GO-C_6-βCD.*

The chemical structure and the βCD loading of the GO derivatives were estimated by X-ray photoelectron spectroscopy (XPS) and elemental analysis (EA).

The XPS survey spectra are showed in Figure 3.4a and Figure 7.3a in the appendix, and the atomic compositions of GO and each modified GO are reported in Table 3.1. The analysed materials were mainly composed of carbon, oxygen, and nitrogen, associated with i) the aromatic sp^2 regions of GO, ii) the C-O/C=O functional groups,

and iii) the nitrogen functional groups (C-N) present in the modified βCD. The effective covalent functionalization of GO is proved by N 1s signal (Figure 3.4b and Figure 7.3b, appendix), which was fitted by using two Voigt curves centred at 400.0 eV for C-NH-C group, associated to epoxide ring opening reaction, and at 402-401.5 eV for the other C-N groups. Unfortunately, the C-NH_2 group, which can be associated to unreacted primary amine, presents a broad assignment in literature: from 402 eV region in dopamine[46] or polydopamine[47] to 400 eV in amino acids,[48] contrarily to the well-established association of 400-400.5 eV signal to C-NH-C, also present in wide XPS polymer literature, as polyamic acid,[49] polydopamine[50] or nylon.[51] Moreover, the pristine GO presents a signal at 401.5 eV, which makes the exact association of 402-401 eV region to a specific functional group ambiguous. The N signal in pristine GO could be ascribed to nitrogen reagents used for GO production and it is reported in literature as graphitic nitrogen.[52]

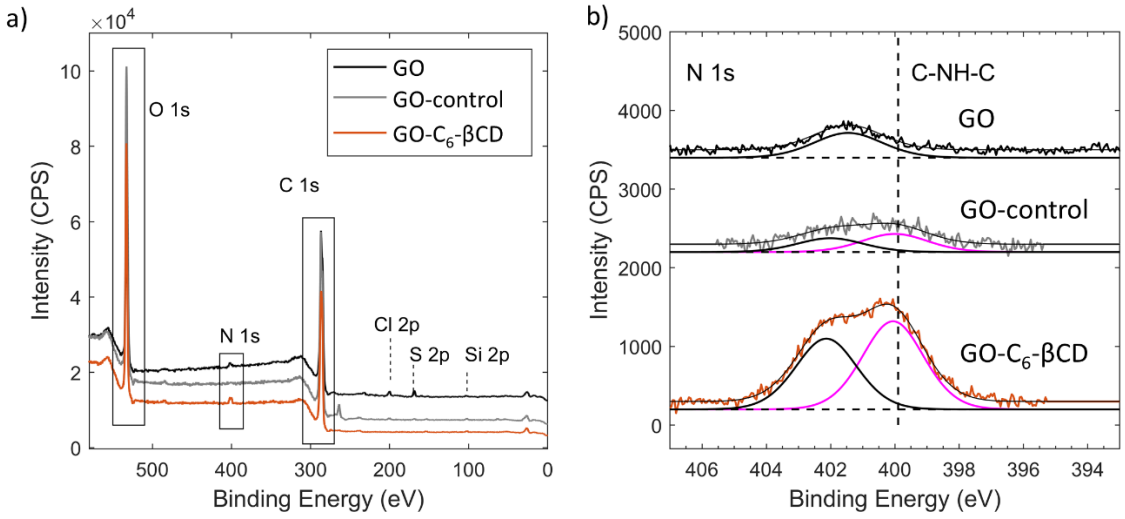

Figure 3.4 *a) XPS survey spectra and b) N 1s signals of GO (black), GO-control (grey) and GO-C_6-βCD (orange). N 1s was fitted by two Voigt curves with binding energies at: i) 400.0 eV (C-NH-C, magenta line) and ii) 402.0 eV (other N atoms, black line). All spectra were shifted for better visualization.*

For the sake of simplicity and in order to have a rough estimation of the C_n-βCD fraction in the whole GO-C_n-βCD, the loading was calculated from the N 1s peak at 400 eV, which is absent in pristine GO and present only as residual of 0.1% in the control sample (GO-control). The atomic percentage of nitrogen (%N 1s) was associated to the number of nitrogen atoms present in C_n-βCD samples. After subtracting the %N of the control material (0.1%) from the N 1s signal at 400 eV of each GO-C_n-βCD in order to consider only the N from C_n-βCD, the loading was estimated calculating the correspondent N : (N+C+O) atom ratio present in the C_n-βCD moiety, which is: 1N : (1 N + 42 C + 34 O)

for C_0-βCD; 2 N : (2 N + 44 C + 34 O) for C_2-βCD; 2 N : (2 N + 48 C + 34 O) for C_6-βCD; 2 N : (2 N + 54 C + 34 O) for C_{12}-βCD. These proportions were used to obtain an indicative estimation of C_n-βCD loading and the results are reported in Table 3.1. Each modified GO were found to span between 12 and 36% loading range. The oxidation degree of the studied materials was determined using the O/C ratio (Table 3.1). The pristine GO and the reference material (GO-control) showed an O/C ratio between the expected interval (0.38 and 0.46, respectively), proving that the experimental conditions used to bind βCD did not lead to the reduction of GO nanosheets. All the GO derivatives showed an O/C ratio comparable to pristine GO (ranging from 0.40 to 0.48), with values that monotonically decreased as the n in C_n aliphatic chain rises from 0 to 12. In the modified materials, the O/C ratio is given by the oxidation degree of the GO nanosheets, which is assumed here to be constant, and the oxidation degree of the modified C_n-βCD, which decreases as the length of the alkyl chain increases (Table 7.2, Appendix).

Table 3.1 *Atomic composition of βCD modified GO obtained by XPS. Errors on C (285 eV) and O (532 eV) were about ± 0.9%, and errors on N were about ± 0.1%. S and Cl were present in GO in low quantities (<1%) and almost absent in GO-C_n-βCD (<0.1%). Si and Na was present in low quantities (<0.5%).*

	Atomic composition %					
Materials	C	O	N (402 eV)	N (400 eV)	O/C ratio	Loading %
GO	70.4	27.0	0.7	-	0.38	-
GO-control	67.9	31.0	0.1	0.1	0.46	-
GO@βCD	70.0	29.4	0.2	0.2	0.42	-
GO-C_0-βCD	67.3	31.9	0.2	0.3	0.47	12
GO-C_2-βCD	66.0	32.0	0.5	1.0	0.48	36
GO-C_6-βCD	67.1	31.0	0.6	0.7	0.46	24
GO-C_{12}-βCD	69.1	27.8	1.1	0.8	0.40	28

Moreover, the C 1s signal (Figure 7.4, Appendix) of GO-C_n-βCD presents a similar shape to that of pristine GO, which is mainly characterized by the presence of aliphatic and aromatic C-C/C=C carbons under the peak in 285 eV region and the different C-O groups present in 286-287 eV region (mainly epoxy/hydroxyl groups for GO and ether/hydroxyl groups for βCD). Combining all of the considerations above, we can conclude that the oxidation degree and the chemical structure of GO-C_n-βCD can be considered as the simple combination of the two reagents, knowing that the epoxy ring opening usually does not affect the overall amount of oxygen.

EA on modified βCD and modified GO was used to determine the bulk composition. The atomic composition (C, H, N, S, O) of each material was in good accordance with that estimated by XPS, and is reported in Tables 7.1-7.2, Appendix. In the modified C_n-βCD, the element content percentage was in good agreement with the expected one from the molecular structure (Table 7.1, Appendix). After the functionalization of GO, the amount of N consistently increases with respect to GO-control, which was taken as reference instead of GO, since it was subjected to the same reaction conditions and further purification used for modified GO.

The N% was used to obtain an indicative estimation of C_n-βCD loading (20% for GO-C_0-βCD, 32% for GO-C_2-βCD, 26% for GO-C_6-βCD, 37% for GO-C_{12}-βCD) and the results are in good agreement with XPS estimation (Table 3.1). The oxidation degree of GO-C_n-βCD obtained from EA presents the same monotonic trend observed by XPS: O/C ratio decreased from 0.91 to 0.66 as n in aliphatic chain C_n rises from 0 to 12 (Table 7.2, Appendix). The observed O/C ratio was systematically overestimated by EA with respect to XPS. This difference can be ascribed to the residual water content in the EA samples. Indeed, XPS is performed in ultra-high vacuum, with almost no residual water, while EA is carried out under ambient room conditions.

The zeta potentials (ζ potentials) of modified GO were measured in deionized water. The obtained values (-36.7 ± 1.4 mV for GO-C_0-βCD; -31.4 ± 0.2 mV for GO-C_2-βCD; -30.2 ± 0.1 mV for GO-C_6-βCD, -34.2 ± 2.2 mV for GO-C_{12}-βCD) were comparable to the one measured for pristine GO (-43.1 ± 2.4 mV), meaning that the experimental conditions used did not affect the surface charge. The morphology of the modified GO was studied by scanning electron microscopy (SEM). The images (Figure 7.5, Appendix) showed that GO-C_6-βCD (taken as a case study) retained the typical morphology of GO nanosheets, with a lateral size of few micrometres.

PFBA adsorption from tap water

GO-C_n-βCD nanosheets were used as sorbent of PFBA from tap water. The concentration of PFBA selected for this study was in the range of the highest ever found in surface waters (0.1-3 μg/L).[53, 54] Adsorption kinetic studies for GO-C_n-βCD (in comparison to GAC) were carried out in batch conditions (i.e. by dispersing the material nanosheets in tap water spiked with PFBA). Figure 3.5a shows the removal of PFBA from tap water at different contact times (15 min, 4 h, and 24 h). For GO samples, the

adsorption equilibrium occurred within 15 minutes, since the removal did not change at longer contact times. On the other hand, GAC showed a slower adsorption rate, reaching the maximum removal capacity after 24 h. It should be noted that the contact time between water and GAC in a real potabilization plant is about 10-20 min. Surprisingly, among the selected case studies, only GO-C_6-βCD showed a PFBA adsorption reaching about 65% removal after only 15 minutes, well competing with the performance of GAC after 24 h (70% removal). Poor removal rates were found for GO and GO@βCD (removal < 5%), this being likely due to the electrostatic repulsion between negatively charged GO nanosheets (ζ potential = -43.1 ± 2.4 mV) and the anionic form of PFBA formed in tap water at neutral pH (pK_a = 0.08-0.4).[55] Similarly to βCD free compounds, poor removal were found for GO-C_0-βCD, GO-C_2-βCD and GO-C_{12}-βCD, meaning that the amount of βCD is not the only parameter promoting the adsorption of PFBA, but a crucial role is also due to the length of the linker.

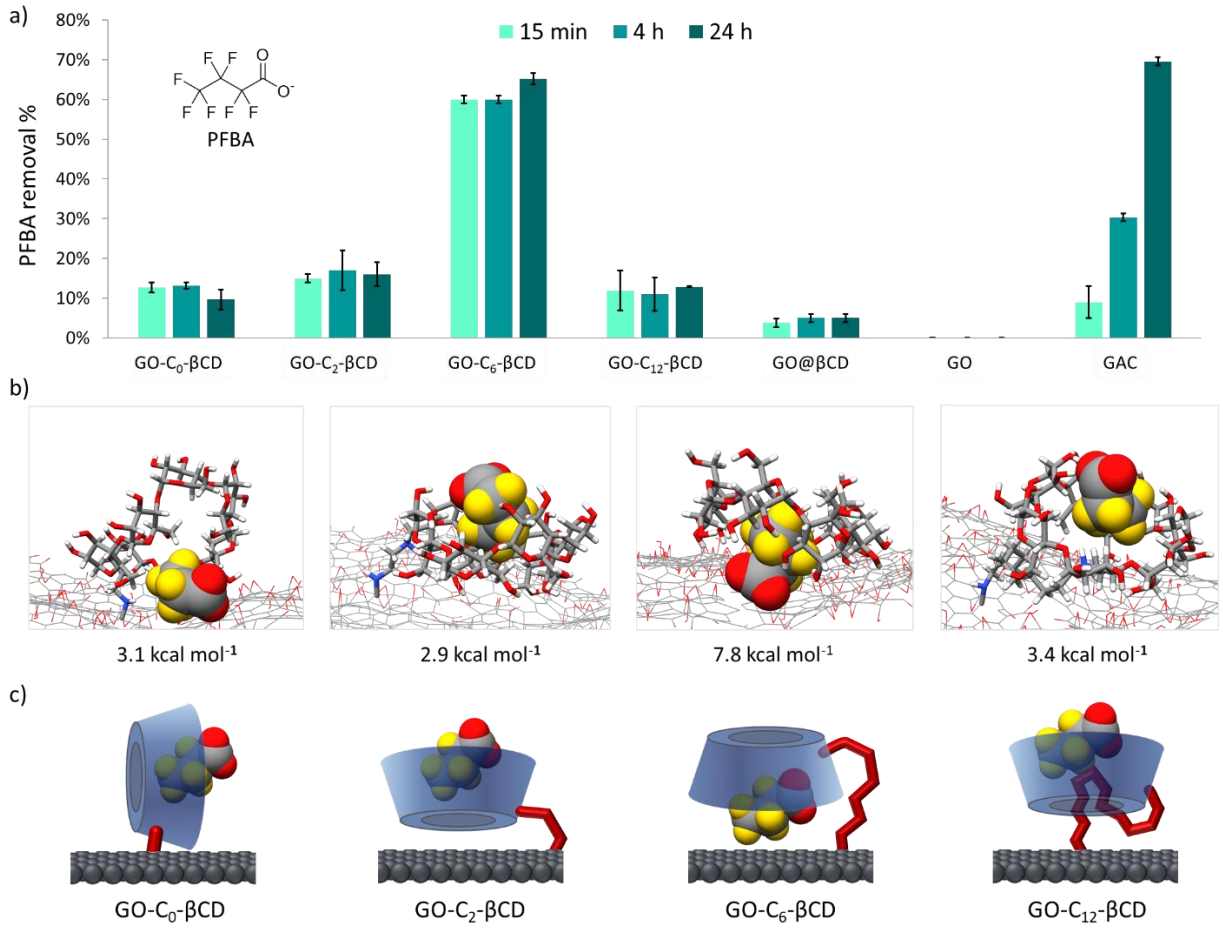

Figure 3.5 a) Removal of PFBA; b) binding affinity gain (kcal mol^{-1}) for PFBA and GO-C_n-βCD obtained at MM-GBSA level and representative snapshots of the MD simulations for the investigated systems; c) schematic representation of the different arrangements of βCD on GO, influencing possible complexation with PFBA. GO is in black, βCD in blue, the different linkers are in red.

To unravel the role of the different linker length on the adsorption, molecular dynamic (MD) simulations were carried out.

MD simulations of the complexes PFBA@βCD, followed by MM-GBSA calculations (Figure 7.6, Appendix), confirmed that βCD can efficiently entrap the PFBA molecule (the binding energy of PFBA inside the βCD is -12.3 kcal mol^{-1}). Van der Waals (E_{vdw}) interactions in PFBA@βCD account for -14.3 kcal mol^{-1} and represent the driving force for the binding. The non-polar solvation term (E_{surf}), i.e. hydrophobic interactions, contributes by -2.6 kcal mol^{-1} to the total affinity, increasing the affinity of the host (βCD) for the guest (PFBA). On the other hand, the electrostatic term (E_{el}) is detrimental for the binding (4.7 kcal mol^{-1}); indeed, the charged PFBA, cannot interact with water molecules while entrapped inside the hydrophobic cavity of the cyclodextrin.

Figure 3.5b shows the energetic gain in binding affinity of PFBA for GO-C_n-βCD (n=0, 2, 6, and 12), due to its covalent attachment on the GO surface. This trend well-reproduces the experimental data, revealing the key role of the linker length on PFBA removal. The highest removal of PFBA by GO-C_6-βCD can be explained by assuming the formation of a “canopy-like” structure, which entraps PFBA between the GO nanosheet and the cavity of the βCD, in a sandwich-like structure. On the other hand, i) in GO-C_0-βCD the absence of the linker rigidly blocks the βCD unit perpendicular to the GO surface, restricting the possibility to interact with PFBA, ii) in GO-C_2-βCD, the βCD units lay on the surface of GO, maximising the interaction between the primary hydroxyl groups of the sugar units of the cyclodextrin and the epoxide/hydroxyl groups of GO. These interactions with the GO surface block one of the two βCD cavity portals. Finally, in GO-C_{12}-βCD the long alkyl chain of the linker shows a strong tendency to self-wrap to maximise the non-polar intramolecular interactions and to interact with the inner hydrophobic cavity of the βCD, reducing the accessibility to PFBA.

Finally, the removal of a mixture of nine PFAS (C_4-C_{13}, Figure 3.6) from tap water was studied. Figure 3.6 shows the removal after 15 min of GO and GO-C_6-βCD. Pristine GO showed high removal (>60%) for long-chain PFAS (C_{12}-C_{14}), while resulted ineffective in the adsorption of short-chain molecules (C_4-C_8). On the other hand, GO-C_6-βCD effectively removed all nine PFAS with values ranging between 50% and 95% of removal, proving the synergic role of GO (adsorbing long-chain PFAS) and βCD (adsorbing the short-chain ones).

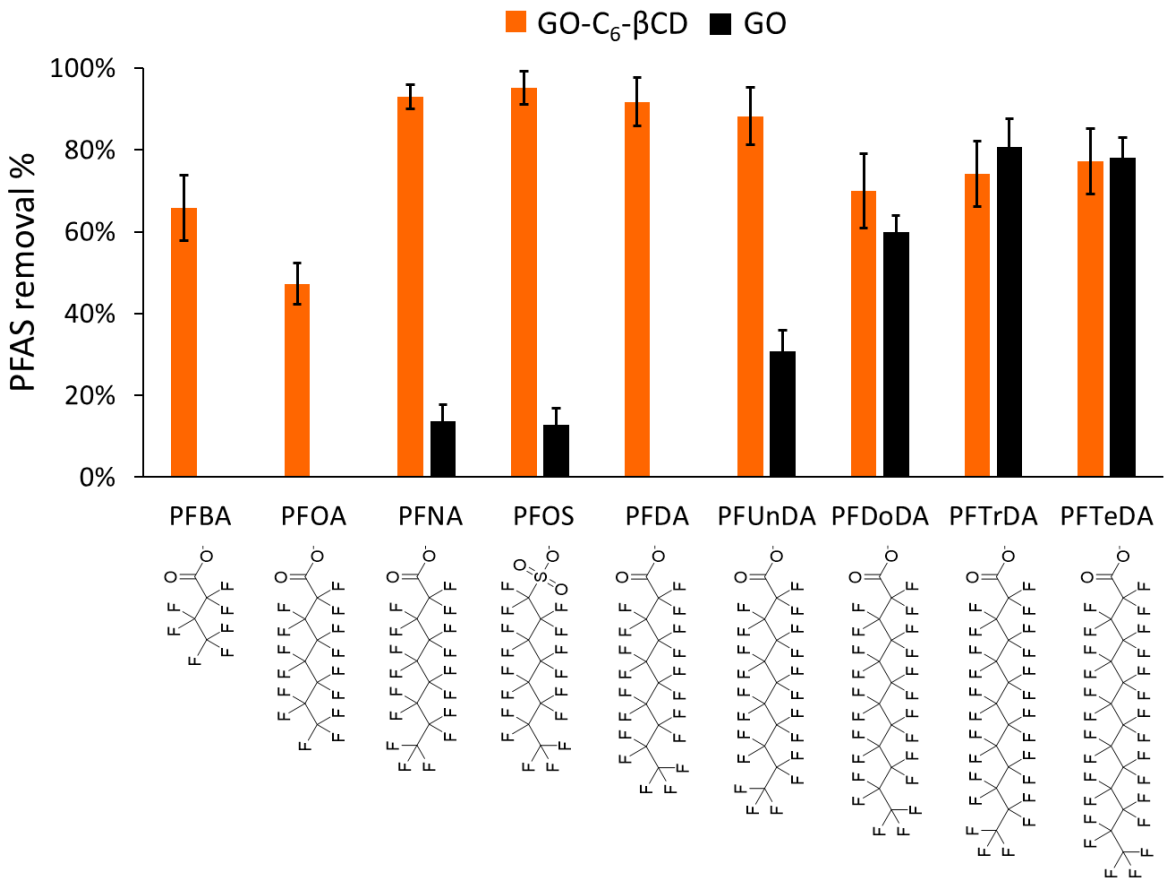

Figure 3.6 *Removal of a mixture of PFAS after 15 minutes.*

3.1.3 Conclusions

Covalent modification of GO with βCD was realized by epoxide ring opening reaction through amino-ended βCD. Tailored alkyl chains with length in the range C_0-C_{12} were exploited as linkers between GO and βCD. The reaction enabled loadings in the range 12-36% and negligible reduction of GO precursor. Covalent binding was demonstrated by comparing ATR-FTIR, TGA, XPS and EA of GO-C_n-βCD to those of two control samples and by the PFBA adsorption test results. Poor adsorption efficiencies were indeed found for control samples. Moreover, the adsorption was not only related to the presence/amount of βCD but mainly to the length of the alkyl linkers. A removal up to 65% after just 15 minutes was found for GO-C_6-βCD only. Molecular dynamic simulations ascribed the observed trend to the complexation of PFBA in the βCD cavity (occurring in all of the GO-C_n-βCD materials tested) and synergic entrapping of PFBA between the GO nanosheet and the cavity of the βCD in a sandwich-like structure, peculiar to the C_6 linker. Remarkably, GO-C_6-βCD outperformed GAC (industrial sorbent benchmark) at short contact time and well compares with the adsorption of GAC after

24 h. The adsorption synergy of GO and βCD was finally proved for a mixture of PFAS of different fluoroalkyl chain length. Long-chain PFAS were well adsorbed by GO and short-chain ones were retained by the βCD unit, this revealing great potential of the presented approach for drinking water purification from emerging contaminants. Future studies will focus on the exploitation of GO-C_6-βCD for engineering technologies, such as membranes, for PFAS removal under flow conditions.

3.1.4 Experimental Section

Materials

GO powder was purchased from Layer One (Norway, previously Abalonyx) and used without further purification (graphene oxide dry powder <35 mesh, product code 1.8). Before using, GO was sonicated in ultrapure water to exfoliate the bulk material into monolayer (>99%) with lateral size of few micrometers.[37, 56] GAC was purchased from CABOT Norit Spa (Ravenna, Italy, Norit GAC 830 AF, MB index min 240 mg/g, BET surface area >1000 m^2/g) and use without further purification. PFAS standards were purchased by Agilent Technologies (Santa Clara, CA, US). The experiments on PFAS were carried out by using polypropylene vials. All other chemicals were purchased from Sigma Aldrich or Termo Fisher and used without any further purification. Purification of modified GO was performed by using microfiltration modules Plasmart 100 MF modules (Versatile® PES hollow fibers, membrane area filtering surface 0.1 m^2, pore average size 100-200 nm) were provided by Medica Spa (Medolla, Italy).

Synthesis of modified β-cyclodextrins

Firstly, tosyl- βCD was obtained by following the procedure reported by Ohashi et al.,[44] with some modifications (Scheme 3.2a).

βCD (5 g; 4.4 mmol) and toluenesulfonyl chloride (TsCl, 3.75 g; 19.6 mmol) were dissolved in an aqueous sodium hydroxide solution (0.4 M, 75 mL) and reacted under vigorous stirring at 0 °C for 1 h. Unreacted TsCl was filtered off, hydrochloric acid was used to neutralize the solution and unrefined tosyl-βCD was obtained as precipitate. 1.2 g of pure tosyl-βCD were obtained from recrystallization of the crude from hot water (90 °C, 25 mL). ^{1}H NMR (400 MHz, DMSO-d_6): δ = 7.73 (d, J= 8.4Hz, 2H), 7.41 (d, J= 8.4Hz, 2H), 5.81 – 5.62 (m, 14H), 4.82 - 4.74 (m, 7H), 4.48 – 4.41 (m, 6H), 4.34-4.29 (m, 1H), 4.19-4.14 (m, 1H), 3.63 – 3.16 (m, 40H, overlapped signal with H_2O), 2.40 (s, 3H) ppm.

C_0-βCD was obtained by following a two-steps reaction reported by Bonnet et al.,[43] with some modifications (Scheme 3.2a).

Tosyl-βCD (1 g; 0.78 mmol) was suspended in deionized water (10 mL) and sodium azide (0.65 g; 0.01 mmol) was added. The reaction was carried out under stirring at 80 °C for 5 h. After cooling to room temperature, acetone (60 mL) was added, and the resulting precipitate was vacuum-dried to obtain 0.9 g of azide-βCD (N_3-βCD). ^{1}H NMR (500 MHz, DMSOd_6): δ = 5.75-5.64 (m, 14H), 4.88-4.83 (m, 7 H), 4.54-4.47 (m, 6H), 3.77−3.56 (m, 28 H), 3.41-3.29 (m, 14 H, overlapped signal with H_2O) ppm. ^{13}C NMR (125 MHz, DMSOd_6): δ = 102.3-101.6 (m), 83.0, 81.8-81.4 (m), 73.0−72.0 (m), 60.1-59.7 (m), 51.1 (CH_2N_3) ppm.

N_3-βCD (540 mg; 0.466 mmol) and triphenylphosphine (206 mg; 0.785 mmol) were dissolved in dimethylformamide (10 mL) and NH_3 (2 mL, 28% aqueous solution) was added. The mixture was stirred at room temperature for 12 h, then acetone (80 mL) was added to obtain the crude product as a white precipitate. To remove by-products, the crude was dissolved in a small quantity of DMF and then precipitated from acetone to obtained 440 mg of C_0-βCD. ^{1}H NMR (500 MHz, D_2O): δ = 5.09 (bs, 7 H), 3.99−3.86 (m, 26H), 3.67-3.51 (m, 13H), 3.49 (t, J= 9.0Hz, 1H), 3.13(d, J= 12Hz, 1H), 2.90 (dd, J= 14.5Hz, J= 7.0Hz, 1H) ppm. ^{13}C NMR (125 MHz, D_2O): δ = 102.3, 102.1, 83.3, 81.6, 81.3, 73.5−72.3, 60.7, 41.7 (CH_2N) ppm.

C_2-βCD, C_6-βCD and C_{12}-βCD were obtained by following the procedure reported by Ohashi et al.,[44] with some modifications (Scheme 3.2a).

Tosyl-βCD (0.5 g; 0.39 mmol) was added in 1,2-ethylenediamine (5.8 mL) or 1,6-hexamethylenediamine (6 g) or 1,12-dodecanediamine (6 g) and stirred at 70 °C for 6 h. The unreacted diamine was removed washing several times with acetone and the obtained white powder was dissolved in a mixture of methanol:water (3:1) by heating and reprecipitation from acetone. The filtered product was washed with acetone to obtain a white solid (C_2-βCD, C_6-βCD and C_{12}-βCD). C_2-βCD: ^{1}H NMR (500 MHz, D_2O): δ = 5.09 (bs, 7H), 4.00-3.87 (m, 26H), 3.68-3.49 (m, 14H), 3.09-3.06 (m, 1H), 2.98-2.94 (m, 2H), 2.91-2.86 (m, 1H), 2.83-2.80 (m, 2H) ppm. ^{13}C NMR (125 MHz, D_2O): δ = 101.8, 101.5, 81.0, 80.9, 73.0, 72.9, 72.9, 72.0, 71.7, 71.7, 70.4, 60.2, 48.8, 38.7 ppm. C_6-βCD: ^{1}H NMR (400 MHz, D_2O): δ = 5.14 (d, J= 3.8Hz, 1H), 5.11-5.08 (m, 6H), 3.99-3.82 (m, 26H), 3.68-3.56 (m, 13H), 3.44 (t, J= 9.2Hz, 1H), 3.10 (bd, J= 12Hz, 1H), 2.93 (t, J=

8.0Hz, 2H), 2.80 (dd, J= 8.8Hz, J= 13.2Hz, 1H), 2.63 (bt, J= 7.6Hz, 2H), 1.69-1.60 (m, 2H), 1.55-1.45 (m, 2H), 1.29-1.45 (m, 4H) ppm. ^{13}C NMR (125 MHz, DMSO-d_6): δ =102.6, 102.4, 82.1, 73.5, 72.9, 72.5, 60.4, 50.0, 49.8, 41.4, 32.3, 30.0, 27.0, 26.6. ppm. C_{12}-βCD: ^{1}H NMR (500 MHz, D_2O): δ = 4.95 (bs, 7H), 3.79-3.55 (m, 26H), 3.51-3.42 (m, 12H), 3.23-3.21 (m, 1H), 2.98-2.94 (d, J= 14Hz, 1H), 2.85-2.77 (m, 2H), 2.63 (bt, J= 14Hz, 1H) ppm, 1.56-1.49 (m, 3H), 1.31-1.13 (m, 20H) ppm. ^{13}C NMR (125 MHz, D_2O): δ = 102.1, 101.9, 80.9, 73.3, 73.2, 72.0, 71.9, 71.7, 65.9, 59.7, 39.7, 39.6, 28.5, 28.4, 28.2, 28.1, 27.9, 27.7, 25.6, 14.0 ppm.

Synthesis and purification of GO-C_n- βCD

100 mg of GO were dispersed in 30 mL of deionized water:EtOH (1:1) and sonicated for 2 h, then a solution of C_0-βCD, C_2-βCD, C_6-βCD or C_{12}-βCD (200 mg in 100 mL of deionized water and EtOH in ratio 1:1) was added under vigorous stirring. The mixture was refluxed overnight, then the crude was purified by microfiltration on commercial Plasmart 100 modules (Medica s.p.a.) accordingly to previously reported procedures.[4] A total volume of about 1 L of water was required to purify the crude. The suspension was freeze-dried to obtain about 140 mg of GO-C_n-βCD (n=0, 2, 6, 12). The first control material (GO@βCD) was prepared with the same procedure using commercial βCD (without alkyl linker). The second control material (GO-control) was prepared under the same experimental conditions without the addition of βCD.

Characterization

ATR FT-IR spectra were recorded with Agilent Cary 630 FTIR Spectrophotometer, and the spectra are expressed by wavenumber (cm^{-1}). Thermogravimetric analysis were recorded with PerkinElmer Thermogravimetric Analyzer TGA 4000 by PerkinElmer, in air atmosphere, from 30 °C to 800 °C, with a scanning temperature of 10 °C/min. High-resolution XPS was performed using a Phoibos 100 hemispherical energy analyser, using Mg Kα radiation (ħω = 1˙253.6 eV; X-Ray power = 125 W) in constant analyser energy (CAE) mode, with analyser pass energies of 10 eV. Base pressure in the analysis chamber during analysis was $4.2x10^{-8}$ mbar. Spectra were fitted by using CasaXPS (www.casaxps.com) after Shirley background subtraction and all spectra were calibrated to the C1s binding energy (285.0 eV). XPS samples were tablet prepared from the dry powder of each material and fixing it on the sample holder by conductive carbon tape. Elemental analysis was performed on powder materials by using an

Elementar Unicube Elemental analyser, method GRAPHITE. ζ potential was measured in deionized water, using NanoBrook Omni Particle Size Analyzer. Scanning electron microscopy (SEM) analyses were performed with a ZEISS LEO 1530 FEG. The samples were deposited on a cleaned silicon wafer by dropping 10 µL of suspension at 0.05 mg/mL in dimethylformamide. The energy of electrons was 5 keV and the signal was acquired using an in Lens detector at a working distance of 3–5 mm. NMR spectra were recorded with a Varian Mercury 400 Spectrometer (400 MHz for ^{1}H-NMR and 100 MHz for ^{13}C-NMR spectra) and Agilent NMR Spectrometer 500 MHz (500 MHz for ^{1}H-NMR, and 125 MHz for ^{13}C-NMR spectra). The chemical shifts (δ) are reported in parts per million (ppm) referred to the signals of the residual solvents (^{1}H $CHCl_3$ = 7.26 ppm; DMSO = 2.48 ppm and H_2O = 4.79 ppm; ^{13}C $CHCl_3$ = 77.0 ppm and DMSO = 40.0 ppm). Coupling constants (J) are reported in Hz and multiplicity are named by the following abbreviations: singlet (s), doublet (d), double of doublets (dd), triplet (t), multiplet (m), broad (b).

Adsorption experiments

25 mg of powder materials (GO, GO-C_0-βCD, GO-C_2-βCD, GO-C_6-βCD, GO-C_{12}-βCD, GO@βCD) were sonicated in 10 mL of ultrapure water for 2 h to exfoliate the bulk material into monolayer nanosheets.[56] After sonication, tap water (15 mL) and PFBA (125 µL of a stock solution of 100 µg/L in MeOH) were added to the suspensions to obtain a final concentration of 0.5 µg/L in a final volume of 25 mL. For non-powder materials (i.e. GAC), 25 mg of samples were directly added to 25 mL of tap water and 125 µL of PFBA (100 µg/L in MeOH) to obtain a final concentration of 0.5 µg/L. Samples were then left under gentle agitation for 15 min, 4 h and 24 h, then each sample was centrifuged (10 min, 10˙000 rpm) and analyzed with UPLC-MS/MS.

PFAS adsorption test were performed using the same experimental conditions. Nine selected PFAS were added to the suspension to reach a final concentration of 0.5 µg/L of each contaminants and samples were left under gentle agitation for 15 min.

PFAS quantification

Samples containing PFAS were analyzed by UPLC-MS/MS (ACQUITY UPLC H-Class PLUS – XEVO TQS Micro mass detector, Waters). 1 mL samples were used as sources for the automated injection. The chromatographic separation was performed on a

reverse phase Waters Acquity UPLC CSH Phenyl-Hexyl (1.7 µm, 2.1x100 mm) column and Waters Isolator Column (2.1x50 mm). The column temperature was 34 °C, the flow rate 0.3 mL/min and the injection volume 40 µL, while the total run time was 8 min for PFBA and 21 min for the mixture of nine PFAS. The mobile phase consisted of a biphasic gradient, NH_4OAc 2 mM in a mixture of ultrapure water:methanol 95:5 as phase A, and NH_4OAc 2 mM in MeOH as phase B. The mobile phase composition varied according to the gradient program reported in Table 7.3-7.4, Appendix. Mass details and the transitions monitored are reported in Table 7.5-7.6, Appendix.

Molecular dynamics simulations

The model-systems representing GO-C_n-βCD (n = 0, 2, 6 and 12) were created on a pristine graphene sheet, generated by VMD, of dimensions 4 nm x 4 nm. Based on the atomic composition obtained by XPS, reported in Table 3.1, oxygen-containing groups (epoxy, hydroxyl, carbonyl and carboxyl) were randomly positioned on the surface, employing the GO-py program. PFAS, βCD, and GO-C_n-βCD were described by the General Amber Force Field (GAFF) force field. The atomic charges were obtained at AM1 level of theory. The systems were fully solvated using TIP3P water molecules, and counterions (necessary to neutralize the total charge of the complexes) were added. All the systems were initially minimized and equilibrated and then 100 ns MD simulations were carried out. Amber16 software was used to perform all the simulation herein reported. The affinities of the PFBA for βCD and GO-C_n-βCD were computed by the Molecular Mechanics-Generalized Born Surface Area (MM-GBSA) algorithm, as implemented in Amber16.

Author Contributions

F. Tunioli: Methodology, Investigation. T. D. Marforio: Investigation, Conceptualization. L. Favaretto: Methodology, Investigation. S. Mantovani: Methodology. A. Pintus: Methodology. A. Bianchi: Methodology, Investigation. A. Kovtun: Investigation, Formal analysis. M. Agnes: Investigation. V. Palermo: Conceptualization, Validation. M. Calvaresi: Investigation, Conceptualization. M. L. Navacchia: Investigation, Formal analysis. M. Melucci: Conceptualization, Validation, Writing – original draft.

Acknowledgements

The authors gratefully acknowledge the support of this work by the projects Life-Remembrance, ENV/IT/001001 Life Resource and Environment LIFE20 ‘Give plastic wastes from the production of hollow-fiber membranes a second life’, project 881603-GrapheneCore3-H2020-SGA-FET- SH1 Graphil- GRAPHENE-FLAGSHIP and PRIN 2017W8KNZW_002 'New Approaches in Nanocarbo-catalysis for organic transformations (NANO-CARBO-CAT)’.

3.1.5 References

1. Yap, P. L.; Nine, M. J.; Hassan, K.; Tung, T. T.; Tran, D. N. H.; Losic, D., Graphene-Based Sorbents for Multipollutants Removal in Water: A Review of Recent Progress. *Adv. Funct. Mater.* **2021,** *31* (9), 2007356.
2. Guo, S.; Garaj, S.; Bianco, A.; Ménard-Moyon, C. J. N. R. P., Controlling covalent chemistry on graphene oxide. **2022,** *4* (4), 247-262.
3. Mantovani, S.; Marforio, T. D.; Khaliha, S.; Pintus, A.; Kovtun, A.; Tunioli, F.; Favaretto, L.; Bianchi, A.; Navacchia, M. L.; Palermo, V.; Calvaresi, M.; Melucci, M., Amino acid-driven adsorption of emerging contaminants in water by modified graphene oxide nanosheets. *Environ. Sci.: Water Res. Technol* **2023,** *9*, 1030.
4. Mantovani, S.; Khaliha, S.; Marforio, T. D.; Kovtun, A.; Favaretto, L.; Tunioli, F.; Bianchi, A.; Petrone, G.; Liscio, A.; Palermo, V.; Calvaresi, M.; Navacchia, M. L.; Melucci, M., Facile high-yield synthesis and purification of lysine-modified graphene oxide for enhanced drinking water purification. *Chem Commun* **2022,** *58* (70), 9766-9769.
5. Wacławek, S.; Krawczyk, K.; Silvestri, D.; Padil, V. V. T.; Řezanka, M.; Černík, M.; Jaroniec, M., Cyclodextrin-based strategies for removal of persistent organic pollutants. *Adv. Colloid Interface Sci.* **2022,** *310*, 102807.
6. Tian, B.; Hua, S.; Tian, Y.; Liu, J., Cyclodextrin-based adsorbents for the removal of pollutants from wastewater: a review. *Environ. Sci. Pollut. Res.* **2021,** *28* (2), 1317-1340.
7. Liu, Q.; Zhou, Y.; Lu, J.; Zhou, Y., Novel cyclodextrin-based adsorbents for removing pollutants from wastewater: A critical review. *Chemosphere* **2020,** *241*, 125043.
8. Köse, K.; Tüysüz, M.; Aksüt, D.; Uzun, L., Modification of cyclodextrin and use in environmental applications. *Environ. Sci. Pollut. Res.* **2022,** *29* (1), 182-209.
9. Syeda, S. E. Z.; Nowacka, D.; Khan, M. S.; Skwierawska, A. M. Recent Advancements in Cyclodextrin-Based Adsorbents for the Removal of Hazardous Pollutants from Waters *Polymers* [Online], 2022, p. 2341.
10. Karoyo, A. H.; Wilson, L. D., Tunable macromolecular-based materials for the adsorption of perfluorooctanoic and octanoic acid anions. *J. Colloid Interface Sci.* **2013,** *402*, 196-203.
11. Takezawa, H.; Murase, T.; Resnati, G.; Metrangolo, P.; Fujita, M., Recognition of polyfluorinated compounds through self-aggregation in a cavity. *J. Am. Chem. Soc.* **2014,** *136* (5), 1786-1788.
12. Karoyo, A. H.; Wilson, L. D., Nano-sized cyclodextrin-based molecularly imprinted polymer adsorbents for perfluorinated compounds—A mini-review. *Nanomaterials* **2015,** *5* (2), 981-1003.
13. Yang, A.; Ching, C.; Easler, M.; Helbling, D. E.; Dichtel, W. R., Cyclodextrin polymers with nitrogen-containing tripodal crosslinkers for efficient PFAS adsorption. *ACS Materials Letters* **2020,** *2* (9), 1240-1245.
14. Weiss-Errico, M. J.; O'Shea, K. E., Enhanced host–guest complexation of short chain perfluoroalkyl substances with positively charged β-cyclodextrin derivatives. *J. Incl. Phenom. Macrocycl. Chem.* **2019,** *95* (1), 111-117.
15. Evich, M. G.; Davis, M. J. B.; McCord, J. P.; Acrey, B.; Awkerman, J. A.; Knappe, D. R. U.; Lindstrom, A. B.; Speth, T. F.; Tebes-Stevens, C.; Strynar, M. J.; Wang, Z.; Weber, E. J.; Henderson, W. M.; Washington, J. W., Per- and polyfluoroalkyl substances in the environment. *Science (New York, N.Y.)* **2022,** *375* (6580), eabg9065.

16. Kancharla, S.; Alexandridis, P.; Tsianou, M., Sequestration of per- and polyfluoroalkyl substances (PFAS) by adsorption: Surfactant and surface aspects. *Curr. Opin. Colloid Interface Sci.* **2022,** *58*, 101571.
17. Li, F.; Duan, J.; Tian, S.; Ji, H.; Zhu, Y.; Wei, Z.; Zhao, D., Short-chain per- and polyfluoroalkyl substances in aquatic systems: Occurrence, impacts and treatment. *Chem. Eng. J.* **2020,** *380*, 122506.
18. Lenka, S. P.; Kah, M.; Padhye, L. P., A review of the occurrence, transformation, and removal of poly- and perfluoroalkyl substances (PFAS) in wastewater treatment plants. *Water Res.* **2021,** *199*, 117187.
19. Thompson, J. T.; Chen, B.; Bowden, J. A.; Townsend, T. G., Per- and Polyfluoroalkyl Substances in Toilet Paper and the Impact on Wastewater Systems. *Env. Sci. Technol. Lett.* **2023,** *10* (3), 234-239.
20. Bertanza, G.; Capoferri, G. U.; Carmagnani, M.; Icarelli, F.; Sorlini, S.; Pedrazzani, R., Long-term investigation on the removal of perfluoroalkyl substances in a full-scale drinking water treatment plant in the Veneto Region, Italy. *Sci. Total Environ.* **2020,** *734*, 139154.
21. Pitter, G.; Re, F. D.; Canova, C.; Barbieri, G.; Jeddi, M. Z.; Daprà, F.; Manea, F.; Zolin, R.; Bettega, A. M.; Stopazzolo, G.; Vittorii, S.; Zambelli, L.; Martuzzi, M.; Mantoan, D.; Russo, F., Serum Levels of Perfluoroalkyl Substances (PFAS) in Adolescents and Young Adults Exposed to Contaminated Drinking Water in the Veneto Region, Italy: A Cross-Sectional Study Based on a Health Surveillance Program. *Environ. Health Perspect.* **2020,** *128* (2), 027007.
22. Mastrantonio, M.; Bai, E.; Uccelli, R.; Cordiano, V.; Screpanti, A.; Crosignani, P., Drinking water contamination from perfluoroalkyl substances (PFAS): an ecological mortality study in the Veneto Region, Italy. *Eur. J. Public Health* **2017,** *28* (1), 180-185.
23. Xu, Y.; Nielsen, C.; Li, Y.; Hammarstrand, S.; Andersson, E. M.; Li, H.; Olsson, D. S.; Engström, K.; Pineda, D.; Lindh, C. H.; Fletcher, T.; Jakobsson, K., Serum perfluoroalkyl substances in residents following long-term drinking water contamination from firefighting foam in Ronneby, Sweden. *Environ. Int.* **2021,** *147*, 106333.
24. Banzhaf, S.; Filipovic, M.; Lewis, J.; Sparrenbom, C. J.; Barthel, R., A review of contamination of surface-, ground-, and drinking water in Sweden by perfluoroalkyl and polyfluoroalkyl substances (PFASs). *Ambio* **2017,** *46* (3), 335-346.
25. Hölzer, J.; Göen, T.; Rauchfuss, K.; Kraft, M.; Angerer, J.; Kleeschulte, P.; Wilhelm, M., One-year follow-up of perfluorinated compounds in plasma of German residents from Arnsberg formerly exposed to PFOA-contaminated drinking water. *Int. J. Hyg. Environ. Health* **2009,** *212* (5), 499-504.
26. Takagi, S.; Adachi, F.; Miyano, K.; Koizumi, Y.; Tanaka, H.; Mimura, M.; Watanabe, I.; Tanabe, S.; Kannan, K., Perfluorooctanesulfonate and perfluorooctanoate in raw and treated tap water from Osaka, Japan. *Chemosphere* **2008,** *72* (10), 1409-1412.
27. Eschauzier, C.; Beerendonk, E.; Scholte-Veenendaal, P.; De Voogt, P., Impact of Treatment Processes on the Removal of Perfluoroalkyl Acids from the Drinking Water Production Chain. *Environ. Sci. Technol.* **2012,** *46* (3), 1708-1715.
28. Flores, C.; Ventura, F.; Martin-Alonso, J.; Caixach, J., Occurrence of perfluorooctane sulfonate (PFOS) and perfluorooctanoate (PFOA) in N.E. Spanish surface waters and their removal in a drinking water treatment plant that combines conventional and advanced treatments in parallel lines. *Sci. Total Environ.* **2013,** *461-462*, 618-626.
29. Gagliano, E.; Sgroi, M.; Falciglia, P. P.; Vagliasindi, F. G. A.; Roccaro, P., Removal of poly- and perfluoroalkyl substances (PFAS) from water by adsorption: Role

of PFAS chain length, effect of organic matter and challenges in adsorbent regeneration. *Water Res.* **2020,** *171*, 115381.
30. Du, Z.; Deng, S.; Bei, Y.; Huang, Q.; Wang, B.; Huang, J.; Yu, G., Adsorption behavior and mechanism of perfluorinated compounds on various adsorbents—A review. *J. Hazard. Mater.* **2014,** *274*, 443-454.
31. https://www.chemsafetypro.com/Topics/EU/REACH_Regulation_EC_No_1907_2006.html.
32. Yuan, J.; Mortazavian, S.; Passeport, E.; Hofmann, R., Evaluating perfluorooctanoic acid (PFOA) and perfluorooctanesulfonic acid (PFOS) removal across granular activated carbon (GAC) filter-adsorbers in drinking water treatment plants. *Sci. Total Environ.* **2022,** *838*, 156406.
33. Belkouteb, N.; Franke, V.; McCleaf, P.; Köhler, S.; Ahrens, L., Removal of per- and polyfluoroalkyl substances (PFASs) in a full-scale drinking water treatment plant: Long-term performance of granular activated carbon (GAC) and influence of flow-rate. *Water Res.* **2020,** *182*, 115913.
34. Baig, N.; Ihsanullah; Sajid, M.; Saleh, T. A., Graphene-based adsorbents for the removal of toxic organic pollutants: A review. *J. Environ. Manage.* **2019,** *244*, 370-382.
35. Ersan, G.; Apul, O. G.; Perreault, F.; Karanfil, T., Adsorption of organic contaminants by graphene nanosheets: A review. *Water Res.* **2017,** *126*, 385-398.
36. Khaliha, S.; Marforio, T. D.; Kovtun, A.; Mantovani, S.; Bianchi, A.; Luisa Navacchia, M.; Zambianchi, M.; Bocchi, L.; Boulanger, N.; Iakunkov, A.; Calvaresi, M.; Talyzin, A. V.; Palermo, V.; Melucci, M., Defective graphene nanosheets for drinking water purification: Adsorption mechanism, performance, and recovery. *FlatChem* **2021,** *29*, 100283.
37. Khaliha, S.; Bianchi, A.; Kovtun, A.; Tunioli, F.; Boschi, A.; Zambianchi, M.; Paci, D.; Bocchi, L.; Valsecchi, S.; Polesello, S.; Liscio, A.; Bergamini, M.; Brunetti, M.; Luisa Navacchia, M.; Palermo, V.; Melucci, M., Graphene oxide nanosheets for drinking water purification by tandem adsorption and microfiltration. *Sep. Purif. Technol.* **2022,** *300*, 121826.
38. Mantovani, S.; Khaliha, S.; Favaretto, L.; Bettini, C.; Bianchi, A.; Kovtun, A.; Zambianchi, M.; Gazzano, M.; Casentini, B.; Palermo, V.; Melucci, M., Scalable synthesis and purification of functionalized graphene nanosheets for water remediation. *Chem Commun* **2021,** *57* (31), 3765-3768.
39. Zambianchi, M.; Khaliha, S.; Bianchi, A.; Tunioli, F.; Kovtun, A.; Navacchia, M. L.; Salatino, A.; Xia, Z.; Briñas, E.; Vázquez, E.; Paci, D.; Palermo, V.; Bocchi, L.; Casentini, B.; Melucci, M., Graphene oxide-polysulfone hollow fibers membranes with synergic ultrafiltration and adsorption for enhanced drinking water treatment. *J. Membr. Sci.* **2022,** *658*, 120707.
40. Zambianchi, M.; Durso, M.; Liscio, A.; Treossi, E.; Bettini, C.; Capobianco, M. L.; Aluigi, A.; Kovtun, A.; Ruani, G.; Corticelli, F.; Brucale, M.; Palermo, V.; Navacchia, M. L.; Melucci, M., Graphene oxide doped polysulfone membrane adsorbers for the removal of organic contaminants from water. *J. Chem. Eng.* **2017,** *326*, 130-140.
41. Kovtun, A.; Bianchi, A.; Zambianchi, M.; Bettini, C.; Corticelli, F.; Ruani, G.; Bocchi, L.; Stante, F.; Gazzano, M.; Marforio, T. D.; Calvaresi, M.; Minelli, M.; Navacchia, M. L.; Palermo, V.; Melucci, M., Core-shell graphene oxide-polymer hollow fibers as water filters with enhanced performance and selectivity. *Faraday Discuss.* **2021,** *227*, 274-290.

42. Vacchi, I. A.; Spinato, C.; Raya, J.; Bianco, A.; Ménard-Moyon, C., Chemical reactivity of graphene oxide towards amines elucidated by solid-state NMR. *Nanoscale* **2016,** *8* (28), 13714-13721.
43. Bonnet, V.; Duval, R.; Tran, V.; Rabiller, C., Mono-N-glycosidation of β-Cyclodextrin − Synthesis of 6-(β-Cyclodextrinylamino)-6-deoxy-D-galactosides and of N-(6-Deoxy-β-cyclodextrinyl)galacto-azepane. *Eur. J. Org. Chem.* **2003,** *24*, 4810-4818.
44. Ohashi, H.; Hiraoka, Y.; Yamaguchi, T., An Autonomous Phase Transition−Complexation/Decomplexation Polymer System with a Molecular Recognition Property. *Macromolecules* **2006,** *39* (7), 2614-2620.
45. Fu, L.; Lai, G.; Yu, A., Preparation of β-cyclodextrin functionalized reduced graphene oxide: application for electrochemical determination of paracetamol. *RSC Advances* **2015,** *5* (94), 76973-76978.
46. Clark, M. B.; Gardella, J. A.; Schultz, T. M.; Patil, D. G.; Salvati, L., Solid-state analysis of eumelanin biopolymers by electron spectroscopy for chemical analysis. *Anal. Chem.* **1990,** *62* (9), 949-956.
47. Zangmeister, R. A.; Morris, T. A.; Tarlov, M. J., Characterization of polydopamine thin films deposited at short times by autoxidation of dopamine. *Langmuir* **2013,** *29* (27), 8619-28.
48. Artemenko, A.; Shchukarev, A.; Štenclová, P.; Wågberg, T.; Segervald, J.; Jia, X.; Kromka, A., Reference XPS spectra of amino acids. *IOP Conf. Ser.: Mater. Sci. Eng.* **2021,** *1050* (1), 012001.
49. Russat, J., Characterization of polyamic acid/polyimide films in the nanometric thickness range from spin-deposited polyamic acid. *Surf. Interface Anal.* **1988,** *11* (8), 414-420.
50. Liebscher, J.; Mrówczyński, R.; Scheidt, H. A.; Filip, C.; Hădade, N. D.; Turcu, R.; Bende, A.; Beck, S., Structure of polydopamine: a never-ending story? *Langmuir* **2013,** *29* (33), 10539-48.
51. Louette, P.; Bodino, F.; Pireaux, J.-J., Nylon 6 (N6) Reference XPS Reference Core Level and Energy Loss Spectra. *Surf. Sci. Spectra* **2006,** *12* (1), 12-17.
52. Shibuya, R.; Takeyasu, K.; Guo, D.; Kondo, T.; Nakamura, J., Chemisorption of CO2 on Nitrogen-Doped Graphitic Carbons. *Langmuir* **2022,** *38* (47), 14430-14438.
53. Wang, P.; Lu, Y.; Wang, T.; Zhu, Z.; Li, Q.; Meng, J.; Su, H.; Johnson, A. C.; Sweetman, A. J., Coupled production and emission of short chain perfluoroalkyl acids from a fast developing fluorochemical industry: Evidence from yearly and seasonal monitoring in Daling River Basin, China. *Environ.Pollut.* **2016,** *218*, 1234-1244.
54. Cao, X.; Wang, C.; Lu, Y.; Zhang, M.; Khan, K.; Song, S.; Wang, P.; Wang, C., Occurrence, sources and health risk of polyfluoroalkyl substances (PFASs) in soil, water and sediment from a drinking water source area. *Ecotoxicol. Environ. Saf.* **2019,** *174*, 208-217.
55. Karoyo, A. H.; Sidhu, P.; Wilson, L. D.; Hazendonk, P., Characterization and Dynamic Properties for the Solid Inclusion Complexes of β-Cyclodextrin and Perfluorooctanoic Acid. *J. Phys. Chem. B* **2013,** *117* (27), 8269-8282.
56. Liscio, A.; Kouroupis-Agalou, K.; Betriu, X. D.; Kovtun, A.; Treossi, E.; Pugno, N. M.; De Luca, G.; Giorgini, L.; Palermo, V., Evolution of the size and shape of 2D nanosheets during ultrasonic fragmentation. *2D Materials* **2017,** *4* (2), 025017.

4 Graphene-biopolymer composites for water treatments

As discussed in the introduction and in the first chapter, GO and, more broadly, GRM are highly effective sorbents when dispersed in water in the form of nanosheets. However, their use as nanomaterials presents challenges for practical applications and large-scale implementation. One key issue is that GRM need to be dispersed in water, often through processes like sonication, to maximize the contact surface area. Moreover, after the treatment process, the nanomaterials must be separated from the water, which typically requires expensive or complex techniques such as centrifugation or additional steps such as filtration.[1] To address these limitations, one approach is to embed the nanomaterials within a polymer matrix. This allows for partial exploitation of the GRM surface area while supporting them in a macroscopic structure. In this context, the use of biopolymers as a matrix to create GRM composites for water treatment has emerged as a widely explored and effective solution.[2-4]

During my PhD, various types of composites were prepared and studied, in collaboration with partner universities involved in European projects. Three examples of composites with distinct geometries are showed in Figure 4.1: planar membranes, cylindrical aerogels and hydrogel beads.

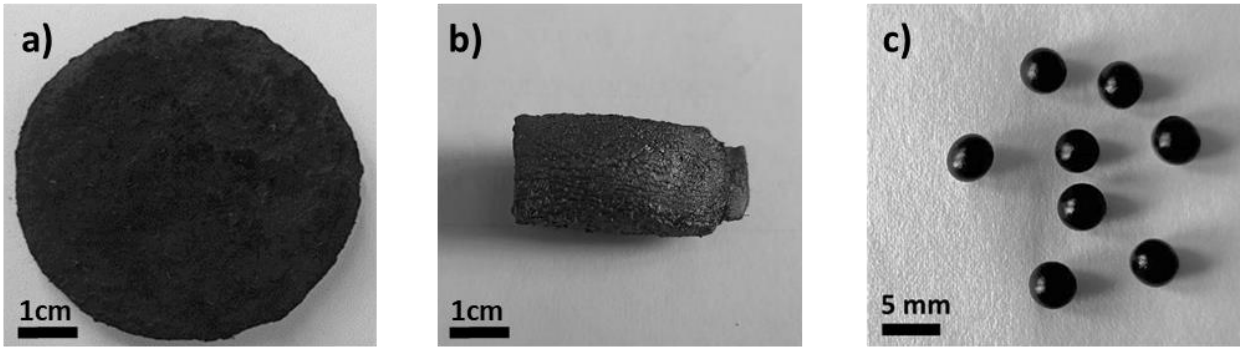

Figure 4.1 *Three composite structures with biopolymers and GRM: a) planar membranes, b) cylindrical aerogels, and c) hydrogel beads.*

In the case of planar membranes, prepared in collaboration with Sabanci University (Istanbul, Turkey), polycaprolactone (PCL) was selected as the biopolymer, while graphene nanoplatelets (GNP) derived from waste tires were used as the GRM. Briefly, an anisotropic 3D hybrid membrane was fabricated. This membrane consists of a salt-leached layer made from polymethyl methacrylate (PMMA) and PCL, covered by thin

PCL nanofibrous mats, both coated with GNP. The goal of this fabrication was to achieve a membrane with an optimal thickness. The salt leaching technique was developed to create a thick substrate, allowing for precise control over porosity by adjusting the quantity of leachable particles. Additionally, the pore size within the porous structure can be modified independently by using particles of different sizes. This method also enables the production of membranes with optimal thickness, well-defined pathways, and adjustable porosity, which together enhance the interaction between the membrane, the deposited GNP, and the wastewater during treatment. These membranes were then tested for the removal of OFLOX under flow conditions and compared with the pure polymer membranes. The results, shown in Figure 4.2, highlight the crucial role of the GRM in the adsorption process, which was absent in the pure polymer membranes. In addition, the results demonstrated the feasibility of using GRM composites under flow conditions. Studies on these planar membranes are ongoing and a paper on this topic is currently in press.

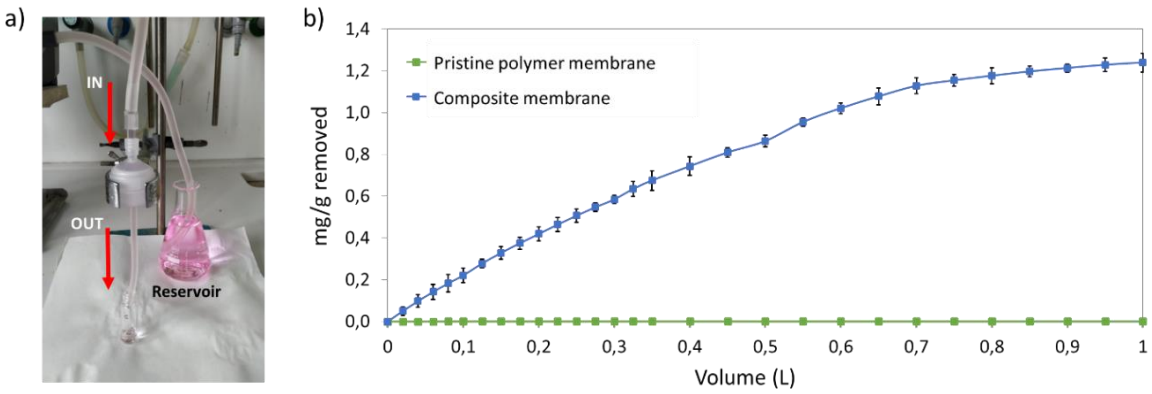

Figure 4.2 *Removal of OFLOX expressed in mg removed per g of membranes in flow condition (0.5 mg/L in tap water, Vtot = 1 L, flow rate = 2 mL/min) obtained by pristine polymer membrane (green), and composite membrane (blue).*

Regarding aerogels, several attempts were made in collaboration with the University of Patras (Greece). Initially, aerogels composed of polylactic acid (PLA) and graphene-related materials (GRM) were tested. In this approach, a suspension containing both components was treated with reducing agents (hypophosphorous acid (H_3PO_2) and iodine (I_2) of weight ratio GO:H_3PO_2:I_2 1:100:10) and then freeze-dried to obtain the composite aerogel. Unfortunately, this preparation method did not allow the polymer to act as a matrix, i.e. as the main component with the addition of GRM as a minority phase. The polymer did not homogenise with the other components, resulting in the formation of separate domains. Consequently, this technique was used to produce GRM-only

aerogels. Using the technique described above, aerogels of GO and GO+GNP (50/50 w/w) were prepared and tested in the removal of a mix of eight ECs in continuous conditions. The Figure 4.3 shows the average removal obtained after 100 mL of treated solution. GO aerogel (blue bars) showed low removal values (12-37%) for all the tested ECs with the exception of BP3, which is absorbed at 82%. GO+GNP aerogel (orange bars) showed increased adsorption capacity towards all ECs. The trend observed considering the removal percentage is also confirmed by the data expressed in mg removed/g of material. GO+GNP had shown an increase in absorption capacity of about 2.3 times the GO (5.54 *vs* 2.44 total mg removed/g of material). The superior performance of the GO+GNP aerogel versus the neat GO aerogel can be attributed to the higher obtained surface area, 27 instead of 16 m^2/g. In this case too, further studies on these aerogels are in progress and an article on this subject is currently in press.

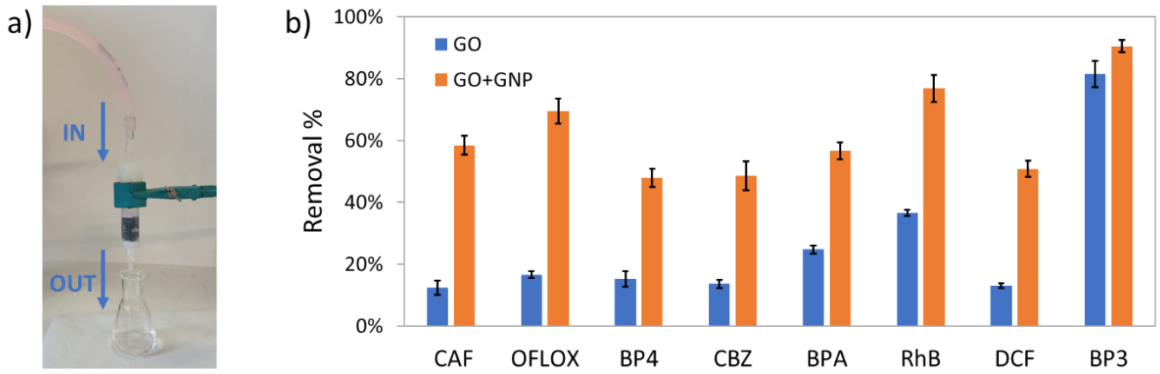

Figure 4.3 *Removal of a mixture of eight organic contaminants (0.5 mg/L each in tap water, Vtot = 100 mL, flow rate = 2 mL/min) by aerogels made by GO (blue) and GO+GNP (orange).*

During my PhD, my research group and I developed composites based on sodium alginate and different types of GRM, including GO-Lys, a modified GO presented in Chapter 3. The composites were prepared by an ion exchange process, resulting in hydrogel beads that were tested for the removal of ECs. This composite system has been extensively studied and the results are collected in the following paper.

4.1 Adsorption of emerging contaminants by graphene related materials and their alginate composite hydrogels

Adapted with permission from Journal of Environmental Chemical Engineering,11, 2023, 109566

DOI 10.1016/j.jece.2023.109566

Abstract

Graphene nanosheets and nanoplatelets were embedded in an alginate hydrogel and the resulting composite gel beads were exploited for the removal of a selected mixture of emerging contaminants (ECs) in tap water, including bisphenol A, ofloxacin and diclofenac. The role of graphene related materials (GRM) on the gel bead structure, adsorption selectivity, kinetic, mechanism, and efficiency was investigated. Combined scanning electron microscopy and confocal Raman microscopy mapping showed a porous structure with pore size in the range of 100-200 μm and a homogeneous distribution of graphene nanosheets or nanoplatelets at the pores surface. The adsorption kinetic of GRM was much faster than that of granular activated carbon (GAC), the industrial sorbent benchmark, with removal capacity of ofloxacin from 2.9 to 4.3 times higher. A maximum adsorption capacity of 178 mg/g for rhodamine B was estimated by adsorption isotherm studies for reduced graphene oxide-based beads (a value comparable to that of powered activated carbon). Regeneration test performed on saturated beads by washing with EtOH, and subsequent reiterated reuses, showed no loss of adsorption performance up to the fifth reuse cycle.

4.1.1 Introduction

The development of new materials and technologies for the removal of emerging contaminants (ECs) from drinking water is one of the current research priority to comply with the Sustainable Development Goal number 6 of the United Nations ‘Ensuring clean water and sanitation for all’, and to help water utilities and operators adopting the new European drinking water directive 2020/2184.[5, 6] ECs include thousands of products used for personal-health care (detergents, pharmaceuticals and cosmetics), and industrial uses (pesticides, plastic additives, etc.).[7, 8] The treatment of such contaminants generally relies on adsorption (i.e. on activated carbons), membrane filtration (i.e. ultrafiltration or reverse osmosis), or the combination of both technologies,

i.e. in domestic point-of-use systems.[9] Reverse osmosis (RO) is currently the most efficient technology for high-performance water purification and desalination, with almost quantitative removal for several classes of contaminants, but its use is bound to some main drawbacks, such as elevated energy consumption needed to force water through the membrane, rejection of the inlet water (still close to 50%), and production of concentrate retentates, which need further treatment or disposal.[10]

Adsorption through granular activated carbon (GAC) remains the most exploited strategy in potabilization plants, as last treatment step for the removal of trace contaminants before the final disinfection steps.[11] Integration of GAC with new, sustainable materials, with wider adsorption versatility toward organic and inorganic contaminants and increased capacity would be particularly advantageous for prolonging the GAC life-time or expanding the range of its applications.

Among carbonaceous nanomaterials, graphene and related materials (GRM) have the largest surface area and adsorption capacity and are commercially available at good and reproducible standard. Moreover, the tunable surface chemistry[12-18] and processability in 3D structures[19] make them particularly appealing for the development of advanced and multifunctional materials.[20-22] The use of nanosheets is the best option to exploit the whole adsorption potential of graphene, but it requires a further microfiltration step to retain the exhausted nanosheets from treated waters.[15, 23] Despite the increasing use of ultrafiltration and microfiltration in multi-train water treatments, the adjustment costs faced by drinking water treatment plants to implement adsorption and/or microfiltration treatments in drinking water production would be too demanding. The engineering of composites, such as membranes, foams, aero-hydrogels, based on porous polymers and GRM, appear as a more convenient and most ready-to-market alternative to exploit graphene in the water purification scenario.[24, 25]

We have recently reported on the development of polysulfone-graphene hollow fibers[26, 27] and granules,[28, 29] as well as on chitosan-graphene sponges, for the removal of ECs in drinking water and on the comparison of the adsorption mechanisms and performance between graphene embedding and graphene coating approaches.[30, 31] We demonstrated that in all of these composites, adsorption was enabled by the exposure of the graphene nanosheets to the contaminated water. Both of embedded and coated structures are active on the removal of different families of pollutants, such as organic

contaminants (ofloxacin, ciprofloxacin, bisphenol A, etc), heavy metals (Pb, Cr(III), Cu), and polyfluoroalkyl substances (PFAS). Notably, graphene-based composites showed adsorption capabilities comparable to or even higher than GAC. For example, polysulfone-graphene hollow fibers showed a performance from 3 to 7 times higher than GAC in the removal of PB, Cr(III), Cu, and short chain PFAS.

Here, we report on alginate graphene composite gel beads synthesized by ion exchange, embedding different types of GRM (Figure 4.4a), i.e. graphene oxide (GO), reduced graphene oxide (rGO), graphene nanoplatelets (GNP), and graphene oxide covalently modified with lysine (GO-Lys).[32, 33] Alginate is a low cost biopolymer with high processability, widely studied for realizing porous gel for adsorption studies.[34-36] On the other hand, the rationale behind GRM selection is their different surface chemistry that is expected to promote different contaminant-nanosheets interactions and the resulting final adsorption properties. GO and rGO have different oxidation ratios with consequent different number of oxygen groups (O/C=0.38 and 0.01, respectively, see Table 7.7, Appendix), and surface charge (-43.1±2.4 mV and -35.3±3.1 mV, respectively). GO-Lys has a more positive surface charge (-35.2±0.8 mV)[28] and slightly higher reduction rate than GO (O/C=0.17), while GNP have an even higher reduction degree (O/C=0.05) and a non-planar shape, with later size comparable to GO-based materials. Overall, these peculiarities are expected to influence the adsorption as well as the properties of their alginate composites. The resulting different surface charge, hydrophilicity and water dispersibility of the GRM are expected to lead to different composite structures (i.e. filler distribution, pore size), ultimately affecting the kinetic, selectivity, and capacity performance.

The alginate gel beads prepared by using the different GRM were used for the removal of a selection of eight organic contaminants (Figure 4.4b). It has been already demonstrated that the encapsulation of GO into a sodium alginate matrix has made the resulting composite material more porous and introduced stabilizing CO bonds between GO and alginate.[37] The adsorption of such composites of Cd (II), Cu (II) and Pb (II), and ciprofloxacin (CIPRO) from aqueous solutions by alginate-graphene beads has been demonstrated.[38-40] The tuning of GO amount as well as GO prefunctionalization was tested to enhance the adsorption capacity. On this line, M. Majdoub et al. showed that hexamethylenediamine (HMDA) covalent binding on GO led to remarkably high adsorption rates for Pb (II), Cu (II) and Cd (II), with only 15 wt% of GO-HMDA

incorporated into the alginate beads, in both single contaminant or mixture solutions in tap water.[39] Similarly, amino post-functionalization of alginate shell increased its maximum adsorption capacity (expressed in mg/g) by 130% and 182% towards Cu (II) and CIPRO, respectively.[41]

On this line, by a combined theoretical and experimental approach, we report on the investigation of the role of graphene type on the adsorption of several contaminants in their mixture. The removal of a mixture of emerging contaminants, in comparison to standard GAC, the regeneration and reuse of the presented composites are also discussed.

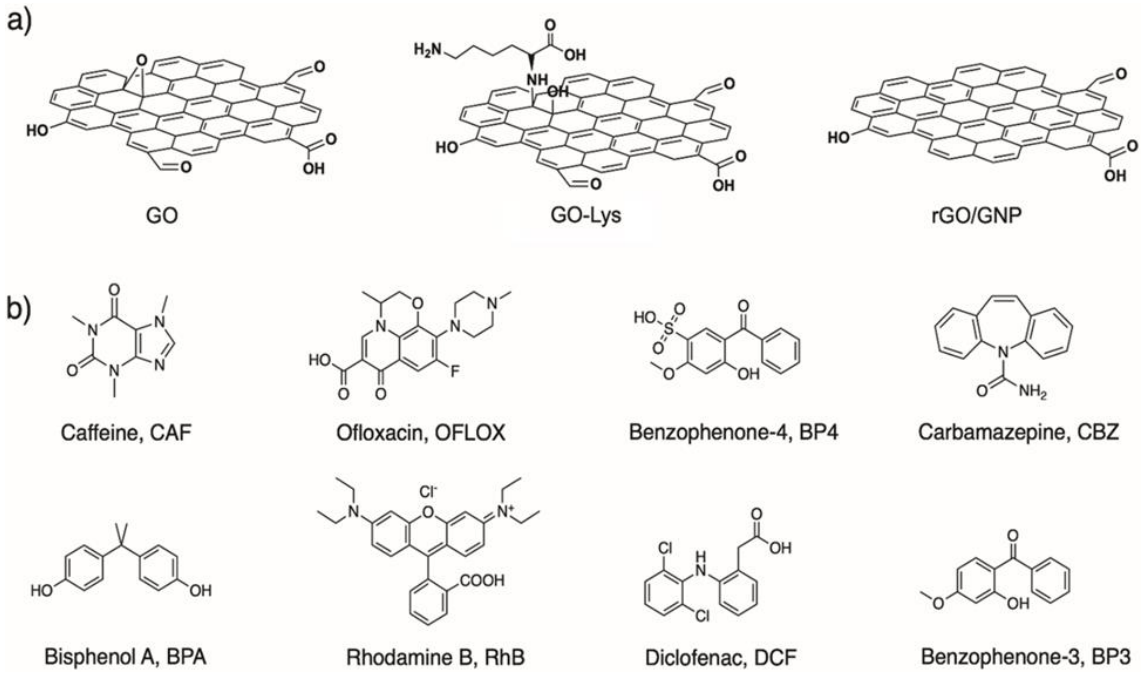

Figure 4.4 *a) Model of GRM used in this work, from left to right: graphene oxide (GO), GO covalently modified with lysine (GO-Lys), reduced graphene oxide (rGO) and graphene nanoplatelets (GNP); b) chemical structure of the selected emerging contaminants (ECs).*

4.1.2 Materials and methods

Materials

GO was purchase from LayerOne (Norway) and used without further purification (graphene oxide powder <35 mesh, product code 1.8). rGO was purchased from LayerOne and used without further purification (rGO powder, fully reduced, carbon content of about 98.5-99 wt%). GAC was purchased from CABOT Norit Spa (Ravenna, Italy, Norit GAC 830 AF, MB index min 240 mg/g, BET surface area >1000 m^2/g). Lysine-modified GO (GO-Lys) was synthesized by microwave-activated amination and purified

by an innovative microfiltration protocol.[28] GNP was obtained from pyrolyzed waste tires provided by NANOGRAFEN Co. (Gebze, Kocaeli, Turkey) and use without further purification. Further information about GRM are shown in Appendix (Table 7.7). All chemicals were purchased from Sigma-Aldrich in the highest available purity and were used without any further purification.

Preparation of alginate-graphene beads

Alginate-graphene beads were obtained by ion exchange, according to previously reported methods.[42] 100 mg of graphene related material (GO, rGO, GNP or GO-Lys) were dispersed in 50 mL of ultrapure water and then sonicated for 2 h. After that, 500 mg of sodium alginate were added to the suspension under magnetic stirring until a dense and homogeneous solution was obtained. The suspension was added dropwise into 150 mL of a 0.2 M $CaCl_2$ solution under gentle magnetic stirring and kept at room temperature for 12 h, to avoid beads aggregation. Finally, the hydrogel beads were washed 3 times with water and stored in ultrapure water at room temperature. The content of water was estimated by firstly weighting the beads (externally dried with filter paper), then drying them in the oven (80° C, 24 h) and weighting them once again.

Structure characterization

Chemical composition of GRM was studied by using X-ray photoelectron spectroscopy (XPS). High-resolution XPS was obtained by using a Phoibos 100 hemispherical energy analyser (Specs GmbH, Berlin, Germany) and Mg Kα photons (ħω = 1,253.6 eV; X-Ray power = 125W) in constant analyser energy mode, with analyser pass energies set to 10 eV. Overall resolution of 0.9 eV was measured on Ag 3d 5/2. Base pressure in the analysis chamber during analysis was 4.2x10-8 mbar. Spectra were fitted by using CasaXPS (www.casaxps.com) after Shirley background subtraction and all spectra were calibrated to the C 1s binding energy (285.0 eV). XPS samples were tablet composed by the dry powder of each material and grounded on the sample holder by conductive carbon tape. The morphology of alginate-graphene beads was studied by SEM after cryo-cutting. The samples were frozen in liquid nitrogen, cut, and then lyophilized to remove water and maintain the original morphology of the beads. The cross section was coated with gold (Lecia EM ACE600) and observed by SEM (JEOL JSM-7800F Prime) at an acceleration voltage of 8 kV. The GRM distribution inside the alginate matrix was studied by Raman confocal mapping performed on a confocal

Raman micro-spectroscope (Alpha300R, WITec, Germany). The light source used was a 532 nm laser with the output power of around 0.7 mW cm^{-2}. The diffraction grating of 600 g/mm was employed together with a 50x microscope objective. A 2 mm step size was used in the *x* and *y* direction for each Raman image with 0.5 s integration time and a spectral range from 0 to 3600 cm^{-1}.

Kinetic selectivity experiments

25 mg of powder materials (GO, rGO, GNP, GO-Lys) were sonicated in 5 mL of ultrapure water for 2 h. The resulting suspensions were added to 20 mL of the mixture of eight organic contaminants (final concentration 0.5 mg/L each in tap water). For non-powder materials (GAC, Alg, Alg-GO, Alg-rGO, Alg-GNP, Alg-GO-Lys), 25 mg of samples were added directly to 25 mL of the mixture of organic contaminants (concentration 0.5 mg/L each in tap water). Samples were then left in darkness under gentle agitation for 24 h. During this time, 200 µL withdrawals were collected after contact times of 15 min, 1 h, 4 h, and 24 h. Each sample was centrifugated (10 min, 10˙000 rpm) and analyzed with HPLC.

High performance liquid chromatography analyses

HPLC analyses of the selected mixture of eight contaminants were performed on a Dyonex Ultimate 3000 system equipped with a diode array detector. 200 µL samples were used as sources for the automated injection. The chromatographic separation was performed on a reverse phase Zorbax XDB-C8 column (4.6 × 150 mm^2, 5 µm) at flow rate of 1.0 mL/min, detection at λ_{max} of each analyte, linear gradient TFA 0.05% aqueous solution/acetonitrile from 80:20 to 0:100. In each experiment, the removal of each analyte was determined by comparison with that of the initial untreated solution. The results are expressed as the mean of two independent experiments ± SD.

Release test

The release test was performed on the alginate-graphene beads used for kinetic experiments. After adsorption, beads were externally dried on filter paper to remove excess water and placed in 25 mL of clean tap water. The samples were kept in darkness under gentle stirring. After 4 h, 200 µL of solution were withdrawn and analyzed by HPLC to check the possible release of the adsorbed contaminants.

Molecular dynamic simulations

A 40 Å × 40 Å graphene sheet was used to model GO, rGO and GO-Lys. The functional groups attached to the different graphene sheets (epoxy, hydroxyl, carbonyl, and carboxylic acid, lysine) were randomly positioned to reproduce the experimental XPS data. The GAFF force field[43] was used to parametrize BP4 and RhB molecules, and graphene nanosheets. QM calculations (HF/ 6-31G(d)), followed by RESP fitting provided the atomic charges of BP4 and RhB. All the simulations were carried out in an explicit solvent box (using the TIP3P water model). Counterions were added to neutralize the system. Molecular dynamic simulations (MD) were carried out using AMBER 16.[44] After equilibration, 100 ns MD simulations were produced. The binding affinity of BP4 and RhB to GO, rGO and GO-Lys were calculated by using the molecular mechanics–generalized Born surface area (MM-GBSA) method[45] extracting the snapshots from the MD trajectories.

Adsorption isotherms

The adsorption isotherms on different graphene powder materials and alginate-graphene beads were performed on rhodamine B (RhB) at a fixed amount of adsorbent material and by varying the contaminant concentration (see details in Appendix, Table 7.8-7.14). In a total volume of 5 mL of ultrapure water, RhB at different concentrations was added to the sorbent materials (powder materials were previously sonicated for 2 h in ultrapure water). The solutions were kept in darkness under gentle stirring for 24 h and then analyzed by UV-Vis spectroscopy (Agilent Cary 3500). Experimental data were fitted by Langmuir and BET models; the plots, the equation, and the R^2 are shown in the Appendix (Table 7.15,7.16, Figure 7.10). For BET model, the saturation concentrations (Cs) was optimized during the fit, selecting 1 mg/mL as the maximum value (maximum RhB solubility experimentally determined).

Regeneration test

Alginate-graphene beads (25 mg) were placed in 25 mL of an RhB solution (concentration 5 mg/L in tap water). Samples were kept in darkness under gentle stirring. After 24 h, the solutions were analyzed by UV-Vis spectroscopy. The same beads were externally dried on filter paper to remove excess water, placed in 25 mL of EtOH for 24 h and the solution analyzed by HPLC to check the possible release. The

beads were recollected and washed in water (25 mL, 30 min) and reused in a new adsorption step. The procedure adsorption-washing-reuse was repeated for four times.

4.1.3 Results and discussion

Preparation and characterization of alginate-graphene beads

The gel beads were prepared by ion exchange. Briefly, GO/GO-Lys/rGO/GNP powders were sonicated in ultrapure water, then sodium alginate was added in ratio 5:1 w/w (alginate:GRM) to the suspension, under magnetic stirring. The dense dispersion was added dropwise into a $CaCl_2$ solution and then left at room temperature, collected, washed, and stored in ultrapure water. The so obtained composites beads are shown in Figure 4.5.

A percentage of water (w/w) between 97-98% was estimated for all each type of bead (Alginate: 97.9%, Alg-GO: 97.2%, Alg-GO-Lys: 97.8%, Alg-rGO: 97.1%, Alg-GNP: 96.9%). The stability of the beads was proved by UV-Vis analysis of the suspensions at different aging times. After ten days, the suspensions were still clear (Figure 4.5c). UV-Vis analysis showed no evidence of signals deriving from nanosheets release. Figure 4.5d shows also the spectrum of a GO standard suspension at 2.5 mg/L, proving that release of GO nanosheets did not occur at this limit of detection.

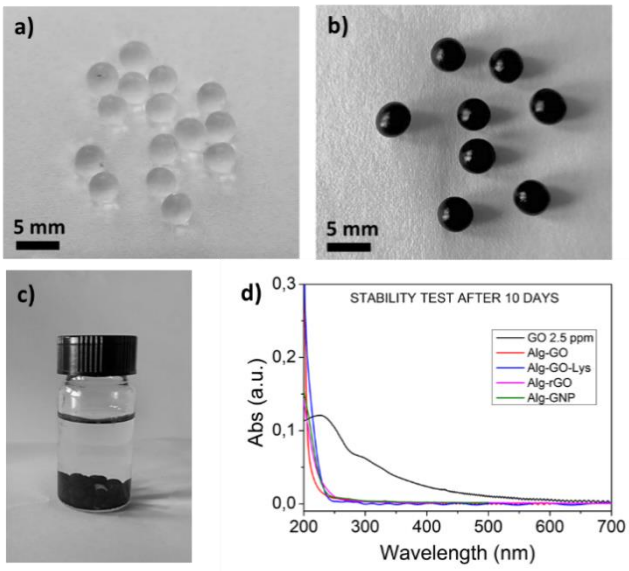

Figure 4.5 *a) Alginate beads and b) alginate-graphene beads; c) stability test of composite beads in mQ water and d) corresponding UV-Vis spectra of solution after 10 days, in comparison to the spectrum of a 2.5 mg/L GO suspension (black line).*

The chemical composition of GRM used in this work was studied by XPS and data are in agreement with previously reported ones.[32,46] The oxidation degree of the studied

materials (expressed as O/C) decreased in the following order: GO (0.38) > GO-Lys (0.17) > GNP (0.05) > rGO (0.01) (details in Table 7.7, Appendix).

The spatial distribution of GRM inside the composite beads, and their morphology, were studied by combining scanning electron microscopy (SEM) and Raman confocal mapping. For these analyses, gel beads were prepared by cryo-cutting. SEM analyses (Figure 4.6) of all samples showed the typical micrometric porous structure of alginate hydrogel with a dense skin layer.

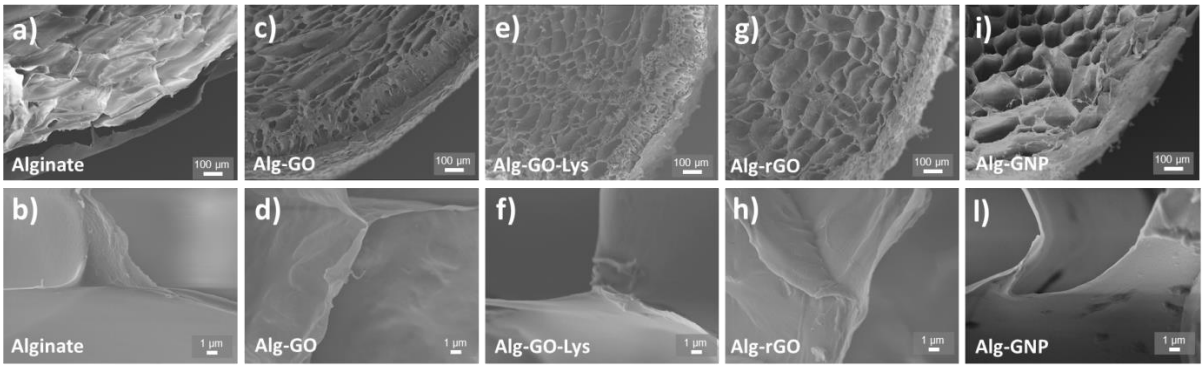

Figure 4.6 *Low and high magnification SEM cross-section images of a,b) alginate, c,d) Alg-GO, e,f) Alg-GO-Lys, g,h) Alg-rGO, i,l) Alg-GNP beads.*

Raman spectra of alginate and alginate-graphene beads are shown in Figure 4.7a. All samples containing GRM showed two characteristic peaks at 1350 and 1596 cm^{-1}, respectively the D band (defects and disorders) and the G band (pristine sp^2 carbon atoms). The G band did not overlap with other characteristic peaks of alginate (2937 cm^{-1}, 1414 cm^{-1}, 1093 cm^{-1}),[47] allowing the study of the GRM distribution inside alginate matrix by Raman mapping. Figure 4.7b-f shows the Raman 2D mapping and the relative optical images. As expected, pristine alginate samples did not show any G peak signal, due to the absence of GRM (Figure 4.7b). Alg-GO and Alg-GO-Lys showed an almost homogeneous distribution of GRM at the edges of pores section, evidence of success in embedding graphene in the alginate matrix. The Alg-rGO was still present along the whole edge, but in some part, as revealed by G signal near the edges, a broader spatial distribution was visible, suggesting the occurrence of aggregations. Among all of the GRM, GNP showed more inhomogeneous distribution inside Alg-GNP, with some regions with no signal at all and other with intense and large spots, showing sign of local agglomeration (Figure 4.7f) and the highest G peak intensity (1E4 CCD cts).

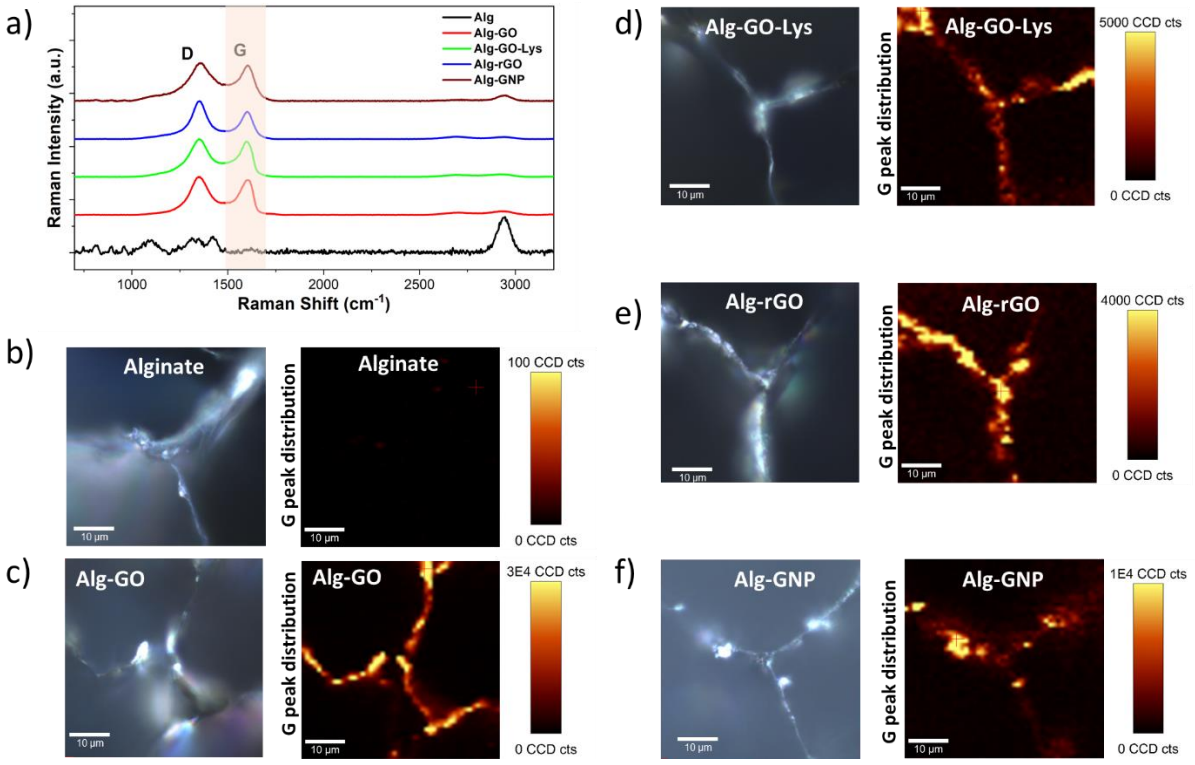

Figure 4.7 *a) Raman spectra of alginate and alginate-graphene beads; b-f) optical images and relative 2D Raman maps of used composites, constructed by using the G-band region.*

Kinetic, selectivity and release experiments

The removal performance of GRM and of alginate and alginate-graphene del beads toward the selected contaminant mixture at 15 min, 1 h, 4 h, and 24 h were studied. At each contact time, an aliquot of treated water was analyzed by HPLC and the results at 1 h and 24 h are shown in Figure 4.8 (data at 15 min and 4 h are reported in the Appendix, Figure 7.8). It can be seen that within the first hour of treatment rGO, GNP, and GO-Lys nanosheets outperformed GAC for almost all contaminants, with GAC becoming competitive only at 24 h (in the range 4-24 h, Figure 7.8b and Figure 4.8b). GO showed a lower performance than the other GRM for CAF, BP4, CBZ, BPA, and DCF. With the exception of CAF, the removal capability of GO remained almost unchanged for these compounds, even at equilibrium conditions (assumed here at 24 h).

Similar selectivity was observed for alginate beads (Figure 4.8c-d and Figure 7.8c-d), indicating that adsorption of the selected contaminants is mainly driven by GRM. Alginate showed almost negligible adsorption, while the performance of beads doped with GO, rGO, GNP, or GO-Lys increased with contact time. Alg-rGO and Alg-GO-Lys

showed high removal after 24 h, with values above 80% for all contaminants. Alg-GNP showed slightly lower adsorption, with removal values ranging between 60% and 99%. As for the free nanosheets, Alg-GO showed lower performances for CAF, BP4, CBZ, and BPA (removal in the range of 5-15%), while effectively removed the other contaminants. The kinetics of the beads was significantly slower than those of the pristine GRM. Indeed, for the composites, the equilibrium time ranges between 4 h and 24 h while for graphene nanosheets most of the adsorption occurred within the first hour and slight increase was found at 24 h. The exfoliated nanosheets expose their whole surface area and are fully available for adsorption. On the other hand, in the composite beads the graphene adsorption sites are distributed in the in-active alginate matrix, this lowering the accessibility of the molecules to the graphene sorption sites ultimately increasing the time required for the adsorption.

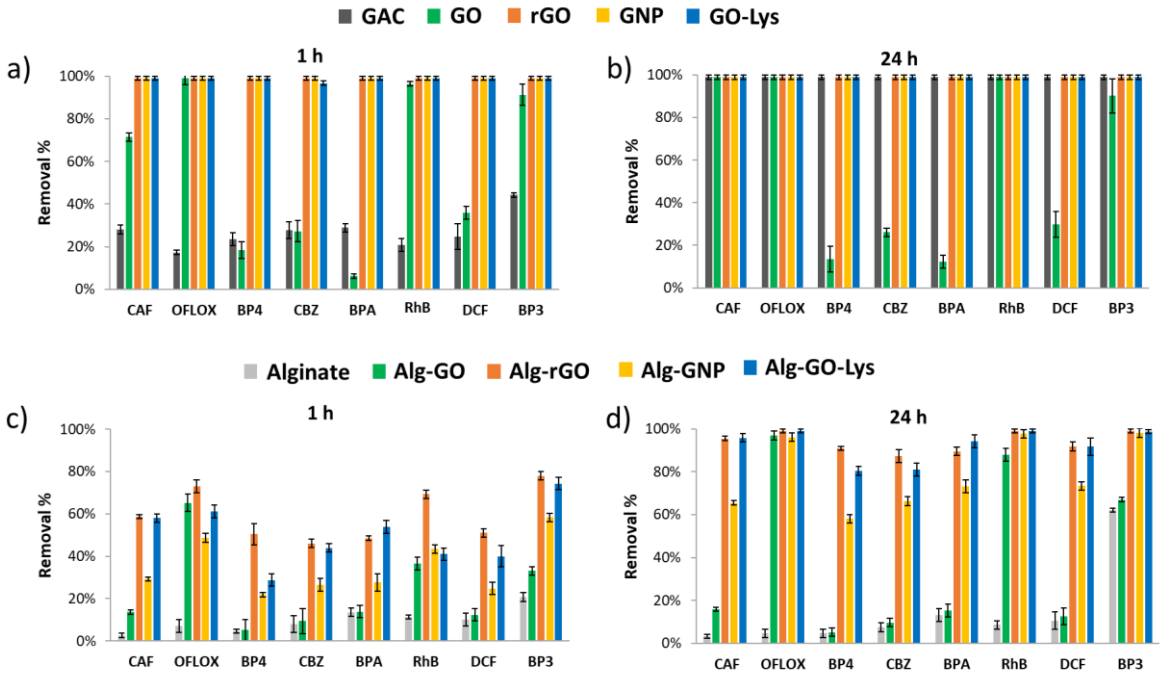

Figure 4.8 *Removal of ECs mix (0.5 mg/L each in tap water, Vtot= 25 mL, 25 mg of sorbent material). On the top, graphene nanosheets removal compared with GAC obtained after contact time of a) 1 h, and b) 24 h. On the bottom, alginate-graphene beds removal compared with pristine alginate beads after contact time of c) 1 h, and d) 24 h.*

The stability of the adsorption of all contaminants on GRM and on alginate composites were tested. To this aim, alginate-graphene gel beads used for the adsorption experiments, thus loaded with the contaminants, were washed and then left in fresh tap water for 4 h. Figure 7.9, reported in the Appendix, shows the ratio between mass adsorbed and released for each contaminant. For Alg-GO-Lys and Alg-rGO, the release

was below the limit of detection of the analytical method (~0.025 mg/L) for all contaminants. Only in the case of CBZ release of about 10% was found (Figure 7.9b-c). Similarly, Alg-GO showed release of CAF and BP3 of 77% and 8% respectively (Figure 7.9a). Alg-GNP showed the higher release with values up to 10-20% for CAF, BP4, CBZ and BPA (Figure 7.9d). Collectively these results highlighted a stable adsorption of almost all contaminants on alginate-graphene composites.

To gain an insight on the adsorption mechanisms driving the observed selectivity we performed molecular dynamic simulations (MD) on the adsorption of BP4 and RhB on GO, rGO and GO-Lys. RhB and BP4 contaminants were selected for their markedly different chemical features, i.e. BP4 is representative of bent shaped, small size and neutral molecule (CAF, CAF, BP4, CBZ, BPA, and DCF) while RhB is large sized, flat aromatic (as OFLOX) and amphiphilic molecule. The three sorbents were selected to unravel the different role of chemical surface groups (i.e. -OH, -COOH or NH_2 Lys pendant groups) on the adsorption of the contaminant molecules. Figure 4.9a shows representative snapshots from MD simulations of the favorite adsorption sites of BP4 and RhB on the GO, rGO and GO-Lys while the values of computed total binding affinity (E_{TOT}) are listed in Figure 4.9b.

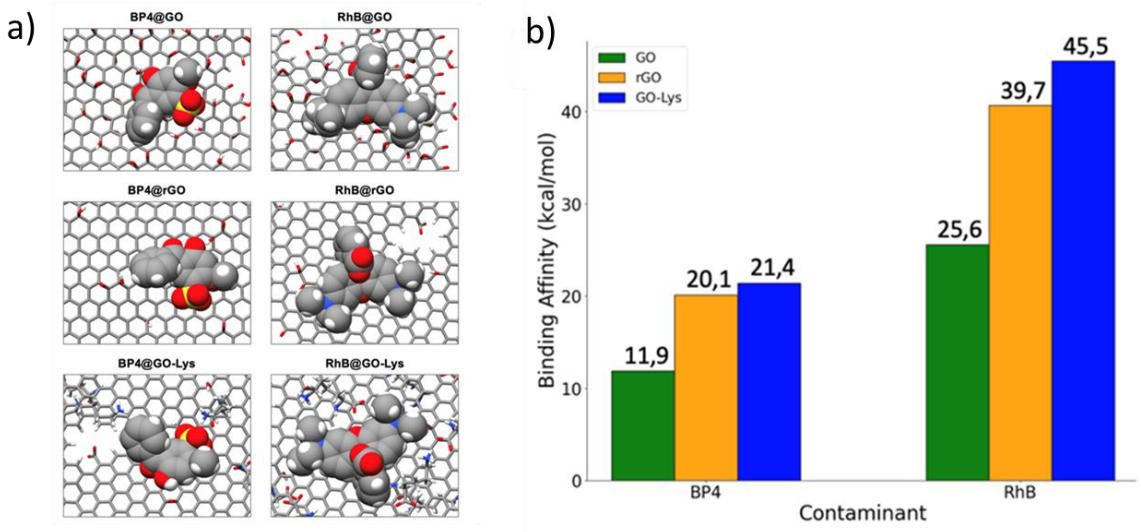

Figure 4.9 *a) Representative snapshots from MD simulations of the favorite adsorption sites of BP4 and RhB on the GO (top), rGO (in the middle) and GO-Lys (bottom); b) bar graph representation of the binding affinity for BP4 and RhB towards GO, rGO and GO-Lys. All energies are reported in kcal/mol.*

It is interesting to note that the lowest adsorption of BP4 by GO shown in Figure 4.8 corresponds to the lowest binding energy calculated by MD (Figure 4.9). The rough surface of GO, due to the surface oxygen groups likely minimize the interaction with

these contaminants and limits the adsorption affinity which increases in the case of rGO having smoother nanosheets surface than GO. In GO-Lys the Lys adsorption sites on the nanosheets increase the binding affinity with BP4 enhancing its removal capacity respect to pristine GO. For large molecules such as RhB, due to their large contact area, adsorption is efficient with all the typologies of the nanosheets. Collectively, the observed selectivity can be ascribed to the complex interplay of nanosheets exposed surface area (as shown by comparison GO vs rGO for BP4) and chemistry (as shown by the comparison GO vs GO-Lys for BP4).

Adsorption isotherms

The adsorption mechanisms and maximum monolayer capacity (Qm) of alginate-graphene beads were studied by adsorption isotherms experiments, which were carried out also for the pristine GRM on RhB (Figure 4.10, Figure 7.10 in the Appendix). RhB was selected as case study for its easy detection by UV-vis analysis and lowest limit of quantification respect to the other molecule and it allows the comparison of performance with respect to already reported materials. Adsorption isotherms were measured and fitted using two different models: i) Langmuir model, which describes an adsorption process with strong molecule-substrate interaction, where molecules are adsorbed in a single monolayer; and ii) Brunauer–Emmett–Teller (BET) model, describing a multilayer adsorption mechanism, where molecule-molecule interaction is comparable to the molecule-substrate one. It is notable that the adsorption of RhB on pristine nanosheets and composite beads were described by the same models, suggesting that the adsorption is driven by GRM, with a negligible role of alginate in molecule-substrate interaction. GO-Lys and GNP adsorption was described by Langmuir model while BET model explained the adsorption data of GO and rGO, reported in a previous work.[15]

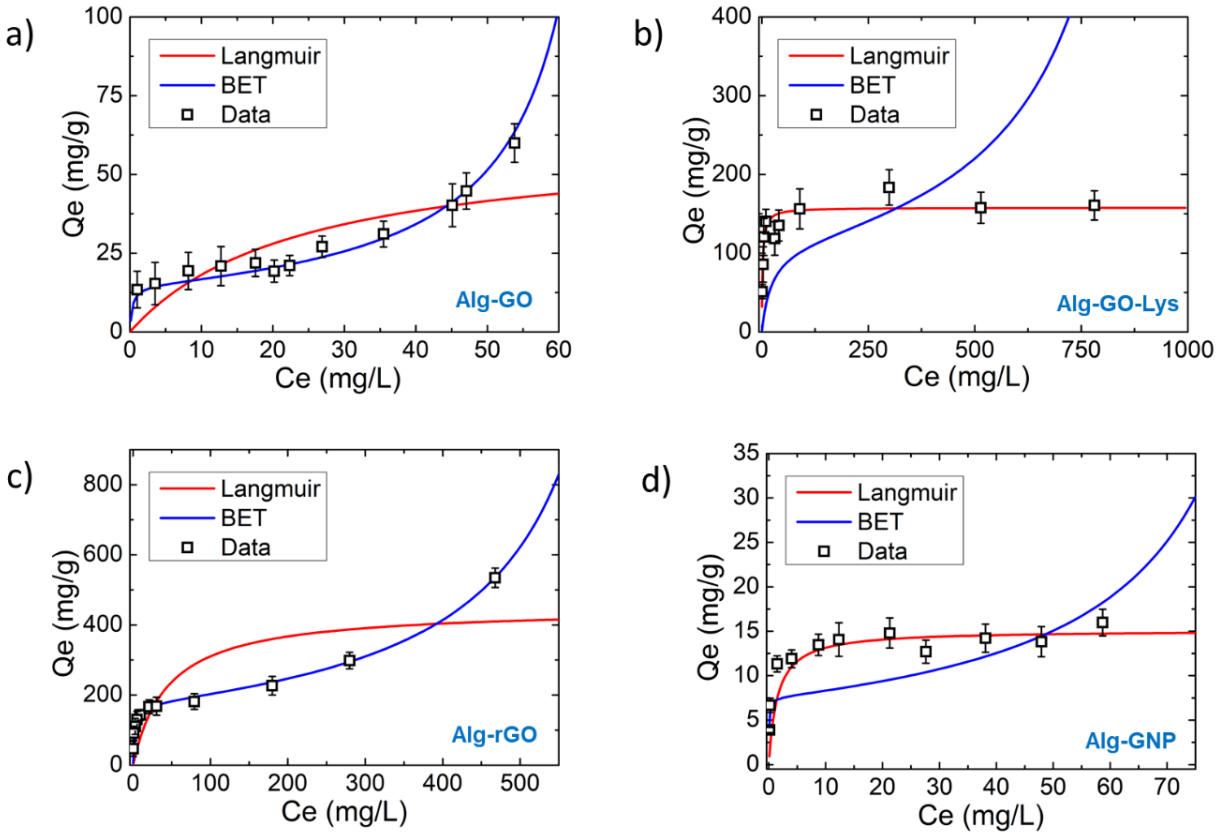

Figure 4.10 *Adsorption isotherm of a) Alg-GO, b) Alg-GO-Lys, c) Alg-rGO, d) Alg-GNP. (0.5 mg of sorbent, 24 h, 5 mL of RhB solution at different concentration). Data referred to GO-Lys and GNP nanosheets and pristine alginate beads are reported in the Appendix, Figure 7.10.*

The maximum monolayer adsorption capacity (Qm) was obtained from the above reported model. Remarkably, we observed that Qm increased with the oxidation degree of GRM (rGO: 220 mg/g < GO-Lys: 312 mg/g < GO: 439 mg/g, Table 4.1 and Table 7.7 in the Appendix). This trend can be explained in terms of the interplay between hydrophilicity and swelling, which influence the effective surface area available for adsorption. The driving force of the sorption for RhB on GRM are π-π interactions, which are deeply related to the accessible surface area of the 2D materials.[15] Oxidized and hydrophilic GRM (i.e. GO) swell in water, this increasing the nanosheets surface available for the adsorption of molecules at higher extent, with respect to hydrophobic materials, which are unable to swell. On the other hand, the relatively lower performance observed for GNP (68 mg/g) was ascribed to their poor water dispersibility, which causes aggregation. Moreover, GNP are a 3D structures formed by several layers of graphitic carbon, which cannot swell in water, contrarily to GO. This leads to a consequent physical lack of surface area exposed to the RhB molecules in water.

Table 4.1 *Maximum adsorption capacity (Qm) of RhB on different GRM and composite obtained from the fit of isotherms.*

Material	Qm (mg/g)		Model fitting
	Nanosheets	Beads	
GO	439*	15	BET
GO-Lys	312	158	Langmuir
rGO	220*	178	BET
GNP	68	15	Langmuir
Alginate	-	0.6	Langmuir

** Data for GO and rGO nanosheets were taken from a previous work.[15]*

The adsorption on beads showed an unexpected behavior since the Qm decreases with the oxidation degree for GO, GO-Lys, and rGO, contrarily to the increase observed for pristine nanosheets (Figure 4.11).

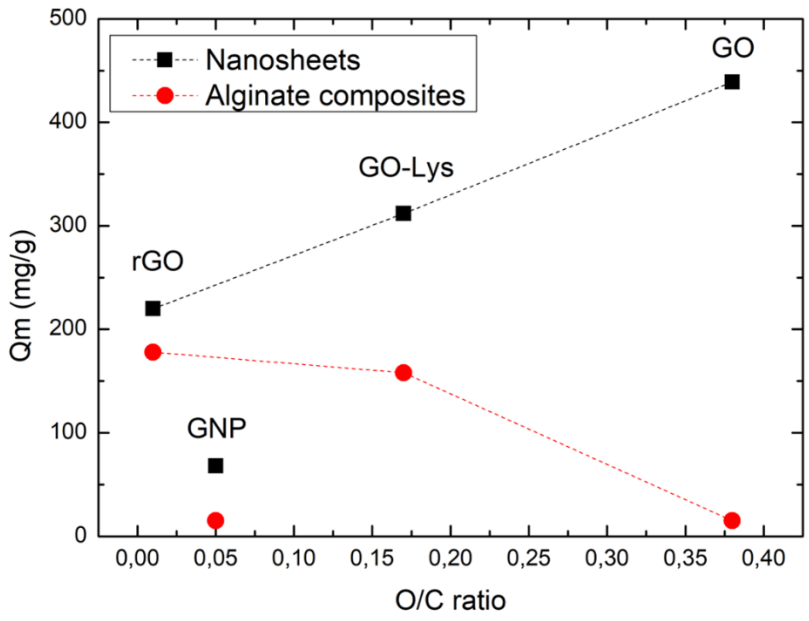

Figure 4.11 *Monolayer adsorption capacity (Qm) of RhB as a function of the oxidation degrees expressed as O/C ratio (rGO: 0.01, GNP: 0.05, GO-Lys: 0.75, GO: 0.38).*

This phenomenon could be related to the inner morphology of the beads and to the dispersion homogeneity of the GRM inside the alginate matrix. Thanks to its high hydrophilicity, GO was homogeneously incorporated in the alginate beads. In contrast, the more hydrophobic rGO nanosheets, were segregated at the composite edges during the bead formation (as confirmed by Raman 2D mapping showed in Figure 4.7). Figure

4.12 shows a sketch of the nanosheets distribution in the porous structure of the alginate matrix. GO is well dispersed inside the matrix, while rGO is aggregated at the pore edges. Therefore, in Alg-GO, the GO nanosheets exposed to the water-pore interface (i.e. the active ones) were less than those exposed by Alg-rGO beads. This explains the remarkably higher adsorption capacity of Alg-rGO, compared to Alg-GO (178 mg/g and 15 mg/g, respectively). Lower water solubility and exposed surface area can also explain the trend observed for Alg-GNP, having GNP a heterogeneous distribution on the alginate beads surface (see Figure 4.7f).

Nevertheless, the Qm values of Alg-rGO and Alg-GO-Lys (178 mg/g and 158 mg/g, respectively) are comparable to the values reported in literature for powder active carbon (Qm= 191 mg/g), the benchmark for dyes adsorption.[48] Moreover, comparing our composites with other materials proposed in literature for RhB adsorption, the Qm obtained from Alg-rGO and Alg-GO-Lys was one order of magnitude higher than nano Zn–Al–Fe_3O_4 blended alginate/Ca beads[49] (Qm=28 mg/g) and duolite C20 resin[50] (Qm=29 mg/g), and was comparable to the value obtained from an activated sugar-based carbon (Qm=123 mg/g).[51]

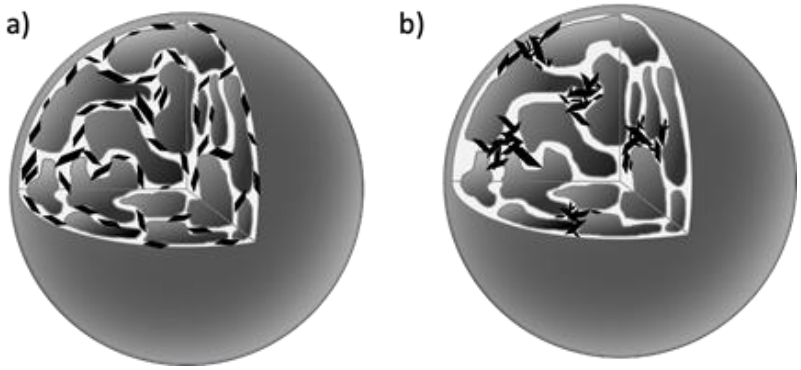

Figure 4.12 *Sketch of a) Alg-GO and b) Alg-rGO beads. The figure highlights the distribution of GO and rGO nanosheets in the porous structure of alginate matrix.*

Regeneration test

The possible regeneration and reuse of alginate-beads was tested on RhB removal. RhB was selected as case study because of its easy detection by UV-Vis spectroscopy. The initial concentration of RhB selected for this experiment was higher than the values expected in real polluted water matrix to allow fast saturation of the sorbents. Five consecutive cycles of RhB adsorption and desorption were performed, in both cases we studied the system once it has reached the equilibrium, while, for practical application,

we expect shortest contact time and reasonably lower performances. The removal efficiency of composite beads after each cycle is shown in Figure 4.13. Beads were placed in contact with a solution of RhB (5 mg/L in tap water) for 24 h, then EtOH was used to wash saturated beads and remove RhB. This cycle was repeated five times without any loss in removal efficiency and any damage on the gel beads structure. The control experiment, that consists only in a sequential use of beads with no use of EtOH, shows a monotonic decline of adsorption performances (see Figure 7.11 reported in the Appendix) after just few cycles in all alginate-graphene composites. Concluding, by observing in detail the trends in Figure 4.13, for Alg-GO and Alg-GNP the regeneration efficiency slowly decreases after each cycle, while the best performances was found for Alg-rGO and Alg-GO-Lys, that are always fully regenerated.

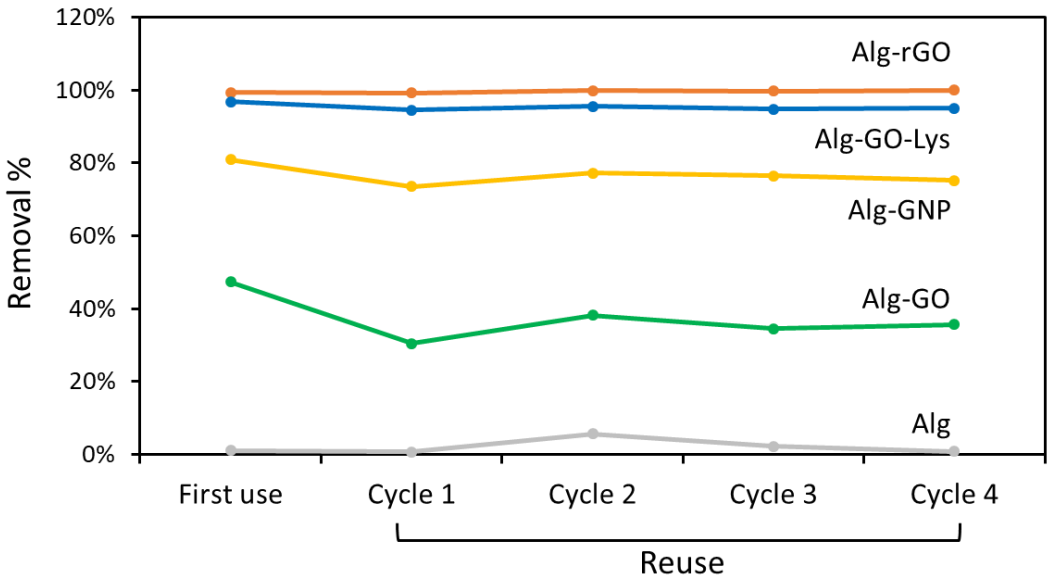

Figure 4.13 *Regeneration test on alginate and alginate-graphene beads. Each cycle includes an adsorption step (25 mg of beads, 25 mL of RhB, 5 mg/L in tap water, 24 h) and a desorption step (beads in 25 mL of EtOH, 24 h).*

4.1.4 Conclusions

In this work, four types of GRM (GO, GO-Lys, rGO, GNP) were effectively incorporated in alginate matrix to form porous composites for water remediation. Morphological characterization confirmed the successful retention of the alginate porous structure after GRM embedding with the nanomaterials exposed at the section edges of the pores. Efficient adsorption of all the eight tested contaminants with removal around 99% was observed for GO-Lys, rGO, GNP. On the other hand, GO showed high removal (99%) toward all contaminants except for bent shaped molecules (BP4, CBZ, BPA, and DCF)

which were removed with efficiency in the range 12-30%. Similar selectivity was found for the alginate composites with higher removal observed for OFLOX, RhB, and BP3 (removal up to 99%). The composite showed slower adsorption with respect to GRM likely due to the lowest active areas exposed by the composites respect to the free nanomaterials. Molecular modelling ascribed the observed selectivity to a complex interplay of molecules-graphene surface interactions with total energy binding values for large flat molecules such as RhB with respect to small and bent molecules such as BP4.

Remarkably, both GRM and alginate composites outperformed GAC after a contact time of 1 h, with removal up to 69% for Alg-rGO versus 21% for GAC toward RhB and up to 74% for Alg-GO versus 44% for GAC toward BP3. Adsorption efficiency was correlated to the oxidation degree of the 2D materials. Alg-GO-Lys and Alg-rGO were the most efficient sorbents for RhB (178 mg/g and 158 mg/g, respectively) taken as case study, with maximum adsorption capacity comparable to the value reported in literature for powder active carbon (190.84 mg/g), the benchmark for dyes adsorption. Moreover, the reusability of alginate-graphene beads after ethanol washing based regeneration was demonstrated.

Collectively, these results prove that the different GRM nanomaterials properties drive the adsorption selectivity and that the observed peculiarity are preserved also once the nanomaterials are embedded in the alginate gel matrix, this aiding the definition of guidelines for designing biopolymer-graphene nanomaterials composites for sustainable water treatment technologies.

Author Contributions

F. Tunioli: Methodology, Investigation. S. Khaliha: Methodology, Investigation. S. Mantovani: Methodology, Investigation. A. Bianchi: Methodology, Investigation. A. Kovtun: Investigation, Formal analysis. Z. Xia: Investigation. M. S. Sorayani Bafqi: Investigation. M. Calvaresi: Investigation, Conceptualization. T. D. Marforio: Investigation. B. Saner Okan: Investigation, Validation. V. Palermo: Conceptualization, Validation. M. L. Navacchia: Investigation, Formal analysis. M. Melucci: Conceptualization, Validation, Writing – original draft.

Acknowledgements

This work was supported by the EU-project 825207 ‘GO-FOR- WATER’.

4.1.5 References

1. Avornyo, A.; Chrysikopoulos, C. V., Applications of graphene oxide (GO) in oily wastewater treatment: Recent developments, challenges, and opportunities. *J. Environ. Manage.* **2024,** *353*, 120178.
2. Mansoori, S.; Davarnejad, R.; Matsuura, T.; Ismail, A. F. J. P. T., Membranes based on non-synthetic (natural) polymers for wastewater treatment. **2020,** *84*, 106381.
3. Matei, E.; Predescu, A. M.; Râpă, M.; Țurcanu, A. A.; Mateș, I.; Constantin, N.; Predescu, C. J. N., Natural polymers and their nanocomposites used for environmental applications. **2022,** *12* (10), 1707.
4. Xie, J. J. S., Application of Graphene Oxide–Natural Polymer Composite Adsorption Materials in Water Treatment. **2023,** *15* (9), 1678.
5. https://sdgs.un.org/goals.
6. https://ec.europa.eu/info/law/better-regulation/initiatives/com-2017-753_en.
7. Schulze, S.; Zahn, D.; Montes, R.; Rodil, R.; Quintana, J. B.; Knepper, T. P.; Reemtsma, T.; Berger, U., Occurrence of emerging persistent and mobile organic contaminants in European water samples. *Water Res.* **2019,** *153*, 80-90.
8. Richardson, S. D.; Ternes, T. A., Water Analysis: Emerging Contaminants and Current Issues. *Anal. Chem.* **2018,** *90* (1), 398-428.
9. van der Hoek, J. P.; Bertelkamp, C.; Verliefde, A. R. D.; Singhal, N., Drinking water treatment technologies in Europe: state of the art – challenges – research needs. *J. of Water Supply: Res. T.-Aqua* **2013,** *63* (2), 124-130.
10. Malaeb, L.; Ayoub, G. M., Reverse osmosis technology for water treatment: State of the art review. *Desalination* **2011,** *267* (1), 1-8.
11. Derbyshire, F.; Jagtoyen, M.; Andrews, R.; Rao, A.; Martin-Gullon, I.; Grulke, E., Carbon materials in environmental applications. *Chemistry and Physics of Carbon* **2000,** *27*, 1-66.
12. Melucci, M.; Treossi, E.; Ortolani, L.; Giambastiani, G.; Morandi, V.; Klar, P.; Casiraghi, C.; Samorì, P.; Palermo, V., Facile covalent functionalization of graphene oxide using microwaves: bottom-up development of functional graphitic materials. *J. Mater. Chem.* **2010,** *20* (41), 9052-9060.
13. Melucci, M.; Durso, M.; Zambianchi, M.; Treossi, E.; Xia, Z.-Y.; Manet, I.; Giambastiani, G.; Ortolani, L.; Morandi, V.; De Angelis, F.; Palermo, V., Graphene–organic hybrids as processable, tunable platforms for pH-dependent photoemission, obtained by a new modular approach. *J. Mater. Chem.* **2012,** *22* (35), 18237-18243.
14. Durso, M.; Borrachero-Conejo, A. I.; Bettini, C.; Treossi, E.; Scida, A.; Saracino, E.; Gazzano, M.; Christian, M.; Morandi, V.; Tuci, G.; Giambastiani, G.; Ottaviano, L.; Perrozzi, F.; Benfenati, V.; Melucci, M.; Palermo, V., Biomimetic graphene for enhanced interaction with the external membrane of astrocytes. *J. Mater. Chem. B* **2018,** *6* (33), 5335-5342.
15. Khaliha, S.; Marforio, T. D.; Kovtun, A.; Mantovani, S.; Bianchi, A.; Luisa Navacchia, M.; Zambianchi, M.; Bocchi, L.; Boulanger, N.; Iakunkov, A.; Calvaresi, M.; Talyzin, A. V.; Palermo, V.; Melucci, M., Defective graphene nanosheets for drinking water purification: Adsorption mechanism, performance, and recovery. *FlatChem* **2021,** *29*, 100283.
16. Mantovani, S.; Khaliha, S.; Favaretto, L.; Bettini, C.; Bianchi, A.; Kovtun, A.; Zambianchi, M.; Gazzano, M.; Casentini, B.; Palermo, V.; Melucci, M., Scalable synthesis and purification of functionalized graphene nanosheets for water remediation. *Chem Commun* **2021,** *57* (31), 3765-3768.

17. Lombardi, L.; Kovtun, A.; Mantovani, S.; Bertuzzi, G.; Favaretto, L.; Bettini, C.; Palermo, V.; Melucci, M.; Bandini, M., Visible-Light Assisted Covalent Surface Functionalization of Reduced Graphene Oxide Nanosheets with Arylazo Sulfones. *Chem. Eur. J.* **2022,** *28* (26).
18. Pintus, A.; Mantovani, S.; Kovtun, A.; Bertuzzi, G.; Bandini, M.; Melucci, M., Recyclable GO-Arginine Hybrids for CO2 Fixation into Cyclic Carbonates. *Chem. Eur. J.* (Acepted Author Manuscript).
19. Yousefi, N.; Lu, X.; Elimelech, M.; Tufenkji, N., Environmental performance of graphene-based 3D macrostructures. *Nat Nanotechnol* **2019,** *14* (2), 107-119.
20. Crini, G., Non-conventional low-cost adsorbents for dye removal: a review. *Bioresour. Technol.* **2006,** *97*, 1061-1085.
21. Perreault, F.; Fonseca de Faria, A.; Elimelech, M., Environmental applications of graphene-based nanomaterials. *Chem. Soc. Rev.* **2015,** *44* (16), 5861-5896.
22. Suárez-Iglesias, O.; Collado, S.; Oulego, P.; Díaz, M., Graphene-family nanomaterials in wastewater treatment plants. *J. Chem. Eng.* **2017,** *313*, 121-135.
23. Khaliha, S.; Bianchi, A.; Kovtun, A.; Tunioli, F.; Boschi, A.; Zambianchi, M.; Paci, D.; Bocchi, L.; Valsecchi, S.; Polesello, S.; Liscio, A.; Bergamini, M.; Brunetti, M.; Luisa Navacchia, M.; Palermo, V.; Melucci, M., Graphene oxide nanosheets for drinking water purification by tandem adsorption and microfiltration. *Sep. Purif. Technol.* **2022,** *300*, 121826.
24. Gandhi, M. R.; Vasudevan, S.; Shibayama, A.; Yamada, M., Graphene and Graphene-Based Composites: A Rising Star in Water Purification - A Comprehensive Overview. *ChemistrySelect* **2016,** *1* (15), 4358-4385.
25. Thakur, K.; Kandasubramanian, B., Graphene and Graphene Oxide-Based Composites for Removal of Organic Pollutants: A Review. *J. Chem. Eng. Data* **2019,** *64* (3), 833-867.
26. Zambianchi, M.; Durso, M.; Liscio, A.; Treossi, E.; Bettini, C.; Capobianco, M. L.; Aluigi, A.; Kovtun, A.; Ruani, G.; Corticelli, F.; Brucale, M.; Palermo, V.; Navacchia, M. L.; Melucci, M., Graphene oxide doped polysulfone membrane adsorbers for the removal of organic contaminants from water. *J. Chem. Eng.* **2017,** *326*, 130-140.
27. Zambianchi, M.; Khaliha, S.; Bianchi, A.; Tunioli, F.; Kovtun, A.; Navacchia, M. L.; Salatino, A.; Xia, Z.; Briñas, E.; Vázquez, E.; Paci, D.; Palermo, V.; Bocchi, L.; Casentini, B.; Melucci, M., Graphene oxide-polysulfone hollow fibers membranes with synergic ultrafiltration and adsorption for enhanced drinking water treatment. *J. Membr. Sci.* **2022,** *658*, 120707.
28. Zambianchi, M.; Aluigi, A.; Capobianco, M. L.; Corticelli, F.; Elmi, I.; Zampolli, S.; Stante, F.; Bocchi, L.; Belosi, F.; Navacchia, M. L.; Melucci, M., Polysulfone Hollow Porous Granules Prepared from Wastes of Ultrafiltration Membranes as Sustainable Adsorbent for Water and Air Remediation. *Adv. Sustain. Syst.* **2017,** *1* (7), 1700019.
29. Kovtun, A.; Zambianchi, M.; Bettini, C.; Liscio, A.; Gazzano, M.; Corticelli, F.; Treossi, E.; Navacchia, M. L.; Palermo, V.; Melucci, M., Graphene oxide-polysulfone filters for tap water purification, obtained by fast microwave oven treatment. *Nanoscale* **2019,** *11* (47), 22780-22787.
30. Kovtun, A.; Bianchi, A.; Zambianchi, M.; Bettini, C.; Corticelli, F.; Ruani, G.; Bocchi, L.; Stante, F.; Gazzano, M.; Marforio, T. D.; Calvaresi, M.; Minelli, M.; Navacchia, M. L.; Palermo, V.; Melucci, M., Core-shell graphene oxide-polymer hollow fibers as water filters with enhanced performance and selectivity. *Faraday Discuss.* **2021,** *227*, 274-290.
31. Kovtun, A.; Campodoni, E.; Favaretto, L.; Zambianchi, M.; Salatino, A.; Amalfitano, S.; Navacchia, M. L.; Casentini, B.; Palermo, V.; Sandri, M.; Melucci, M.,

Multifunctional graphene oxide/biopolymer composite aerogels for microcontaminants removal from drinking water. *Chemosphere* **2020,** *259*, 127501.
32. Mantovani, S.; Khaliha, S.; Marforio, T. D.; Kovtun, A.; Favaretto, L.; Tunioli, F.; Bianchi, A.; Petrone, G.; Liscio, A.; Palermo, V.; Calvaresi, M.; Navacchia, M. L.; Melucci, M., Facile high-yield synthesis and purification of lysine-modified graphene oxide for enhanced drinking water purification. *Chem Commun* **2022,** *58* (70), 9766-9769.
33. Mantovani, S.; Marforio, T. D.; Khaliha, S.; Pintus, A.; Kovtun, A.; Tunioli, F.; Favaretto, L.; Bianchi, A.; Navacchia, M. L.; Palermo, V.; Calvaresi, M.; Melucci, M., Amino acid-driven adsorption of emerging contaminants in water by modified graphene oxide nanosheets. *Environ. Sci.: Water Res. Technol* **2023,** *9*, 1030.
34. Zhao, H.; Ouyang, X.-K.; Yang, L.-Y., Adsorption of lead ions from aqueous solutions by porous cellulose nanofiber–sodium alginate hydrogel beads. *J. Mol. Liq.* **2021,** *324*, 115122.
35. Shen, J.; Xu, X.; Ouyang, X.-k.; Jin, M.-c., Adsorption of Pb(II) from Aqueous Solutions Using Nanocrystalline Cellulose/Sodium Alginate/K-Carrageenan Composite Hydrogel Beads. *J Polym Environ* **2022,** *30* (5), 1995-2006.
36. Fan, L.; Lu, Y.; Yang, L.-Y.; Huang, F.; Ouyang, X.-k., Fabrication of polyethylenimine-functionalized sodium alginate/cellulose nanocrystal/polyvinyl alcohol core–shell microspheres ((PVA/SA/CNC)@PEI) for diclofenac sodium adsorption. *J Colloid Interface Sci* **2019,** *554*, 48-58.
37. Platero, E.; Fernandez, M. E.; Bonelli, P. R.; Cukierman, A. L., Graphene oxide/alginate beads as adsorbents: Influence of the load and the drying method on their physicochemical-mechanical properties and adsorptive performance. *J Colloid Interface Sci* **2017,** *491*, 1-12.
38. Algothmi, W. M.; Bandaru, N. M.; Yu, Y.; Shapter, J. G.; Ellis, A. V., Alginate-graphene oxide hybrid gel beads: an efficient copper adsorbent material. *J Colloid Interface Sci* **2013,** *397*, 32-8.
39. Majdoub, M.; Amedlous, A.; Anfar, Z.; Jada, A.; El Alem, N., Engineering of amine-based binding chemistry on functionalized graphene oxide/alginate hybrids for simultaneous and efficient removal of trace heavy metals: Towards drinking water. *J Colloid Interface Sci* **2021,** *589*, 511-524.
40. Fei, Y.; Li, Y.; Han, S.; Ma, J., Adsorptive removal of ciprofloxacin by sodium alginate/graphene oxide composite beads from aqueous solution. *J Colloid Interface Sci* **2016,** *484*, 196-204.
41. Sun, Y.; Zhou, T.; Li, W.; Yu, F.; Ma, J., Amino-functionalized alginate/graphene double-network hydrogel beads for emerging contaminant removal from aqueous solution. *Chemosphere* **2020,** *241*, 125110.
42. Ajeel, S. J.; Beddai, A. A.; Almohaisen, A. M. N., Preparation of alginate/graphene oxide composite for methylene blue removal. *Mater. Today: Proc.* **2022,** *51*, 289-297.
43. Wang, J.; Wolf, R. M.; Caldwell, J. W.; Kollman, P. A.; Case, D. A., Development and testing of a general amber force field. *Journal of computational chemistry* **2004,** *25* (9), 1157-74.
44. D. A. Case, R. M., D. S. Cerutti, T. E. Cheatham III, T. A. Darden, R. E. Duke, T. J. Giese, H. Gohlke, A. W. Goetz, N. Homeyer, S. Izadi, P. Janowski, J. Kaus, A. Kovalenko, T. S. Lee, S. LeGrand, P. Li, C. Lin, T. Luchko, R. Luo, B. Madej, D. Mermelstein, K. M. Merz, G. Monard, H. Nguyen, H. T. Nguyen, I. Omelyan, A. Onufriev, D. R. Roe, A. Roitberg, C., Sagui, C. L. Simmerling, W. M. Botello-Smith, J. Swails, R.

C. Walker, J. Wang, R. M. Wolf, X. Wu, L. Xiao and P. A. Kollman, AMBER. **2016**, University of California, San Francisco.
45. Miller, B. R., III; McGee, T. D., Jr.; Swails, J. M.; Homeyer, N.; Gohlke, H.; Roitberg, A. E., MMPBSA.py: An Efficient Program for End-State Free Energy Calculations. *J. Chem. Theory Comput.* **2012,** *8* (9), 3314-3321.
46. Berktas, I.; Ghafar, A. N.; Fontana, P.; Caputcu, A.; Menceloglu, Y.; Okan, B. S., Facile Synthesis of Graphene from Waste Tire/Silica Hybrid Additives and Optimization Study for the Fabrication of Thermally Enhanced Cement Grouts. *Molecules* **2020,** *25* (4), 886.
47. Campos-Vallette, M. M.; Chandía, N. P.; Clavijo, E.; Leal, D.; Matsuhiro, B.; Osorio-Román, I. O.; Torres, S., Characterization of sodium alginate and its block fractions by surface-enhanced Raman spectroscopy. *J. Raman Spectrosc.* **2009**, n/a-n/a.
48. Liu, S.; Wang, Y.; Wang, B.; Huang, J.; Deng, S.; Yu, G., Regeneration of Rhodamine B saturated activated carbon by an electro-peroxone process. *J. Clean. Prod.* **2017,** *168*, 584-594.
49. Kumar, M.; Vijayakumar, G.; Tamilarasan, R., Synthesis, Characterization and Experimental Studies of Nano Zn–Al–Fe3O4 Blended Alginate/Ca Beads for the Adsorption of Rhodamin B. *J. Polym. Environ.* **2019,** *27* (1), 106-117.
50. Xiao, W.; Garba, Z. N.; Sun, S.; Lawan, I.; Wang, L.; Lin, M.; Yuan, Z., Preparation and evaluation of an effective activated carbon from white sugar for the adsorption of rhodamine B dye. *J. Clean. Prod.* **2020,** *253*, 119989.
51. Al-Rashed, S. M.; Al-Gaid, A. A., Kinetic and thermodynamic studies on the adsorption behavior of Rhodamine B dye on Duolite C-20 resin. *J. Saudi Chem. Soc.* **2012,** *16* (2), 209-215.

5 Graphene-synthetic polymer composites for water treatments

5.1 Graphene oxide-polysulfone hollow fibers membranes

As highlighted in the introduction, GRM, in particular GO, can be incorporated into polymeric matrices of synthetic origin. In POU systems, filtration systems based on polymeric membranes, either in planar form or as hollow fibers, are commonly used. These membranes work by blocking particles according to their pore size, making them highly effective in filtration applications.

The research group I joined for my PhD has established a long-term collaboration with Medica spa (Medolla, Italy), a company specialized in the production of filtration systems for the biomedical sector. Medica has extensive experience in the development of microfiltration devices (cut-off = 100-200 nm), based on polyethersulfone (PES) hollow fibre membranes, as well as ultrafiltration devices (cut-off = 20-50 nm), using polysulfone (PSU) hollow fibre membranes. Taking advantage of the knowledge of filter devices already on the market, the aim of the collaboration was to implement these filters by adding GO in the polymer matrix to obtain devices that can be used in water treatment. This collaboration led to a European project (Graphil) funded by the Graphene Flagship, and notably to prototype filters ready for commercialization.

Briefly, the proposed devices are polysulphone-graphene oxide hollow-fibre membranes (PSU-GO HFs) with simultaneous adsorption and ultrafiltration capabilities for POU drinking water purification.[1] The PSU-GO HFs were prepared by phase inversion extrusion in a customized semi-industrial plant and different GO:PSU ratio were studied (Figure 5.1).

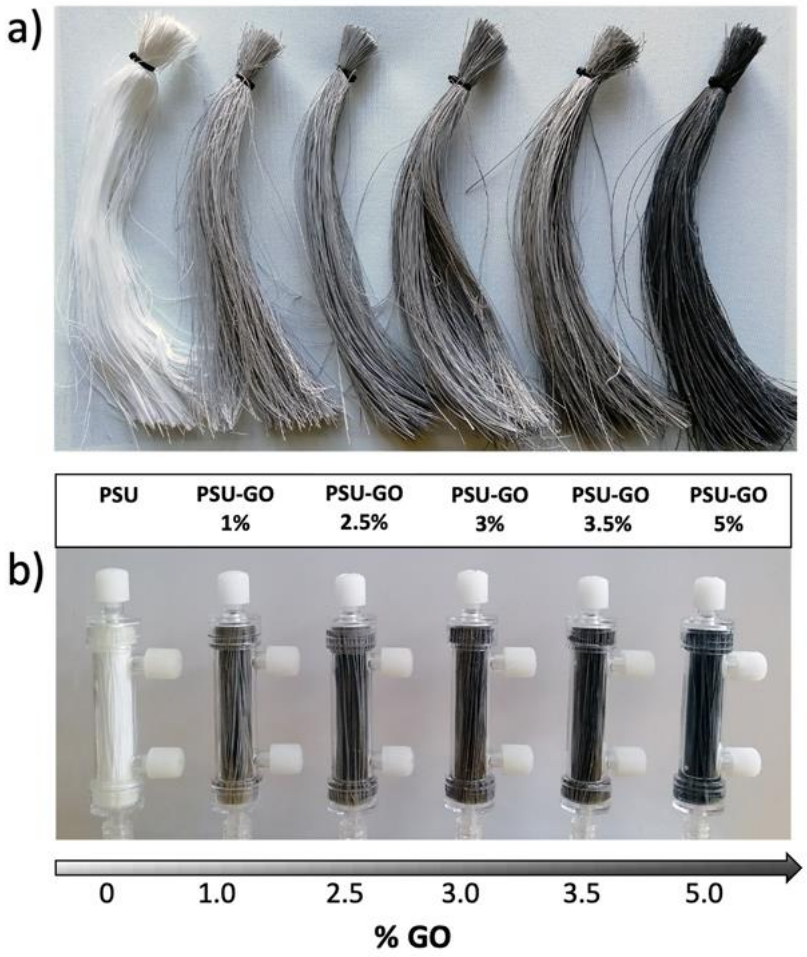

Figure 5.1 *a) PSU HFs and b) filtration modules, with different amounts of GO (w/ w). From left to right: pristine PSU; PSU-GO 1%; PSU-GO 2.5%; PSU-GO 3%; PSU-GO 3.5%; PSU-GO 5%.*

PSU-GO HFs modules preserve ultrafiltration properties of commercial PSU HF modules, but also exhibited the adsorption properties typical of GO nanosheets, which was demonstrated by studying the adsorption maximum capacity of ciprofloxacin antibiotic (CIPRO) vs GO ratio. Loading of 3.5% GO vs PSU was selected as case study, representing the best compromise between performance and GO nanofiller amount.

The removal of heavy metals (Pb, Cu and Cr(III)) and PFAS from tap water was competitive and in some cases exceeded that of granular activated carbon (GAC), the standard industrial sorbent (Figure 5.2). In addition, Surface Enhanced Raman Spectroscopy (SERS) analysis of the treated water excluded the release of GO from the PSU-GO modules in operation, with a limit of quantification of 0.1 μg/L for GO nanosheets.

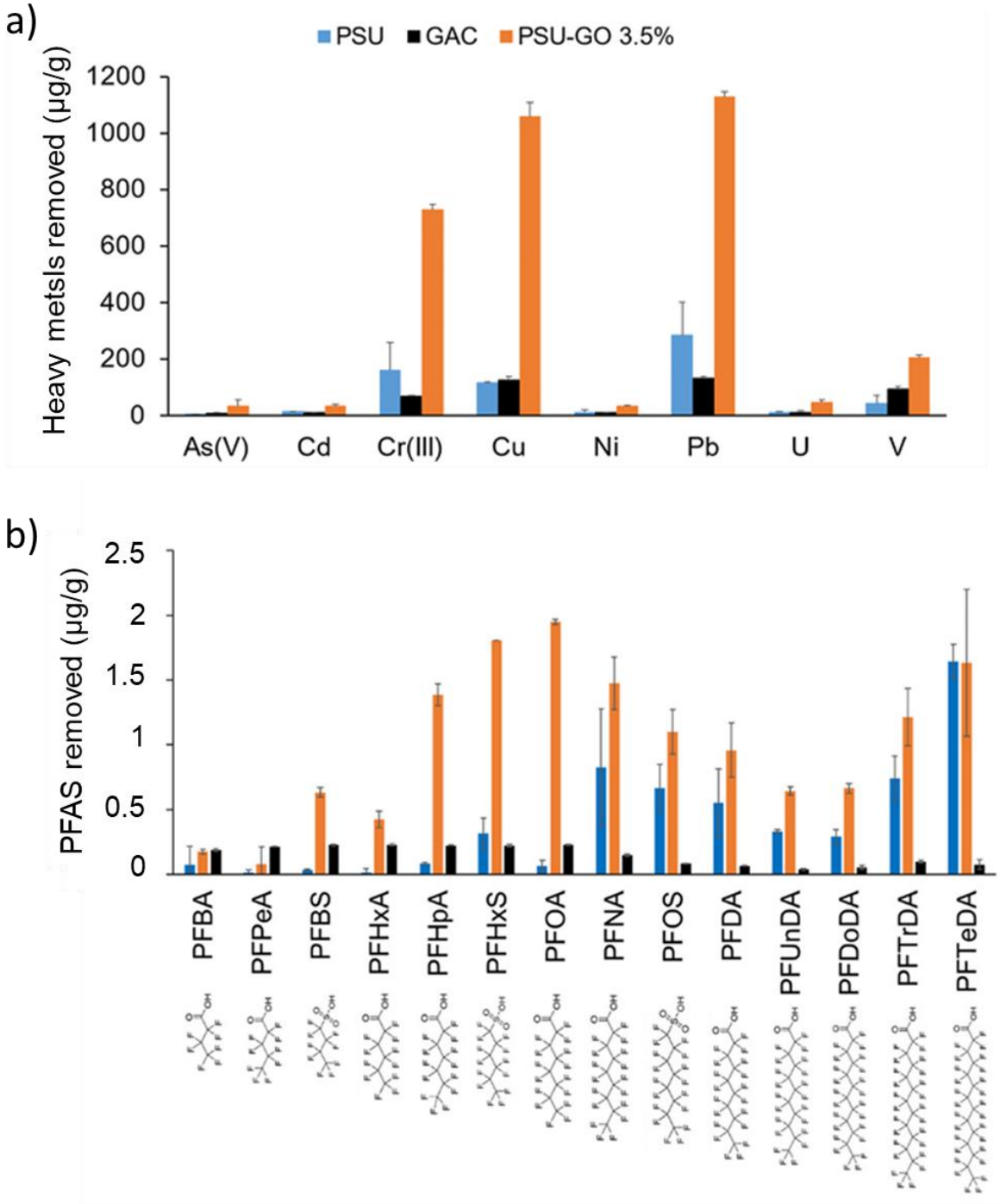

Figure 5.2 *Adsorption capacity (µg/g) towards a mixture of a) eight heavy metals and metalloids (flow rate = 5 mL/min, Vtot = 3 L, C_{IN} =100 µg/L each), and b) fourteen PFAS (flow rate = 5 mL/min, Vtot = 1 L, CIN =0.5 µg/L each) obtained by PSU HFs (blue), PSU-GO 3.5% HFs (orange) and GAC (black).*

More detailed information can be found in the full article (Khaliha et al).[1] Notably, this work has resulted in an innovative material (PSU-GO HFs) that acts simultaneously as a filter and a sorbent and has been commercialised as a POU device for water treatment.

However, the production of commercial PSU-HF and PSU-GO-HF cartridges requires a hot-wire cutting process to cut the as-spun hollow fibre bundle and adapt it to the size of the final cartridge. The process generates PSU-GO-HF scrap (about 10% of the total mass produced), which has to be disposed of, resulting in economic and environmental costs. To address this issue, the European project 'Life Remembrance' has been created to reduce waste and promote circular economy practices. The project aims to recycle PSU-GO-HF scraps by producing a high quality granular sorbents. This recycled material has been tested for the removal of different classes of ECs and the results are included in the following article.

5.2 Upcycling of plastic membrane industrial scraps and reuse as sorbent for emerging contaminants in water

Adapted with permission from Environmental Science Water Research & Technology, 10, 2024, 1097

DOI 10.1039/d3ew00900a

Abstract

Scraps obtained as waste of the industrial production of polysulfone (PSU) and polysulfone-graphene oxide hollow fiber membranes (PSU-HF and PSU-GO-HF, respectively) are converted into granular materials and used as sorbents for several classes of emerging and standard water contaminants, such as drugs, heavy metal ions and a mixture of per- and poly-fluoroalkyl substances (PFAS). The millimetric sized granules outperformed granular activated carbon (GAC), the industrial sorbent benchmark, in the adsorption of lead, diclofenac, and PFOA from tap water. Adsorption mechanism insight is achieved by molecular dynamic simulations, demonstrating the key role of graphene oxide (GO), on the adsorption selectivity and capacity. GO enables hydrophobic interactions with contaminant molecules promoting their adsorption on granules surface. Materials safety was assessed by surface enhanced Raman spectroscopy, excluding GO nanosheets leaching, and combined potability test. Overall, our work proves that scraps conversion and reuse it is a valuable strategy to reduce plastic industrial waste disposal and to integrate standard technology for enhanced water purification.

5.2.1 Introduction

The last seventy years have seen a fiftyfold increase in the production of chemicals, which is expected to triple again by 2050.[2] Such chemicals are applied in thousands of industrial and civil products, and it is extremely challenging to introduce safe and sustainable technologies for their removal from the environment. The saturation limit capacity for some of these chemicals (e.g. per- and poly-fluoroalkyl substances, PFAS) has already been reached,[3-5] calling for the urgent adoption of risk-mitigation actions and the development of new remediation strategies. Nowadays, great attention is focused on the removal of 'emerging contaminants' (ECs), *i.e.* pharmaceuticals, cosmetics, pesticides, from water sources. Adsorption on granular activated carbon (GAC) is the most exploited technology to remove ECs from water in potabilization plants[6, 7] and more than 5 million tons of GAC are produced annually for water treatment applications.[8] The environmental impact of GAC production, activation, transport, regeneration, and disposal is almost incalculable. Moreover, GAC shows poor adsorption performance for several classes of ECs, such as short chain PFAS and other small polar molecules, or metal and heavy metal ions.[9, 10] Finding alternative materials and strategies to replace GAC and to widen removal selectivity and efficiencies toward ECs is extremely challenging.

In the last decade, new materials and technologies, including biochar,[11] metal-organic frameworks[12] and graphene related nanomaterials,[13, 14] have been proposed as adsorbent materials of various class of contaminants with maximum adsorption capacity higher than those of GAC (i.e. for Ofloxacin antibiotic, 650 mg g_{GO}^{-1} vs 95 mg g_{GAC}^{-1}).[13]

Given the large global request of materials for water treatment, sustainability issues related to their production should be considered when proposing new solutions. In this respect, sorbents deriving from industrial wastes are particularly interesting. Due to their abundance and easy processability, plastic waste deriving from the production of polyethylene (PE), polypropylene (PP), polyvinylchloride (PVC), polystyrene (PS), and polyethylene terephthalate (PET) have been widely investigated. It has been shown that they can adsorb a wide range of pollutants, including toxic hydrophobic, persistent, and bio-accumulative substances, such as polycyclic aromatic hydrocarbons (PAHs), polychlorinated biphenyls (PCBs), dichloro-diphenyl-trichloroethanes (DDTs), heavy metals, and others.[15-17]

On this line, our group recently reported on the conversion of plastic waste deriving from the industrial production of polysulfone hollow fiber (PSU-HF) membranes into porous granules.[18] PSU-HF are the most exploited membranes for the production of ultrafiltration cartridges for biomedical filtration,[19] gas separation,[20] water disinfection,[21] and nanomaterials purification.[13, 22-26]

Their graphene oxide modified version (PSU-GO-HF, Medica Spa) has further expanded their application range to drinking water purification thanks to the simultaneous filtration and adsorption properties, enabled by GO nanosheets.[27, 28]

The production of commercial PSU-HF and PSU-GO-HF cartridges requires a hot-wire cutting process to cut the as-spun hollow fibers bundle to fit the final cartridge size (Figure 5.3a). The process originates PSU-GO-HF scraps (about 10% of the total mass produced, Figure 5.3b), which must be disposed, with consequent economic and environmental costs. It has been estimated that the current yearly production of hollow fiber membranes is approaching the hundreds of thousand tons scale and due to the increasing number of applications (*i.e.* ultrafiltration, membrane contactors, pervaporation, microfiltration, reverse osmosis, forward osmosis, pressure retarded osmosis, and many other liquid/liquid or liquid/solid separation), the hollow fiber membrane global market projections foresee an annual growth rate of 14.3% from 2023 to 2030, reaching USD 1.76 billion by 2030, meaning also a massive increase of the scraps byproducts.[29]

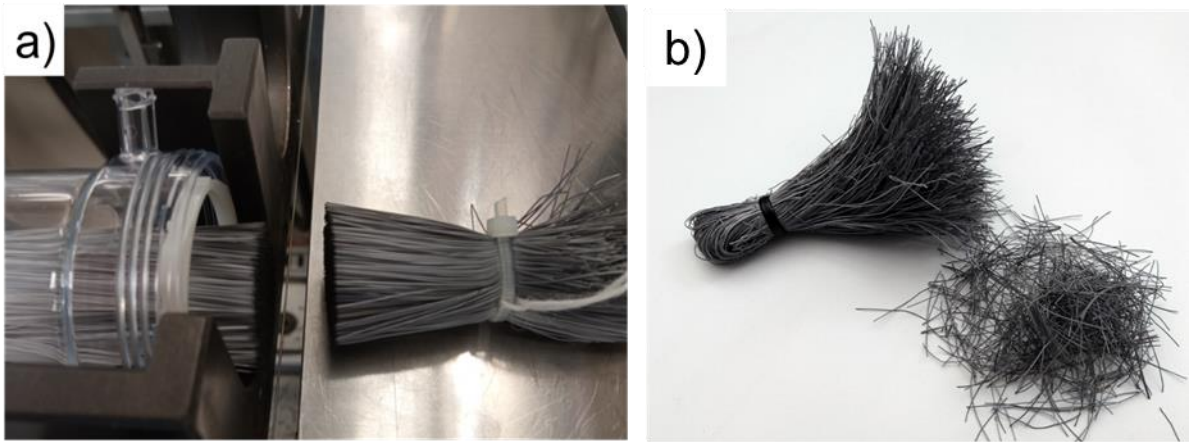

Figure 5.3 *a) Industrial hot-wire cutting of hollow fiber bundles, generating membrane scraps, b) PSU-GO-HF scraps. From Medica Spa production plant (SarMed Srl., IT).*

Here, we demonstrate that PSU-HF and PSU-GO-HF membrane scraps, from here named PSU and PSU-GO, can be converted into granular porous materials with

excellent adsorption capacity toward emerging contaminants, including PFAS and high potential for drinking water treatment. The selectivity of PSU and PSU-GO toward drugs (*i.e.,* ofloxacin, carbamazepine, and diclofenac),[30-32] PFAS (*i.e.* $(CF)_3$-$(CF)_{13}$, where $(CF)_n$ indicates the number of fluorinated carbons), [33-35] and heavy metals (*i.e.* U, V, Cr, As, Cu, and Pb),[36-38] chosen for environmental relevance[39], was studied. Moreover, adsorption capacity tests were performed on three selected contaminants of environmental concern, i.e. diclofenac (DCF),[30-32] perfluorooctanoic acid (PFOA)[33-35] and lead (Pb).[36-38] Production scale up allowing automatic grinding of scraps precursors is reported and allowed the validation of PSU and PSU-GO in standard sized commercial cartridges. Validation of such cartridges in real tap conditions in comparison to commercial standard technologies (GAC and hollow fibers ultrafiltration modules) was also performed.

5.2.2 Experimental

Material

Ofloxacin (OFLOX), diclofenac (DCF), benzophenone-4 (BP4), carbamazepine (CBZ), bisphenol A (BPA), benzophenone-3 (BP3), rhodamine B (RhB), and caffeine (CAF) were purchased from Sigma-Aldrich (DE) and used without further purification (Figure 4.3b). PFAS standard mixture (CH_3CN: H_2O 9:1, 200 µg mL^{-1}) were purchased from Agilent Technologies (Santa Clara, CA, USA) (Figure 7.12, Appendix). Ethanol absolute anhydrous was purchased from Carlo Erba Reagents (Val-de-Reuil, Cedex, FR). Metals salts were purchased by CPA chem Ltd. (BG) as $UO_2(OOCCH_3)_2$, NH_4VO_3, $Cr(NO_3)_3$, H_3AsO_4, $Cu(NO_3)_2$, $Pb(NO_3)_2$, $Cd(NO_3)_2$, Ni $(NO_3)_2$ in HNO_3 2% solution. Nitric acid (≥ 89.0%) was purchased from Honeywell (FR). Granular activated carbon (GAC) was purchased from CABOT Norit Spa (Ravenna, IT, Norit), product reference: GAC 830 AF (MB index min 240 mg g^{-1}, BET surface area > 1000 m^2 g^{-1}, details in Table 7.17, Appendix). To remove sub-millimetric particles, GAC was washed with deionized water at a mild flux, then dried overnight in an oven at 40 °C.

Preparation of PSU-GO granules and cartridges assembling

PSU and PSU-GO granules were prepared by manual or mechanical grinding of commercial PSU-HF and PSU-GO-HF, [7] coextruded with a 3.5% content of GO with respect to PSU weight (Figure 7.13, Appendix). [28] For mechanical grinding, a commercial blade grinder (Ceramic Instruments Srl, IT, sieve cut-off = 2 mm, Figure

7.28, Appendix), with a production capacity of 0.75 Kg h^{-1}, was used. Small prototype cartridges (14 mm diameter, 65 mm length, dead volume 6 mL, Empty Bed Contact Time (EBCT) = 0.5 min, bed volume = 0.01 L, Medica Spa, IT) were filled with PSU granules, PSU-GO granules, or GAC (Figure 7.14, Appendix). The final weight of material in the cartridges was 0.4 g for PSU, 0.73 g for PSU-GO, and 2.3 g for GAC. These cartridges were used for the lab scale test reported in Figure 5.5 and 5.7. For real conditions test (Figure 5.8), commercial standard sized and reusable cartridges (49 mm diameter, 250 mm length, dead volume 250 mL, EBCT = 0.14 min, bed volume = 0.5 L, Medica Spa, IT) were filled with 33 g of PSU-GO mechanical grinded granules or 33 g of PSU granules or 130 g of GAC (Figure 7.14, Appendix).

Characterization

Optical microscopy was performed using a Nikon DS-2Mv digital camera, mounted on a Nikon Eclipse 80i optical microscope (Nikon, Melville, NY, USA). Scanning electron microscopy (SEM) analyses were acquired with ZEISS LEO 1530 FEG. The energy of electrons was 5 keV and inLens detector at a working distance of 3-5 mm acquired the signal. Attenuated total reflection Fourier-transform infrared (ATR FT-IR) spectra were recorded with Agilent Cary 630 FTIR spectrophotometer and the spectra are expressed by wavenumber (cm^{-1}). Thermogravimetric analysis (TGA) has been investigated using a PerkinElmer TGA4000 apparatus in air atmosphere, from 30 °C to 800 °C, with a scanning temperature of 10 °C min^{-1}.

Adsorption bench-scale test

A tap water solution of eight heavy metals and metalloids (i.e. Pb, Cu, Cd, Ni, Cr(III), As(V), V, and U) at a final concentration of 100 µg L^{-1} each was prepared and then filtered on the cartridges using the filtration set up in Figure 7.15, Appendix. Samples were collected every 250 mL. Each fraction was immediately acidified with 1% HNO_3 and analyzed by ICP-MS. All the determinations were carried out with inductively coupled plasma triple quadrupole mass spectrometry (ICP-MS). A PerkinElmer NexION 1˙000 instrument was used for the analysis of the mixture of eight heavy metals and metalloids, and for loading curve experiments of lead. The operating conditions are listed below: nebulizer gas flow rates: 0.94 L min^{-1}; auxiliary gas flow: 1.2 L min^{-1}; plasma gas flow: 15 L min^{-1}; ICP RF power: 1˙600 W. Detection limit=1 µg L^{-1}.

A solution of eight emerging contaminants, including OFLOX, DCF, BP4, CBZ, BPA, BP3, RhB, and CAF (structures in Figure 4.3b), at 0.5 mg L^{-1} each, was prepared and then filtered. Samples were collected every 100 mL and analyzed by HPLC-UV. HPLC analyses of the selected emerging contaminants in mixture were performed on a Dyonex Ultimate 3˙000 system equipped with a diode array detector. 0.5 mL samples were used as sources for the automated injection. The chromatographic separation was performed on a reverse phase Zorbax XDB-C8 column (4.6 × 150 mm, 5 µm) at flow rate of 1.0 mL min^{-1}, detection at λ_{max} of each analyte, linear gradient TFA 0.05% aqueous solution/acetonitrile from 80:20 to 0:100. In every experiment, the removal of each analyte was determined by comparison with that of the initial untreated solution. The results are expressed as the mean of three independent experiments ± SD. Detection limit = 0.05 mg L^{-1}.

A solution of fourteen PFAS with alkyl chains in the range $(CF)_3$ – $(CF)_{13}$ (structures in Figure 7.12, Appendix) with concentration of 0.5 µg L^{-1} each in tap water was prepared and filtered on the tested cartridges. Samples were collected after 0.5 L and 1 L of filtration and analyzed by UPLC-MS/MS (Waters ACQUITY® UPLC H-Class PLUS – XEVO TQS Micro mass detector). UPLC-MS/MS analyses on PFAS were performed by using an UPLC-MS/MS Waters ACQUITY UPLC H-Class PLUS – XEVO TQS Micro mass detector. The chromatographic separation was performed on a reverse phase Waters Acquity UPLC CSH Phenyl-Hexyl (1.7µm, 2.1 x 100 mm) column and Waters Isolator Column (2.1 x 50 mm). The column temperature was 34 °C, the flow rate 0.3 mL min^{-1} and the injection volume 40 µL, while the total run time was 21 minutes for PFAS and 11 minutes for PFOA analyses. The mobile phase consists of a biphasic gradient, NH_4OAc 2 mM in a mixture of ultrapure water:methanol 95:5 as phase A, and NH_4OAc 2 mM in MeOH as phase B. The mobile phase composition varied according to the gradient program reported in Table 7.18 in the Appendix for PFAS and in Table 7.19 for PFOA analyses. Mass details and the transitions monitored for each analyte are reported in Table 7.20. The calibration curves were calculated by using the average value of 2 subsequent UPLC-MS/MS injections. Calibration curve solutions (0.01, 0.05, 0.1, 0.5, 1, 2.5 µg L^{-1}) were freshly prepared diluting methanolic PFAS stock solution with laboratory phase A and injected before each analytical batch. Regression equations of calibration curves were linear in the range of 2.5-0.01 or 0.05 or 0.1 µg L^{-1} depending on the analyte (see Table 7.20, LOQ). The results are expressed as the mean of 2 ±

SD. Laboratory drinking water was checked for PFAS contamination: no PFAS were detected above LOD value.

In each case, the total filtered volume of water was 1 L and samples were collected in polypropylene test tubes. Filtration on PSU, PSU-GO, and GAC small cartridges was carried out at a constant flow of 20 mL min^{-1}, corresponding to an EBCT = 0.5 min (set up in Figure 7.15, Appendix). New cartridges were used for each class of contaminants, and all tests were carried out in duplicate, with results reported as mean value with standard deviation.

Molecular dynamic modelling

The generalized AMBER force field (GAFF) [40] was used to parameterize PFAS molecules. Atomic charges were calculated at HF/6-31G(d) level, followed by restrained electrostatic potential (RESP) fitting. The model-systems representing GO was modelled on a 40 Å x 40 Å graphene sheet created with visual molecular dynamics (VMD) [41]. The epoxy, hydroxyl, carbonyl, and carboxylic acid groups were randomly positioned on graphene sheet to reproduce the experimental XPS data. The GAFF force field was also used to describe GO. In this case, the atomic charges were obtained by AM1 calculations. Each PFAS/GO complex was inserted into a box of TIP3P water molecules and counterions were added to neutralize the total charge. The resulting systems were minimized using a two-steps procedure employing Amber16 [42]. First, harmonic constraints (500 kcal mol^{-1} $Å^{-2}$) on the PFAS/GO complex, relaxing only the position of waters molecules and ions. Second, all the system is free to move. The resulting minimized structures were used as starting points for molecular dynamics simulations. An equilibration step of 10 ns was carried out gradually heating the system from 0 to 298 K, using an Andersen thermostat and periodic boundary conditions (PBC). Then 100 ns of molecular dynamics simulations were carried out (production runs). Molecular mechanics – generalized Born surface area (MM-GBSA) calculations were carried out to compute the binding affinity of PFAS to GO. For each calculation, 5˙000 frames were used, extracting the snapshots from the MD trajectories.

Bench-scale loading curves on DCF, PFOA, and Pb

Experiments were carried out by flowing the spiked tap water through PSU, PSU-GO, and GAC small cartridges (20 mL min^{-1}, EBCT = 0.5 min) and by sampling aliquots at

predefined intervals for further analyses and quantification of the contaminant. The experiments were carried out until cartridge saturation was reached (meaning when input concentration equals output concentration, $C_{IN} = C_{OUT}$) or until the removal was about 50% of the initial value. Filtration set up is reported in Figure 7.15 in the Appendix. The initial concentration was C_{IN} = 100 µg L^{-1} (Pb), 1 mg L^{-1} (DCF) and 1 µg L^{-1} (PFOA). The concentration was chosen as the lowest possible in accordance to our detection limits and in good correlation with the maximum concentration found in water (*i.e.*, 50 µg L^{-1} Pb,[43] 836 µg L^{-1} DCF[44] and 5-25 µg L^{-1} PFOA[45]). New cartridges were used for each contaminant, and all tests were carried out in duplicate, with results reported as mean value with standard deviation.

Cartridge integrity, regeneration and reuse

For GO leaching studies on PSU-GO cartridges, 5 L of ultrapure water were filtered at 100 mL min^{-1} and fractions were collected after each liter. Finally, 10 L were recirculated for 1 h at 100 mL min^{-1}. At the end of the experiment, 11 L of water were filtered. Samples were analyzed by surface-enhanced Raman spectroscopy (SERS). The preparation of the substrates for the SERS analysis was carried out according to the following steps: Si/SiO_2 substrate was placed on a heating plate at 50 °C. Then 20 µL of the AuNPs solution (10.7 nM) were added by drop casting and, finally, 1˙200 µL of the standard test or sample were added. The prepared substrates were analyzed by SERS using an InVia Renishaw microspectrometer equipped with a 532 nm point-based laser. The power density was set at 50 mW and an acquisition time of 1 s was employed for all measurements. 3˙000 points per substrate were measured and the 3˙000 spectra were averaged to give a single spectrum for each replica, using a program generated in MATLAB R2020a with our own code. The spectrum of AuNPs was used as a control and was subtracted in all the samples. Samples of treated water were analyzed in order to detect release of GO, using the methodology previously described.[46] This method allows the quantification of GO nanosheets in water using SERS. The intensity of the D-band is used as analytical signal (Figure 7.16, Appendix) and correlated with the concentration to obtain a calibration curve in the range 0.1-10.0 µg L^{-1}. The characteristic G band of GO cannot be used as analytical signal because of the interferences with the gold nanoparticle signal. No peaks around 1˙350 cm^{-1} were found in the Raman spectrum of PSU (Figure 7.17) and no interferences are observed. The practical limit of quantification of this methodology was 0.1µg L^{-1}. This value is defined

as the minimum amount of GO that can be measured with accuracy higher than 80% and relative standard deviation lower than 10%. Three replicates were carried out for each analyzed sample. Moreover, the relative standard deviation of the intensity values was calculated, for each sample (Table 7.20, Appendix).

The release of substances from the cartridges was studied flowing 1 L of fresh tap water in saturated cartridges at 20 mL min^{-1}. The final concentration of DCF, PFOA, and Pb was analyzed by UV–Vis, UPLC-MS/MS, and ICP-MS analyses, respectively.

Regeneration experiments were performed on a PSU-GO cartridges previously used for PFOA loading curve in Figure 5.7 and then washed by using ultrapure water/EtOH (1 L) at different ratio (70:30 → 50:50 →0:100 v/v)[35] that was flowed at 20 mL min^{-1}. After washing, a solution of PFOA (2 L, 1 µg L^{-1}) was flowed at 20 mL min^{-1}.

Release test of chromium from PSU-GO and PSU granules.

We studied the release of Cr in water from PSU and PSU-GO granules to exclude a significant presence of chromium caused by the blades during the grinding. 1 g of unwashed PSU granules was stirred in 200 mL of tap water for 3 days, then filtered on a mixed cellulose esters filter (cut-off 0.22 mm) to separate the granules from the aqueous phase. The latter was immediately acidified with 1% NHO_3 and analysed with an ICP-MS. The same procedure was performed on 1 g of PSU-GO granules.

Pilot-plant adsorption tests

Adsorption tests were performed on commercial standard sized cartridges already suitable for point-of-use applications and filled by PSU (33 g), PSU-GO (33 g), GAC (130 g) and on PSU-HF and PSU-GO-HF commercial ultrafiltration modules. Experiments were performed in dedicated automatized pilot (flow rate about 3 L min^{-1}, EBCT = 0.14 min, in non-continuous sampling mode). Tap water solution of Pb (C_{IN} = 30 µg L^{-1}) and PFOA (C_{IN} = 0.5 µg L^{-1}) were used. For each contaminant a new cartridge was used.

As shown in Figure 5.8a, the system comprises two tanks with a capacity of 100 L each (Namely tank “1”, on the left, and tank “2” on the right) allowing water circulation (with the chance of by-passing the filter under test), and it is connected to the tap with a pump driving water into the first tank. Pressurization is controlled by a valve, and the inlet pressure was maintained at a constant 2 bars to represent average tap pressure.

The pilot system includes flow rate measurement and the capability to program start-stop cycles with real-time monitoring of pressure, flow rate, and partial/total volume. During the experiments, tank 1 is filled with spiked tap-water, which is then pumped through the filtering cartridge. A new cartridge was used for each contaminant. After the cartridge, a tap allows for the collection of filtered water samples at predefined intervals for further analyses and quantification. The remaining water is then collected in tank 2. After treating 100 L, the maximum capacity of the tanks, water can be re-pumped into the first tank, by-passing the cartridge, in order to recycle the contaminated water. The concentration of the contaminant is then quantified and re-adjusted to ensure constant initial concentration during all the experiment.

5.2.3 Results and discussion

Materials preparation and characterization

Optical microscope and SEM analyses of PSU and PSU-GO prepared by manual cutting of PSU-HF and PSU-GO-HF showed granules with size in the range of 300 µm - 2 mm (Figure 5.4). The cutting process preserved the inner lumen size (250-300 µm), wall section thickness (about 50 µm), inner wall skin porosity (5-80 nm), and outer wall porosity (5-10 µm) of the pristine hollow fibers. Finger-like pore channels in the section of the fibers were also preserved (Figure 5.4e, 5.4f).

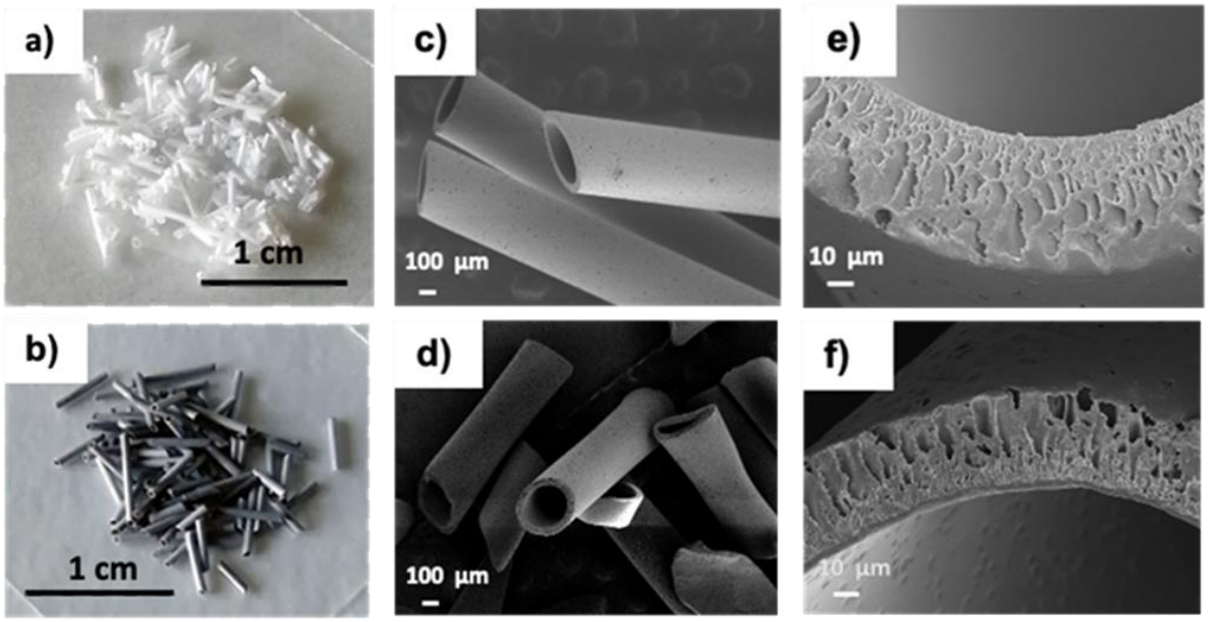

Figure 5.4 *Images of PSU (a) and PSU-GO (b) granules, and SEM images at different magnification of PSU (c, e) and PSU-GO (d, f).*

ATR FT-IR and TGA analyses on PSU and PSU-GO showed almost identical features, likely due to the low percentage of GO in the matrix (Figure 7.18, 7.19, Appendix). TGA curves displayed similar profiles with a slight increase in decomposition temperature for PSU-GO (536°C vs 528°C, and 657°C vs 647°C for PSU and PSU-GO, respectively, Figure 7.19, Appendix). The extensive characterization of PSU-GO fibers (before the manual cutting) was reported in our previous work, including Scanning Electron Microscopy (SEM), Liquid-Liquid-Displacement-Porometer, contact angle and Raman confocal microscope. In particular, Raman spectra revealed homogeneous distribution of GO inside the hollow fiber, with no aggregation.[28]

Bench-scale adsorption selectivity tests

The selectivity of PSU and PSU-GO was studied in flow conditions, on mixtures of heavy metals and different classes of organic contaminants in comparison to GAC. Removal results were normalized respect to the sorbent weight and are shown in Figure 5.5 (results in % Removal and full data are reported in Figure 7.20-7.23, Appendix). PSU-GO showed higher selectivity respect to PSU for all tested metals, in particular toward Pb (103 µg g^{-1} *vs* 48 µg g^{-1}), Cu (90 µg g^{-1} *vs* 8 µg g^{-1}) and Cr (58 µg g^{-1} *vs* 27 µg g^{-1}), while GAC showed negligible adsorptions for all considered metals (Figure 5.5b). The observed trend suggests a mechanism , primarily driven by electrostatic interactions between the metal ions and the negatively charged GO surface, as already highlighted in literature.[47] Indeed, the affinity of PSU-GO follows the order Pb (II) > Cu (II) > Cr (III), which well correlates with the electronegativity of the metals (2.3, 1.9, and 1.6, respectively).

With respect to organic contaminants, PSU-GO showed higher selectivity for OFLOX, BP4, and DCF than GAC and PSU (Figure 5.5c). On the other hand, the removal of f RhB and BP3 was slightly higher for PSU than PSU-GO.

With respect to PFAS, PSU-GO showed higher selectivity, compared to GAC, for PFAS with a chain length > $(CF)_3$. PSU showed comparable performance to PSU-GO for > $(CF)_8$. GAC was the only sorbent able to capture perfluorobutyric acid (PFBA, $(CF)_3$) and perfluoropentanoic acid (PFPeA, $(CF)_4$), with a removal > 99%, which decreased down to 40% with longer chain length (Figure 5.5d).

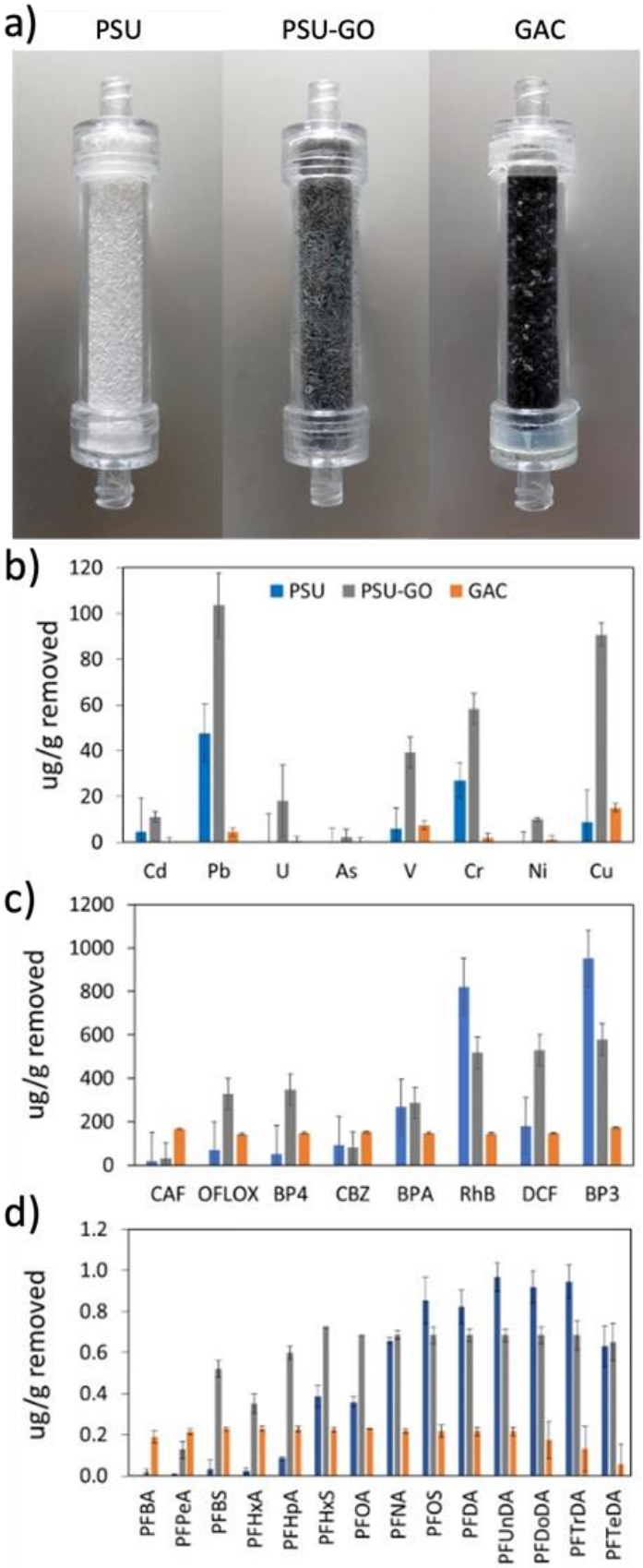

Figure 5.5 *a) PSU, PSUGO and GAC cartridges and adsorption selectivity on b) heavy metals, c) organic contaminants, and d) PFAS.*

PFAS adsorption mechanism

Due to the critical environmental relevance of PFAS, and to the higher performance of PSU-GO respect to PSU on their removal (Figure 5.5d), we investigate the adsorption mechanism of PFAS on GO. The adsorption trend of PSU-GO as a function of the n-octanol/water partition coefficient ($logK_{ow}$) of each molecule (expressing the hydrophobicity) for carboxylate PFAS is plotted in Figure 5.6a.

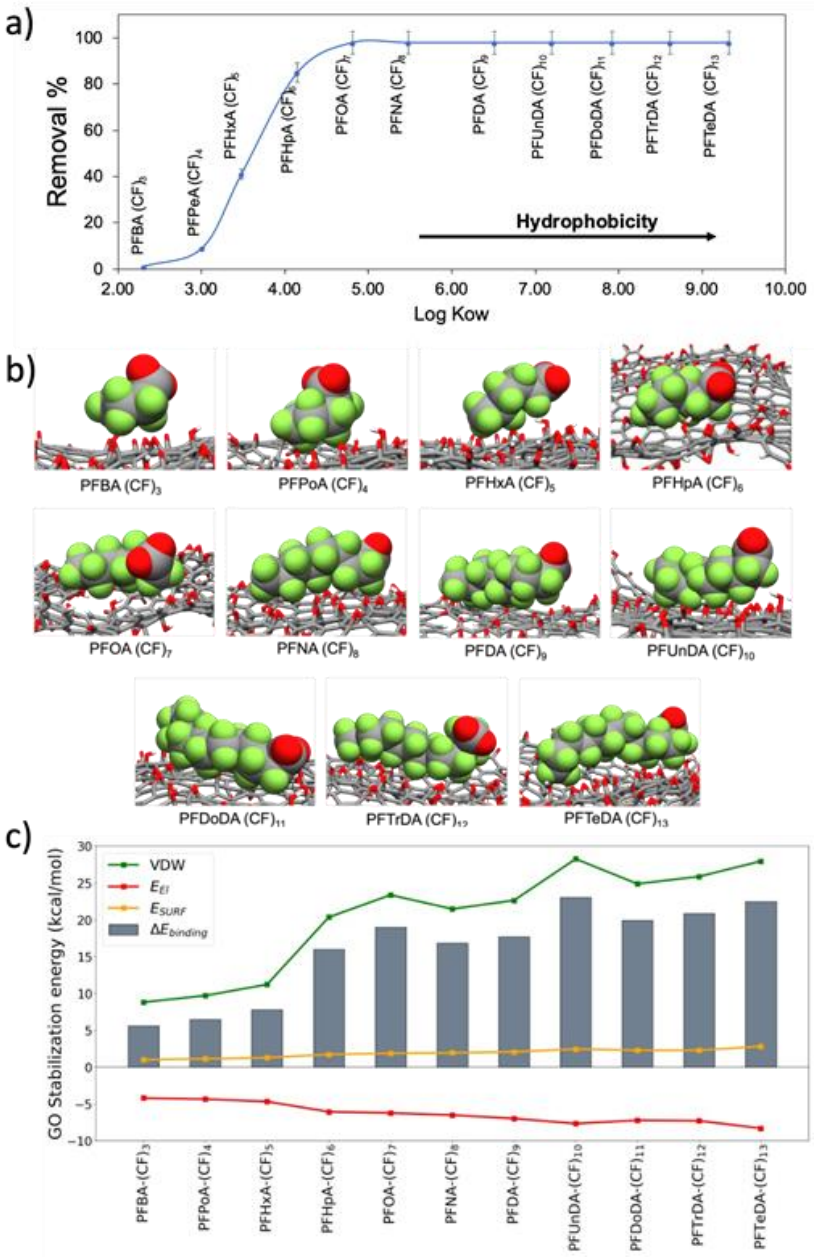

Figure 5.6 *a) Trend of removal vs $logK_{ow}$ of carboxylates PFAS ($(CF)_3$-$(CF)_{13}$); b) adsorption of PFAS of different chain length on GO nanosheets (representative snapshots taken from MD simulations); c) energy components of the $\Delta E_{binding}$ for PFAS of different length with GO. Total binding energy ($\Delta E_{binding}$, grey bars), van der Waals interactions (E_{vdW}, green line), nonpolar solvation ($E_{nonpolar\ solvation}$, yellow line), electrostatic terms (E_{el}, red line).*

The removal efficiency increased with the hydrophobicity of the contaminant (see Table 7.22, Appendix).[35] According to previous studies,[35, 48, 49] the two driving forces that need to be considered in PFAS adsorption are electrostatic repulsion and hydrophobic interaction. The comparison between the removals of sulfonate and carboxylate PFAS with the same amount of CF ($(CF)_4$: PFBS vs PFPeA; $(CF)_6$: PFHxS vs PFHpA; $(CF)_8$: PFOS vs PFNA) highlights that i) there is a correlation between the number of CF groups and the removal, ii) due to a higher hydrophobicity of the sulfonate group, sulfonate PFAS are better adsorbed than the carboxylate ones by both PSU and PSU-GO, (Figure 7.24 and Table 7.23, Appendix).

The binding energy ($\Delta E_{binding}$) between PFAS and GO is obtained by the sum of three energetic terms: electrostatic interactions, van der Waals interactions, and surface energy (Figure 5.6c). As the PFAS chain elongates, the $\Delta E_{binding}$ with GO increases, well reproducing the experimental trend. The driving force controlling the adsorption process are the van der Waals (VDW) interactions, originated between the perfluoroalkyl chains and the GO sheet. VDW contribution is hydrophobic in nature and strongly depends on the adsorbate chain length: the longer the PFAS chain, the stronger the interaction with GO. Additionally, the surface energy E_{SURF} contribution (hydrophobic effect) assists the binding with an almost constant value among the different PFAS, even if in terms of magnitude E_{SURF} is smaller than the VDW interactions. The surface energy term originates from the hydrophobic perfluoroalkyl chain of the PFAS that interact with the hydrophobic surface of the GO instead of interacting with water, with which the interaction is unfavorable. While VDW and E_{SURF} contributions favour the adsorption process, the electrostatic term (E_{el}) is detrimental to the binding. This term takes into consideration i) the Coulombic repulsion between the negatively charged GO ($\zeta_{potential}$ = -43.1 ± 2.4 mV) and the negatively charged carboxylate of PFAS, and ii) the polar solvation term. The hydrophilic portions of PFAS are forcedly desolvated upon the formation of the complex with GO, causing an overall destabilization of the system. Taken together, the results confirm that, as previously reported in literature,[35] when the hydrophobic interactions (van der Waals plus hydrophobic effect) overcome the electrostatic repulsion between PFAS and GO, the binding of PFAS, and their consequent removal, occurs.

Bench-scale adsorption capacity tests

Based on the selectivity observed in previous experiments (Figure 5.5), we selected one contaminant per each class (*i.e.,* DCF, PFOA and Pb) and we tested the adsorption capacity of PSU-GO, PSU and GAC with respect to them. Figure 5.7 shows the results in Removal % vs Bed volume, while results expressed as function of output concentration (C_{OUT}), or cumulative µg of contaminant removed on g of sorbent (µg g^{-1}) are reported in the Appendix (Figure 7.25). To simulate real applications, the cartridge adsorption capacity tests were carried in flow conditions, using fresh spiked tap water, with EBCT = 0.5 min. Experiments were carried on until saturation conditions occurred (*i.e.,* $C_{OUT} = C_{IN}$) or when the adsorption capacity was half of the initial value.

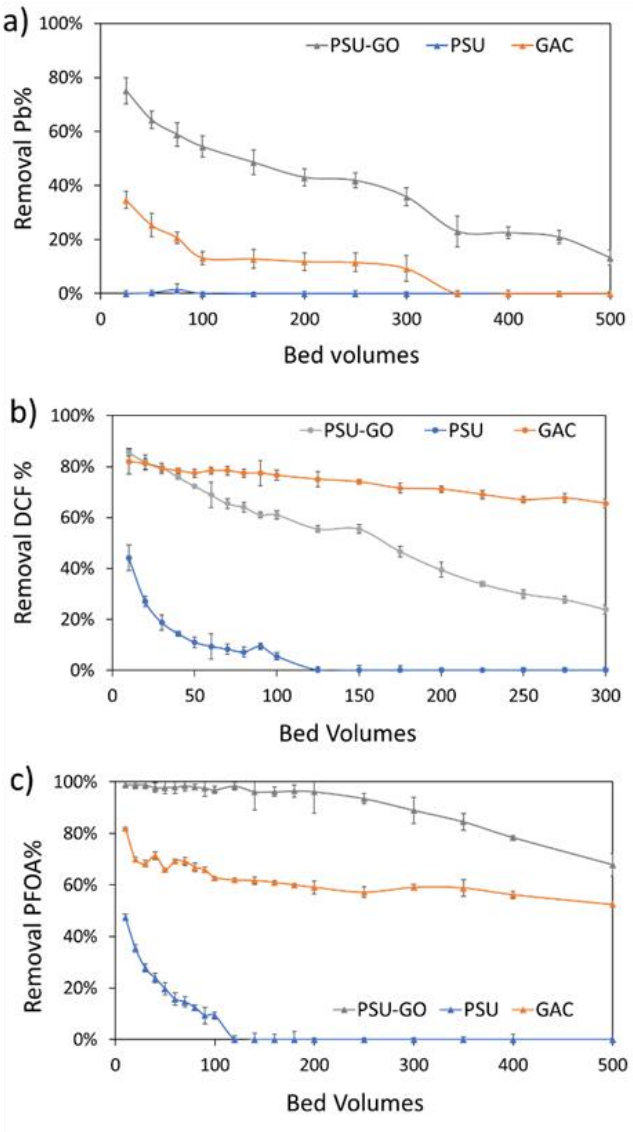

Figure 5.7 *Loading curve of a) Pb, b) DCF, and c) PFOA expressed as Removal % vs Bed volumes of PSU (blue lines), PSU-GO (grey lines) and GAC (orange lines).*

In Figure 5.7a, PSU-GO adsorbed Pb with maximum removal approaching values in the range 75-43%, after 500 bed volumes, while PSU was ineffective, and GAC saturated after 100 bed volumes. Similarly, PSU-GO showed higher adsorption capacity than PSU (Figure 5.7b) toward DCF, and no saturation was observed even though the adsorption capacity decreases faster than for GAC. With regards to PFOA, PSU-GO adsorption capacity remained almost constant even after 500 bed volumes (Figure 5.7c), outperforming GAC and PSU.

Table 5.1 summarizes the total amount of contaminant (*i.e.,* Pb, DCF, PFOA) removed normalized per gram of sorbent. In the case of Pb, the mass removed by PSU-GO were 10 times higher than that obtained with GAC, while PSU showed negligible adsorption. The amount of DCF and PFOA globally removed by PSU-GO was 2 and 6 times higher than the amount adsorbed by GAC and PSU, respectively. This evidence supports our previous study showing that the SSA for N_2 measured by BET is not representative of the sorbent capacity in the liquid phase (SSA for N_2 being 23 $m^2\ g^{-1}$ *vs*. 1000 $m^2\ g^{-1}$).[50]

Table 5.1 *Adsorption capacity values normalized per gram of adsorbent, estimated at the plateau of the loading curve.*

	Adsorption capacity (mass of contaminant/mass of adsorbent; µg g^{-1})		
Contaminant	PSU	GAC	PSU-GO
Pb	1.1	21.5	230.1
DCF	389.8	951.6	2400.2
PFOA	1.1	3.2	6.1

To date, the best sorption performances for Pb, DCF and PFOA have been achieved by using carbonaceous materials, including i) GAC (PFOA 112 mg g^{-1},[35] DCF 6.85 mg g^{-1},[51] Pb 58 mg g^{-1} [52]), ii) GO (PFOA 0.4 mg g^{-1},[53] DCF 128 mg g^{-1},[54] Pb 55.80 mg g^{-1} [55]), iii) Carbon-nanotubes (Pb 97 mg g^{-1},[56] PFOA 124 mg g^{-1} [57]) or iv) nanocomposites, such as modified graphene aerogel (Pb 368 mg g^{-1},[58, 59] PFOA 1575 mg g^{-1} [60]). However, it should be noted that the above-mentioned materials and performance, were estimated from batch experiments and related adsorption isotherms at the equilibrium time (not under flow as in this work), carried out in ultrapure water (not tap drinking water as in this work) and with contact times of hours (rather than seconds as in this work). Overall, these discrepancies prevent a proper and direct comparison of our results with

the literature. To overcome this issue, we characterized GAC and PSU/PSUGO-HF standard cartridges in the same experimental conditions of our materials.

Materials integrity, regeneration and reuse

We investigated the potential leaching of GO nanosheets from PSU–GO cartridges by surface-enhanced Raman spectroscopy (SERS) analysis of filtered water. This methodology is based on the deposition of the analyte on a SERS active substrate based on gold nanoparticles and allows the quantification of GO down to 0.1 μg L^{-1}.[46] No significant differences were found between tap water, used as control, and the PSU–GO treated water samples (Figure 7.17 and Table 7.21, Appendix), indicating that no release of GO occurred. In addition, chemical and biological water potability was verified on tap water after filtration (Table 7.24, Appendix).

Moreover, stable adsorption of contaminants was tested by washing the saturated cartridges with fresh tap water and measuring the concentration of the contaminants in the washing solution. Releases lower than 8% for Pb, 6% for DCF, and 1.5% for PFOA (Figure 7.26, Appendix) were found.

Finally, given the importance of cartridge regeneration, we carried out some preliminary regeneration test on cartridge saturated with PFOA. To this aim, the cartridge was washed with ultrapure H_2O/EtOH solution at different ratio and the amount of PFOA recovery in the different conditions was estimated. The best recovery in terms of maximum amount recovered (2.1 μg, 45.3%) was achieved by using a solution at 70:30 v/v ratio (ultrapure H_2O/EtOH). The washed cartridge was then used for a second filtration cycle and showed adsorption capacity (Figure 7.27, Appendix). Both cycles showed adsorption efficiency of about 98% suggesting that it is possible to regenerate and reuse PSU-GO cartridges. Further studies on different contaminants will be addressed to fully assess the reuse possibility for these materials.

Granules production upscale and pilot-plants tests

The scraps grinding process was upscaled by using a commercial blade mechanical grinder with steel blades and production capability of 0.75 Kg h^{-1} (Figure 7.28, Appendix). Chromium release from the blades during the grinding was excluded by dedicated tests, with release Cr(III) < 5 ng g^{-1}. The size of the granules was in the range 0.3-2 mm (due to the grinder cut-off) and a real scale standard cartridge was filled with

the obtained granules (Figure 7.28c, Appendix). Due to the mechanical stress applied during the grinding process, the granules displayed a flattened and partially opened structure in comparison to manually ground granules, which exhibited a homogeneous tubular shape (Figure 7.29, Appendix). However, despite the different morphology the granules showed adsorption performance very similar to those obtained by manual grinding (Figure 7.30, Appendix).

Commercial standard cartridges were filled with PSU-GO granules (Figure 7.14, Appendix) and characterized in a pilot plant test on Pb removal. As shown in Figure 5.8b, PSU showed negligible adsorption of Pb (total removal about 8 µg g^{-1}), while PSU-GO removed up to 250 µg g^{-1} with the highest removal within the first 100 L treated (Figure 5.8b and Figure 7.31, Appendix). Remarkably, comparable adsorption capacity was obtained with small and larger cartridges (230 µg g^{-1} vs 250 µg g^{-1}), despite the different concentration of Pb (100 µg L^{-1} vs 30 µg L^{-1}) and EBCT (0.5 min vs 0.14 min). GAC was not tested since no Pb adsorption was observed in lab test. In addition, we compared the granules adsorption performance on Pb to the performance of standard commercially available PSU-HF and PSU-GO-HF cartridges, which are the precursors of the granules. As shown in Figure 8b neither PSU granules nor PSU-HF removed Pb. On the contrary, PSU-GO granules and PSU-GO HF showed high Pb removal capacity with values of 195 µg g^{-1} and 202 µg g^{-1}, respectively (treated volume 420 L) suggesting that i) granules and HF are characterized by the same adsorption selectivity and capacity and ii) the adsorption of lead is exclusively promoted by GO.

In the same experimental set-up, PSU and PSU-GO cartridges were tested on PFOA removal and compared to GAC and PSU cartridges (Figure 5.8c). Remarkably, PSU-GO overcome GAC and PSU in the adsorption of PFOA with maximum capacities of 12 µg g^{-1} *vs.* 1.63 µg g^{-1} *vs*. 0.8 µg g^{-1}, respectively.

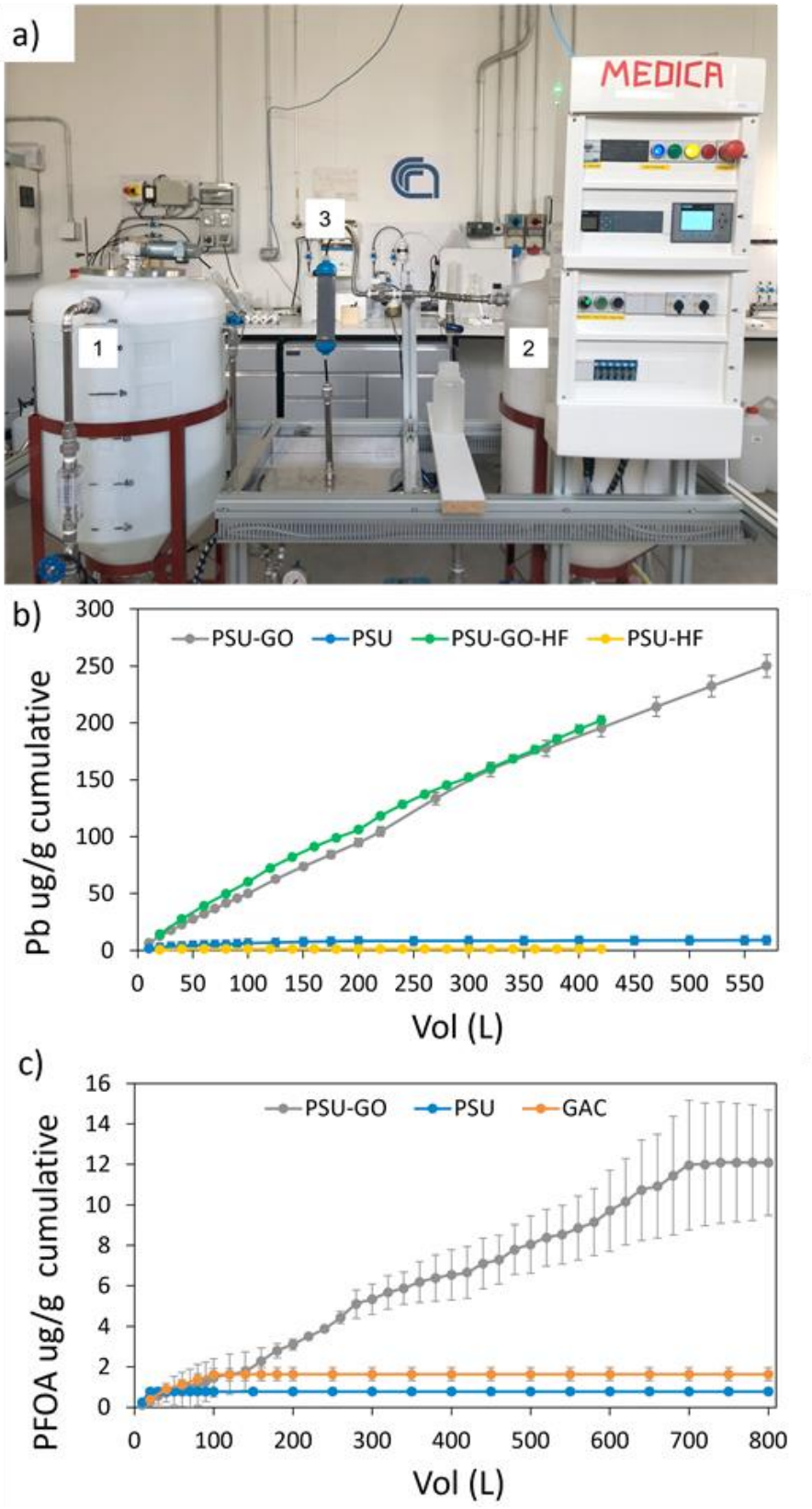

Figure 5.8 *a) Set-up of the real scale automatized pilot plant. Spiked water in tank 1 (100 L capacity) is flowed through the cartridge (PSU-GO in the picture, filter 3) and filtered water is collected in tank 2 (100 L capacity). After 100 L are filtered, water is pumped from tank 2 to tank 1 (bypassing the cartridge) and the concentration checked and adjusted to the target initial value. b) and c) Comparison between removal capacity on Pb and PFOA.*

5.2.4 Conclusion

In conclusion, we reported new sorbent materials derived from waste of the industrial production of polymeric hollow fiber membranes. The scraps were converted into granules (PSU and PSU-GO) through mechanical grinding and their adsorption properties toward selected water contaminants, including PFAS, were characterized.

Cartridges of PSU and PSU-GO materials showed excellent adsorption properties toward several contaminants, higher than GAC, this highlighting their potential for drinking water purification. In general, respect to GAC, PSU showed higher selectivity for BP3 and RhB and for PFAS with chain length > $(CF)_8$. PSU-GO showed higher selectivity, compared to GAC, for Pb, Cu, Cr, OFLOX, BP4, DCF and for PFAS with chain length $(CF)_3$ → $(CF)_{13}$. Given the interest for PFAS removal and their structural similarity, the adsorption mechanism on GO was investigated by molecular dynamic simulations. Calculations showed that the GO active sites mainly drive the adsorption process and favor the removal of hydrophobic molecules. In terms of adsorption capacities, PSU-GO removal of DCF and PFOA were more than 2 times higher than GAC and 6 times higher than PSU. Moreover, the maximum Pb removal capacity of PSU-GO was 10 times higher than that obtained with GAC.

A grinding scale up through an automatic grinder with a production capability close to 1 Kg h^{-1} was demonstrated, allowing the fabrication and test of larger cartridges (commercial standard size) and treatment of water volumes up to 800 L. Test performed in real tap conditions, showed that PSU-GO performances on Pb and PFOA are poorly affected by the flow rate and overcome GAC standard material.

Considering the massive global membrane production and the related mass of scraps byproducts, which is expected to further increase in the next few years, the approach herein described, and the suggested application could contribute to the reduction of plastic waste from the membrane producers. Moreover, the granular materials obtained from these scraps could be exploited in synergy with other standard technologies, including activated carbon sorption and membrane filtration. Studies in this direction are underway *in situ* in a municipal potabilization plant (Hera, Fe, Italy, po river source) for drinking water production.

Author Contributions

S. Khaliha: methodology, investigation, data curation, editing. F. Tunioli: methodology, investigation. L. Foti: methodology, investigation. A. Bianchi: methodology, reviewing and editing. A. Kovtun: investigation, formal analysis. M. Zambianchi: methodology, investigation. C. Bettini: methodology, investigation. T. D. Marforio: investigation, methodology, formal analysis. M. L. Navacchia: investigation, formal analysis. E. Briñas: investigation. E. Vázquez: methodology, investigation. L. Bocchi: conceptualization, methodology, resources. V. Palermo: conceptualization, validation. M. Calvaresi: methodology, investigation. M. Melucci: conceptualization, validation, writing – original draft.

Acknowledgements

The authors gratefully acknowledge the support of this work by the projects Life-Remembrance, ENV/IT/001001 Life Resource and Environment LIFE20 ‘Give plastic wastes from the production of hollow-fiber membranes a second life’, project PNRR MUR project ECS_00000033_ECOSISTER.

MM thanks M. Bergamini and M. Brunetti (Gruppo HERA Spa, Bologna, Italy) for providing samples of GAC used in their municipal plants.

5.2.5 References

1. Zambianchi, M.; Khaliha, S.; Bianchi, A.; Tunioli, F.; Kovtun, A.; Navacchia, M. L.; Salatino, A.; Xia, Z.; Briñas, E.; Vázquez, E.; Paci, D.; Palermo, V.; Bocchi, L.; Casentini, B.; Melucci, M., Graphene oxide-polysulfone hollow fibers membranes with synergic ultrafiltration and adsorption for enhanced drinking water treatment. *J. Membr. Sci.* **2022,** *658*, 120707.
2. Guardian Chemical pollution has passed safe limit for humanity, say scientists https://www.theguardian.com/environment/2022/jan/18/chemical-pollution-has-passed-safe-limit-for-humanity-say-scientists.
3. Teymoorian, T.; Munoz, G.; Vo Duy, S.; Liu, J.; Sauvé, S., Tracking PFAS in Drinking Water: A Review of Analytical Methods and Worldwide Occurrence Trends in Tap Water and Bottled Water. *ACS ES&T Water* **2023,** *3* (2), 246-261.
4. Persson, L.; Carney Almroth, B. M.; Collins, C. D.; Cornell, S.; de Wit, C. A.; Diamond, M. L.; Fantke, P.; Hassellöv, M.; MacLeod, M.; Ryberg, M. W.; Søgaard Jørgensen, P.; Villarrubia-Gómez, P.; Wang, Z.; Hauschild, M. Z., Outside the Safe Operating Space of the Planetary Boundary for Novel Entities. *Environ. Sci. Technol.* **2022,** *56* (3), 1510-1521.
5. *Scientists Letter: The World Health Organization should significantly revise or withdraw its draft PFAS drinking water guidelines*.
6. Bertanza, G.; Capoferri, G. U.; Carmagnani, M.; Icarelli, F.; Sorlini, S.; Pedrazzani, R., Long-term investigation on the removal of perfluoroalkyl substances in

a full-scale drinking water treatment plant in the Veneto Region, Italy. *Sci. Total Environ.* **2020,** *734*, 139154.
7. Zhang, Y.; Tan, X.; Lu, R.; Tang, Y.; Qie, H.; Huang, Z.; Zhao, J.; Cui, J.; Yang, W.; Lin, A., Enhanced Removal of Polyfluoroalkyl Substances by Simple Modified Biochar: Adsorption Performance and Theoretical Calculation. *ACS ES&T Water* **2023**.
8. *Activated Carbon Market Size, Share & Trends Analysis Report By Type (Powdered, Granular), By Application (Liquid Phase, Gas Phase) By End Use (Water Treatment, Air Purification), By Region, And Segment Forecasts, 2022 - 2030*; 978-1-68038-073-6; 2020.
9. Crini, G.; Lichtfouse, E., Advantages and disadvantages of techniques used for wastewater treatment. *Environ. Chem. Lett.* **2019,** *17* (1), 145-155.
10. Quesada, H. B.; de Araújo, T. P.; Vareschini, D. T.; de Barros, M.; Gomes, R. G.; Bergamasco, R., Chitosan, alginate and other macromolecules as activated carbon immobilizing agents: A review on composite adsorbents for the removal of water contaminants. *Int. J. Biol. Macromol.* **2020,** *164*, 2535-2549.
11. Shi, Q.; Wang, W.; Zhang, H.; Bai, H.; Liu, K.; Zhang, J.; Li, Z.; Zhu, W., Porous biochar derived from walnut shell as an efficient adsorbent for tetracycline removal. *Bioresour. Technol.* **2023,** *383*, 129213.
12. Dhaka, S.; Kumar, R.; Deep, A.; Kurade, M. B.; Ji, S.-W.; Jeon, B.-H., Metal–organic frameworks (MOFs) for the removal of emerging contaminants from aquatic environments. *Coord. Chem. Rev.* **2019,** *380*, 330-352.
13. Khaliha, S.; Marforio, T. D.; Kovtun, A.; Mantovani, S.; Bianchi, A.; Navacchia, M. L.; Zambianchi, M.; Bocchi, L.; Boulanger, N.; Iakunkov, A.; Calvaresi, M.; Talyzin, A. V.; Palermo, V.; Melucci, M., Defective graphene nanosheets for drinking water purification: Adsorption mechanism, performance, and recovery. *FlatChem* **2021,** *29*, 100283.
14. Zhao, L.; Deng, J.; Sun, P.; Liu, J.; Ji, Y.; Nakada, N.; Qiao, Z.; Tanaka, H.; Yang, Y., Nanomaterials for treating emerging contaminants in water by adsorption and photocatalysis: Systematic review and bibliometric analysis. *Sci. Total Environ.* **2018,** *627*, 1253-1263.
15. Bakir, A.; Rowland, S. J.; Thompson, R. C., Competitive sorption of persistent organic pollutants onto microplastics in the marine environment. *Mar. Pollut. Bull.* **2012,** *64* (12), 2782-2789.
16. Brennecke, D.; Duarte, B.; Paiva, F.; Caçador, I.; Canning-Clode, J., Microplastics as vector for heavy metal contamination from the marine environment. *Estuar. Coast. Shelf Sci.* **2016,** *178*, 189-195.
17. Provencher, J. F.; Avery-Gomm, S.; Liboiron, M.; Braune, B. M.; Macaulay, J. B.; Mallory, M. L.; Letcher, R. J., Are ingested plastics a vector of PCB contamination in northern fulmars from coastal Newfoundland and Labrador? *Environ. Res.* **2018,** *167*, 184-190.
18. Zambianchi, M.; Aluigi, A.; Capobianco, M. L.; Corticelli, F.; Elmi, I.; Zampolli, S.; Stante, F.; Bocchi, L.; Belosi, F.; Navacchia, M. L.; Melucci, M., Polysulfone Hollow Porous Granules Prepared from Wastes of Ultrafiltration Membranes as Sustainable Adsorbent for Water and Air Remediation. **2017,** *1* (7), 1700019.
19. Dumitriu, C.; Voicu, S. I.; Muhulet, A.; Nechifor, G.; Popescu, S.; Ungureanu, C.; Carja, A.; Miculescu, F.; Trusca, R.; Pirvu, C., Production and characterization of cellulose acetate – titanium dioxide nanotubes membrane fraxiparinized through polydopamine for clinical applications. *Carbohydr. Polym.* **2018,** *181*, 215-223.

20. Li, G.; Kujawski, W.; Válek, R.; Koter, S., A review - The development of hollow fibre membranes for gas separation processes. *International Journal of Greenhouse Gas Control* **2021,** *104*, 103195.
21. Thakur, V. K.; Voicu, S. I., Recent advances in cellulose and chitosan based membranes for water purification: A concise review. *Carbohydr. Polym.* **2016,** *146*, 148-165.
22. Kovtun, A.; Bianchi, A.; Zambianchi, M.; Bettini, C.; Corticelli, F.; Ruani, G.; Bocchi, L.; Stante, F.; Gazzano, M.; Marforio, T. D.; Calvaresi, M.; Minelli, M.; Navacchia, M. L.; Palermo, V.; Melucci, M., Core–shell graphene oxide–polymer hollow fibers as water filters with enhanced performance and selectivity. *Faraday Discuss.* **2021,** *227* (0), 274-290.
23. Mantovani, S.; Khaliha, S.; Favaretto, L.; Bettini, C.; Bianchi, A.; Kovtun, A.; Zambianchi, M.; Gazzano, M.; Casentini, B.; Palermo, V.; Melucci, M., Scalable synthesis and purification of functionalized graphene nanosheets for water remediation. *Chem. Commun.* **2021,** *57* (31), 3765-3768.
24. Khaliha, S.; Bianchi, A.; Kovtun, A.; Tunioli, F.; Boschi, A.; Zambianchi, M.; Paci, D.; Bocchi, L.; Valsecchi, S.; Polesello, S.; Liscio, A.; Bergamini, M.; Brunetti, M.; Navacchia, M. L.; Palermo, V.; Melucci, M., Graphene oxide nanosheets for drinking water purification by tandem adsorption and microfiltration. *Sep. Purif. Technol.* **2022,** *300*, 121826.
25. Mantovani, S.; Khaliha, S.; Marforio, T. D.; Kovtun, A.; Favaretto, L.; Tunioli, F.; Bianchi, A.; Petrone, G.; Liscio, A.; Palermo, V.; Calvaresi, M.; Navacchia, M. L.; Melucci, M., Facile high-yield synthesis and purification of lysine-modified graphene oxide for enhanced drinking water purification. *Chem. Commun.* **2022,** *58* (70), 9766-9769.
26. Qiu, Y.; Depuydt, S.; Ren, L.-F.; Zhong, C.; Wu, C.; Shao, J.; Xia, L.; Zhao, Y.; Van der Bruggen, B., Progress of Ultrafiltration-Based Technology in Ion Removal and Recovery: Enhanced Membranes and Integrated Processes. *ACS ES&T Water* **2023**.
27. Zambianchi, M.; Durso, M.; Liscio, A.; Treossi, E.; Bettini, C.; Capobianco, M. L.; Aluigi, A.; Kovtun, A.; Ruani, G.; Corticelli, F.; Brucale, M.; Palermo, V.; Navacchia, M. L.; Melucci, M., Graphene oxide doped polysulfone membrane adsorbers for the removal of organic contaminants from water. *Chem. Eng. J.* **2017,** *326*, 130-140.
28. Zambianchi, M.; Khaliha, S.; Bianchi, A.; Tunioli, F.; Kovtun, A.; Navacchia, M. L.; Salatino, A.; Xia, Z.; Briñas, E.; Vázquez, E.; Paci, D.; Palermo, V.; Bocchi, L.; Casentini, B.; Melucci, M., Graphene oxide-polysulfone hollow fibers membranes with synergic ultrafiltration and adsorption for enhanced drinking water treatment. *J. Membr. Sci.* **2022,** *658*, 120707.
29. Research, G. V., Hollow Fiber Filtration Market Size, Share & Trends Analysis Report By Membrane Material (Polysulfone), By Process (Single-use Hollow Fiber Membranes), By Technology, By Application, By End-users, By Region, And Segment Forecasts, 2023 - 2030. **2022**, 150.
30. Vieno, N.; Sillanpää, M., Fate of diclofenac in municipal wastewater treatment plant — A review. *Environ. Int.* **2014,** *69*, 28-39.
31. Vieno, N. M.; Härkki, H.; Tuhkanen, T.; Kronberg, L., Occurrence of Pharmaceuticals in River Water and Their Elimination in a Pilot-Scale Drinking Water Treatment Plant. *Environ. Sci. Technol.* **2007,** *41* (14), 5077-5084.
32. Anand, U.; Adelodun, B.; Cabreros, C.; Kumar, P.; Suresh, S.; Dey, A.; Ballesteros, F.; Bontempi, E., Occurrence, transformation, bioaccumulation, risk and analysis of pharmaceutical and personal care products from wastewater: a review. *Environ. Chem. Lett.* **2022,** *20* (6), 3883-3904.

33. Glüge, J.; Scheringer, M.; Cousins, I. T.; DeWitt, J. C.; Goldenman, G.; Herzke, D.; Lohmann, R.; Ng, C. A.; Trier, X.; Wang, Z., An overview of the uses of per- and polyfluoroalkyl substances (PFAS). *Environmental Science: Processes & Impacts* **2020,** *22* (12), 2345-2373.
34. Valsecchi, S.; Rusconi, M.; Mazzoni, M.; Viviano, G.; Pagnotta, R.; Zaghi, C.; Serrini, G.; Polesello, S., Occurrence and sources of perfluoroalkyl acids in Italian river basins. *Chemosphere* **2015,** *129*, 126-34.
35. Gagliano, E.; Sgroi, M.; Falciglia, P. P.; Vagliasindi, F. G. A.; Roccaro, P., Removal of poly- and perfluoroalkyl substances (PFAS) from water by adsorption: Role of PFAS chain length, effect of organic matter and challenges in adsorbent regeneration. *Water Res.* **2020,** *171*, 115381.
36. Shahid, M. N.; Khalid, S.; Saleem, M., Unrevealing arsenic and lead toxicity and antioxidant response in spinach: a human health perspective. *Environ. Geochem. Health* **2022,** *44* (2), 487-496.
37. Nag, R.; Cummins, E., Human health risk assessment of lead (Pb) through the environmental-food pathway. *Sci. Total Environ.* **2022,** *810*, 151168.
38. Chowdhury, I. R.; Chowdhury, S.; Mazumder, M. A. J.; Al-Ahmed, A., Removal of lead ions (Pb2+) from water and wastewater: a review on the low-cost adsorbents. *Appl. Water Sci.* **2022,** *12* (8), 185.
39. Tröger, R.; Ren, H.; Yin, D.; Postigo, C.; Nguyen, P. D.; Baduel, C.; Golovko, O.; Been, F.; Joerss, H.; Boleda, M. R.; Polesello, S.; Roncoroni, M.; Taniyasu, S.; Menger, F.; Ahrens, L.; Yin Lai, F.; Wiberg, K., What's in the water? – Target and suspect screening of contaminants of emerging concern in raw water and drinking water from Europe and Asia. *Water Res.* **2021,** *198*, 117099.
40. Wang, J.; Wolf, R. M.; Caldwell, J. W.; Kollman, P. A.; Case, D. A., Development and testing of a general amber force field. *J. Comput. Chem.* **2004,** *25* (9), 1157-1174.
41. Humphrey, W.; Dalke, A.; Schulten, K., VMD: Visual molecular dynamics. *J. Mol. Graphics* **1996,** *14* (1), 33-38.
42. D.A. Case, R. M. B., D.S. Cerutti, T.E. Cheatham, III, T.A. Darden, R.E. Duke, T.J. Giese, H. Gohlke, A.W. Goetz, N. Homeyer, S. Izadi, P. Janowski, J. Kaus, A. Kovalenko, T.S. Lee, S. LeGrand, P. Li, C. Lin, T. Luchko, R. Luo, B. Madej, D. Mermelstein, K.M. Merz, G. Monard, H. Nguyen, H.T. Nguyen, I. Omelyan, A. Onufriev, D.R. Roe, A. Roitberg, C. Sagui, C.L. Simmerling, W.M. Botello-Smith, J. Swails, R.C. Walker, J. Wang, R.M. Wolf, X. Wu, L. Xiao and P.A. Kollman, *AMBER*. University of California, San Francisco., 2016.
43. Zamora-Ledezma, C.; Negrete-Bolagay, D.; Figueroa, F.; Zamora-Ledezma, E.; Ni, M.; Alexis, F.; Guerrero, V. H., Heavy metal water pollution: A fresh look about hazards, novel and conventional remediation methods. *Environmental Technology & Innovation* **2021,** *22*, 101504.
44. Shamsudin, M. S.; Azha, S. F.; Ismail, S., A review of diclofenac occurrences, toxicology, and potential adsorption of clay-based materials with surfactant modifier. *J. Environ. Chem. Eng.* **2022,** *10* (3), 107541.
45. Johnson, G. R.; Brusseau, M. L.; Carroll, K. C.; Tick, G. R.; Duncan, C. M., Global distributions, source-type dependencies, and concentration ranges of per- and polyfluoroalkyl substances in groundwater. *Sci. Total Environ.* **2022,** *841*, 156602.
46. Briñas, E.; González, V. J.; Herrero, M. A.; Zougagh, M.; Ríos, Á.; Vázquez, E., SERS-Based Methodology for the Quantification of Ultratrace Graphene Oxide in Water Samples. *Environ. Sci. Technol.* **2022,** *56* (13), 9527-9535.

47. Gao, Z.; Bandosz, T. J.; Zhao, Z.; Han, M.; Qiu, J., Investigation of factors affecting adsorption of transition metals on oxidized carbon nanotubes. *J. Hazard. Mater.* **2009,** *167* (1), 357-365.
48. Hotová, G.; Slovák, V.; Zelenka, T.; Maršálek, R.; Parchaňská, A., The role of the oxygen functional groups in adsorption of copper (II) on carbon surface. *Sci. Total Environ.* **2020,** *711*, 135436.
49. Adel, M.; Ahmed, M. A.; Elabiad, M. A.; Mohamed, A. A., Removal of heavy metals and dyes from wastewater using graphene oxide-based nanomaterials: A critical review. *Environmental Nanotechnology, Monitoring & Management* **2022,** *18*, 100719.
50. Kovtun, A.; Zambianchi, M.; Bettini, C.; Liscio, A.; Gazzano, M.; Corticelli, F.; Treossi, E.; Navacchia, M. L.; Palermo, V.; Melucci, M., Graphene oxide-polysulfone filters for tap water purification, obtained by fast microwave oven treatment. *Nanoscale* **2019,** *11* (47), 22780-22787.
51. Genç, N.; Durna, E.; Erkişi, E., Optimization of the adsorption of diclofenac by activated carbon and the acidic regeneration of spent activated carbon. *Water Sci. Technol.* **2021,** *83* (2), 396-408.
52. Johns, M. M.; Marshall, W. E.; Toles, C. A., Agricultural by-products as granular activated carbons for adsorbing dissolved metals and organics. *J. Chem. Technol. Biotechnol.* **1998,** *71* (2), 131-140.
53. Lath, S.; Navarro, D.; Losic, D.; Kumar, A.; McLaughlin, M., Sorptive remediation of perfluorooctanoic acid (PFOA) using mixed mineral and graphene/carbon-based materials. *Environ. Chem.* **2018,** *15*.
54. Guerra, A. C. S.; de Andrade, M. B.; Tonial Dos Santos, T. R.; Bergamasco, R., Adsorption of sodium diclofenac in aqueous medium using graphene oxide nanosheets. *Environ. Technol.* **2021,** *42* (16), 2599-2609.
55. Azam, M. G.; Kabir, M. H.; Shaikh, M. A. A.; Ahmed, S.; Mahmud, M.; Yasmin, S., A rapid and efficient adsorptive removal of lead from water using graphene oxide prepared from waste dry cell battery. *J. Water Process Eng.* **2022,** *46*, 102597.
56. Saeidi, N.; Parvini, M.; Niavarani, Z., High surface area and mesoporous graphene/activated carbon composite for adsorption of Pb(II) from wastewater. *J. Environ. Chem. Eng* **2015,** *3* (4, Part A), 2697-2706.
57. Cao, F.; Wang, L.; Yao, Y.; Wu, F.; Sun, H.; Lu, S., Synthesis and application of a highly selective molecularly imprinted adsorbent based on multi-walled carbon nanotubes for selective removal of perfluorooctanoic acid. *Environ. Sci. Water Res. Technol.* **2018,** *4* (5), 689-700.
58. Pan, L.; Wang, Z.; Yang, Q.; Huang, R., Efficient Removal of Lead, Copper and Cadmium Ions from Water by a Porous Calcium Alginate/Graphene Oxide Composite Aerogel. *Nanomaterials (Basel, Switzerland)* **2018,** *8* (11).
59. Yousefi, N.; Lu, X.; Elimelech, M.; Tufenkji, N., Environmental performance of graphene-based 3D macrostructures. *Nat. Nanotechnol.* **2019,** *14* (2), 107-119.
60. Tian, D.; Geng, D.; Tyler Mehler, W.; Goss, G.; Wang, T.; Yang, S.; Niu, Y.; Zheng, Y.; Zhang, Y., Removal of perfluorooctanoic acid (PFOA) from aqueous solution by amino-functionalized graphene oxide (AGO) aerogels: Influencing factors, kinetics, isotherms, and thermodynamic studies. *Sci. Total Environ.* **2021,** *783*, 147041.

6 Conclusions and future perspectives

Water pollution is a critical and rapidly evolving issue that is driving research and industry to find new solutions in the field of water treatment. Chemistry and materials science offer diverse insights and perspectives to address this pressing global challenge with innovative and advanced materials. Among the most promising developments, nanotechnology - particularly graphene related materials - has emerged as a key actor, offering innovative solutions that could not be achieved by traditional methods. This thesis contributes to this evolving field by investigating the potential of GRM as effective sorbents for the removal of ECs from drinking water.

The first part of my research was more fundamental and focused on the adsorption mechanisms of water-dispersed GRM nanosheets. It demonstrated their fast kinetics, high selectivity and adsorption capacity for a wide range of contaminants. Among the various GRM, the unique properties of GO, including its large surface area, water dispersibility and surface oxygen groups, have been shown to play a crucial role in its effectiveness as sorbent. Despite the potential of GO, its negatively charged surface and structural properties make it ineffective in the removal of some specific ECs, such as anionic dyes and PFAS. With this in mind, this thesis investigated the effect of covalent chemical modifications on GO. The aim was to tune its adsorptive properties, i.e. selectivity and capacity, by modifying its surface through covalent functionalization. Epoxide ring-opening reactions have been used to graft various functional groups, including amino acids and β-cyclodextrin, onto the GO surface. In particular, functionalization with βCD proved to be very effective in the removal of perfluorobutanoic acid (PFBA), a persistent PFAS. By controlling the length of the alkyl chain used to bind the βCD to the GO, the adsorption efficiency in tap water was significantly improved from no removal of pristine GO to 65% removal in the case of the best performing GO-βCD. Molecular dynamic simulations provided further insight into the adsorption mechanisms and enhanced the understanding of how these modifications affect adsorption. Indeed, in this case, the length of the linker used in the covalent modification significantly influences the position of the βCD with respect to the GO and thus its adsorption properties.

The research then focused on a more application-oriented part. While GRM have shown excellent properties that make them attractive candidates as sorbents, they are also

difficult to implement in traditional water treatment systems. Their use as nanomaterials presents challenges for practical applications and large-scale implementation. One of the main problems is that GRM need to be dispersed in water, often through processes such as sonication, to maximize the contact surface area. In addition, after the treatment process, the nanomaterials must be separated from the water to avoid secondary contamination, and this process typically requires expensive or complex techniques such as centrifugation or additional steps such as filtration. To address these limitations, my approach was to embed the nanomaterials within a polymer matrix, which can be easily removed from the treated solution. This allows for partial exploitation of the GRM surface area while supporting them in a macroscopic structure.

In this context, the use of biopolymers as a matrix to create GRM composites for water treatment has emerged as a widely explored and effective solution. I started with the use of biopolymers as a matrix to create GRM composites for water treatment. I have collaborated with several universities, partners in European projects, on the preparation of different composites for water treatment at the laboratory scale. We have explored different geometries, i.e. planar membranes, cylindrical aerogels and hydrogel beads, and different biopolymers, such as polycaprolactone or sodium alginate. Among the examples reported, alginate-GRM hydrogel composites were taken as a case study. These materials demonstrated the ability to remove contaminants even when the GRM are within a polymer matrix, while maintaining their original selectivity. In particular, lysine modified GO and reduced graphene oxide showed adsorption capacities comparable to the industrial benchmark, i.e. granular activated carbon. These composites showed slower adsorption kinetics than the respective nanomaterials used as powder, as the surface area available for contaminant interaction is definitely smaller and more difficult to access. However, the incorporation of GRM into the alginate matrix greatly simplifies the process of separating the sorbent from the treated solution, and it is also possible to regenerate them and exploit their potential for repeated use in water treatment applications.

Finally, my focus shifted to synthetic polymer-based composites, with particular emphasis on polysulfone hollow fiber membranes co-extruded with graphene oxide (PSU-GO HFs). These membranes were optimized for point-of-use water filtration and tested for the removal of a range of contaminants, including PFAS, heavy metals and organic contaminants. This work has resulted in an innovative material that acts

simultaneously as a filter and a sorbent and has been commercialised as a POU device for water treatment. In addition, an innovative approach was introduced to recycle PSU-GO industrial scrap into granular sorbents, promoting circular economy actions. These granules were tested in pilot plants mimicking real tap water conditions and proved effective in removing pharmaceuticals, heavy metals and PFAS without releasing GO into the water, confirming their safety and applicability.

In conclusion, this thesis demonstrates that graphene-related materials, especially when chemically modified or integrated with polymers, represent a promising approach to address the challenge of emerging contaminants in drinking water. By optimizing adsorption selectivity, enhancing material stability, and ensuring safe and sustainable use, GRM hold great potential for advancing water treatment technologies. Future work will prioritise the development of methods to regenerate exhausted materials to reduce the environmental impact of proposed technologies. In addition, biopolymer composites can be further engineered to achieve better performance and thus move from laboratory scale to point-of-use.

7 Appendix: Methodology and supporting information

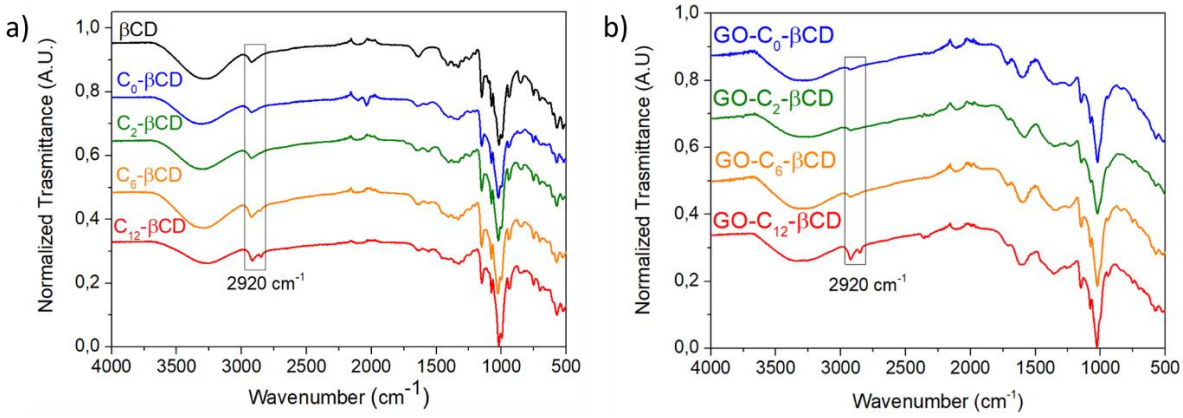

Figure 7.1 *ATR-FTIR spectra of a) βCD (black), C_0-βCD (blue), C_2-βCD (green), C_6-βCD (orange), C_{12}-βCD (red), and b) GO-C_0-βCD (blue), GO-C_2-βCD (green), GO-C_6-βCD (orange), GO-C_{12}-βCD (red).*

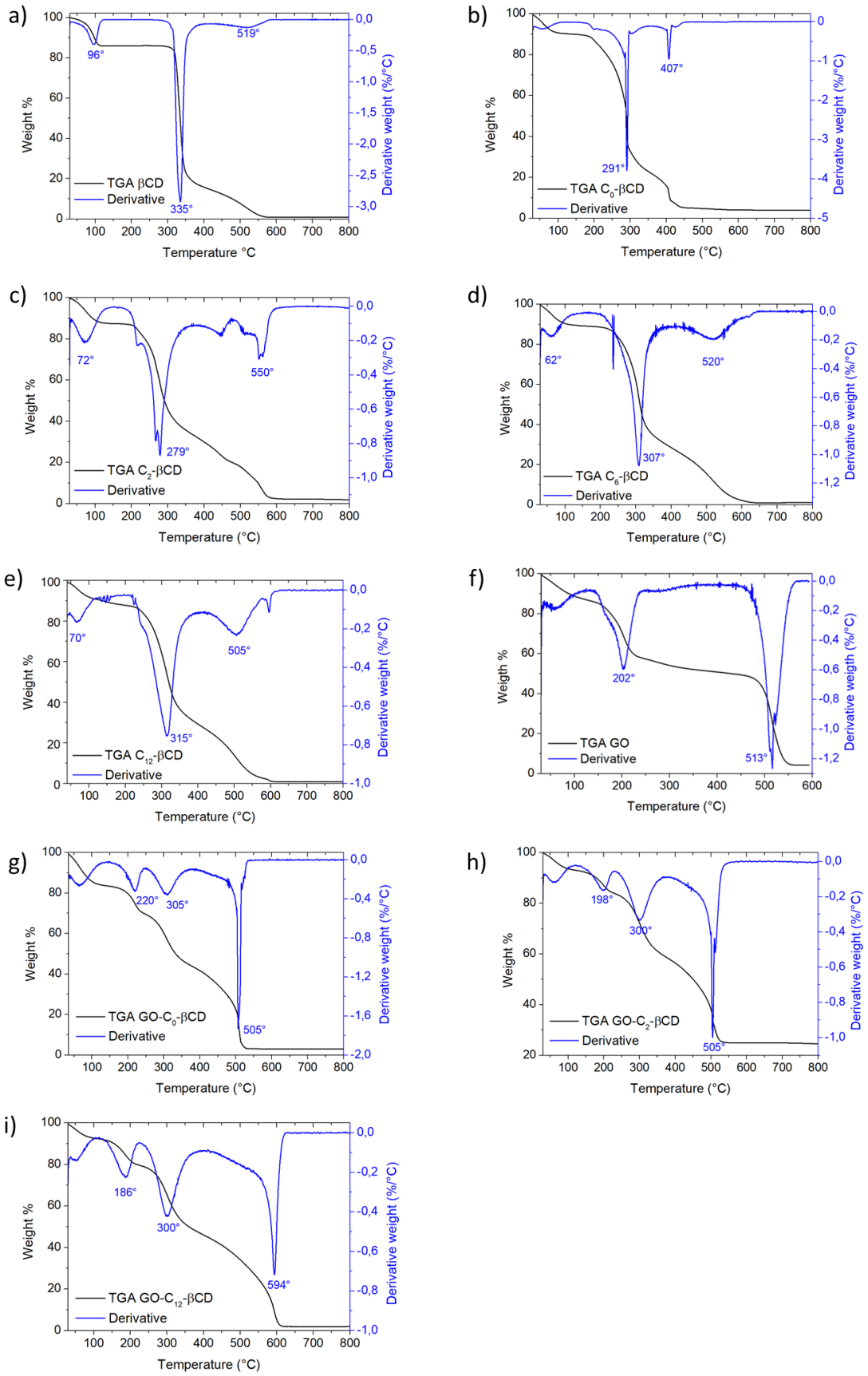

Figure 7.2 *TGA of a) βCD, b) C_0-βCD, c) C_2-βCD, d) C_6-βCD, e) C_{12}-βCD, f) GO, g) GO-C_0-βCD, h) GO-C_2-βCD, i) GO-C_{12}-βCD (10 °C/min in air).*

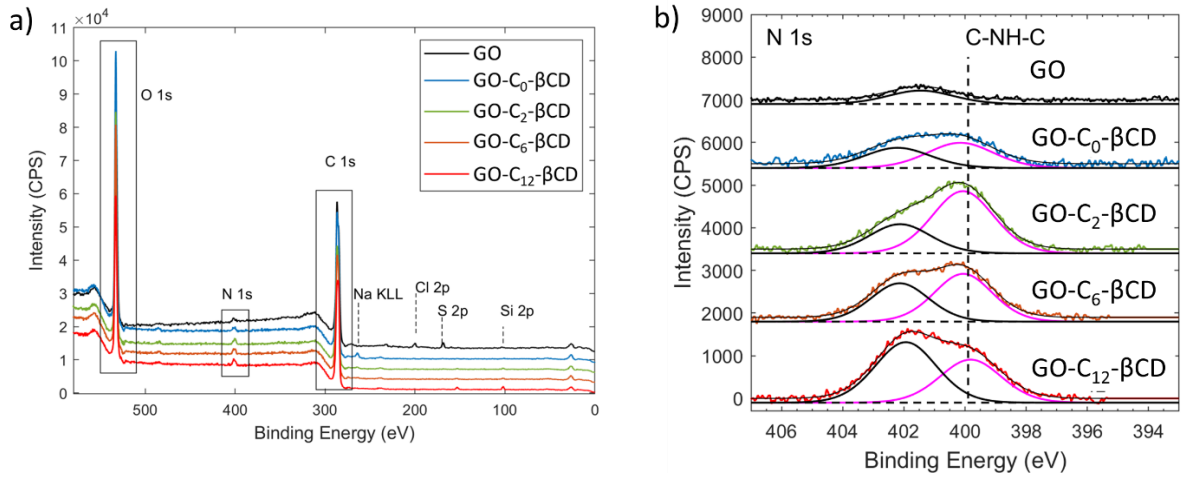

Figure 7.3 *a) XPS survey spectra and b) N 1s signals of GO (black), GO-C_0-βCD (blue), GO-C_2-βCD (green), GO-C_6-βCD (orange), and GO-C_{12}-βCD (red). N 1s was fitted by two voigt curves with binding energies at: i) 400.0 eV (C-NH-C, magenta line) and ii) 402.0 eV (other N atoms, black line). All spectra were shifted for better visualization.*

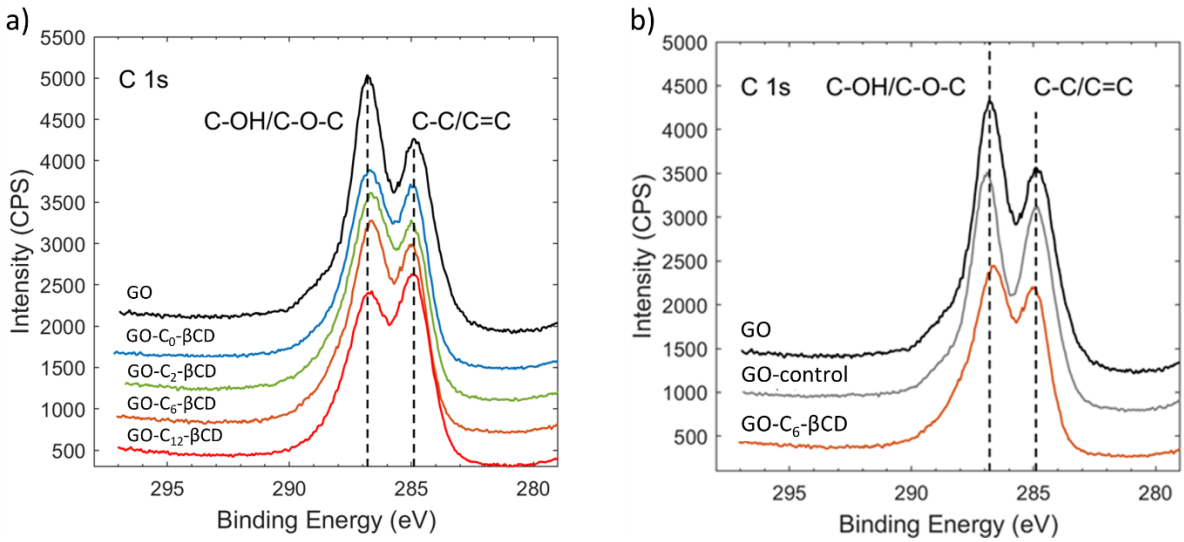

Figure 7.4 *C 1s XPS signal of a) GO (black), GO-C_0-βCD (blue), GO-C_2-βCD (green), GO-C_6-βCD (orange), GO-C_{12}-βCD (red), and b) GO (black), GO-control (grey) and GO-C_6-βCD (orange).*

Table 7.1 *Element content (wt. %) of C_0-βCD ($C_{42}H_{71}NO_{34}$), C_2-βCD ($C_{44}H_{76}N_2O_{34}$), C_6-βCD ($C_{48}H_{84}N_2O_{34}$), and C_{12}-βCD ($C_{54}H_{96}N_2O_{34}$).*

		Element content (wt. %)				
		C	**H**	**N**	**S**	**O**
C_0-βCD	**calculated**	44.5	6.3	1.2	-	48.0
	found	37.5	6.5	1.8	0.09	49.6
C_2-βCD	**calculated**	44.9	6.5	2.4	-	46.2
	found	38.0	6.9	2.4	0.1	47.9
C_6-βCD	**calculated**	46.8	6.9	2.3	-	44.1
	found	41.1	7.1	1.8	0.03	48.2
C_{12}-βCD	**calculated**	49.2	7.4	2.1	-	41.3
	found	44.8	7.7	2.2	0.09	43.8

Table 7.2 *Atomic composition and atomic ratios of βCD, C_0-βCD, C_2-βCD, C_6-βCD, C_{12}-βCD, GO, GO-control, GO@βCD, GO-C_0-βCD, GO-C_2-βCD, GO-C_6-βCD, and GO-C_{12}-βCD.*

	Atomic composition (%)					Molar ratio			
	C	**H**	**N**	**S**	**O**	**C/O**	**C/H**	**C/N**	**O/C**
βCD	23.39	51.12	0.00	0.04	25.45	**0,92**	**0,46**	**-**	**1,09**
C_0-βCD	24.35	50.45	1.00	0.02	24.17	**1.01**	**0.48**	**24.31**	**0.99**
C_2-βCD	24.00	51.97	1.29	0.03	22.71	**1.06**	**0.46**	**18.57**	**0.95**
C_6-βCD	25.15	51.73	0.96	0.03	22.12	**1.14**	**0.49**	**26.07**	**0.88**
C_{12}-βCD	26.08	53.69	1.08	0.02	19.14	**1.36**	**0.49**	**24.17**	**0.73**
GO	40.05	28.60	0.08	0.46	30.81	**1.30**	**1.40**	**-**	**0.77**
GO-control	39.14	31.02	0.10	0.08	29.65	**1.32**	**1.26**	**-**	**0.76**
GO@βCD	44.08	26.12	0.03	0.30	29.47	**1.50**	**1.69**	**-**	**0.67**
GO-C_0-βCD	32.03	38.51	0.35	0.03	29.08	**1.10**	**0.83**	**91.33**	**0.91**
GO-C_2-βCD	34.54	40.69	0.90	0.02	23.86	**1.45**	**0.85**	**38.31**	**0.69**
GO-C_6-βCD	34.69	41.53	0.75	0.02	23.01	**1.51**	**0.84**	**46.28**	**0.66**
GO-C_{12}-βCD	33.73	42.94	1.02	0.02	22.29	**1.51**	**0.79**	**32.99**	**0.66**

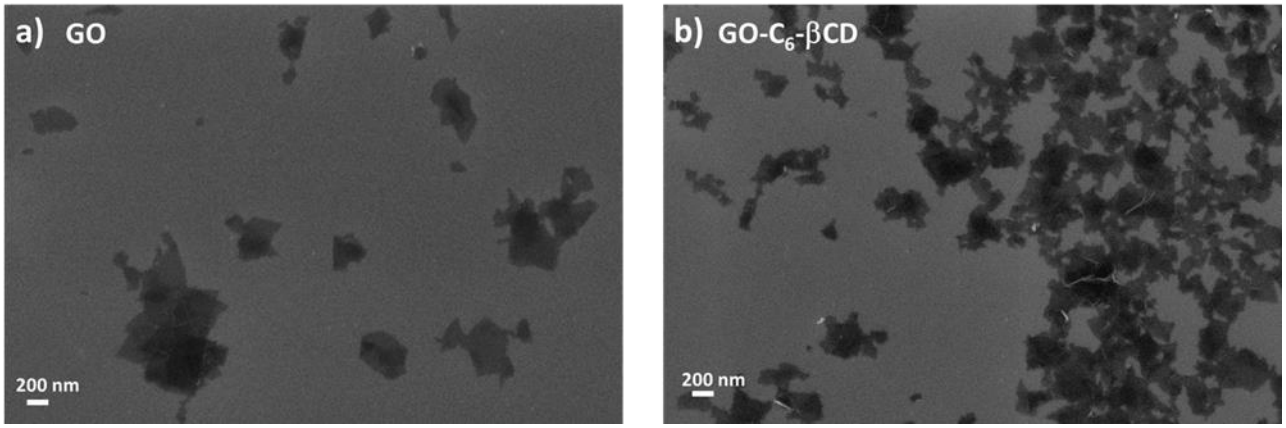

Figure 7.5 *SEM images of a) pristine GO, and b) GO-C_6-βCD.*

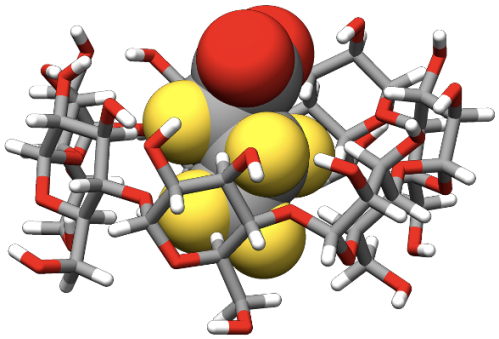

	PFBA@βCD
van der Waals	-14.3
Electrostatic	4.7
E_{SURF}	-2.6
Total Affinity	-12.3

Figure 7.6 *A representative snapshot, taken form MD simulation, of the interaction between PFBA and βCD. Computed total affinity and its contributions i.e., Van der Waals, electrostatic and non-polar solvation (Esurf) for PFBA inside βCD. All energies are reported in kcal mol^{-1}.*

Table 7.3 *Elution gradient used for PFBA analyses. Mobile phases: (A) MeOH:aqueous NH_4OAc 2 mM 95:5; (B) NH_4OAc 2 mM in MeOH.*

Time (min)	Analytical pump		
	Flow (mL min^{-1})	A%	B%
0	0.3	100	0
1	0.3	80	20
5	0.3	60	40
6	0.3	100	0
8	0.3	100	0

Table 7.4 *Elution gradient used for the analyses of the mixture of nine PFAS. Mobile phases: (A) MeOH:aqueous NH_4OAc 2 mM 95:5; (B) NH_4OAc 2 mM in MeOH.*

Time (min)	Analytical pump		
	Flow (mL min^{-1})	A%	B%
0	0.3	100	0
1	0.3	80	20
6	0.3	55	45
13	0.3	20	80
15	0.35	5	95
17	0.35	5	95
18	0.3	100	0
21	0.3	100	0

Table 7.5 *LC-MS/MS parameters for PFBA using UPLC-MS/MS ACQUITY UPLC H-Class PLUS – XEVO TQS Micro MS.*

Analyte	Monitored transition (ES-)	Collision energy (eV)	Limit of quantification (µg/L)
Perfluorobutanoic acid (PFBA)	212.97→168.99	8	0.01

Table 7.6 *LC-MS/MS parameters for the mixture of nine PFAS using UPLC-MS/MS ACQUITY UPLC H-Class PLUS – XEVO TQS Micro MS.*

Analyte	Monitored transition (ES-)	Collision energy (eV)	Limit of quantification (µg/L)
Perfluorobutanoic acid (PFBA)	212.97→168.99	8	0.01
Perfluorodecanoic acid (PFOA)	412.98→168.98	18	0.01
Perfluoroundecanoic acid (PFNA)	462.96→218.97	16	0.01
Perfluorododecanoic acid (PFOS)	498.90→79.90	54	0.01
Perfluorotridecanoic acid (PFDA)	513.12→469.00	10	0.01
Perfluorotetradecanoic acid (PFUnDA)	562.96→519.06	10	0.05
Perfluorobutanesulfonic acid (PFDODA)	613.06→569.04	14	0.05
Perfluorohexanesulfonic acid (PFTrDA)	622.90→168.97	28	0.05
Perfluorooctanesulfonic acid (PFTA)	712.96→168.96	32	0.1

Table 7.7 *Atomic composition (% at.) and O/C ratio of GO, GO-Lys, rGO and GNP.*

Transition	GO	GO-Lys	rGO	GNP
C 1s 285 eV	70.4 ± 0.8	81.5 ± 0.8	98.8 ± 0.3	94.5 ± 0.8
O 1s 532 eV	27.0 ± 0.5	13.9 ± 0.5	1.1 ± 0.2	4.7 ± 0.4
N 1s 400eV	0.7 ± 0.3	3.1 ± 0.3	-	-
Na KLL KE 990 eV	-	1.2 ± 0.3	-	-
Cl 2p 200eV	0.8 ± 0.2	0.3 ± 0.1	0.3 ± 0.1	-
S 2p 168 eV	1.0 ± 0.2	-	0.11 ± 0.04	0.6 ± 0.1
Fe $2p_{3/2}$ 712 eV	-	-	-	0.16 ± 0.05
O/C ratio	0.38	0.17	0.01	0.05

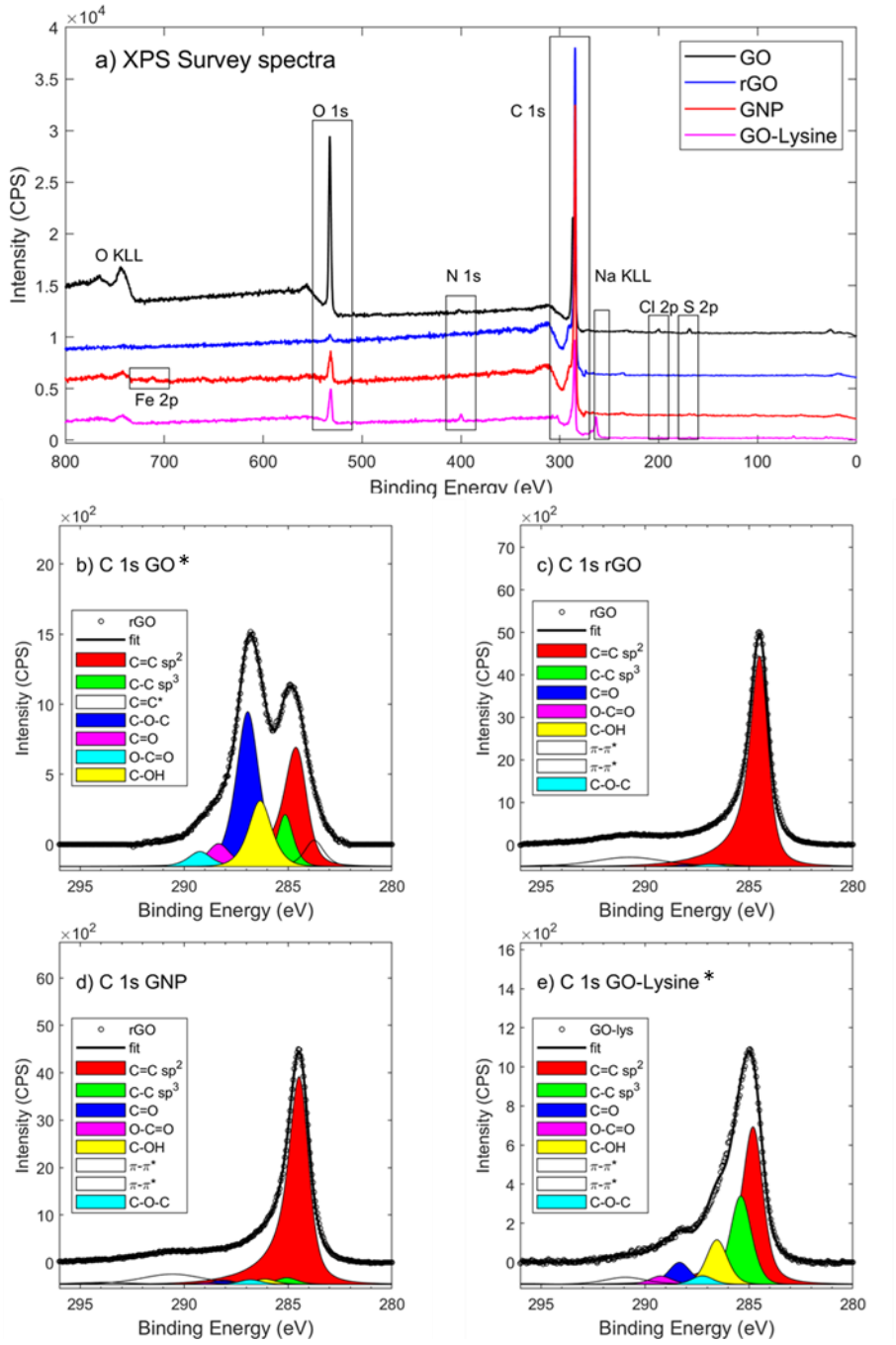

Figure 7.7 *Survey a) and C 1s spectra of b) GO, c) rGO, d) GNP and e) GO-Lysine. C=C sp^2 relative abundance obtained from C 1s fit (red component) was 36 %, 98%, 92% and 52 %, respectively.*

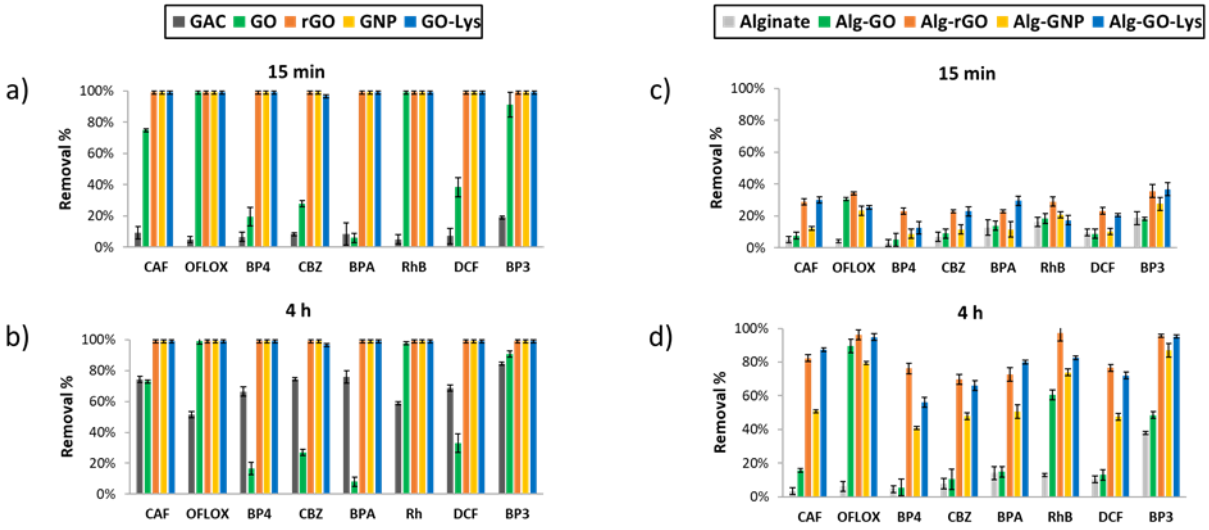

Figure 7.8 *Removal of ECs mix (0.5 mg/L each in tap water, V_{tot}= 25 mL, 25 mg of sorbent material). On the left, graphene nanosheets removal compared with GAC obtained after contact time of a) 15 min, and b) 4 h. On the right, alginate-graphene beds removal compared with pristine alginate beads after contact time of c) 15 min, and d) 4 h.*

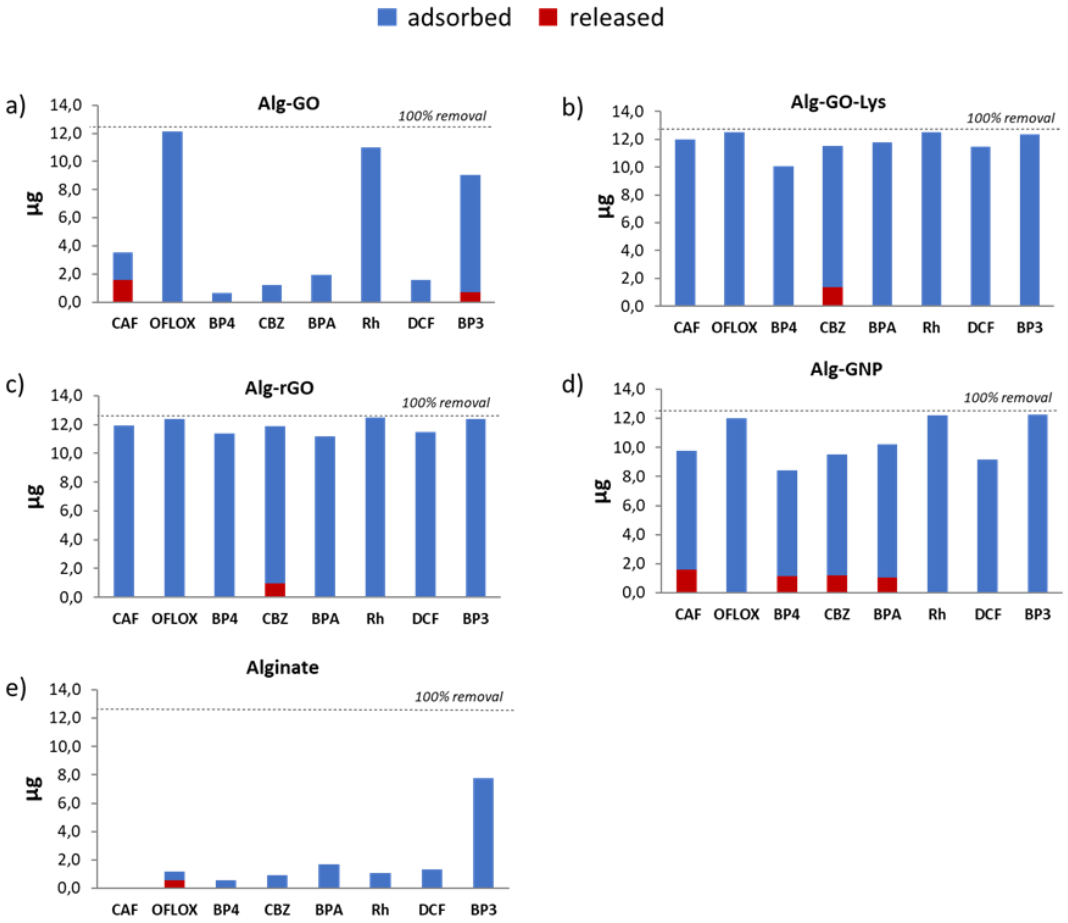

Figure 7.9 *Release test on a) Alg-GO, b) Alg-GO-Lys, c) Alg-rGO, d) Alg-GNP, and e) Alginate. Blue bars show the mass in µg adsorbed during kinetic test, red bars correspond to the mass in µg of contaminants released in fresh tap water (25 mg of beads used for kinetic test, V_{tot}=25 mL of tap water, contact time= 4 h).*

Table 7.8 *Experimental parameters of solutions used for isotherms studies on GO-Lys.*

Sample	Volume (mL)	C_0 RhB (mg/L)	GO-Lys (mg)
1	5	1	7
2	5	1	5
3	5	1	2
4	5	0.5	10
5	5	0.5	5
6	5	0.5	2
7	5	0.2	5
8	5	0.2	2

Table 7.9 *Experimental parameters of solutions used for isotherms studies on GNP.*

Sample	Volume (mL)	C_0 RhB (mg/L)	GNP (mg)
1	5	0.2	10
2	5	0.2	7
4	5	0.2	5
5	5	0.1	7
6	5	0.1	5
7	5	0.1	2
8	5	0.05	5
9	5	0.05	2

Table 7.10 *Experimental parameters of solutions used for isotherms studies on Alginate.*

Sample	Volume (mL)	C_0 RhB (mg/L)	Alginate (mg)
1	5	0.0005	1
2	5	0.0025	4
4	5	0.005	3
5	5	0.01	2
6	5	0.015	4
7	5	0.015	3
8	5	0.04	4
9	5	0.04	4
10	5	0.05	4

Table 7.11 *Experimental parameters of solutions used for isotherms studies on Alg-GO.*

Sample	Volume (mL)	C_0 RhB (mg/L)	Alg-GO (mg)
1	5	0.0025	0.5
2	5	0.005	0.5
4	5	0.010	0.5
5	5	0.015	0.5
6	5	0.020	0.5
7	5	0.025	0.5
8	5	0.030	0.5
9	5	0.040	0.5
10	5	0.050	0.5
11	5	0.060	0.5
12	55	0.070	0.5

Table 7.12 *Experimental parameters of solutions used for isotherms studies on Alg-GO-Lys.*

Sample	Volume (mL)	C_0 RhB (mg/L)	Alg-GO-Lys (mg)
1	5	0.010	0.5
2	5	0.015	0.5
4	5	0.020	0.5
5	5	0.040	0.5
6	5	0.050	0.5
7	5	0.100	0.5
8	5	0.300	0.5
9	5	0.500	0.5
10	5	0.750	0.5

Table 7.13 *Experimental parameters of solutions used for isotherms studies on Alg-rGO.*

Sample	Volume (mL)	C_0 RhB (mg/L)	Alg-rGO (mg)
1	5	0.005	0.5
2	5	0.010	0.5
4	5	0.015	0.5
5	5	0.020	0.5
6	5	0.025	0.5
7	5	0.040	0.5
8	5	0.050	0.5
9	5	0.100	0.5
10	5	0.200	0.5
11	5	0.300	0.5
12	5	0.500	0.5

Table 7.14 *Experimental parameters of solutions used for isotherms studies on Alg-GNP.*

Sample	Volume (mL)	C_0 RhB (mg/L)	Alg-GNP (mg)
1	5	0.0005	0.5
2	5	0.0010	0.5
4	5	0.0025	0.5
5	5	0.005	0.5
6	5	0.010	0.5
7	5	0.025	0.5
8	5	0.030	0.5
9	5	0.040	0.5
10	5	0.050	0.5
11	5	0.060	0.5

Table 7.15 *Fit parameters of the adsorption isotherms on rhodamine B (RhB) by GRM nanosheets.*

	Langmuir	$Q_e = Q_m \cdot \frac{C_e \cdot K_L}{1+K_L \cdot C_e}$		**BET**	$Q_e = \frac{Q_m \cdot C_{BET} \cdot x}{(1-x) \cdot (1+C_{BET} \cdot x-x)}$,	$x = \frac{C_e}{C_s}$	
	Q_m *[mg/g]*	**K_L** *[mL/mg]*	**R^2**	**Q_m** *[mg/g]*	**C_s** *[mg/mL]*	**C_{BET}**	**R^2**
GO-Lys	312	107	0.9704	167	1	600	0.5855
GNP	68	1519	0.9969	57	1	1763	0.9945

Table 7.16 *Fit parameters of the adsorption isotherms on rhodamine B (RhB) by alginate-GRM composites.*

	Langmuir $Q_e = Q_m \cdot \frac{C_e \cdot K_L}{1+K_L \cdot C_e}$			**BET** $Q_e = \frac{Q_m \cdot C_{BET} \cdot x}{(1-x) \cdot (1+C_{BET} \cdot x - x)}, \quad x = \frac{C_e}{C_s}$			
	Q_m *[mg/g]*	**K_L** *[mL/mg]*	**R^2**	**Q_m** *[mg/g]*	**C_s** *[mg/mL]*	**C_{BET}**	**R^2**
Alginate	0.6	229	0.9784	0.2	0.07	828	0.8268
Alg-GO	61	42	0.6035	15	0.07	226	0.99
Alg-GO-Lys	158	507	0.9975	113	1	44	0.841
Alg-rGO	449	22	0.8144	178	0.7	242	0. 9995
Alg-GNP	15	661	0.9877	7	0.1	1326	0.9576

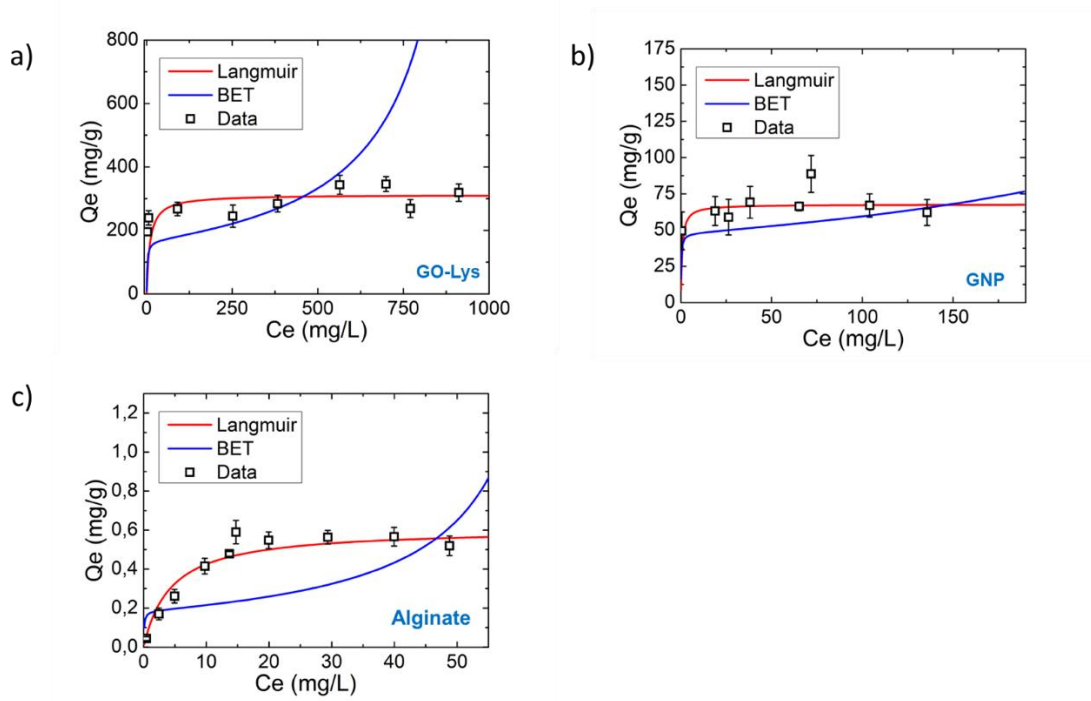

Figure 7.10 *Adsorption isotherm of (a) GNP, (b) GO-Lys, (c) alginate.*

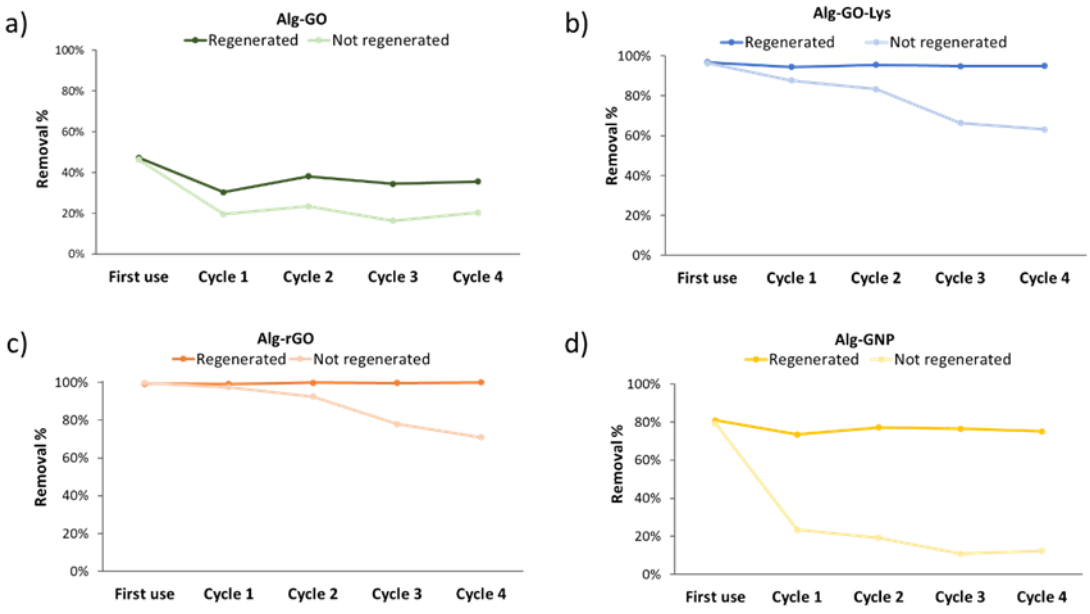

Figure 7.11 *Comparison between regenerated and not regenerated beads of (a) Alg-GO, (b) Alg-GO-Lys, (c) Alg-rGO and Alg-GNP.*

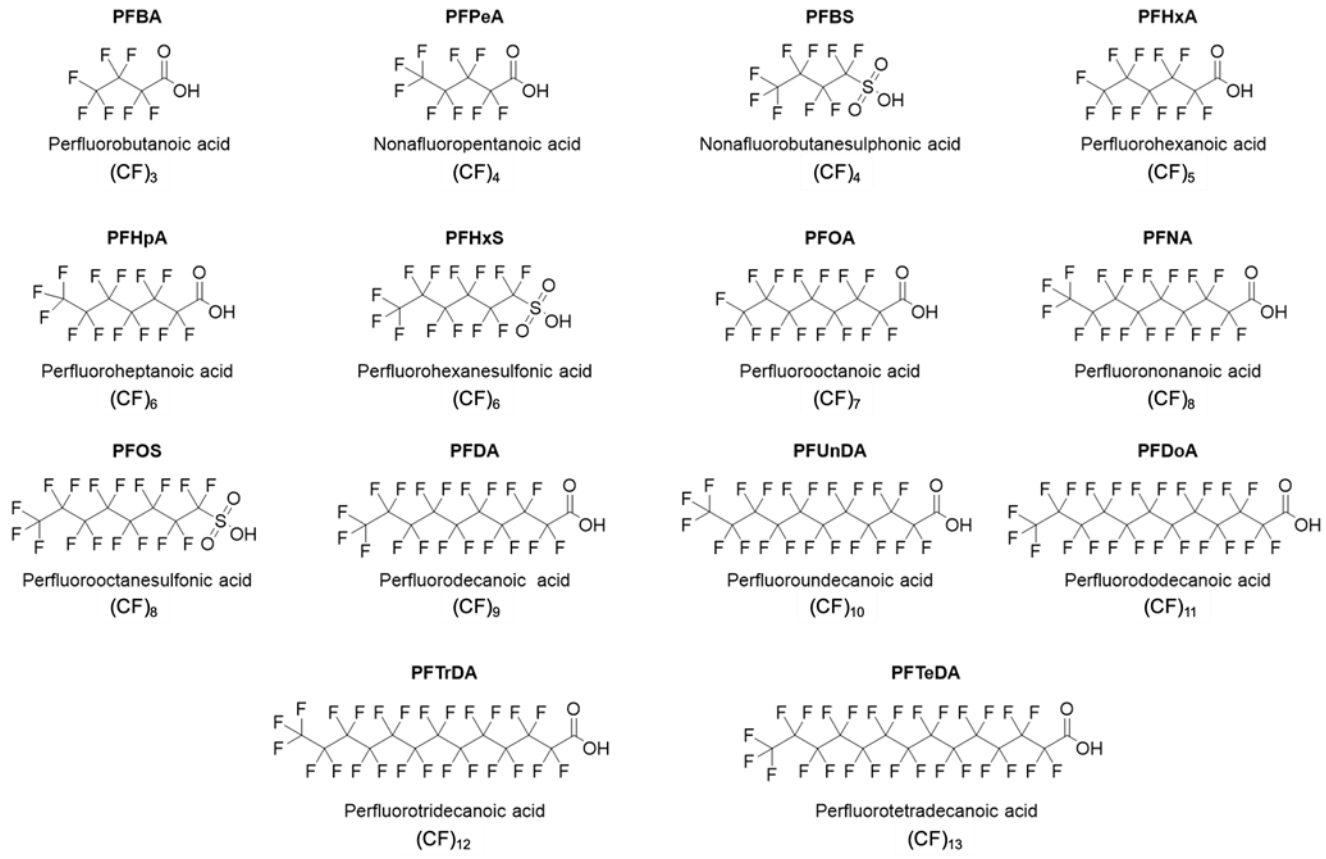

Figure 7.12 *Molecular structure of selected PFAS.*

Table 7.17 *Technical details of GAC purchased from CABOT Norit Spa (Ravenna, IT, Norit GAC 830 AF). NORIT GAC 830 is a granular activated carbon produced by steam activation of select grades of coal.*

Specifications	
Iodine number *(ASTM D 4607, 2014)*	> 1000 mg/g
Methylene blue index *(MU 182:98 M35)*	> 240 mg/g
Water soluble ashes *(MU 182:98 M33)*	< 11%
Granulometry >8 US mesh *(MU 182:98 M32)*	< 5 %
Granulometry <30 US mesh *(MU 182:98 M32)*	< 5%
Moisture (as packed)	< 5%
Ball-pan hardness *(ASTM D 3802)*	> 90
Apparent density *(MU 182:98 M31)*	> 450 kg/m^3
Molasses index *(Norit Standard Test Method)*	> 230
Pores distribution	Micro: > 45%; Meso: > 30%
Total pores volume	0.9-1.1 mL/g
Surface area *(BET method)*	> 1000 m^2/g
Uniformity coefficient	> 1.9
Density backwashed and drained	> 400 kg/m^3
Bed expansion	> 8% at linear rate 12.5 m/h at 20 °C

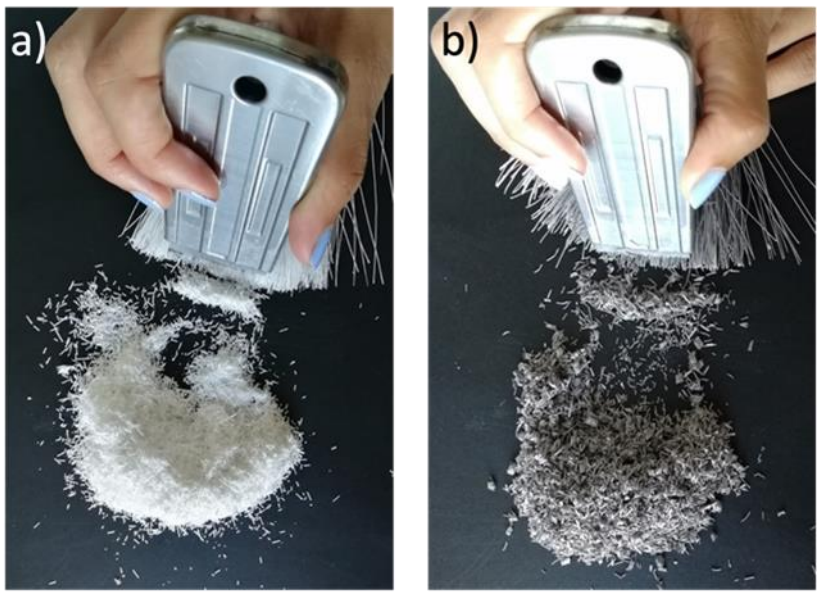

Figure 7.13 *Manual grinding PSU (a) and PSU-GO (b).*

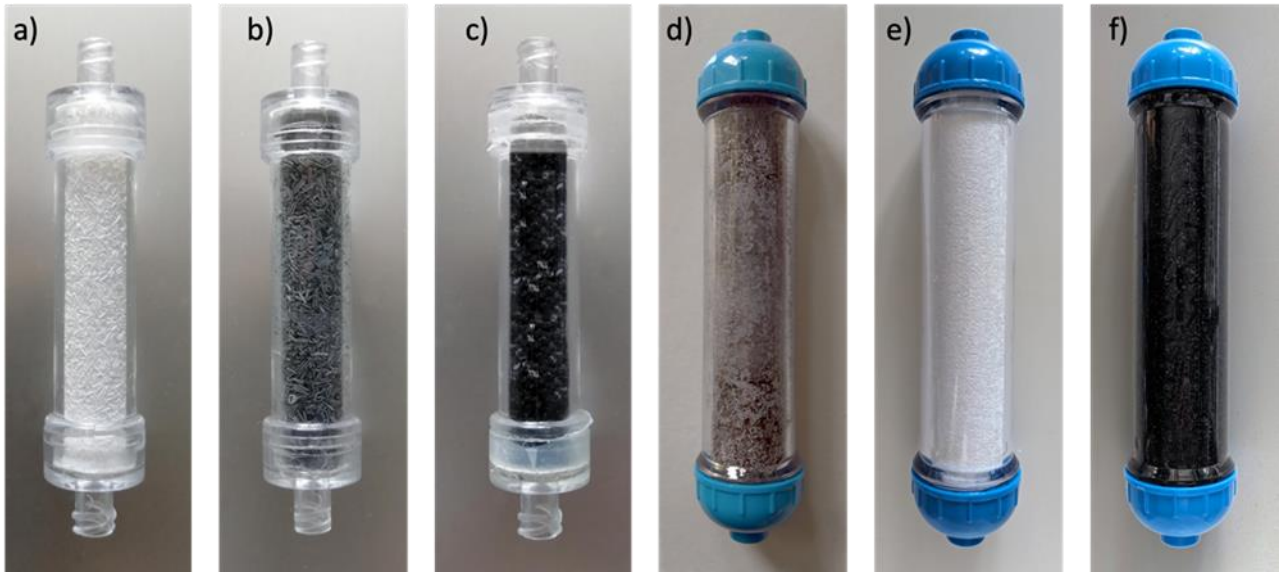

Figure 7.14 *Modules filled with granules: a) PSU (0.4 g), b) PSU-GO (0.73 g), c) GAC (2.3 g), d) PSU-GO granules (33 g), e) PSU granules (33 g),f) GAC (130 g). a) – c) Small modules (mm 14 x 65, EBCT = 0.5 min, Bed volume= 0.01 L), d-f) large module (mm 49 x 250, EBCT = 0.14 min, Bed volume 0.5 L).*

Table 7.18 *Elution gradients used for PFAS analyses. Mobile phases: (A) MeOH:aqueous NH_4OAc 2 mM 95:5; (B) NH_4OAc 2 mM in MeOH.*

Time (min)	Flow (mL/min)	%A	%B
0.00	0.300	100.0	0.0
1.00	0.300	80.0	20.0
6.00	0.300	55.0	45.0
13.00	0.300	20.0	80.0
15.00	0.350	5.0	95.0
17.00	0.350	5.0	95.0
18.00	0.300	100.0	0.0
21.00	0.300	100.0	0.0

Table 7.19 *Elution gradients used for PFOA analyses. Mobile phases: (A) MeOH:aqueous NH_4OAc 2 mM 95:5; (B) NH_4OAc 2 mM in MeOH.*

Time (min)	Flow (mL/min)	%A	%B
0.00	0.300	70.0	30.0
5.00	0.300	5.0	95.0
7.00	0.300	5.0	95.0
8.00	0.300	70.0	30.0
11.00	0.300	70.0	30.0

Table 7.20 *LC-MS/MS parameters for all PFAS target analytes using UPLC-MS/MS Waters ACQUITY UPLC H-Class PLUS – XEVO TQS Micro mass detector.*

	Name	Monitored transition (ES^-)	Collision energy (eV)	LOQ µg/L)
PFBA	Perfluorobutanoic acid	212.97→168.99	8	0.01
PFPeA	Perfluoropentanoic acid	263.09→218.93	6	0.01
PFBS	Perfluorohexanoic acid	299.03→79.84	32	0.01
PFHxA	Perfluoroheptanoic acid	312.90→269.02	6	0.01
PFHpA	Perfluorooctanoic acid	262.90→168.98	6	0.01
PFHxS	Perfluorononanoic acid	398.96→79.90	38	0.01
PFOA	Perfluorodecanoic acid	412.98→168.98	18	0.01
PFNA	Perfluoroundecanoic acid	462.96→218.97	16	0.01
PFOS	Perfluorododecanoic acid	498.90→79.90	54	0.01
PFDA	Perfluorotridecanoic acid	513.12→469.00	10	0.01
PFUnDA	Perfluorotetradecanoic acid	562.96→519.06	10	0.05
PFDODA	Perfluorobutanesulfonic acid	613.06→569.04	14	0.05
PFTrDA	Perfluorohexanesulfonic acid	622.90→168.97	28	0.05
PFTA	Perfluorooctanesulfonic acid	712.96→168.96	32	0.1

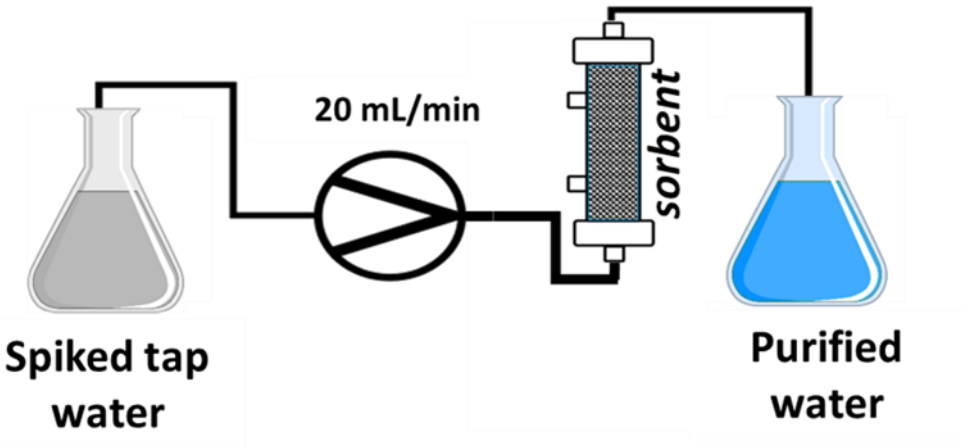

Figure 7.15 *Scheme of the experimental set up used for the adsorption test. The spiked solution flowed through the filtration module and the purified water was analyzed. Flow rate: 20 mL/min, EBCT = 0.5 min. The same set-up was used to wash the module before use, in order to remove glycerin. In this case, ultrapure water was filtered through the module.*

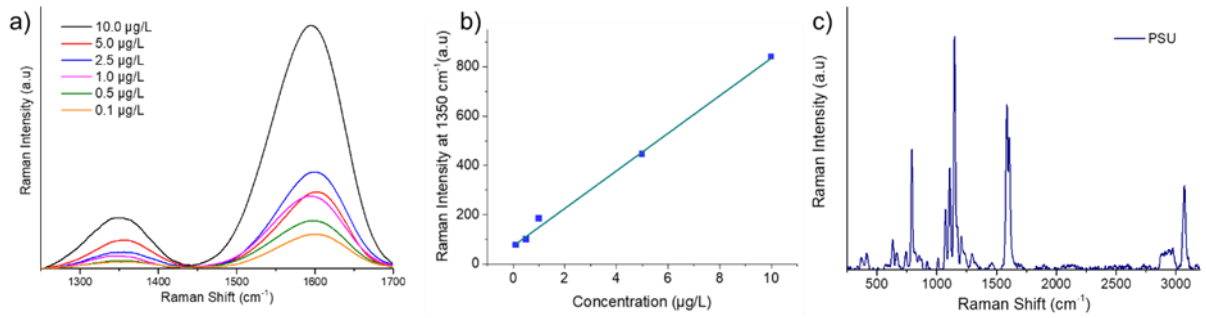

Figure 7.16 *a) SERS spectra of different GO concentrations in the range of 0.1−10 µg L^{-1}, b) calibration curve, c) Raman spectrum of PSU.*

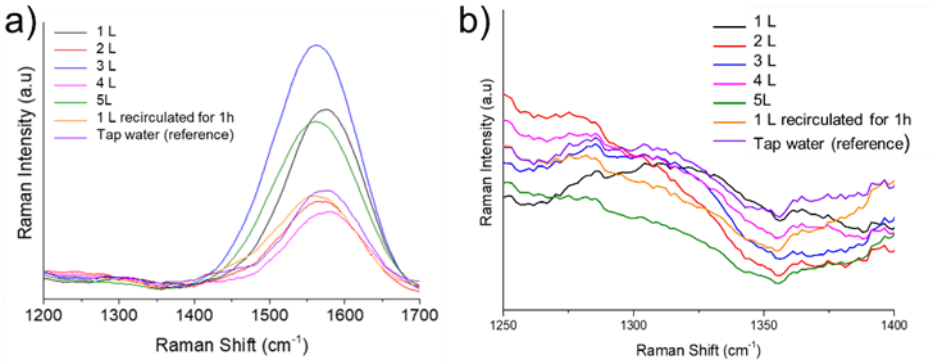

Figure 7.17 *a) SERS spectra of filtered water, from 1 L to 5 L, 1 L recirculated for 1 h, and tap water, b) Zoom at 1˙350 cm^{-1} of SERS spectra.*

Table 7.21 *Filtered water samples and intensity values (1˙350 cm^{-1}) measured on SERS substrates. Relative standard deviation (RSD) of intensity values (3˙000 points per sample) and obtained GO concentration (µg/L)*

Sample	**Intensity (A.U.)**	**%Rsd**	**Concentration (µg/L)**
1 L	18.20	4.03	<0.1
2 L	12.30	5.28	<0.1
3 L	14.12	5.02	<0.1
4 L	15.98	4.97	<0.1
5 L	11.12	7.86	<0.1
1 L recirculate for 1h	14.37	3.63	<0.1
TAP water (reference)	17.64	8.22	-

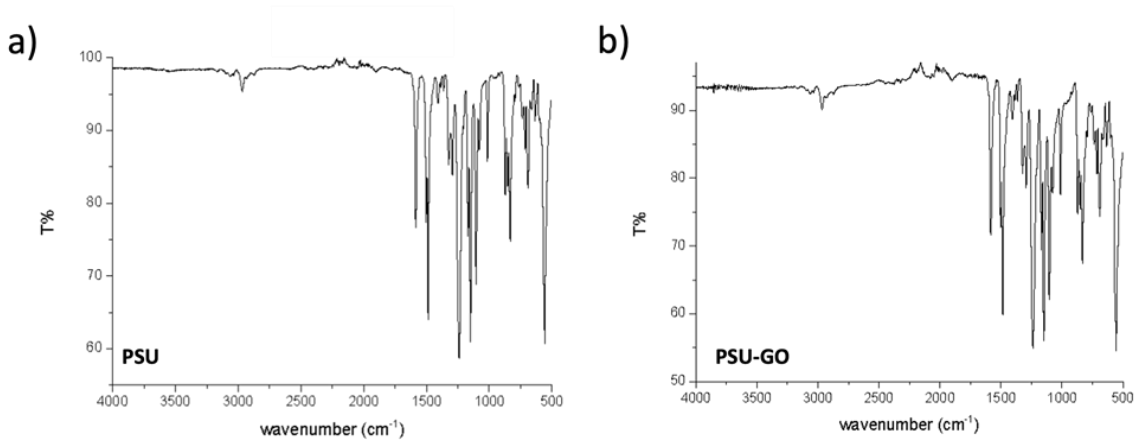

Figure 7.18 *Attenuated total reflection Fourier-transform infrared (ATR FT-IR) spectra on a) PSU and b) PSU-GO samples.*

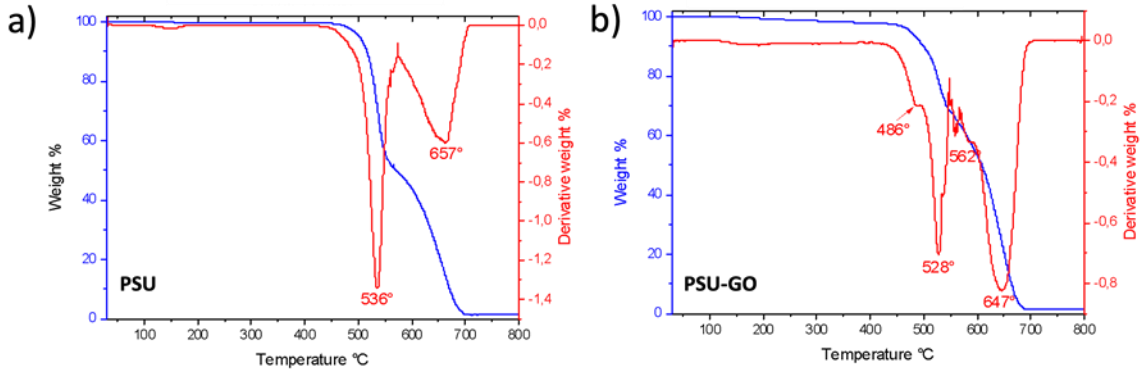

Figure 7.19 *Thermogravimetric analysis (TGA) on a) PSU and b) PSUGO samples.*

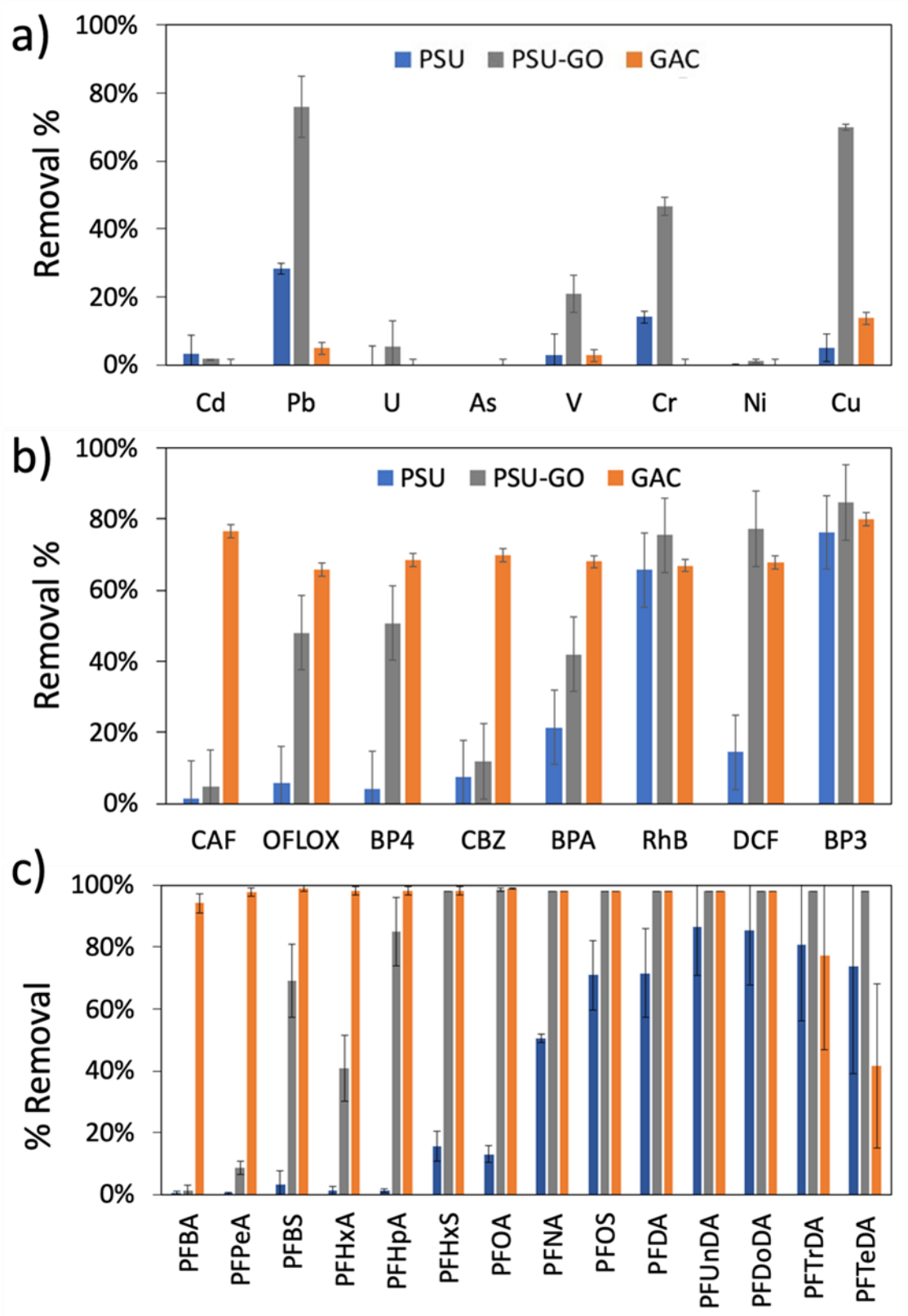

Figure 7.20 *Adsorption selectivity of modules of PSU (0.4g) PSU-GO (0.73g) and GAC (2.3g) towards mixture in tap water (flow rate = 20 mL/min, EBCT = 0.5 min, total treated volume 1 L, 100 bed volumes) of a) metals (C_{IN} = 100 µg/L each), b) selected organic contaminants (C_{IN} = 0.5 mg/L each), c) PFAS (C_{IN} = 0.5 µg/L each). PSU (blue bars), PSU-GO (grey bars) and GAC (orange bars) modules.*

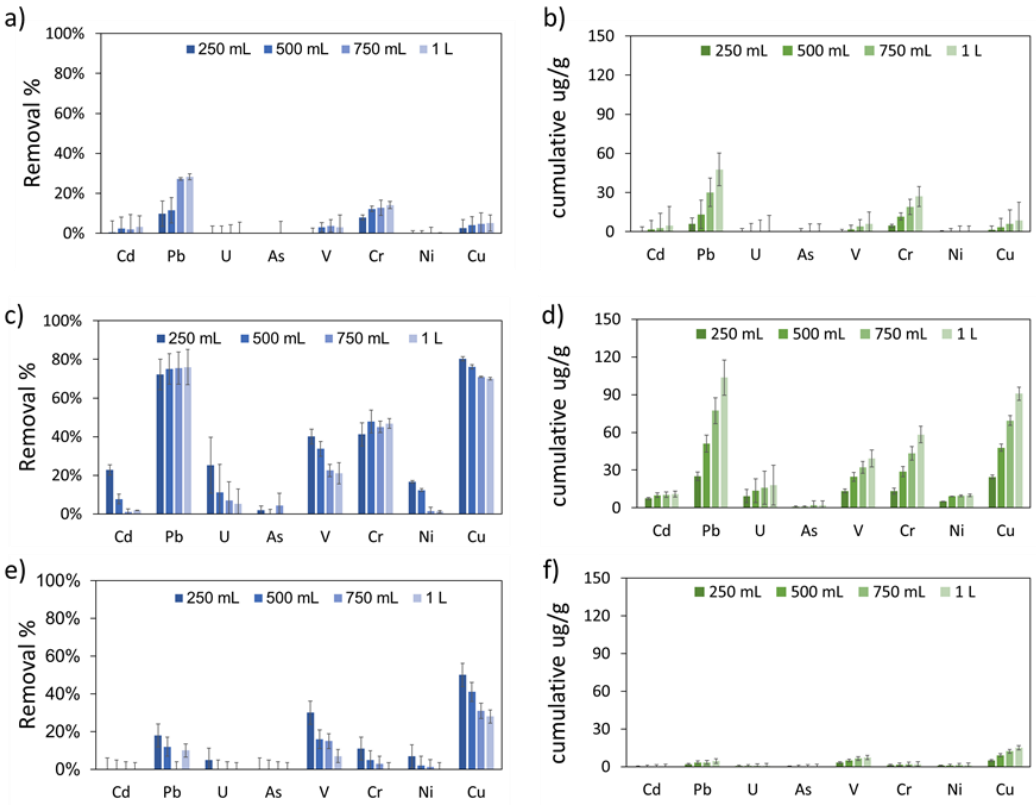

Figure 7.21 *Removal of a) PSU, c) PSU-GO, and e) GAC on a mixture of eight heavy metals and metalloids in tap water. Cumulative µg removed/g of b) PSU, d) PSU-GO and f) GAC. (C_{IN} = 100 µg/L each, V_{TOT} = 1 L, flow rate = 20 mL/min, EBCT = 0.5 min, bed volume=0.01 L).*

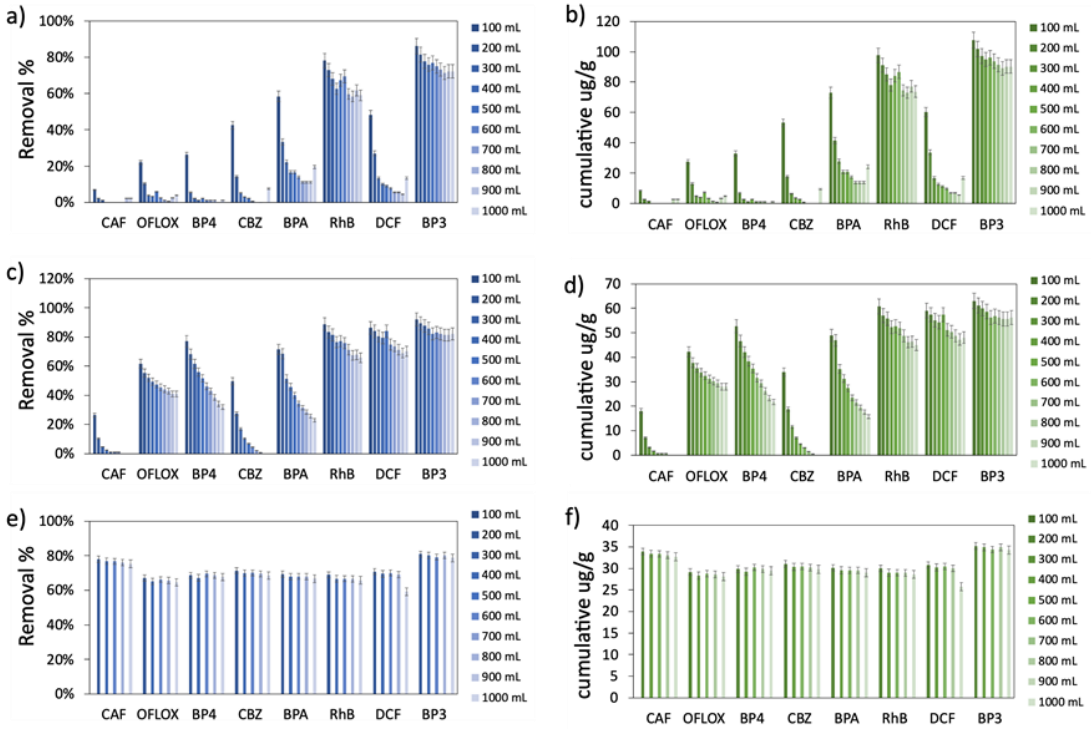

Figure 7.22 *Removal of a) PSU, c) PSU-GO, and e) GAC on a mixture of eight organic contaminants in tap water. Cumulativeµg removed/g of b) PSU, d) PSU-GO and f) GAC. (C_{IN} = 0.5 mg/L each, V_{TOT} = 1 L, flow rate = 20 mL/min, EBCT = 0.5 min, bed volume=0.01 L).*

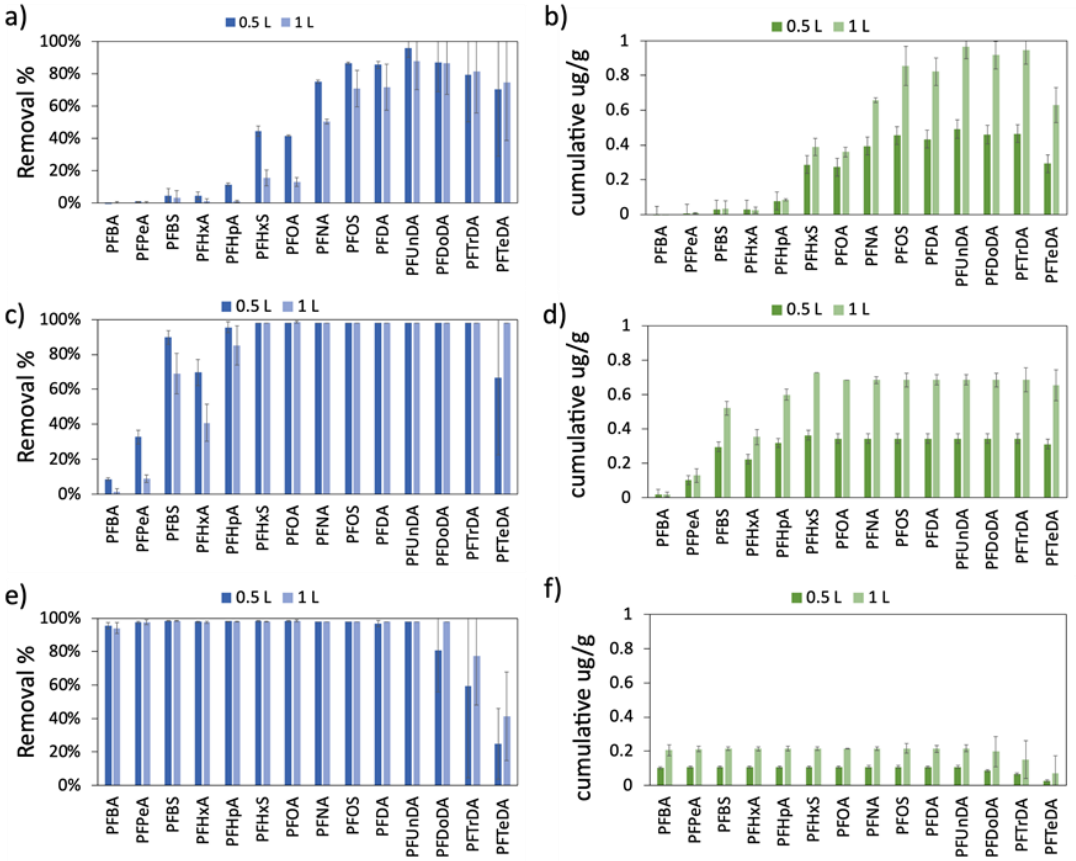

Figure 7.23 *Removal of a) PSU, b) PSU-GO and c) GAC on a mixture of fourteen PFAS in tap water. Cumulative µg removed/g of b) PSU, d) PSU-GO and f) GAC. (C_{IN} = 0.5 µg/L each, V_{TOT} = 1 L, flow rate = 20 mL/min, EBCT = 0.5 min, bed volume=0.01 L).*

Table 7.22 *n-Octanol/water partition coefficient ($logK_{ow}$) of carboxylic PFAS, and removal for PSU and PSU-GO.*

	Log K_{ow}	PSU		PSU-GO	
		µg/g	Removal %	µg/g	Removal %
PFBA (CF_3)	2.31	0.001	0	0.017	1
PFPeA (CF_4)	3.01	0.007	0	0.128	9
PFHxA (CF_5)	3.48	0.024	1	0.352	41
PFHpA (CF_6)	4.15	0.085	1	0.600	85
PFOA (CF_7)	4.81	0.359	13	0.683	98
PFNA (CF_8)	5.48	0.657	51	0.685	98
PFDA (CF_9)	6.51	0.822	72	0.685	98
PFUnDA (CF_{10})	7.20	0.967	88	0.685	98
PFDoDA (CF_{11})	7.92	0.918	86	0.685	98
PFTrDA (CF_{12})	8.62	0.946	82	0.685	98
PFTeDA (CF_{13})	9.32	0.630	75	0.652	98

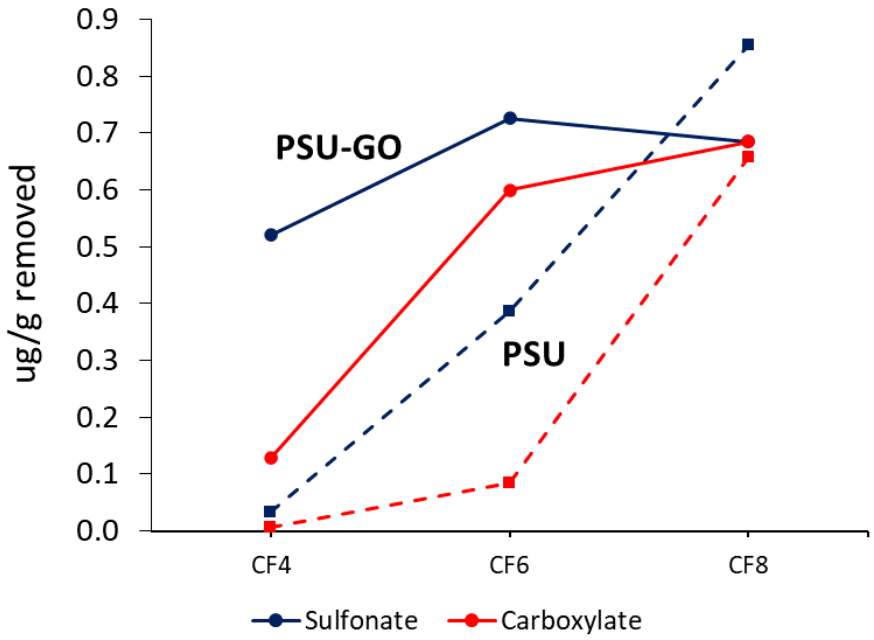

Figure 7.24 *Comparison between the mg of PFAS/g removed by PSU-GO (solid line) and PSU (dotted line). The µg removed of sulfonate (blue) and carboxylate (red) PFAS have been correlated to the number of fluorinated carbon (CF_n).*

Table 7.23 *Comparison between the removal of sulfonate and carboxylate PFAS correlated to the number of fluorinated carbon (CF_n) and K_{ow}.*

	Log K_{ow}	PSU		PSU-GO	
		µg/g	Removal %	µg/g	Removal %
PFBA (CF_3)	1.82	0.03	3	0.52	69
PFPeA (CF_4)	3.01	0.01	0	0.13	9
PFHxA (CF_5)	3.16	0.39	16	0.73	98
PFHpA (CF_6)	4.15	0.09	1	0.60	85
PFOA (CF_7)	4.49	0.85	71	0.68	98
PFNA (CF_8)	5.48	0.66	51	0.68	98

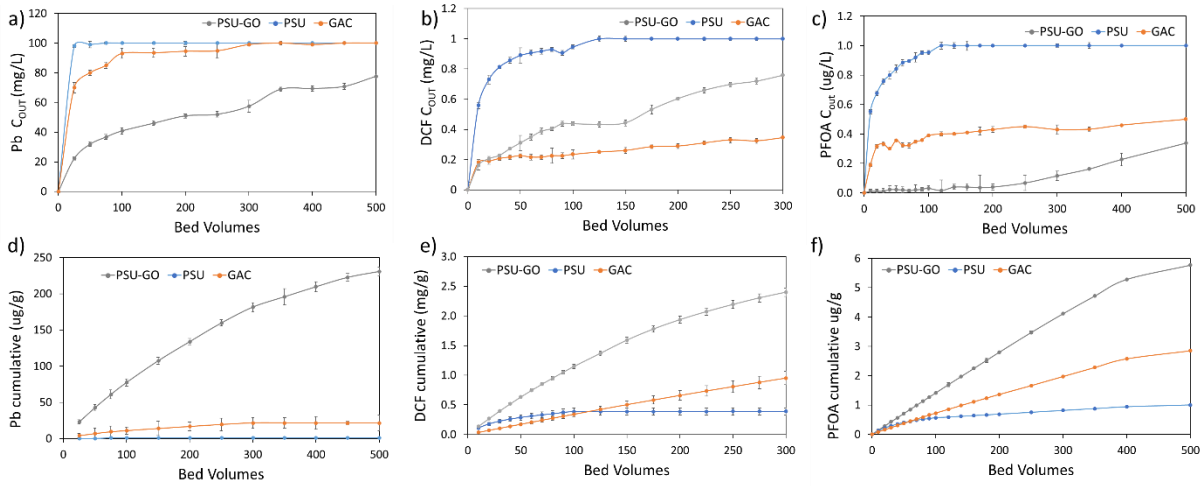

Figure 7.25 *Loading curve of a) Pb , b) DCF, c) PFOA; cumulative mg/g removed for d) Pb, e) DCF and f) PFOA. Results are expressed in Bed Volumes (Vol treated/V modules).*

Table 7.24 *Potability test on tap water after filtration.*

Parameter *Method*	*PSU-GO*		*Limits*
Turbidity	*<0.02*		
APAT CNR IRSA 2110 Man 29 2003			
Smell	*Odorless*		
APAT CNR IRSA 2050 Man 29 2003			
Taste	*Tasteless*		
APAT CNR IRSA 2080 Man 29 2003			
Color	*Colorless*		
APAT CNR IRSA 2020 A Man 29 2003			
pH	*8*	*±0.4*	*6.5/9.5*
APAT CNR IRSA 2060 Man 29 2003			
TOC (mg/L)	*< 1*		
UNI EN 1484:1999			
Conductivity (microS/cm)	*508*	*±38*	*<2500*
APAT CNR IRSA 2030 Man 29 2003			
Water hardness (°F)	*55*	*±11*	*15/50*
APAT CNR IRSA 3010 B			
+ APAT CNR IRSA 3020 Man 29 2003			
Fixed residue a 180°C (mg/L)	*389.0*	*±31.1*	*<1500*

APAT CNR IRSA 2090 B Man 29 2003			
Ammoniacal nitrogen$^{(NH4+)}$ (mg/L)	*<0.02*		
UNI 11669:2017			
Chloride (mg/L)	*38.50*	*±3.85*	*<250*
APAT CNR IRSA 4020 Man 29 2003			
Sulphate (mg/L)	*117.1*	*±14.1*	*<250*
APAT CNR IRSA 4020 Man 29 2003			
Nitrite (mg/L)	*0.07*	*±0.01*	*<0.5*
APAT CNR IRSA 4020 Man 29 2003			
Iron (ICP-MS) (µg/L)	*9.2*	*±0.8*	*<200*
EPA 6020B 2014			
Aluminium (ICP-MS) (µg/L)	*7.6*	*±0.7*	*<200*
EPA 6020B 2014			
Manganese (ICP-MS) (µg/L)	*<0.1*		*<50*
EPA 6020B 2014			
Sodium (mg/L)	*38.81*	*±5.59*	*<200*
APAT CNR IRSA 3010 B			
+ APAT CNR IRSA 3020 Man 29 2003			
Escherichia coli	*0*		*<0*
UNI EN ISO 9308-1:2017			
Intestinal Enterococci	*0*		*<0*
UNI EN ISO 7899-2:2003			
Antimony (ICP-MS) (µg/L)	*<0.1*		*<0.5*
EPA 6020B 2014			
Arsenic (ICP-MS) (µg/L)	*<0.1*		*<10*
EPA 6020B 2014			
Boron (mg/L)	*0.12*	*±0.02*	
APAT CNR IRSA 3010 B + APAT CNR IRSA 3020 Man 29 2003			
Cadmium (ICP-MS) (µg/L)	*0.01*	*±0.002*	*<5.0*
EPA 6020B 2014			
Chromium (ICP-MS) (µg/L)	*0.6*	*±0.09*	*<50*
EPA 6020B 2014			

Mercury (ICP-MS) (µg/L)	*<0.1*		*<1.0*
EPA 6020B 2014			
Nichel (ICP-MS) (µg/L)	*0.5*	*±0.07*	*<20*
EPA 6020B 2014			
Lead (ICP-MS) (µg/L)	*0.5*	*±0.07*	*<10*
EPA 6020B 2014			
Copper (mg/L)	*<0.01*		
APAT CNR IRSA 3010 B + APAT CNR IRSA 3020 Man 29 2003			
Selenium (mg/L)	*<0.06*		
APAT CNR IRSA 3010 B + APAT CNR IRSA 3020 Man 29 2003			
Vanadium (ICP-MS) (µg/L)	*0.3*	*±0.04*	*<50*
EPA 6020B 2014			
1.2-Dichloroethane (µg/L)	*<0.1*		
EPA 5030C 2003 + EPA 8260D 2018			
Fluorides (mg/L)	*0.09*	*±0.02*	
APAT CNR IRSA 4020 Man 29 2003			
Nitrate (mg/L)	*3.21*	*±0.48*	*<50*
APAT CNR IRSA 4020 Man 29 2003			
Nitrite (mg/L)	*0.07*	*±0.01*	*<0.5*
APAT CNR IRSA 4020 Man 29 2003			
Trihalomethanes (Total) (µg/L)	*<0.05*		
EPA 5030C 2003 + EPA 8260D 2018			
Vinyl chloride (µg/L)	*<0.1*		
EPA 5030C 2003 + EPA 8260D 2018			
Chlorites (µg/L)	*<0.1*		
APAT CNR IRSA 4020 Man 29 2003			
Benzo(a)pyrene (µg/L)	*<0.002*		
APAT CNR IRSA 4020 Man 29 2003			
Benzene (µg/L)	*<0.1*		
EPA 5030C 2003 + EPA 8260D 2018			
Acrylamide (µg/L)	*<0.01*		
EPA 5030C 2003 + EPA 8260D 2018			

Brominated (mg/L)	*<0.1*
APAT CNR IRSA 4020 Man 29 2003	
Free Cyanides (µg/L)	*<0.05*
APAT CNR IRSA 4020 Man 29 2003	
Polycyclic Aromatic Hydrocarbons (µg/L)	*<0.002*
EPA 8272 2007	
Total Pesticide (µg/L)	*<0.02*
APAT CNR IRSA 4020 Man 29 2003	
Epichlorohydrin (µg/L)	*<0.1*
EPA 5030C 2003 + EPA 8260D 2018	
Tetrachloroethylene + trichloroethylene (µg/L)	*<0.1*
EPA 5030C 2003 + EPA 8260D 2018	

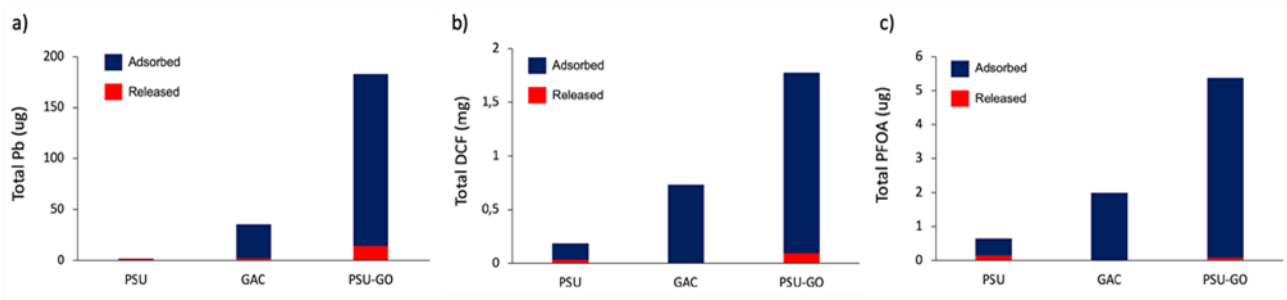

Figure 7.26 *Release of a) Pb, b) DCF, and c) PFOA for saturated PSU, PSU-GO, and GAC modules with tap water.*

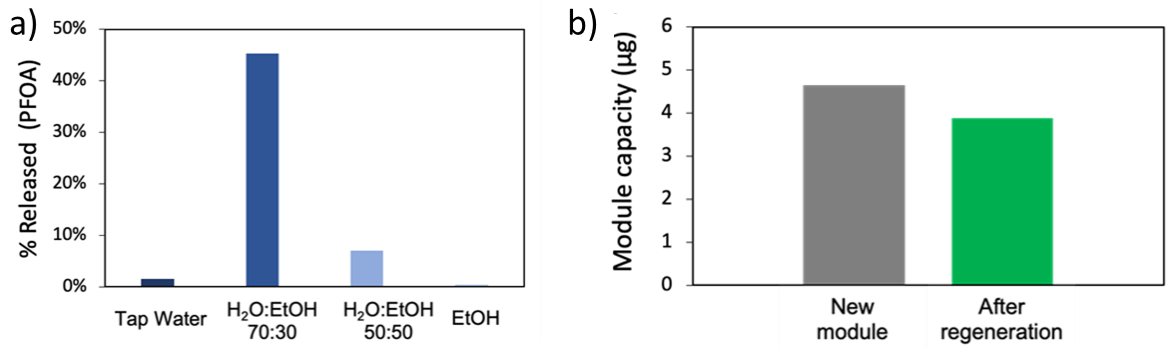

Figure 7.27 *a) Release of PFOA for PSU-GO washed with different ultrapure H_2O:EtOH mixtures and b) mg of PFOA adsorbed by a module before and after regeneration.*

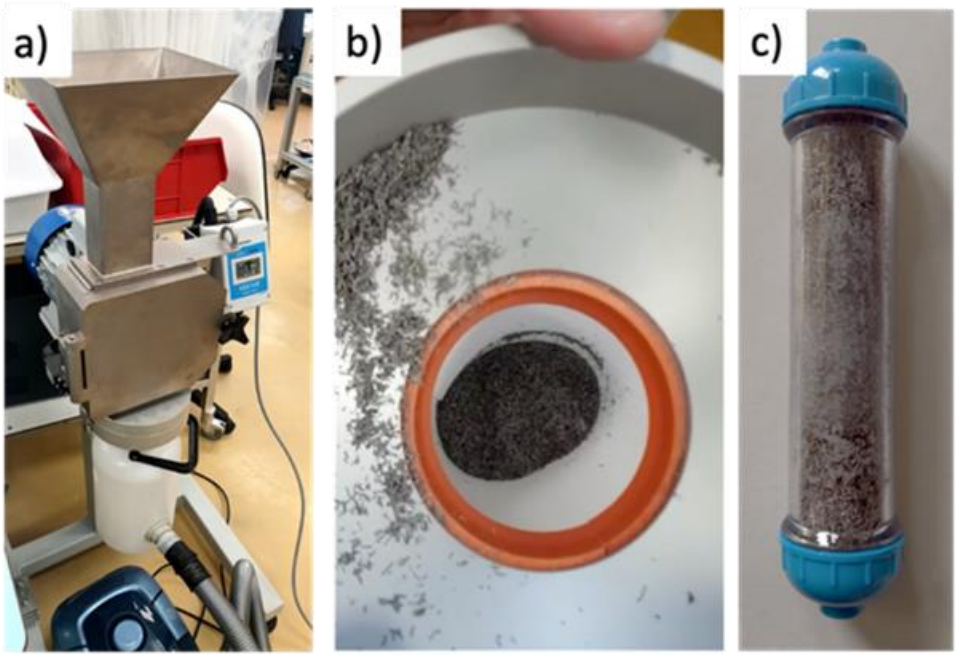

Figure 7.28 *a) Mechanical blade grinder, b) zoom of PSU-GO granules obtained, c) larger modules filled with the obtained granules (49 mm diameter, 250 mm length, EBCT = 0.14 min, bed volume = 0.5 L) of PSU-GO.*

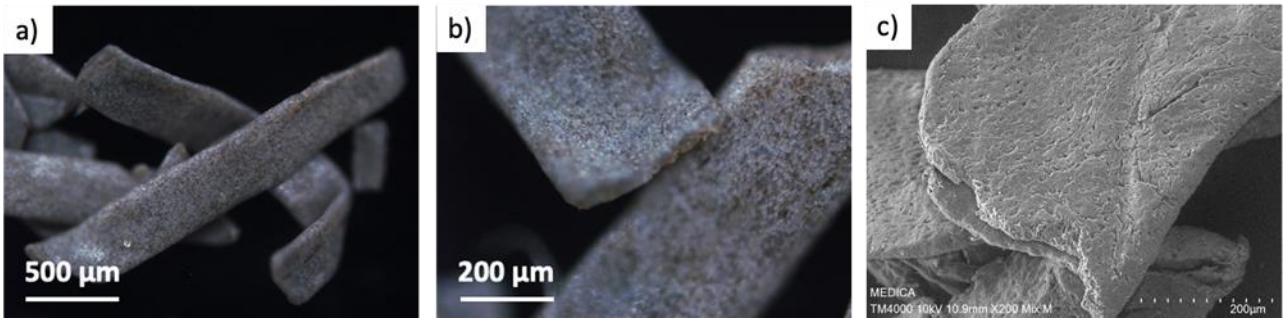

Figure 7.29 *a, b) Optical microscopy images at different magnification and c) SEM image of granules obtained by mechanical grinding of scraps of PSU-GO-HF.*

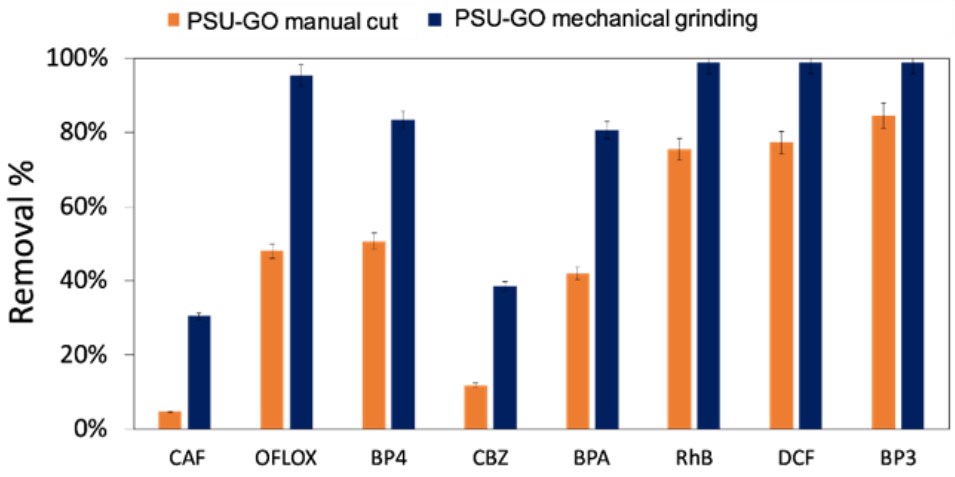

Figure 7.30 *Comparison of the adsorption of manually grinded PSU-GO and mechanically grinded PSU-GO. Small modules (Figure 7.13) filled by 0.7 g of material were used. Tap water solution (1 L), 0.5 mg/L each contaminant, flow rate = 20 mL/min, EBCT= 0.5 min, bed volumes= 0.01 L.*

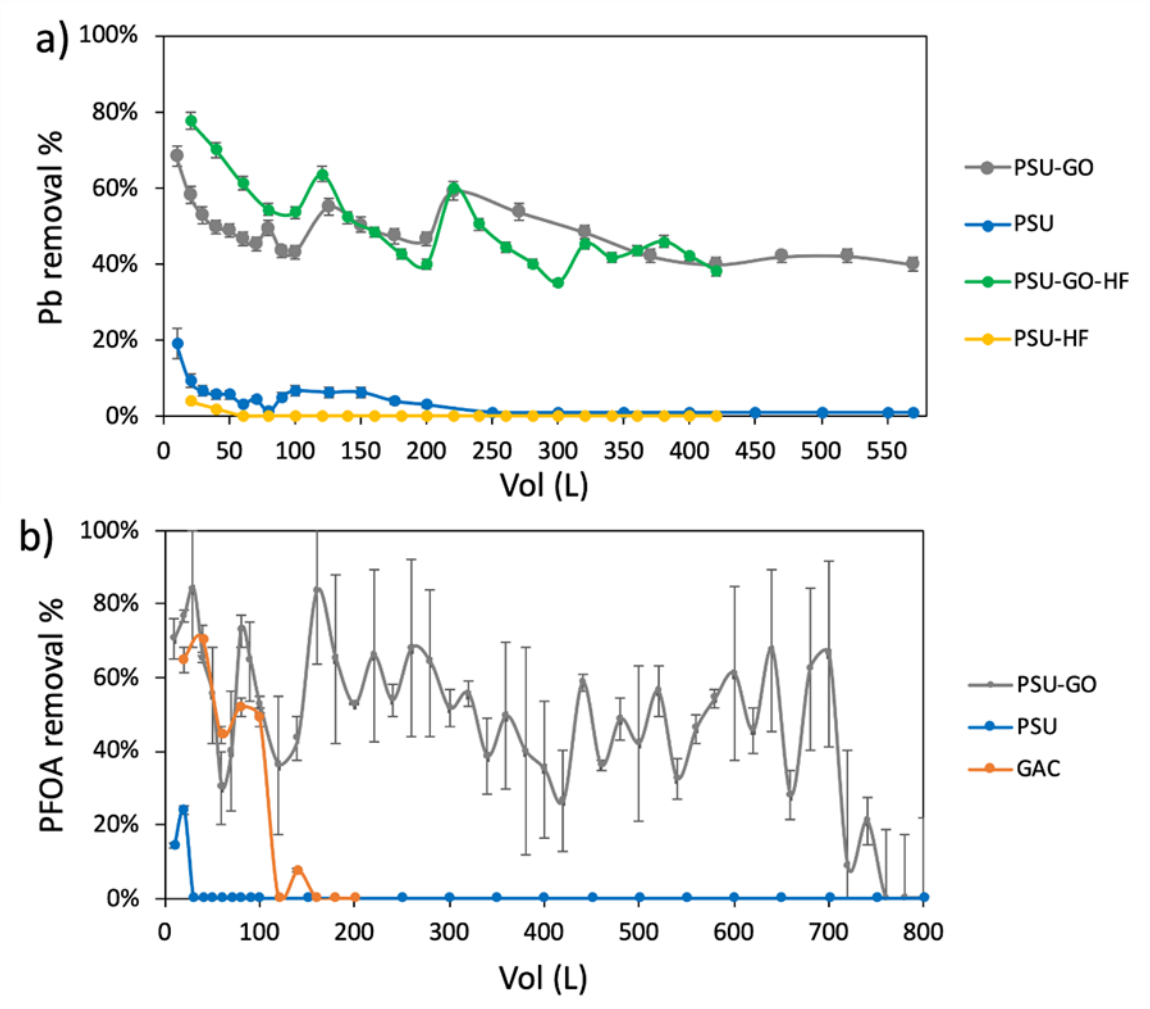

Figure 7.31 *Comparison between removal capacity of tested module on a) Pb and b) PFOA.*